
The Radon Transform and Medical Imaging

CBMS-NSF REGIONAL CONFERENCE SERIES IN APPLIED MATHEMATICS

A series of lectures on topics of current research interest in applied mathematics under the direction of the Conference Board of the Mathematical Sciences, supported by the National Science Foundation and published by SIAM.

- GARRETT BIRKHOFF, *The Numerical Solution of Elliptic Equations*
D. V. LINDLEY, *Bayesian Statistics, A Review*
R. S. VARGA, *Functional Analysis and Approximation Theory in Numerical Analysis*
R. R. BAHAUDUR, *Some Limit Theorems in Statistics*
PATRICK BILLINGSLEY, *Weak Convergence of Measures: Applications in Probability*
J. L. LIONS, *Some Aspects of the Optimal Control of Distributed Parameter Systems*
ROGER PENROSE, *Techniques of Differential Topology in Relativity*
HERMAN CHERNOFF, *Sequential Analysis and Optimal Design*
J. DURBIN, *Distribution Theory for Tests Based on the Sample Distribution Function*
SOL I. RUBINOW, *Mathematical Problems in the Biological Sciences*
P. D. LAX, *Hyperbolic Systems of Conservation Laws and the Mathematical Theory of Shock Waves*
I. J. SCHOENBERG, *Cardinal Spline Interpolation*
IVAN SINGER, *The Theory of Best Approximation and Functional Analysis*
WERNER C. RHEINBOLDT, *Methods of Solving Systems of Nonlinear Equations*
HANS F. WEINBERGER, *Variational Methods for Eigenvalue Approximation*
R. TYRRELL ROCKAFELLAR, *Conjugate Duality and Optimization*
SIR JAMES Lighthill, *Mathematical Biofluidynamics*
GERARD SALTON, *Theory of Indexing*
CATHLEEN S. MORAWETZ, *Notes on Time Decay and Scattering for Some Hyperbolic Problems*
F. HOPPENSTEADT, *Mathematical Theories of Populations: Demographics, Genetics and Epidemics*
RICHARD ASKEY, *Orthogonal Polynomials and Special Functions*
L. E. PAYNE, *Improperly Posed Problems in Partial Differential Equations*
S. ROSEN, *Lectures on the Measurement and Evaluation of the Performance of Computing Systems*
HERBERT B. KELLER, *Numerical Solution of Two Point Boundary Value Problems*
J. P. LASALLE, *The Stability of Dynamical Systems*
D. GOTTLIEB AND S. A. ORSZAG, *Numerical Analysis of Spectral Methods: Theory and Applications*
PETER J. HUBER, *Robust Statistical Procedures*
HERBERT SOLOMON, *Geometric Probability*
FRED S. ROBERTS, *Graph Theory and Its Applications to Problems of Society*
JURIS HARTMANIS, *Feasible Computations and Provable Complexity Properties*
ZOHAR MANNA, *Lectures on the Logic of Computer Programming*
ELLIS L. JOHNSON, *Integer Programming: Facets, Subadditivity, and Duality for Group and Semi-Group Problems*
SHMUEL WINOGRAD, *Arithmetic Complexity of Computations*
J. F. C. KINGMAN, *Mathematics of Genetic Diversity*
MORTON E. GURTIN, *Topics in Finite Elasticity*
THOMAS G. KURTZ, *Approximation of Population Processes*
JERROLD E. MARSDEN, *Lectures on Geometric Methods in Mathematical Physics*
BRADLEY EFRON, *The Jackknife, the Bootstrap, and Other Resampling Plans*
M. WOODROOFE, *Nonlinear Renewal Theory in Sequential Analysis*
D. H. SATTINGER, *Branching in the Presence of Symmetry*
R. TEMAM, *Navier-Stokes Equations and Nonlinear Functional Analysis*

- MIKLÓS CSÖRGÖ, *Quantile Processes with Statistical Applications*
J. D. BUCKMASTER AND G. S. S. LUDFORD, *Lectures on Mathematical Combustion*
R. E. TARJAN, *Data Structures and Network Algorithms*
PAUL WALTMAN, *Competition Models in Population Biology*
S. R. S. VARADHAN, *Large Deviations and Applications*
KIYOSI ITÔ, *Foundations of Stochastic Differential Equations in Infinite Dimensional Spaces*
ALAN C. NEWELL, *Solitons in Mathematics and Physics*
PRANAB KUMAR SEN, *Theory and Applications of Sequential Nonparametrics*
LÁSZLÓ LOVÁSZ, *An Algorithmic Theory of Numbers, Graphs and Convexity*
E. W. CHENEY, *Multivariate Approximation Theory: Selected Topics*
JOEL SPENCER, *Ten Lectures on the Probabilistic Method*
PAUL C. FIFE, *Dynamics of Internal Layers and Diffusive Interfaces*
CHARLES K. CHUI, *Multivariate Splines*
HERBERT S. WILF, *Combinatorial Algorithms: An Update*
HENRY C. TUCKWELL, *Stochastic Processes in the Neurosciences*
FRANK H. CLARKE, *Methods of Dynamic and Nonsmooth Optimization*
ROBERT B. GARDNER, *The Method of Equivalence and Its Applications*
GRACE WAHBA, *Spline Models for Observational Data*
RICHARD S. VARGA, *Scientific Computation on Mathematical Problems and Conjectures*
INGRID DAUBECHIES, *Ten Lectures on Wavelets*
STEPHEN F. MCCORMICK, *Multilevel Projection Methods for Partial Differential Equations*
HARALD NIEDERREITER, *Random Number Generation and Quasi-Monte Carlo Methods*
JOEL SPENCER, *Ten Lectures on the Probabilistic Method, Second Edition*
CHARLES A. MICCHELLI, *Mathematical Aspects of Geometric Modeling*
ROGER TEMAM, *Navier-Stokes Equations and Nonlinear Functional Analysis, Second Edition*
GLENN SHAFER, *Probabilistic Expert Systems*
PETER J. HUBER, *Robust Statistical Procedures, Second Edition*
J. MICHAEL STEELE, *Probability Theory and Combinatorial Optimization*
WERNER C. RHEINBOLDT, *Methods for Solving Systems of Nonlinear Equations, Second Edition*
J. M. CUSHING, *An Introduction to Structured Population Dynamics*
TAI-PING LIU, *Hyperbolic and Viscous Conservation Laws*
MICHAEL RENARDY, *Mathematical Analysis of Viscoelastic Flows*
GÉRARD CORNUÉJOLS, *Combinatorial Optimization: Packing and Covering*
IRENA LASIECKA, *Mathematical Control Theory of Coupled PDEs*
J. K. SHAW, *Mathematical Principles of Optical Fiber Communications*
ZHANGXIN CHEN, *Reservoir Simulation: Mathematical Techniques in Oil Recovery*
ATHANASSIOS S. FOKAS, *A Unified Approach to Boundary Value Problems*
MARGARET CHENEY AND BRETT BORDEN, *Fundamentals of Radar Imaging*
FIORALBA CAKONI, DAVID COLTON, AND PETER MONK, *The Linear Sampling Method in Inverse Electromagnetic Scattering*
ADRIAN CONSTANTIN, *Nonlinear Water Waves with Applications to Wave-Current Interactions and Tsunamis*
WEI-MING NI, *The Mathematics of Diffusion*
ARNULF JENTZEN AND PETER E. KLOEDEN, *Taylor Approximations for Stochastic Partial Differential Equations*
FRED BRAUER AND CARLOS CASTILLO-CHAVEZ, *Mathematical Models for Communicable Diseases*
PETER KUCHMENT, *The Radon Transform and Medical Imaging*

PETER KUCHMENT

Texas A&M University
College Station, Texas

The Radon Transform and Medical Imaging



SOCIETY FOR INDUSTRIAL AND APPLIED MATHEMATICS
PHILADELPHIA

Copyright © 2014 by the Society for Industrial and Applied Mathematics.

10 9 8 7 6 5 4 3 2 1

All rights reserved. Printed in the United States of America. No part of this book may be reproduced, stored, or transmitted in any manner without the written permission of the publisher. For information, write to the Society for Industrial and Applied Mathematics, 3600 Market Street, 6th Floor, Philadelphia, PA 19104-2688 USA.

Trademarked names may be used in this book without the inclusion of a trademark symbol. These names are used in an editorial context only; no infringement of trademark is intended.

MATLAB is a registered trademark of The MathWorks, Inc. For MATLAB product information, please contact The MathWorks, Inc., 3 Apple Hill Drive, Natick, MA 01760-2098 USA, 508-647-7000, Fax: 508-647-7001, info@mathworks.com, www.mathworks.com.

Figure 11.6 reprinted with kind permission of Springer Science and Business Media.

Figure 12.2 reprinted with permission from IOP Publishing.

Figure 12.4 reprinted with permission from the American Institute of Mathematical Sciences.

Figure 12.5 reprinted with permission from de Gruyter.

Library of Congress Cataloging-in-Publication Data

Kuchment, Peter, 1949- author.

The radon transform and medical imaging / Peter Kuchment.

p. ; cm. -- (CBMS-NSF regional conference series in applied mathematics ; 85)

Includes bibliographical references and index.

ISBN 978-1-611973-28-0

I. Society for Industrial and Applied Mathematics, issuing body. II. Title. III.

Series: CBMS-NSF regional conference series in applied mathematics ; 85.

[DNLM: 1. Tomography--methods--Lectures. 2. Mathematics--Lectures. 3.

Radon--Lectures. WN 206]

RC78.7.U4

616.07'543--dc23

2013038338

*Dedicated to the memory
of Leon Ehrenpreis,
Larry Shepp,
Iosif Shneiberg,
dear friends and mathematicians.*



Contents

List of Figures	xiii
Preface	xv
I Introduction	1
1 Why Use Mathematics in Medical Imaging?	3
1.1 Types of medical imaging	3
1.2 Tomography. Computed tomography (CT). Inverse problems	3
1.3 Applications	4
1.4 General types of CT	5
1.5 What kind of mathematics is involved?	5
2 A Brief and Incomplete History of CT	7
3 Some Major CT Modalities and Their Features to Watch for	11
3.1 Tomographic modalities	11
3.2 What features one should pay attention to?	12
3.3 PDE classification	13
4 Organization of the Book	15
II Traditional Computed Tomography Techniques and Integral Geometry	19
5 “Standard” CT and X-ray and Radon Transforms	21
5.1 X-ray projection imaging: X-ray pictures and “old” tomography	21
5.2 X-ray CT	22
5.3 Beer’s law and the X-ray/Radon transforms	23
5.4 Some notation and conventions	28
5.5 Properties of X-ray (= Radon) transform in two dimensions .	30
5.6 Backprojection	34
5.7 Inversion formulas	36

5.8	Stability of inversion	42
5.9	Fourier series and Cormack inversion formulas	44
5.10	Range conditions for the Radon transform	45
5.11	Support (or “hole”) theorem	48
5.12	Chapter’s final remarks and conclusions	48
6	Emission Tomography	53
6.1	Radiative transfer (transport) equation (RTE)	53
6.2	Attenuated X-ray transform and SPECT (single photon emission computed tomography)	54
6.3	PET (positron emission tomography)	59
6.4	Chapter’s final remarks and conclusions	60
7	Artifacts, Incomplete Data, Microlocal Analysis, and Such	65
7.1	Some common artifacts	65
7.2	Microlocal detection of singularities: Wavefront sets of distributions	68
7.3	Detection of singularities, stability, and incomplete data problems	70
7.4	Local (high frequency) tomography—Sharpening singularities	72
7.5	Chapter’s final remarks and conclusions	73
8	More about 3D Radon and X-ray Transforms	77
8.1	3D Radon transform	77
8.2	X-ray transform: Overdetermined parametrization and John’s equation	79
8.3	Projectivization, \mathbf{x} -operator, and such	80
8.4	Fully 3D X-ray CT	80
9	A Brief Overview of Numerical Methods	83
9.1	Analytic techniques	83
9.2	Algebraic reconstruction techniques (ART)	84
9.3	Optimization techniques	84
9.4	Statistical techniques	85
9.5	Parametrix + ART	85
9.6	Some MATLAB [®] sources	86
9.7	Numerical techniques for inverse problems	86
10	MRI, EIT, OT, Elastography, UT	87
10.1	MRI (magnetic resonance imaging)	87
10.2	EIT (electrical impedance tomography)	88
10.3	Optical tomography (OT)	90
10.4	Elastography	91
10.5	Ultrasound imaging and tomography (UT)	91

III	Hybrid (Coupled Physics) Imaging Techniques	93
11	Thermo-, Photo-, and Optoacoustic Tomography (TAT/PAT/OAT)	97
11.1	Mathematical model	98
11.2	Analysis of TAT: Acoustically homogeneous medium case	105
11.3	Analysis of TAT: Acoustically inhomogeneous media	116
11.4	Reconstruction methods in TAT/PAT	121
11.5	Chapter's final remarks and conclusions	137
12	Ultrasound Modulation in EIT and OT	141
12.1	AET (acousto-electric tomography)	142
12.2	Synthetic focusing	144
12.3	Ultrasound modulated optical tomography (UMOT)	147
12.4	Chapter's final remarks and conclusions	149
13	Inverse Problems with Interior Information	151
13.1	The QPAT example worked out (well, sketched)	154
13.2	Other examples	155
13.3	Generic linearized uniqueness	156
IV	Appendices	157
A	Notation	159
A.1	Sets, vectors, etc.	159
A.2	Multi-index notation and derivatives	159
A.3	Some useful functions	160
A.4	Radon transform	161
A.5	Some linear algebra	162
B	Brief Notes on the Fourier Transform and Harmonic Analysis	165
B.1	Harmonic analysis	165
B.2	Fourier series expansions	167
B.3	Properties of Fourier series expansions	168
B.4	Smoothness of $f(x) \Leftrightarrow$ decay of Fourier coefficients f_k	169
B.5	Relations with shifts and derivatives	170
B.6	Product-convolution relations	171
B.7	Convolution on \mathbb{R}^n	171
B.8	Fourier transform (FT)	172
B.9	Properties of the FT	173
B.10	FT of some common functions	174
B.11	The Paley–Wiener theorem	174
B.12	Smoothness and decay of the FT	175
B.13	Smoothing	175
B.14	Sobolev spaces	176

B.15	Sampling	177
B.16	Mellin transform	179
B.17	Wavefront sets of distributions	180
C	Geometric Rays, Trapping, Energy Decay	181
C.1	Geometric rays	181
C.2	Trapping	182
C.3	Local energy decay	182
D	Some Classes of Linear Operators and Operator Functions	183
D.1	Some notation concerning linear operators	183
D.2	Fredholm and semi-Fredholm operators. Fredholm index.	183
D.3	Schatten–von Neumann classes	185
D.4	Regularized determinants	187
D.5	Analytic Fredholm operator functions	188
E	Recommended Books and Surveys	191
Bibliography		193
Index		237

List of Figures

5.1	X-ray picture and old tomography.	21
5.2	X-ray CT. Parallel beam geometry.	23
5.3	X-ray CT. Fan beam and cone beam geometry	24
5.4	Parametrization of a line, $x \cdot \omega = t$	28
5.5	Sinogram (density plot of the X-ray transform) of two squares with parallel sides touching at a vertex.	28
5.6	Geometry of the backprojection.	35
5.7	A phantom (left) and its reconstruction (right).	39
6.1	SPECT procedure.	55
6.2	PET procedure.	59
6.3	Two half-rays in PET.	60
7.1	Full data: phantom and its reconstruction.	65
7.2	A disk phantom and its reconstruction with an undersampling in t	66
7.3	Reconstruction with too few (20) projections.	66
7.4	A phantom and its reconstruction with a 120 degree observation angle	67
7.5	Exterior problem. A phantom, its exterior reconstruction, and reconstruction showing the black central region that was avoided	67
7.6	X-ray projection of the characteristic function of the unit disk at the origin.	71
7.7	A phantom and its local reconstruction. One sees the boundaries sharpened.	72
11.1	TAT/PAT procedure with a partially surrounding acquisition surface S	97
11.2	The observation surface S and the domain Ω containing the object to be imaged.	99
11.3	Coxeter cross of N lines.	108
11.4	The conjectured structure of a most general nonuniqueness set in three dimensions.	109
11.5	Reconstruction from incomplete data using a closed-form inversion formula in two dimensions	113

11.6	(a) Some rays starting along the interval $x \in [-0.7, -0.2]$ in the vertical directions escape on the right; (b) a flat phantom with “invisible wavefront”; (c)–(f) propagation of the flat front: most of the energy of the signal leaves the square domain through the “hole” on the right	119
11.7	Reconstruction with the same sound speed as in Fig. 11.6	119
11.8	Reconstruction with the same sound speed as in Fig. 11.6	120
11.9	Reconstruction of a square phantom from full data in the presence of a trapping parabolic sound speed	121
11.10	Example of a reconstruction using formula (11.25)	133
11.11	Examples of reconstruction from incomplete data using the technique of [464].	137
12.1	The AET procedure	142
12.2	An example of AET reconstruction	143
12.3	An N-shaped pulse.	145
12.4	Comparison of AET reconstructions using ideal focusing versus synthetic focusing (of spherical pulse waves)	146
12.5	UMOT reconstructions: Top row—the phantoms; middle row—initial run of the algorithms; bottom row—reconstructions after 40 iterations (see [15]).	148
B.1	A function “invisible” at the given sequence of points.	177

Preface

This text addresses the topics covered in ten lectures delivered by the author during the 2012 CBMS-NSF conference “Mathematical methods of computed tomography.” The goals of the lectures were

- to describe the main problems and techniques of some well-established imaging modalities,
- to emphasize the most important mathematical ideas involved, and
- to give a brief overview of several imaging techniques that are less common and/or currently being developed.

Writing this text, though, I realized that a more precise (and modest) title should be “The Radon Transform and Medical Imaging.” Indeed, I mostly (but not exclusively) concentrate on modalities allowing integral geometry approaches. Moreover, all the techniques I discuss in any detail come from medical imaging.

The audience of the conference included a wide range of people—from graduate students to mature researchers. These lectures aim to the same mixed crowd. This is why I have tried to keep the exposition self-contained as much as possible, with some background information included in Appendices. Experts should in most cases skip those, to avoid feeling patronized.

I have also tried to keep technicalities to a minimum, emphasizing the main mathematical ideas, with details to be developed to the full extent by the reader and/or found in the literature. In many cases I just provide pointers to the literature.

Concerning the list of the references, it could have grown indefinitely if I tried to make it comprehensive (and even then it would not be complete). I tried to make sure that the reader is referred to main surveys and monographs, and when needed, to original papers. In the case of the many areas that I could touch only tangentially, I threw in a hodgepodge of related pointers, hoping that the reader will dig out further information and references from there. You will be the judges of how well I succeeded.

I also have to confess that the book is addressing mostly analytic techniques. Thus, the highly nontrivial numerical issues—discretization, sampling, efficient algorithms, etc.—are mentioned only in passing in Chapter 9, with pointers to the literature provided.

In my work in tomography I am indebted to many colleagues, coworkers, and students, from whom I have learned a lot. I would not have been able to do this work if not for their books, papers, lectures, and many discussions. I thus express my thanks to M. Agranovsky, V. Aguilar, M. Allmaras, G. Ambartsoumian, H. Ammari, M. Anastasio, S. Arridge, G. Bal, C. Berenstein, G. Beylkin, J. Bowman, E. Bonnetier, L. Borcea, A. Bukhgeim, P. Burgholzer, R. Carroll, M. Cheney, D. Colton, B. Cox, D. Darrow, M. de Hoop, D. Dobson, M. Eastwood, R. Ehman, L. Ehrenpreis, A. Faridani, D. Finch, A. Fokas, I. Gelfand, S. Gindikin, F. Gonzalez, A. Greenleaf, E. Grinberg, F. A. Grünbaum, M. Haltmeier, S. Helgason, Y. Hristova, D. Isaacson, V. Isakov, H. Kang, A. Katsevich, L. Kunyansky, Y. Kurylev, B. Mallick, K. Lancaster, M. Lassas, M. Lenox, V. Lin, S. Lissianoi, A. Louis, S. Lvin, D. Ma, A. Markoe, J. McLaughlin, G. Milton, M. Mogilevsky, S. Moon, J. Mueller, A. Nachman, F. Natterer, L. Nguyen, O. Öktem, G. Ólafsson, A. Olson, L. Päivärinta, V. Palamodov, G. Papanicolaou, V. Papanicolaou, S. Patch, I. Ponomarev, E. T. Quinto, J. Ragusa, Rakesh, E. Ritman, B. Rubin, W. Rundell, F. Santosa, O. Scherzer, J. Schotland, L. Shepp, I. Shneiberg, M. Shubin, S. Siltanen, D. Solmon, P. Stefanov, D. Steinhauer, R. Strichartz, J. Sylvester, A. Tamasan, F. Terzioglu, G. Uhlmann, B. Vainberg, J. Vargo, M. Vogelius, L. Wang, M. Xu, Y. Xu, X. Xun, H. Zhao, N. Zobin, and others, whom I may have inadvertently forgotten to mention.

I also thank L. Kunyansky and Y. Hristova for their help with pictures.

I am grateful to L. Kunyansky, S. Lvin, M. Mogilevsky, D. Steinhauer, F. Terzioglu, as well as the reviewers, for reading parts of the manuscript and making many useful suggestions. On the other hand, I claim ownership and copyright of all the bloopers a reader might (and most probably will) find in this text.

My thanks also go to T. Aktosun, G. Ambartsoumian, and J. Chung for the flawless organization of the conference, as well as to all participants, who patiently suffered through the whole week of my lectures.

This work was partially supported by the CBMS, DHS, and NSF. The author expresses his deep gratitude to these agencies, as well as to the Mathematics Department and IAMCS (Institute of Applied Mathematics and Computational Science) of Texas A&M and KAUST for this important support.

I am indebted to the SIAM publishing editors and staff, especially Sara Murphy and Gina M. Rinelli for patiently working with me on this book.

Last, but not least, my deep gratitude goes to my family for the love and patience they provided during my writing of this text.

*Peter Kuchment
College Station, TX
August, 2013*

Chapter 1

Why Use Mathematics in Medical Imaging?

The classifications of types of imaging, tomography, etc., provided here can be found in a more detailed form in [85, Prologue].

1.1 • Types of medical imaging

Medical imaging involves several important parts, each of which requires sophisticated mathematics (see the handbook [85] on mathematics of imaging).

- **Image reconstruction** deals with producing an image from the data supplied by a scanner.
- **Image processing** addresses improvements of quality of the obtained image, e.g. sharpening edges, de-blurring, etc.
- **Image understanding** is devoted to extracting some features of interest from the image, e.g. blood vessels.

Although these areas are interconnected, we will be addressing the **tomographic**, i.e., image reconstruction part only.

1.2 • Tomography. Computed tomography (CT). Inverse problems

The term **tomography** comes from the Greek words $\tau\omega\mu\sigma$ (slice) and $\gamma\rho\alpha\psi\epsilon\tau\epsilon$ (write). Tomography attempts to find the internal structure of a nontransparent object by sending some signals (waves, particles) through it. For instance, electromagnetic waves of various frequencies (radio and microwaves, visual light, X-rays, γ -rays) and acoustic waves are common.

In **computed tomography (CT)**, the measurements coming from the scanner do not provide a ready image, as in the usual X-ray pictures, but rather the image is the result of an intricate mathematical processing of the measured data.

Tomography thus is an **inverse problem**, where the unknown parameters of a system need to be estimated from the known reaction of the system to external

signals. See [155, 164, 165, 201, 305, 383, 386, 387, 398, 410, 414, 416, 751, 769, 771, 775] for surveys and references on inverse problems.

A typical kind of an inverse problem is the **recovery of coefficients of a differential equation** on a domain from some information about its solutions obtained at the domain's boundary. As we will see, tomography mostly falls into this category.

We will also see that knowing the type of the equation (elliptic, hyperbolic, transport) whose coefficients need to be recovered from boundary measurements already tells us a lot about what to expect from the method in terms of, for instance, resolution and stability.

Here is another example of an inverse problem: the famous Mark Kac problem, “**Can one hear the shape of the drum?**” [394]. The question here is: Can one determine the shape of an oscillating membrane by listening to the pure tones it produces? In other words, can one recover the shape of a domain Ω knowing the spectrum of Laplace operator on Ω with appropriate (e.g., Dirichlet) boundary conditions? This is an example of an **inverse spectral problem**, or a **spectral geometry problem**. See [84, 129, 155, 184, 293, 335, 336, 397] and references therein about that fascinating field. Although it does have some relations to imaging, we will not be able to address it in this text.

1.3 • Applications

One can easily come up with a long list of areas where tomographic techniques would be desirable. Here is such a (partial) list of already existing applications:

- **Medicine:** noninvasive diagnostics, CT guided surgery, CT guided radiotherapy [142, 168].
- **Industry:** nondestructive testing (e.g., finding internal cracks and other defects) [399].
- **Homeland security:** detection of illicit nuclear materials, airport screening [17].
- **Geology/geophysics/seismology:** oil prospecting, deep Earth imaging, earthquake prediction [102, 190, 281, 373, 529, 814].
- **Astronomy** has been one of the main users and developers of tomographic methods; see, e.g., [105, 122, 124].
- **Archeology:** CT scans of mummies, e.g., of Tutankhamen [343].
- **Fusion reactors:** plasma diagnostics in Tokamaks [744].
- **Radar and sonar** [123, 157, 158, 498, 573].

We will concentrate on the imaging modalities arising in medical diagnostics, although our approaches are also applicable in most of other areas listed above.

1.4 • General types of CT

We provide below an important classification of tomographic setups; they can be and sometimes are combined in a single device:

- **Transmission:** The radiation traverses the body and is detected emerging “on the other side.” Example: standard clinical X-ray CT.
- **Reflection:** The radiation bounces back and is detected where it was emitted. Examples: some instances of ultrasound and geophysics imaging.
- **Emission:** The radiation is emitted inside the body and is detected emerging outside. Examples: clinical SPECT (single photon emission tomography) and PET (positron emission tomography), plasma diagnostics, nuclear reactor testing, detection of illicit nuclear materials.

This classification, however, is not all-inclusive. There are various types of tomographic techniques that are hard to classify this way, such as various hybrid methods (see Part III), luminescence optical tomography, magnetic resonance imaging, etc.

1.5 • What kind of mathematics is involved?

The wide range of important applications of CT explains why it has been attracting the close attention of scientists for the past half century. However, putting its usefulness aside, there is another treasure hidden in CT, which makes it so dear for so many “pure” and “applied” mathematicians.¹ Indeed, the mathematics of CT is beautiful, diverse, and keeps producing new delightful challenges to researchers. One can find in CT a wide range of mathematical techniques and problems: Fourier (harmonic) analysis, differential equations, geometry (integral, differential, and algebraic), complex analysis (including several variables), microlocal analysis, group representation theory, discrete mathematics, probability theory and statistics, numerical analysis; you name it.

¹The quotation marks indicate that this author does not believe in the existence of any significant distinction between “pure” and “applied” mathematics and finds separating them harmful for both.

Chapter 2

A Brief and Incomplete History of CT

The author understands that it is fair to add to the above adjectives also “amateurish.” He nevertheless dares to provide the sketch below. One can find much better witness accounts, biographic notes, and historical overviews of various parts of this fascinating story (including the major development of integral geometry in the second half of the 20th century), for instance, in [103, 130, 136, 169, 170, 172, 193, 270, 352, 355, 371, 372, 384, 393, 497, 511, 514, 575, 603, 673, 674, 691, 703, 707, 712, 772, 785, 800].

- 1880: A. G. Bell discovers the photoacoustic effect [89, 90], which leads, more than a hundred years later, to the design of a new exciting medical imaging technique (see Chapter 11).
- 1895: W. C. Röntgen discovers a new radiation, which he calls the X-ray.
- 1896: F. H. Williams in Boston and C. Schleussner (Frankfurt a.Main) take X-ray pictures.
- 1901: W. C. Röntgen receives the first Nobel Prize in physics.
- 1903: E. A. O. Pasche develops a **collimator** for suppressing scattered radiation.
- 1904: H. Minkowski introduces [531] what was later called the **Minkowski–Funk transform** and proves its invertibility.
- 1905–1906: H. Lorentz’s “Radon transform” inversion in three dimensions (unpublished), used by H. Bockwinkel [104].
- 1916: P. Funk finds inversion formulas for the Minkowski–Funk transform [244].
- 1917: J. Radon publishes his reconstruction formula [663].
- 1925: P. Ehrenfest solves the n -dimensional problem.

- 1930–1931: **Traditional (“old”) tomography** arises: A. Vallebona develops stratigraphy, and B. Ziedses des Plantes develops planigraphy.
- 1936: H. Cramér and H. Wold solve the reconstruction problem in statistics, recovering a probability distribution from its marginal distributions.
- 1936: A. Eddington recovers the distribution of star velocities from their radial components.
- 1938–1946: I. Rabi discovers the phenomenon of nuclear magnetic resonance in molecular beams (1944 Nobel Prize in Physics); F. Bloch and E. Purcell (1946) extend it to liquids and solids (1952 Nobel Prize in Physics).
- 1940: F. Firestone achieves ultrasound detection of internal defect of a metal structure.
- 1950–1953: G. Brownell and W. Sweet develop a positron emission imaging device.
- 1952: J. Wild and J. Reid take first 2D ultrasound scan.
- 1956: R. Bracewell solves an inverse problem of radio astronomy.
- 1956–1958: B. Korenblum, S. Tetelbaum, and A. Tyutin solve the CT problem theoretically and implement it experimentally, developing an X-ray scanner for medical purposes [425, 757, 758]. This work became known outside the Ukraine in the 1980s, by which time all traces of their device had disappeared.
- 1963: A. M. Cormack implements tomographic reconstructions for an X-ray scanner.
- 1963: D. Kuhl, L. Chapman, and R. Edwards run first laboratory SPECT experiment (no computers used).
- 1969: G. N. Hounsfield builds an X-ray scanner.
- 1968–1972: G. L. Brownell, C. A. Burnham, and coworkers develop the first PET system.
- 1972: G. N. Hounsfield builds (with J. Ambrose) the first medical CT scanner in 1972.
- 1972: R. Damadian obtains first patent for clinical MRI scan.
- 1973: P. Lauterbur records the first NMR images.
- 1974: First CT system available from a manufacturer (EMI).

- 1976: P. Mansfield and A. A. Maudsley record first human MRI image (a live finger). (2003 Nobel Prize in Medicine to P. Lauterbur and P. Mansfield; read about the tumultuous history of this in Wikipedia: https://en.wikipedia.org/wiki/Magnetic_resonance_imaging).
- 1979: G. N. Hounsfield and A. M. Cormack receive Nobel Prize in medicine for the invention of the CT scanner.
- 1978–1984: Electrical impedance tomography (EIT) is invented by J. Webster and developed further by D. Barber and B. Brown (see Wikipedia: http://en.wikipedia.org/wiki/Electrical_impedance_tomography).
- 2000: PET/CT scanner (by D. Townsend and Nutt) named by TIME Magazine the medical invention of the year.

In this brief historical overview, we have left out many other milestone events in developing CT (e.g., emission tomography, optical tomography, major mathematical developments coming out of electrical impedance tomography, various recent hybrid methods, such as thermo- and photo-acoustic tomography, elastography, etc.). Some additional information about those is provided throughout the book. The author apologizes for possible errors and omissions.

Chapter 3

Some Major CT Modalities and Their Features to Watch for

3.1 • Tomographic modalities

It is hard to list all the types of CT currently used and/or being developed (see, e.g., Wikipedia's article on Tomography, as well as [85, 168, 577]). We list just some, in loose categories.

More or less standard by now:

- X-ray CT is the most commonly used version. The next two are also well known.
- MRI (magnetic resonance imaging), based upon the nuclear magnetic resonance effect
- UT (ultrasound tomography)
- SPECT (single photon emission tomography)
- PET (positron emission tomography)
- OT (optical tomography)
- EIT (electrical impedance tomography)

Many more (not all listed here, but where general considerations of these lectures are often still applicable):

- Elastography [389, 485, 518, 519, 521, 522, 525, 527, 604], electron tomography [237, 282, 283, 333, 334, 507, 601, 662, 721], Doppler tomography [577], radar and sonar [157, 158, 498, 573], microwave tomography [166], discrete tomography [359, 360], quantum tomography [727], polarization tomography, luminescence tomography, etc.

Including “weird” ones like this:

- Internet tomography [533]

And the hype of the day, hybrid methods:

- Thermoacoustic tomography (TAT), photo-optoacoustic tomography (PAT/OAT), ultrasound modulated optical tomography (UMOT, UOT), magnetic resonance electrical impedance tomography (MREIT), magnetic resonance elastography (MRE), sonoelastography, acousto-electric tomography (AET), current density imaging (CDI, CDII), magneto-acoustic, and more. See Part III.

3.2 ▪ What features one should pay attention to?

There are several features one should pay attention to, when considering a particular CT technique:

Mathematics-related:

- **Contrast:** variation in different tissues' responses to the radiation being used. Low contrast means that the technique cannot distinguish between different tissues of interest (e.g., cancerous and healthy cells).
- **Resolution:** size of smallest distinguishable details. If the resolution is insufficient, tumors can be discovered only when they are too large to be treated. Making small blood vessels visible also requires high resolution. As is well known (see Section B.15 and references therein), the high frequency content of the data is responsible for the resolution.
- **Uniqueness** of determining the unknown quantity. Do we collect enough data to uniquely reconstruct a picture? If not, we might be in trouble!
- **Inversion** methods (formulas, algorithms). One needs to be able to present a picture (tomogram) to a physician, rather than just say “Look, we have enough data, but we do not have an image for you ...”
- **Stability** of inversion, which means that the picture (tomogram) does not react too wildly to always present errors in the measured data. The bad news is that essentially all CT problems are unstable (also called **ill-posed**)! The good news, however, is that the degree of instability (ill-posedness) varies significantly. For instance, X-ray CT, MRI, and some other techniques are only very mildly unstable and thus allow for amazingly sharp reconstructions. Some others, such as OT or EIT, which have very good contrast, are extremely unstable. These issues and ways to work around them will be discussed in this text.
- **Linearity:** Some of the CT techniques lead to solving linear problems (X-ray CT, MRI, TAT, PET, SPECT; the last two only if the attenuation map is known). In many cases, one deals with (very significantly) nonlinear problems, e.g., in EIT, OT, UT, etc. Nonlinearity aggravates both mathematical

analysis and numerical solution. Maybe not surprisingly, to add insult to injury, very often nonlinearity comes together with strong instability.

- **Incomplete data is a frequent occurrence in CT.** This means that not all views are available. One is interested, then, in understanding and, if possible, alleviating the arising **incomplete data artifacts**.
- In CT, the forward operator that maps a section of a body to the data measured by the scanner usually has a very small, of infinite co-dimension, range. This means that perfect data would have to satisfy an infinite set of so-called **range conditions**. Knowing such conditions turns out to be important for understanding and developing tomographic techniques. For instance, such information is used to improve inversion algorithms, complete incomplete data, discover and compensate for certain data errors, etc. (see, e.g., [253, 349, 500, 559, 602, 620, 631, 643] and references therein).

Nonmathematical:

- **Safety:** Does the imaging procedure cause any adverse effect on the patient and/or doctor?
- **Cost:** You probably understand this part. If not, check your medical insurance statement after having a CT or MRI scan. ☺

3.3 ■ PDE classification

As we have already mentioned, most imaging methods reduce mathematically to inverse problems of determining coefficients of a partial differential equation (PDE) from boundary data.

The dependence of the boundary values on the coefficients is usually highly nonlinear, which complicates the analytic and numerical treatment substantially. We are lucky that problems arising in some of the main CT modalities (e.g., X-ray CT) are linear or can be approximated well by linear ones.

Some of the features we discussed in the previous section (e.g., stability) are closely related to the type of PDE involved. The main types of PDEs arising here are as follows:

- **Transport equation** (X-ray CT, SPECT, PET)
- **Elliptic equations** (OT, EIT)
- **Wave, or more general hyperbolic equations** (TAT/PAT, SAR, ultrasound imaging)

We will see later on that the type of the underlying PDE already gives hints to what properties to expect. The main thing, as will be discussed in Chapter 7, is whether the possible internal singularities of the quantities in question propagate to the boundary where the observation is done.

Lately, a new breed of tomographic techniques has been arising, the so-called **hybrid** (or **coupled physics**) **methods** (Part III), where one can rely upon some additional *internal* information. It is sometimes hard to classify them according to the options above.

Chapter 4

Organization of the Book

The content of Part II is clearly stated by its title, Traditional Computed Tomography Techniques and Integral Geometry.

It starts with Chapter 5, where the basic imaging procedure and its mathematical model are introduced, leading to the X-ray (the same as Radon in two dimensions) transform. We then study the rich invariance properties of this transform. In accordance with the idea of harmonic analysis, viewed in Appendix B, this naturally leads to the usage of the Fourier transform, Fourier series, and Mellin transform. We derive the main formula of this part—the projection-slice (Fourier-slice or central slice) formula and show that all the information about inversion, stability, and range of the 2D X-ray transform can be extracted from it. Along the way we introduce and explain the notion of the backprojection and discuss the parts of the filtered backprojection formula. The chapter ends, as do many other chapters of the main text, with a section containing final remarks and conclusions; an effort was made to emphasize here the main important lessons to draw, which will remain valuable in discussing other types of tomographic imaging.

The next chapter, Chapter 6, addresses the so-called emission tomography methods (SPECT and PET). Although the main lessons learned about X-ray CT remain valid, there are some new circumstances and difficulties arising here.

The important Chapter 7 starts by discussing common artifacts arising in X-ray CT. Several of them can be explained and predicted using the powerful technique of **microlocal analysis**. We introduce the notion of the **wavefront set** and relate it to the situations in which some parts of the picture get blurred. The microlocal explanation is very easy to use, although if one wants to get into the proofs (which we skip), things get rather technical. Local tomography, which amplifies singularities, is also introduced here. It is useful, for instance, for imaging small blood vessels or other tissue interfaces.

It is hard to overstate the importance of the microlocal technique in tomography. A more advanced part of this analysis, the techniques of **pseudodifferential operators** (Ψ D O s) and **Fourier integral operators** (FIOs) is also crucial but remains mostly behind the scene, since it is hard to introduce to the novice in this

text. Recommended literature can be found in Appendix E. The microlocal facts and techniques will be used throughout the remaining chapters.

Having addressed so far only the 2D case, in Chapter 8, we switch to discussing 3D Radon and X-ray transforms. The analysis of the 3D Radon transform² is rather similar to that of the 2D one. An important difference between them concerns the locality feature. On the other hand, the X-ray transform in three dimensions, which is needed for the still developing so-called **fully 3D X-ray computed tomography**, is a more complex creature. Namely, there are “too many” lines in three dimensions, so the data becomes overdetermined. Reducing dimension can be done by doing slice-by-slice 2D CT, or by using the X-ray cone-beam source moving along a curve. The latter is the choice for the contemporary 3D CT. We describe here the overdetermined **John’s parametrization** of lines in three dimensions and the related ultrahyperbolic **John’s equation**, which removes the overdeterminacy. This naturally leads to the famous χ -operator developed and used by I. Gelfand’s school of integral geometry. This technique, undeservedly, is not well known in the tomographic community. We cannot give it (as well as other topics of this chapter) full justice, so we stop at pointing to the relevant literature. The same goes for the last part, devoted to the cone-beam transform with sources on a curve, where wonderful work has been done in the last decade; more is needed.

Chapter 9 provides a very superficial overview of various numerical techniques, as well as some relevant references. A more detailed account would have required another (and possibly larger) book, as well as an author more competent in the numerical issues of tomography.

The last chapter of Part II, Chapter 10, provides brief looks at some other important modalities: magnetic resonance imaging, electrical impedance imaging, optical tomography, etc. Most of them are mathematically much more complex than what the reader has seen by that point in the book.

The next major part, Part III, addresses the slew of new, mostly not in clinics yet, but highly promising **hybrid or coupled physics** techniques. The first and largest chapter, Chapter 11, is devoted to the best-developed hybrid technique of thermo-/photo-acoustic tomography. We discuss this wonderful (both mathematically and with respect to its medical potential) technique in some detail. Our experience with X-ray CT, Radon transform, and microlocal analysis will be very useful here.

Chapter 12 provides brief accounts of how ultrasonic modulation can make the high contrast, safe, and cheap modalities like EIT and OT more stable and thus lead to high quality tomograms. This work is still in active development and thus very fluid.

An observation made repeatedly in the chapters of this part leads one to believe that “internal information,” provided in most hybrid methods, should be responsible for their improved stability. Indeed, this happens to be the case, as is explained in Chapter 13. Simple microlocal (here you go again!) calculations

²Used, for instance, in some implementations of MRI.

can provide the researcher with an *a priori* understanding of whether stability is expected and, if not, what experimental design can achieve it. The calculation also shows the exact level (i.e., the correct smoothness of the spaces) where stability estimates are expected to hold. This technique, albeit very useful and simple, is no magic wand, and more technical efforts are needed and are being devoted to providing exact answers.

The Appendices (Part IV) provide some relevant (usually elementary) information on linear algebra, harmonic analysis, PDEs, and operator theory. The last appendix contains recommendations of books and surveys devoted to the topics of the book.

The book ends with the list of references and a subject index.

Chapter 5

“Standard” CT and X-ray and Radon Transforms

5.1 • X-ray projection imaging: X-ray pictures and “old” tomography

In the standard X-ray picture procedure⁴ (Fig. 5.1, left), the X-rays from a source pass through the patient’s body and leave a trace on the film. Therefore, the resulting X-ray picture is essentially the overlap of images of all slices (parallel to the film) of the body. This makes reading X-ray pictures an art and requires a lot of training: Even trained professionals might not be able to detect a small tumor hiding behind a dense bone. Almost a hundred years ago, doctors came up with a smart idea (now called “old” or traditional tomography). One of its versions involves moving the source with a constant speed parallel to the film and simultaneously moving the film in the opposite direction with a coordinated constant speed. A simple planar geometry consideration (Fig. 5.1, right) shows that there is a single slice/layer parallel to the film (its location dependent on the chosen motion speed) which will be projected onto the same location of the film and thus sharpened, while the images of all other slices will move and thus blur. Hence, this simple technique sharpens the image of a chosen layer while blurring the rest

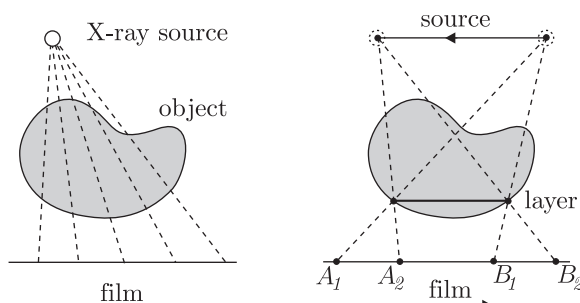


Figure 5.1. X-ray picture and old tomography.

⁴Also called, for natural reasons, projection imaging.

of them. However, the blurred remnants of noninteresting layers are still present and still cause problems while reading X-ray pictures.

The X-ray projection imaging, producing X-ray picture and old tomography are examples of **direct imaging** methods. This means that the machine’s output is an image, without any further mathematical processing of the acquired data.

Can one truly see a single layer in isolation (without cutting the patient open)? This is where **computed tomography (CT)** kicks in.

5.2 ■ X-ray CT

The setup of the now “standard” X-ray CT is as follows: One sends a very narrow (“pencil”) beam of X-rays through a patient’s body. The original intensity (i.e., the number of photons per unit of time) of the beam is known, and a detector finds the outgoing intensity at beam’s exit. The exit intensity is clearly lower than the original one, due to photons being absorbed and scattered inside of the body. So, one collects the two numbers, the initial and terminal intensities. Then the direction of the beam is changed, and a new pair of numbers is collected. This procedure is repeated for a large number of rays (say, on the order of 10^6), which provides a large set of numerical data. Since the rate of weakening of the beam depends on the type of tissues it passes through (e.g., a bone would attenuate the beam much more than a soft tissue), there is a hope of recovering the internal structure of the body from the collected data.

Here a few remarks are due:

- As we have already mentioned, this method requires a “very thin” beam of X-rays. It is clear that this is practically unfeasible. What is usually done to make the beams indeed thin is called **collimation**. Namely, a thin lead tube (**collimator**) is placed in front of the X-ray source; it absorbs all beams except the ones in a small angle around its axis. There is still a cone, rather than a line, of allowed directions, which, at a distance of dozens of centimeters spreads significantly. Collimating the detector on the other side helps to alleviate this issue to a large degree.

In what follows, we will use the mathematical idealization of beams as infinitely thin rays.

- Collimation clearly reduces the signal, by absorbing most of the available photons. Thus, in situations when the signal is not strong to start with (e.g., in SPECT, astronomy, or in some homeland security applications), one wants to avoid collimation. However, without any collimation, one loses the crucial information about the directions of incoming photons. So-called **Compton cameras** (see [17, 623, 623, 722, 723, 765] and references therein) can provide some less specific directional information without collimation.
- Another issue with using collimators is that by reducing the intensity of the beam (i.e., the number of photons per unit of time), it increases **statistical**

(shot) noise. Indeed, if the intensity of the beam is high, the detector, due to the law of large numbers, essentially measures the well-defined expectation (the mean value) of the number of photons per unit of time. However, in low intensity situations (e.g., SPECT or homeland security), the deviations from the mean become significant, which then requires the use of statistical methods (see, e.g., [17, 40, 86, 133, 266, 362, 398, 532, 751, 813]).

Let us now discuss the most popular scan geometries. In the parallel beam setup, one sends a large (often on the order of 10^3) number of beams parallel to a single direction. The collected data is called a single **parallel beam projection**; see Fig. 5.2. Then the procedure is repeated for a large number of different directions (projections).

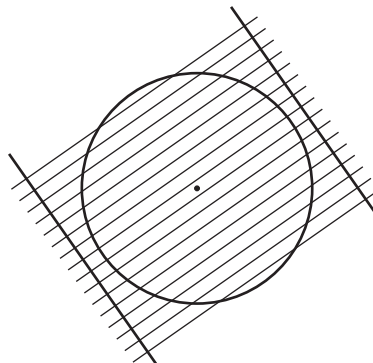


Figure 5.2. X-ray CT. Parallel beam geometry.

A more efficient and frequently used scan geometry is called a **fan-beam (cone-beam in three dimensions) projection**. Here the source runs along a curve, emitting an uncollimated fan (cone in three dimensions) of beams, which are detected on the opposite side by properly collimated detectors (see Fig. 5.3).

One might argue that ideally, when “all” (infinitely many) beams are used, the difference between the fan beam and parallel geometries is just in parametrization of the same data. Although this is true, when fan- (cone-) beam data is collected, one is better off using the appropriate parametrization for reconstruction. Also, different geometries lead to different choices of finitely many beams to use (see the detailed discussion of the sampling issues in [559]).

5.3 • Beer's law and the X-ray/Radon transforms

Well, it is time now to develop a mathematical model of the data collected by an X-ray CT scanner. One needs to start here with a simple physics law (see a more detailed discussion of the radiative transport equation (RTE) in section 6.1).

5.3.1 • Beer's law

Let us consider a pencil beam L , ideally just a line. The intensity of the beam drops during the propagation from its original value, which we denote I_0 , to the

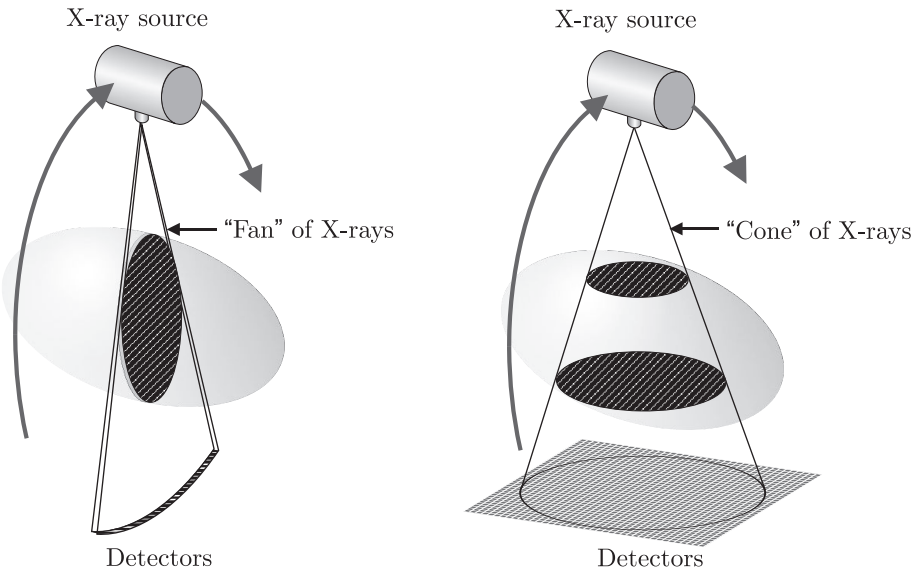


Figure 5.3. X-ray CT. Fan beam (left) and cone beam (right) geometry.

terminal intensity, I_1 . As we have already discussed, the numbers I_0 and I_1 are provided by the scanner. Let us denote by $I(x)$ the intensity of the beam L at a location x . Beer’s law provides a simple ordinary differential equation (ODE) for the function $I(x)$ along the beam L .

Namely, the infinitesimal relative drop of intensity at a distance Δx from the location x should be proportional to the distance traveled:

$$\frac{\Delta I}{I} = -\mu(x)\Delta x, \quad (5.1)$$

where $\mu(x)$ is the **attenuation coefficient** of the tissue at the point x . Notice that one assumes that the attenuation coefficient depends only on the location but not on the direction of the beam passing through this location.

This, so far unknown, function $\mu(x)$ is the tomogram we are looking for!

The relation (5.1) is essentially the first natural guess one can make. Indeed, it is clear that there must be dependence of the relative loss on the distance Δx traveled, with the loss increasing with Δx . When Δx is equal to zero, it is natural to assume that the intensity loss is also equal to zero. Now, the simplest guess for a function that vanishes at zero and then increases is linear, which is exactly what Beer’s law (5.1) states.

Now, (5.1) leads to the ODE

$$\frac{dI}{dx} = -\mu(x)I.$$

Thus, if the initial intensity is I_0 and after traversing the line L the intensity at the

detector is I_1 , then

$$I_1 = I_0 e^{-\int_L \mu(x) dx}$$

or

$$\int_L \mu(x) dx = \log \frac{I_0}{I_1}. \quad (5.2)$$

Remark 5.1. Later (Section 6.1) we'll see a deeper explanation through the *radiative transfer equation (RTE)*.

Hence, the scanner provides us with all (only theoretically, in practice just a finite number) of the line integrals (5.2) of $\mu(x)$. The question thus becomes:

Q: Can one recover a (piecewise smooth, compactly supported⁵) function $f(x)$ of two (or three) variables from all its line integrals?

This is indeed the question that J. Radon posed and resolved in 1917 [663]. And the answer is ... (cue tension-building music here!):

A: Yes (under some reasonable conditions).

In order to obtain this answer, we need to study what is called the X-ray (or Radon⁶) transform.

5.3.2 ■ X-ray and Radon transforms

As we have seen, Beer's law tells us that the scanner data provides us with the line integrals (5.2) of the unknown tomogram $\mu(x)$. This leads to the following definition.

Definition 5.2. The *X-ray (Radon) transform* maps a function $f(x)$ in two dimensions into the set of all its line integrals:

$$f(x) \mapsto (Rf)(l) = g(l) := \int_l f(x) ds,$$

where ds is the arc length measure along the line l .

A *divergent beam (or ray) transform*,

$$(Df)(a, \omega) := \int_0^\infty f(a + t\omega) dt \quad \text{with } a, \omega \in \mathbb{R}^2, |\omega| = 1,$$

is another incarnation of essentially the same operation. Here a is the source location and ω is the direction vector of the beam.

⁵Bodies of all patients tend to be compactly supported. ☺

⁶The difference between the two arises only in dimensions three and higher.

Remark 5.3.

- The X-ray transform is clearly linear. This is a property that one should treasure. No such luck in many other important imaging modalities.
- One should certainly assume appropriate conditions on the function $f(x)$ for its X-ray transform to be defined. For instance, piecewise continuity and compactness of support (or a sufficiently fast decay) suffice.⁷ In most cases, to avoid unnecessary distractions from the main issues, we will not spell out exactly the conditions on the function class involved. Instead, the reader is directed to the multitude of sources where these technical details are available (see, e.g., [349, 354, 511, 559, 577]).
- The name “X-ray transform” is very natural in the X-ray CT scan setting. “Radon transform” means exactly the same thing, if one deals with the 2D situation. In higher dimensions, however, these two notions split. Namely, X-ray is used for the same line integrals transform. However, the term Radon transform is used to denote the operation that maps a function into its integrals over all (affine, i.e., not necessarily passing through the origin) hyperplanes.

We see that if one wants to do imaging slice-by-slice, the X-ray CT problem boils down to inverting the 2D X-ray⁸ transform of a function. With fully 3D imaging, one needs to invert the 3D X-ray transform. These are problems addressed in **integral geometry**. The name comes from studying functions and other geometric objects by their nonlocal, integral rather than local, differential properties. The reader is directed to [252, 253, 325, 326, 328, 349, 354].

5.3.3 • 3D and higher-dimensional transforms

We have already alluded to higher-dimensional situations, but due to its practical importance, it is worthwhile to address the 3D case again (see also Chapter 8 for additional discussions).

In three dimensions, **X-ray transform** still produces line integrals,

$$f(x) \mapsto Pf = g(L) := \int_L f(x) ds,$$

where L is an affine (i.e., not necessarily passing through the origin) line in three dimensions, while **Radon transform** uses planar integrals,

$$f(x) \mapsto Rf = g(\Pi) := \int_{\Pi} f(x) d\sigma,$$

⁷Compactness of support, or at least sufficiently fast decay at infinity, is more important for the validity of analytic results but is automatically satisfied in medical practice.

⁸The same as Radon in two dimensions.

where Π is an affine (i.e., not necessarily passing through the origin) plane in three dimensions.

In two dimensions the X-ray/Radon transform maps a function of two variables into a function of a line, which is again a function of two variables. There are, however, “too many lines” in three dimensions. Indeed, the space of lines in three dimensions is four-dimensional. Thus, in three dimensions, as in higher dimensions, the X-ray data is over determined, meaning that the transform of a function depends on more variables than does the function itself. The Radon data, however, is determined in all dimensions, since there is an n -dimensional variety of affine hyperplanes in \mathbb{R}^n .

More options, besides the X-ray (also called **John's transform**) and Radon transforms, are available in higher dimensions. Indeed, for any $1 \leq k \leq n - 1$ one can consider the **k -plane transform**,⁹ which integrates a function on \mathbb{R}^n over all k -dimensional affine planes. When $k = 1$, we obtain the X-ray (= John's) transform, while when $k = n - 1$, we get the Radon transform.

5.3.4 • Parameterizations of the Radon transform

In order to be able to do computations with the X-ray (Radon) transform, we need to parameterize the space of lines (hyperplanes). We introduce here the common parametrization by so-called **normal coordinates**, which works for the Radon transform in any dimension (and in particular, for the X-ray transform in two dimensions). Indeed, any hyperplane (or line in two dimensions) can be described by a **unit normal vector** $\omega \in S^{n-1}$ and the **signed distance** from the origin $t \in \mathbb{R}$, by means of the linear equation $x \cdot \omega = t$, where x is a vector:

$$(Rf)(t, \omega) = g(t, \omega) := \int_{x \cdot \omega = t} f(x) dx.$$

In two dimensions, the formula can also be written as follows:

$$(Rf)(t, \omega) = g(t, \omega) := \int_{-\infty}^{\infty} f(t\omega + s\omega^\perp) ds.$$

Here ω^\perp is the counterclockwise rotation through 90° of $\omega = (\omega_1, \omega_2)$: $\omega^\perp = (-\omega_2, \omega_1)$ (see Fig. 5.4).

The reader should notice the simple but important fact that (t, ω) and $(-t, -\omega)$ denote the same line. Thus, $g(t, \omega) = g(-t, -\omega)$.

Remark 5.4. *The normal parametrization is not the only possibility, and there are cases when one needs to deal with other parametrizations, as in the paragraphs below.*

⁹Sometimes the name **Radon–John transform** is also used, as kind of an interpolation between the two extreme cases $k = n - 1$ and $k = 1$.

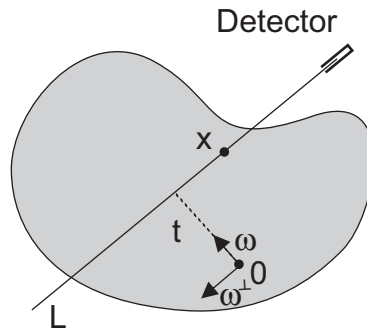


Figure 5.4. Parametrization of a line, $x \cdot \omega = t$.

In particular, as we have mentioned, the normal parametrization works for the Radon transform in any dimension, while for the X-ray transform it is fine in two dimensions only.

Another useful, albeit overdetermined, parametrization, which leads to the John’s transform, is discussed in Chapter 8.

5.3.5 • Sinograms

A **sinogram** is the density plot of the X-ray transform of a 2D function; see Fig. 5.5.

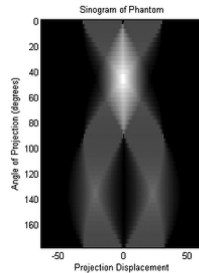


Figure 5.5. Sinogram (density plot of the X-ray transform) of two squares with parallel sides touching at a vertex.

Exercise 5.5. Why is it called a sinogram?

Hint: (a) Look at the picture. (b) What is the X-ray transform of a small single dot?

5.4 • Some notation and conventions

We will adhere to the following notation (see also Appendix B for more discussion of Fourier transforms):

- $S^1 \subset \mathbb{R}^2$ —the circle of unit vectors $\omega \in \mathbb{R}^2$, $|\omega| = 1$.
- $T := \mathbb{R} \times S^1$ —cylinder of points (t, ω) labeling the lines: $x \cdot \omega = t$.

- Points (t, ω) and $(-t, -\omega)$ in T , which correspond to the same line, will often need to be identified, which turns T into the (infinitely wide) Möbius strip.
- Ω —the unit disk $\{x \in \mathbb{R}^2 \mid |x| < 1\}$ in \mathbb{R}^2 .
- We will often assume that our objects (functions) are located (supported) inside Ω .
- We will often use the spaces $L_2(\mathbb{R}^2)$ of square integrable functions on the plane with the inner product

$$(f_1, f_2) = \int_{\mathbb{R}^2} f_1(x) \overline{f_2(x)} dx$$

and the similar space $L_2(T)$ on the cylinder T with

$$(g_1, g_2) = \int_T g_1(t, \omega) \overline{g_2(t, \omega)} d\omega dt.$$

- We will use the notation $\mathcal{S}(\mathbb{R}^2)$ (or just \mathcal{S}) for the Schwartz space of infinitely differentiable functions on the plane, which decay with all their derivatives faster than any power of $|x|$ at infinity: for any α and $N > 0$

$$\left| \frac{\partial^\alpha f(x)}{\partial x^\alpha} \right| \leq C_{N,\alpha} (1 + |x|)^{-N}.$$

Analogous Schwartz space $\mathcal{S}(T)$ can be defined on the cylinder T , where decay is understood with respect to the linear variable $t \in \mathbb{R}$.

- We will denote by $C_0^\infty(\mathbb{R}^2)$ the space of smooth compactly supported functions on the plane, and a similar space $C_0^\infty(T)$ on the cylinder T . Analogously, $C_0^\infty(U)$ consists of C_0^∞ -functions with support in U .
- X-ray/Radon transform in two dimensions acts as follows:

$$f(x) \mapsto g(t, \omega) := Rf(t, \omega) := \int_{x \cdot \omega = t} f(x) ds = \int_{-\infty}^{\infty} f(t\omega + s\omega^\perp) ds, \quad (5.3)$$

where ω^\perp is the counterclockwise rotation through 90° of $\omega = (\omega_1, \omega_2)$; i.e., $\omega^\perp = (-\omega_2, \omega_1)$.

- The **2D Fourier transform** of a function $f(x)$ on \mathbb{R}^2 will be denoted by $\tilde{f}(\xi)$:

$$\tilde{f}(\xi) := \int f(x) e^{-i\xi \cdot x} dx. \quad (5.4)$$

- The 1D Fourier transform of a function $g(t)$ on \mathbb{R} will be denoted by $\hat{g}(\sigma)$:

$$\hat{g}(\sigma) := \int g(t)e^{-i\sigma t} dt. \quad (5.5)$$

The same notation will be applied to functions $g(t, \omega)$:

$$\hat{g}(\sigma, \omega) := \int g(t, \omega)e^{-i\sigma t} dt. \quad (5.6)$$

5.5 • Properties of X-ray (= Radon) transform in two dimensions

Here we explore the rich and fascinating properties of the Radon transform on the plane, which make it extremely useful not only in tomography but also in many other areas of pure and applied mathematics, such as PDEs, group representation theory, special functions, mathematical physics, etc. (see the preamble to Part II). Again, we will not deal here with precise conditions on the functions involved, assuming them to be “sufficiently nice” (whatever this means in each particular case).

Many wonderful properties and applications of X-ray and Radon transforms stem from quite a few symmetries (invariances) that they possess.

5.5.1 • Shift invariance and Fourier transform

Let $\alpha \in \mathbb{R}^2$, and let $T_\alpha f(x) := f(x + \alpha)$ be the corresponding shift operator acting on functions on the plane. Analogously, $T_s g(t, \omega) := g(t + s, \omega)$ is the (axial) shift on the cylinder T .

Proposition 5.6. *The following commutation relation holds:*

$$R(T_\alpha f)(t, \omega) = (T_{\alpha \cdot \omega} R)f(t, \omega). \quad (5.7)$$

Indeed,

$$\begin{aligned} R(T_\alpha f)(t, \omega) &= \int_{x \cdot \omega = t} f(x + \alpha) dx \\ &= \int_{y \cdot \omega = t + \alpha \cdot \omega} f(y) dy = Rf(t + \alpha \cdot \omega, \omega) = (T_{\alpha \cdot \omega} R)f(t, \omega). \text{ QED.} \end{aligned}$$

The resulting equality (5.7) shows the **shift invariance of the Radon transform**.

Thus, according to the discussion in Appendix B, especially Section B.1, **Fourier transform** must be useful when studying the Radon transform.

What the shift invariance property says is geometrically easy to understand: instead of integrating a function over a shifted line, one can integrate the appropriately shifted function along the original line.

5.5.2 • Rotation invariance and Fourier series

Let A be a 2×2 rotation matrix, and $M_A f(x) = f(Ax)$ be the corresponding rotation operator. Abusing notation, one can also use the same notation for the rotation operator on T : $M_A g(t, \omega) := g(t, A\omega)$. (Notice that, since A is a rotation, $A\omega$ is a unit vector whenever ω is.)

Proposition 5.7. *The following commutation relation holds for any rotation matrix A :*

$$RM_A = M_A R. \quad (5.8)$$

Indeed,

$$\begin{aligned} RM_A f(t, \omega) &= \int_{x \cdot \omega = t} f(Ax) dx = \int_{A^{-1}y \cdot \omega = t} f(y) dy \\ &= \int_{y \cdot A\omega = t} f(y) dy = Rf(t, A\omega) = M_A Rf(t, \omega). \end{aligned}$$

We used here that since matrix A represents a rotation, its determinant is equal to 1, and so no Jacobian factor arises during the change of variables. QED.

The equality $RM_A = M_A R$ shows the **rotation invariance of the Radon transform**.

This property, like the shift invariance, has a simple geometric meaning: instead of integrating a function over a rotated line, one can integrate the appropriately rotated function along the original line.

Thus, **Fourier series expansion** must be useful when studying the Radon transform.

Exercise 5.8. *What is the analogue of (5.8) when A is an arbitrary invertible matrix (not necessarily a rotation)?*

5.5.3 • Dilation invariance and Mellin transform

Let $r > 0$ be a positive number, and D_r be the radial dilation operator $D_r f(x) := f(rx)$. An analogous operator acts (in the axial variable) on functions on the cylinder T : $D_r g(t, \omega) := g(rt, \omega)$.

Proposition 5.9. *The following commutation relation holds:*

$$RD_r = \frac{1}{r} D_r R. \quad (5.9)$$

Again, this is proven by a straightforward calculation:

$$(RD_r f)(t, \omega) = \int_{x \cdot \omega = t} f(rx) dx = \frac{1}{r} \int_{y \cdot \omega = rt} f(y) dy = \frac{1}{r} D_r (Rf)(t, \omega). \text{ QED.}$$

The (quasi-)invariance with respect to dilations shows that **Mellin transform** (see Section B.16) must be useful when studying the Radon transform.

5.5.4 ■ Relations with the Fourier transform: Projection-slice theorem

The shift invariance shows that the Fourier transform should be a good friend (maybe even a close relative) of the Radon transform.

The next statement (called the **projection-slice, Fourier-slice, or central slice formula/theorem**) is indeed central for studying the *X*-ray and Radon transforms.

Theorem 5.10. *Under appropriate conditions on a function $f(x)$ on \mathbb{R}^2 (e.g., being in L_2 suffices), the following relation holds:*

$$\widehat{Rf}(\sigma, \omega) = \tilde{f}(\sigma\omega). \quad (5.10)$$

Before proving this theorem, we just notice that it says that, taking a 1D Fourier transform of the Radon transform Rf of a function f on the plane, one recovers the 2D Fourier transform of f (albeit in polar coordinates). Thus, one immediately gets the following consequences concerning uniqueness of reconstruction of f from Rf and inversion formulas.

Corollary 5.11.

1. **Uniqueness of reconstruction:** If f is in L_2 and $Rf = 0$ almost everywhere, then $f = 0$ almost everywhere. Indeed, given its Fourier transform, an L_2 -function is uniquely determined almost everywhere.

2. **Factorization formula:**

$$\mathcal{F}_{1,t \rightarrow \sigma} R = \mathcal{F}_{2,x \rightarrow \xi}. \quad (5.11)$$

Here \mathcal{F}_j is the j -dimensional Fourier transform between the functions of variables indicated in the subscript.

One can say that Fourier transform factors through the Radon transform.

3. **An inversion procedure:** Function f can be recovered from its Radon transform Rf by the following formula (**Fourier inversion**):

$$f = (\mathcal{F}_{2,x \rightarrow \xi})^{-1} \mathcal{F}_{1,t \rightarrow \sigma} Rf. \quad (5.12)$$

In addition to having the above implications, the projection-slice formula will be useful in other ways as well. One can say, without any exaggeration, the following:

The projection-slice formula = the whole analysis of the Radon transform.

So, after this propaganda, let us finally prove the thing!

Proof of Theorem 5.10. Let us write the Radon transform of f as follows:

$$Rf(t, \omega) = \int_{-\infty}^{\infty} f(t\omega + s\omega^\perp) ds.$$

Then

$$\widehat{Rf}(\sigma, \omega) = \int dt \int ds f(t\omega + s\omega^\perp) e^{-i\sigma t} = \int_{\mathbb{R}^2} f(x) e^{-i\sigma x \cdot \omega} dx = \tilde{f}(\sigma \omega). \quad (5.13)$$

QED.

Exercise 5.12. *The relation with the Fourier transform (i.e., the fact that Fourier transform factors through the Radon transform) has a useful generalization. Namely, a function $\Phi(x)$ is said to be a **ridge function** if it depends only on the dot product $x \cdot \omega$ for a fixed ω , i.e., $\Phi(x) = \phi(x \cdot \omega)$.*

1. Show that the functional $f(x) \mapsto \int f(x)\Phi(x)dx$ factors through the Radon transform of f .
2. Find the relation of this fact with the Fourier-slice formula.

5.5.5 • X-ray/ Radon transform as a mapping between function spaces

Consider the weighted space $L_2([-1, 1] \times S^1, (1-t^2)^{-1/2})$ that consists of functions on the finite cylinder $[-1, 1] \times S^1$ that have finite weighted L_2 -norm,

$$\int_{-1}^1 \int_{S^1} |g(t, \omega)|^2 \frac{d\omega dt}{\sqrt{1-t^2}}.$$

We denote, as before, by Ω the unit disk in \mathbb{R}^2 centered at the origin and assume that the function is supported inside Ω .

Theorem 5.13. *The Radon transform R is a continuous linear operator from $L_2(\Omega)$ to $L_2([-1, 1] \times S^1, (1-t^2)^{-1/2})$.*

Indeed, consider a function $f \in L_2(\Omega)$ (i.e., it is square integrable and supported in the unit disk). Then

$$|Rf(t, \omega)|^2 = \left| \int_{-\sqrt{1-t^2}}^{\sqrt{1-t^2}} f(t\omega + s\omega^\perp) ds \right|^2.$$

Consider the function

$$\chi(s) = \begin{cases} 1 & \text{when } |s| \leq \sqrt{1-t^2}, \\ 0 & \text{otherwise.} \end{cases}$$

Then the last integral can be rewritten as

$$\int_{-\infty}^{\infty} \chi(s) f(t\omega + s\omega^\perp) ds.$$

Thus, using the Cauchy–Schwarz inequality $|\int \chi f|^2 \leq \int \chi^2 \int f^2$, one gets

$$|Rf(t, \omega)|^2 \leq 2\sqrt{1-t^2} \int_{-\infty}^{\infty} |f(t\omega + s\omega^\perp)|^2 ds.$$

Now dividing both sides by $\sqrt{1-t^2}$ and integrating with respect to ω and t , one gets the required inequality. QED.

Remark 5.14.

- Notice that R is also continuous as a mapping into the larger space $L_2(S^1 \times [-1, 1])$ without a weight. This is a weaker statement than the theorem above.
- Since the weight in the L_2 -norm on the cylinder blows up when t approaches 1, this means that the Radon transform has a certain decay there, which compensates for the blow up. What does this feature reflect? (Hint: Recall that the function is supported in Ω .)
- This theorem might create the wrong impression that a Radon transform does not change the smoothness class of a function. In fact, as we will see later (Section 5.8), it does make functions smoother. This happens to be a crucially important circumstance in the theory.

5.6 ■ Backprojection

Backprojection is the dual operator $R^\sharp : L_2(T) \mapsto L_2(\mathbb{R}^2)$ to $R : L_2(\mathbb{R}^2) \mapsto L_2(T)$, i.e., such that

$$(Rf, g)_{L_2(T)} = (f, R^\sharp g)_{L_2(\mathbb{R}^2)}.$$

A simple calculation starting with the left-hand side and changing the order of

integration should reveal what R^\sharp is:

$$\begin{aligned}
 (Rf, g)_{L_2(T)} &= \int_{S^1} d\omega \int_{-\infty}^{\infty} dt Rf(t, \omega) g(t, \omega) \\
 &= \int_{S^1} d\omega \int_{-\infty}^{\infty} dt \left(\int_{x \cdot \omega = t} f(x) dx \right) g(t, \omega) \\
 &= \int_{S^1} d\omega \int_{\mathbb{R}^2} dx f(x) g(x \cdot \omega, \omega) \\
 &= \int_{\mathbb{R}^2} f(x) \left(\int_{S^1} g(x \cdot \omega, \omega) d\omega \right) dx.
 \end{aligned}$$

Thus,

$$R^\sharp g(x) = \int_{S^1} g(x \cdot \omega, \omega) d\omega. \quad (5.14)$$

Geometrically, to get the value of $R^\sharp g$ at a point x , one chooses a line passing through x , which implies that the parameters of this line are $(x \cdot \omega, \omega)$; picks the corresponding measured data $g(x \cdot \omega, \omega)$; and then averages over all lines passing through x (see Fig. 5.6).

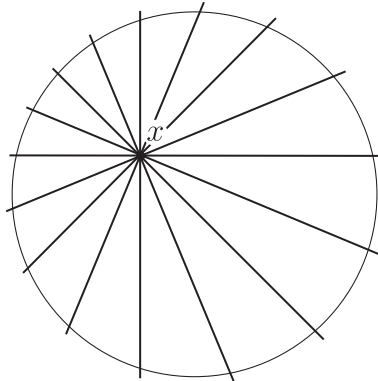


Figure 5.6. Geometry of the backprojection.

The name “backprojection” can be explained by the following simple interpretation of its action. Imagine that whenever a detector is hit by a photon coming from a direction L , the detector “projects it back,” or geometrically draws the line L . As the result, one gets a web of lines, the density of which can be understood as $R^\sharp g$. In other words, a single point source will produce the overlap of a bunch of lines passing through it (see again Fig. 5.6). A calculation shows that this is the

same as saying (denoting by $\delta(x)$ the delta-function) that

$$R^\# \delta = \frac{2}{|x|}, \quad (5.15)$$

and thus instead of the sharp δ -pick, one gets its blurred version $2/|x|$.

It is a common thing when solving a linear system $Ax = b$ numerically to consider the system $A^*Ax = A^*b$ instead. The new system has the matrix A^*A , the so-called **normal operator** corresponding to A . Its advantage is self-adjointness and positivity. Doing spectral analysis of A^*A , one also finds the so-called **singular values** of A , which tell one how ill conditioned the problem of solving the system is (see any numerical linear algebra textbook, e.g., [761]). If the original matrix A was unitary, then this procedure even inverts it, since $A^*A = I$. (The Fourier inversion formula is an instance of this remark.)

It is thus natural to compute the composition $R^\# R$, which is a straightforward calculation. Indeed,

$$\begin{aligned} R^\# R f(x) &= \int_{S^1} Rf(x \cdot \omega, \omega) d\omega \\ &= \int_{S^1} \int_{-\infty}^{\infty} f((x \cdot \omega)\omega + t\omega^\perp) dt d\omega. \end{aligned}$$

Thus, we integrate $f(x)$ over each line passing through x and then integrate over the angle. This is almost like the polar integration with the pole at x , except for two things: (1) the integral is doubled, since we integrate over the whole lines rather than polar rays; (2) the radius factor needed for the polar integration is missing. So, if we take these issues into account and introduce the radial factor, we end up with

$$R^\# R f(x) = \int \frac{2f(y)}{|x-y|} dy = \frac{2}{|x|} * f(x). \quad (5.16)$$

Thus, backprojecting the Radon data, one gets a blurred version of the original image $f(x)$. We will learn how to deblur it later.

Exercise 5.15. Show that the formulas (5.15) and (5.16) say the same thing.

5.7 • Inversion formulas

An explicit inversion formula can be obtained by using the projection-slice formula (5.10) and Fourier inversion formula (5.12). Indeed, passing from Cartesian

coordinates ξ to the polar ones (σ, ω) (where $\xi = \sigma \omega$), we obtain

$$f(x) = \frac{1}{(2\pi)^2} \int_{\mathbb{R}^2} \tilde{f}(\xi) e^{ix \cdot \xi} d\xi \quad (5.17)$$

$$= \frac{1}{(2\pi)^2} \int_{S^1} \int_0^\infty \tilde{f}(\sigma \omega) e^{i\sigma x \cdot \omega} \sigma d\sigma d\omega \quad (5.18)$$

$$= \frac{1}{2} \frac{1}{(2\pi)^2} \int_{S^1} \int_{-\infty}^\infty \tilde{f}(\sigma \omega) e^{i\sigma x \cdot \omega} |\sigma| d\sigma d\omega, \quad (5.19)$$

where we used that $\tilde{f}((-x)(-\omega)) = \tilde{f}(x\omega)$.

Now we use the projection-slice formula (5.10) to get

$$\begin{aligned} f(x) &= \frac{1}{2} \frac{1}{(2\pi)^2} \int_{S^1} \int_{-\infty}^\infty \hat{g}(\sigma, \omega) e^{i\sigma x \cdot \omega} |\sigma| d\sigma d\omega \\ &= \frac{1}{4\pi} \int_{S^1} d\omega \left(\frac{1}{2\pi} \int_{\mathbb{R}} \hat{g}(\sigma, \omega) e^{i\sigma t} |\sigma| d\sigma \right) \Big|_{t=x \cdot \omega}. \end{aligned} \quad (5.20)$$

Here, as before, $g = Rf$.

Looking at the expression in parentheses, one recognizes the inverse 1D Fourier transform applied in variable σ to $\hat{g}(\sigma, \omega)|\sigma|$. If it were just $\hat{g}(\sigma, \omega)$, the result would be $g(t, \omega)$. What is the role of the factor $|\sigma|$? If it were $i\sigma$, we would get $\frac{\partial g(t, \omega)}{\partial t}$. Writing $|\sigma| = -i \operatorname{sgn}\sigma \times i\sigma$, where

$$\operatorname{sgn}x = \begin{cases} 1 & \text{when } x > 0, \\ -1 & \text{when } x < 0, \end{cases}$$

one sees that one has in the parenthesis the function

$$H \frac{\partial g}{\partial t}(t, \omega).$$

Here we have denoted by H the **Hilbert transform** that acts on a function $u(t)$ as follows:

$$Hu(t) = \frac{1}{2\pi} \int_{\mathbb{R}} \hat{u}(\sigma) e^{i\sigma t} (-i \operatorname{sgn}\sigma) d\sigma.$$

This transform happens to be well known and important and can be rewritten without using Fourier transform as follows:

$$Hu(t) = \frac{1}{\pi} p.v. \int_{-\infty}^{\infty} \frac{u(s)}{t-s} ds. \quad (5.21)$$

The improper integral in this formula diverges at the point $s = t$. It has to be understood in the **principal value** (*p.v.*) sense, i.e., as

$$\lim_{\epsilon \downarrow 0} \left(\int_{-\infty}^{t-\epsilon} + \cdots + \int_{t+\epsilon}^{\infty} \cdots \right),$$

or, equivalently, as

$$-\lim_{\epsilon \downarrow 0} \int_{\epsilon}^{\infty} \frac{u(t+s) - u(t-s)}{t-s} ds.$$

So,

$$Hu(t) = -\frac{1}{\pi} \lim_{\epsilon \downarrow 0} \int_{\epsilon}^{\infty} \frac{u(t+s) - u(t-s)}{t-s} ds. \quad (5.22)$$

Finally, we look at the last operation to be performed in (5.20),

$$u(t, \omega) \rightarrow \int_{S^1} u(x \cdot \omega, \omega) d\omega,$$

to recognize in it the backprojection $R^\# u(x)$. Thus, we get the celebrated

FILTERED BACKPROJECTION (FBP) FORMULA
(goes back to J. Radon [663]):

$$f = \frac{1}{4\pi} R^\# H \frac{d}{dt} (Rf). \quad (5.23)$$

Hurray!

Here the **filtration** part is $H \frac{d}{dt}$, and the **backprojection** is $R^\#$, which explains the name of the formula.

Remark 5.16.

- *The filtration is responsible for removing the blur, which, as we know, would have occurred if just the backprojection were used.*
- *The filtration can also be done after the backprojection:*

$$f = \frac{1}{4\pi} \Lambda R^\# (Rf), \quad (5.24)$$

where $\Lambda = \sqrt{-\Delta}$ is the **Calderon operator**. This formula is sometimes called **ρ -filtered backprojection** (and don't ask me, why!).

- *One can also do a filtering partially before and partially after the backprojection. In order to do this, one needs to introduce the **Riesz potential operator** I^α , acting on functions defined on \mathbb{R}^n , when $\alpha < n$:*

$$\widetilde{I^\alpha f}(\xi) := |\xi|^{-\alpha} \tilde{f}(\xi). \quad (5.25)$$

Then the following series of inversion formulas hold in two dimensions:

$$f = \frac{1}{4\pi} I^{-\alpha} R^\# I^{\alpha-1}(Rf), \quad \alpha < 2. \quad (5.26)$$

Then $\alpha = 0$ corresponds to the filtered backprojection, and $\alpha = 1$ to the ρ -filtered one.

- In dimension n an analogous series of inversion formulas hold for the Radon (not the X-ray) transform:

$$f = \frac{1}{4\pi} I^{-\alpha} R^\# I^{\alpha-n+1}(Rf), \quad \alpha < n. \quad (5.27)$$

- The projection-slice formula, as we have already mentioned, leads to what is called the Fourier inversion formula (5.12).

5.7.1 • It works!!!

Well, we have proven the theorems, but do they really work numerically? The author, even after doing all the proofs, had not been sure, till he did his first actual reconstruction. Fig. 5.7 shows the density plot of a function $f(x)$ (a so-called **numerical phantom**), whose Radon transform was computed numerically and then reconstructed using the FBP formula. This picture shows that, surprisingly, the theorems did not lie. ☺

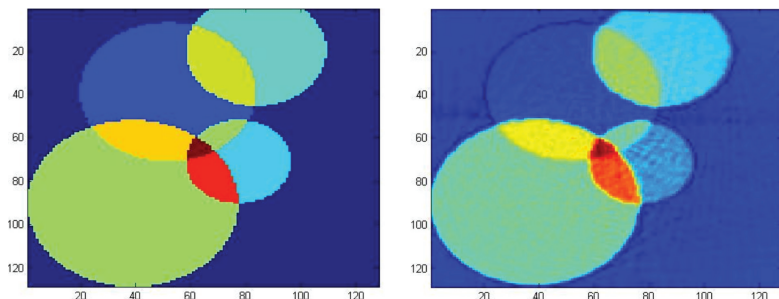


Figure 5.7. A phantom (left) and its reconstruction (right).

To spoil the fun, a few words of caution are due, as follow.

Remark 5.17.

- As we know, tomographic reconstructions, like most inverse problems, are unstable (at least to some degree). It is thus very important, when testing algorithms on numerical phantoms, to use the direct and inverse algorithms that “do not know” about each other. In other words, one should use direct and inverse procedures that are as different as possible: different meshes, no mesh alignment along the picture interfaces, etc. Otherwise, the reconstruction can

*turn out to be too good to be true, cheating even its author. This is the so-called **inverse crime** (for committing which, one should go to an inverse jail, or at least suffer a public admonishment during a conference).*

*There is no such danger when using **physical phantoms** (i.e., actual physical objects scanned by the scanner).*

- *There is often a temptation to demonstrate the success of your reconstruction algorithm by reconstructing something really complicated, such as *Mona Lisa*. Although this might be a good boardroom presentation idea, it is not advisable when testing algorithms. Indeed, most artifacts can be found much more easily on simple phantoms, even as simple as a combination of a few disks of various densities. On such phantoms you can intentionally try to corner your algorithm into producing a variety of well-known artifacts (see their discussion in Chapter 7).*

5.7.2 ▪ Another word of caution: Left inversion versus inversion

One might be surprised that there are several (in fact, infinitely many) different inversion formulas (5.26). Why would one need several inversions for the same operator? Don’t they all give the same result? The answer is a resounding “no.” What’s up here?

As we already know, the Radon transform has zero kernel on “reasonably good” (e.g., compactly supported and piecewise continuous) functions. Thus, such an f can be uniquely reconstructed from Rf . However, the word “inversion” that we used carries some danger of misunderstanding. Namely, the absence of a kernel does NOT necessarily mean invertibility, even for finite matrices. The following standard linear algebra exercise helps us to figure out what is going on (apologies to everyone beyond the linear algebra level ☺).

Exercise 5.18.

1. *Prove that if A is a square matrix with zero kernel, it is invertible, i.e., that there exists $B := A^{-1}$ such that $BA = I$, $AB = I$.*
2. *Prove that if the kernel of any (not necessarily square) matrix A is zero, then there exists a left inverse B such that $BA = I$. Show that if the matrix is not square but rectangular, this is not a right inverse.*
3. *Prove that the left inverse is NOT uniquely defined.*
4. *Prove that a matrix with zero kernel is square (and thus truly invertible) if and only if its range coincides with the whole ambient space.*

This exercise shows that absence of the kernel implies unique recovery of f , but the reconstruction in principle can be done by *different left inverses*. It also shows that a unique inversion procedure arises only if we know additionally that

the range of the matrix is the whole space. Thus, knowledge of the range of the Radon transform is germane to its inversion. We will tackle the range later and see that it is far from being the whole space, which explains the multitude of different “inverses.”

Certainly, all left inverses coincide on any element from the range of the operator. However, they act differently on functions outside the range. Since one never has precise data, the chance that the data collected by a scanner belongs to the range is zero. And then, **on the data with errors, different left inverses give different results.**¹⁰ This emphasizes the importance of knowing the range.

5.7.3 ■ Nonuniqueness (too many words of caution??)

Well, one should not get too elated about our uniqueness of inversion theorem. It requires us to know the line integrals of a function over **all** lines. Clearly, we can measure by the scanner only finitely many such integrals. Then there cannot be any uniqueness: A function from an infinite-dimensional space cannot be recovered from the values of finitely many linear functionals. It seems that the situation is even worse. Namely, we have the following result.

Theorem 5.19 (see [726]). *Let $\omega_1, \dots, \omega_k$ be a finite set of unit vectors, $K \subset \mathbb{R}^2$ be compact, and $f \in C_0^\infty(K)$. Let $K_0 \subset U \subset K$, where K_0 is compact and U is open. Then there exists $f_0 \in C_0^\infty(K)$ such that $f_0 = f$ on K_0 and $Rf_0(\cdot, \omega_j) = 0$, $j = 1, \dots, k$.*

This seems to be rather devastating: Even unrealistically allowing all values of the linear variable t , but restricting to a finite number of projections (projection directions), one gets nonuniqueness. However, it is known (although we will not show this here) that the Fourier transform of any function f , “invisible” under the k projections, has the following representation in polar coordinates:

$$\tilde{f}(\sigma\omega) = \sum_{m>k} i^m \sigma^{-1} J_{m+1}(\sigma) q_m(\omega),$$

where J_m is the Bessel function of order m of the first kind and q_m is a polynomial of degree m . Thus, due to the known behavior of Bessel functions, the Fourier transform $\tilde{f}(\xi)$ is mostly concentrated in the set where $|\xi| > k$. This means that such “invisible” functions are highly oscillatory, and the contributions of their Fourier transforms inside the ball $|\xi| < k$ are small (see Appendix B). Hence, this “not too oscillatory” part of the Fourier transform of the function one is trying to reconstruct can be determined rather reliably. Thus, for a large number of projections, one should feel rather safe.

This gives us the following rule of thumb: A function is reliably determined from its k Radon projections if the following are true:

¹⁰Indeed, in SPECT (Chapter 6) the difference between a straightforward and a smarter inversion formula can be very significant [344, 718].

1. it is *a priori* expected that $|\tilde{f}(\xi)|$ is small for $|\xi| > b > 0$ (this is called **essential b -band limitedness** of f), for some $b < k$,
and
2. the reconstruction algorithm produces a function which is also essentially b -band limited.

See [494, 495, 559] for a detailed discussion.

5.8 ■ Stability of inversion

By **stability of reconstruction** of the tomogram f from the measured data g we mean that small (in an appropriate norm) variations of g lead to small variations of the reconstructed tomogram f , also measured by an appropriate norm. In other words, small errors in the data lead to small errors in the reconstruction.

We will try to give the reader a feeling of the general state of affairs around stability, referring to the literature (e.g., [387, 559, 577]) for further exact details.

We will consider as functional spaces the standard Sobolev spaces H^s of smoothness s (see Appendix Section B.14 and [2, 196, 515]). We will also, as before, denote by R the Radon operator transforming the unknown function f on \mathbb{R}^2 into the data g on T .

Let us recall the notions of **Lipschitz** and **Hölder** stability. An even weaker **logarithmic stability** will not be addressed here. The reader can find discussion of general stability notions and issues, as applied to inverse problems, in [387].

Definition 5.20. *The operation of reconstructing f from $g = Rf$ is said to be Lipschitz stable between the spaces H^{s_2} and H^{s_1} if the following estimate holds for some constant C :*

$$\|f\|_{H^{s_1}} \leq C\|g\|_{H^{s_2}}.$$

The reconstruction is said to be Hölder stable (a weaker concept) if there are constants $s_1, s_2, s_3, C, \mu > 0$ and $\delta > 0$ such that

$$\|f\|_{H^{s_1}} \leq C\|g\|_{H^{s_2}}^\mu$$

for all f such that $\|f\|_{H^{s_3}} \leq \delta$.

Inversion of the Radon transform in \mathbb{R}^2 is only mildly unstable. Namely, the following result holds.

Theorem 5.21. *Let $B \subset \mathbb{R}^2$ be a ball and $s \geq 0$. There exists a positive constant $C_{B,s}$ such that, for any function $f \in H^s$ supported inside B , the following estimate holds:*

$$\frac{1}{C_{B,s}}\|Rf\|_{H^{s+1/2}} \leq \|f\|_{H^s} \leq C_{B,s}\|Rf\|_{H^{s+1/2}}. \quad (5.28)$$

The right-hand-side inequality is not hard to establish. Let us show it for $s = 0$. We have

$$\|f\|_{L^2}^2 = \text{const} \|\tilde{f}\|_{L^2}^2 = \text{const} \int |\tilde{f}(\xi)|^2 d\xi.$$

Switching to polar coordinates $\xi = \sigma\omega$ and using the projection-slice formula gives

$$\begin{aligned} \|f\|_{L^2}^2 &= \text{const} \int |\tilde{f}(\sigma\omega)|^2 |\sigma| d\sigma d\omega \\ &= \text{const} \int \left(|\widehat{Rf}(\sigma, \omega)| |\sigma|^{1/2} \right)^2 d\sigma d\omega \leq \|g\|_{H^{1/2}}^2. \end{aligned}$$

This claim follows from (5.20), where the $|\sigma|$ term is responsible for gaining the “1/2 of a derivative” in the norm of Rf . In other words, Rf is “1/2 of a derivative smoother than f .”

The left-hand-side inequality in (5.28) is also based upon the projection-slice formula, but it requires somewhat more work to prove (see its proof in [559]).

Consider now the n -dimensional Radon transform that integrates a function f over hyperplanes in \mathbb{R}^n . Analogously to Theorem 5.21, one can prove that it smoothes function by “adding $(n-1)/2$ derivatives” (a half of a derivative for each dimension of integration). Namely, it maps continuously H^s functions in Ω into the Radon projections of class $H^{s+(n-1)/2}$. Moreover, the reconstruction procedure is Lipschitz stable between these spaces (see [559] for detailed discussion). Analogous estimates also hold for k -plane Radon transforms.

This “smoothing” is responsible for some instability of the reconstruction (see a related discussion in Appendix Section B.13). Indeed, for instance, in two dimensions, the inversion formula involves multiplication of the Fourier transform $\widehat{g}(\sigma, \omega)$ of the data by the **filter** $|\sigma|$. Let the data have a small but fast oscillating error. It thus makes a small contribution to the data, located at high values of the frequency σ . Due to the growing factor $|\sigma|$, the contribution of this error to the reconstruction will be much larger. The situation would have been worse if the needed filter grew as a higher power of σ or, even worse, exponentially. In the latter case of **exponentially unstable problems** (such as EIT or OT), only a very blurred (low frequency) version of f could be reconstructed.

Stability can also be interpreted in the terms of the decay of the **singular values** σ_j (see Appendix Section D.3) of the forward operator $f \mapsto g$ in L^2 . The faster the decay is, the more unstable the reconstruction becomes. Fortunately, some common modalities, such as X-ray CT, whose singular values have at most power (and not a high power), decay when $j \rightarrow \infty$. The problems with singular values decaying faster than any power of j are considered to be extremely unstable. Even worse are the problems with exponential decay of singular values (analytic continuation or solving a Cauchy problem for an elliptic operator belong to this class).

Note that since the forward mapping is smoothing (it “adds derivatives” to the smoothness level of a function), the inversion should produce functions that are less smooth than the data, which is an unstable operation. The rule of thumb

(which can be justified by applications of appropriate Sobolev embedding theorems [196, 515]) is that the stronger is the smoothing, the less stable is the inversion (this can be rigorously recast in the language of the decay of singular values). Thus, problems that require reconstructing nonsmooth functions from infinitely differentiable (or, even worse, analytic) data are extremely unstable (with superalgebraic or exponential decay of singular values correspondingly). See also additional comments on the relations between smoothness and ill-posedness in Section 5.12 (the paragraph dealing with the Shatten–von Neumann operator ideals).

5.9 • Fourier series and Cormack inversion formulas

As we have seen, there are different inversion formulas for the Radon transform (since they are in fact only left inverses). In particular, although the FBP inversion essentially goes back to J. Radon, neither of the Nobel laureates A. Cormack and J. Hounsfield used (or probably even knew) this formula. While Hounsfield used what is known as an **algebraic reconstruction technique**, which does not require knowledge of any inversion formulas, Cormack did find an inversion method. While we came to FBP using the shift invariance of the Radon transform, and thus the Fourier transform, Cormack essentially used the rotational and dilation invariances and correspondingly Fourier series and the Mellin transform.

When we discovered the rotational invariance of the Radon transform, this indicated that Fourier series expansions should be useful. Let $f(x)$ be a function on \mathbb{R}^2 . We can write it in polar coordinates as $f(r, \theta)$ and then expand into the Fourier series with respect to the polar angle θ :

$$f(r, \theta) = \sum_{n=-\infty}^{\infty} f_n(r) e^{in\theta}.$$

Analogously, $g(t, \omega) = Rf(t, \omega)$ can be expanded into the Fourier series with respect to the polar angle ϕ , where $\omega = (\cos \phi, \sin \phi)$:

$$g(t, \phi) = \sum_{n=-\infty}^{\infty} g_n(t) e^{in\phi}.$$

Exercise 5.22. Use the rotational invariance of the Radon transform to prove (without direct computation) that if $g = Rf$, then g_n depends on f_n only.

Then one can find direct formulas relating these Fourier coefficients. Indeed, according to the previous exercise,

$$g_n(t) e^{in\phi} = R(f_n(r) e^{in\theta}).$$

Thus, it is sufficient to compute only the case when $\phi = 0$ (i.e., “vertical” line L).

Exercise 5.23. Do this calculation to show that

$$g_n(t) = 2 \int_t^{\infty} f_n(r) \cos n \arccos \left(\frac{t}{r} \right) \frac{rd r}{\sqrt{r^2 - t^2}}. \quad (5.29)$$

The expression $T_n(x) := \cos n \arccos x$ is known to be a polynomial, called the **n th Tchebychev polynomial** of the first kind. Thus,

$$g_n(t) = 2 \int_t^\infty f_n(r) T_n\left(\frac{t}{r}\right) \frac{rdr}{\sqrt{r^2 - t^2}}. \quad (5.30)$$

Thus, inversion of the Radon transform R reduces to the inversion of the sequence of integral transforms (5.29), which are called **transforms of Abel type**.

Exercise 5.24. Determine how the Abel transform (5.29)–(5.30) commutes with the dilation $f(r) \rightarrow f(ar)$.

Dilation invariance shows that one should expect this transform to be a convolution operator on the multiplicative group of positive reals. Thus, Mellin transform might be able to invert it explicitly. Fortunately, this is indeed possible, and was done by A. Cormack (see, e.g., [559]).

5.10 • Range conditions for the Radon transform

As we have already discussed in Section 5.7.2, knowledge that the range of R is the whole space (whatever this means) is needed to know that the left inversion is indeed the true inversion and thus is unique. Alas, we will see that the range of R in appropriate function spaces is in fact very small, of infinite co-dimension, and so there exists a huge variety of nonequivalent (for imperfect data) inversion procedures.

We start with a simple exercise.

Exercise 5.25. Let $f(x)$ be a locally integrable function on the plane such that it decays at infinity faster than any power of $|x|$. Prove that $Rf(t, \omega)$ decays when $t \rightarrow \infty$ faster than any power of $|t|$.

We can now state the two **range conditions** that a function $g(t, \omega)$ must satisfy to be the Radon transform of a function $f(x)$ of the class of the above exercise. Namely, such a function must display the following:

1. **Evenness:** $g(t, \omega) = g(-t, -\omega)$.
2. **Moment conditions:** for any integer $k \geq 0$, the k th moment

$$G_k(\omega) := \int_{-\infty}^{\infty} t^k g(t, \omega) dt \quad (5.31)$$

is the restriction to the unit circle S^1 of a homogeneous polynomial of degree k with respect to ω .

Indeed, the evenness is straightforward (just recall that (t, ω) and $(-t, -\omega)$ correspond to the same line).

The moment conditions, as soon as they are formulated, can be checked by the direct calculation:

$$G_k(\omega) = \int_{\mathbb{R}^2} (x \cdot \omega)^k f(x) dx.$$

Since for any vector x the function $(x \cdot \omega)^k$ of ω is linear and homogeneous, we conclude that $(x \cdot \omega)^k$ is a homogeneous polynomial of degree k with respect to ω . Coefficients of this polynomial depend on x as a parameter. Clearly, integrating with respect to x , we still get a homogeneous polynomial of degree k .

Notice that without sufficient decay of f , the moments cannot even be defined. This is why the previous exercise was offered.

As it turns out, the evenness and moment conditions happen to be also sufficient, as seen in the next result.

Theorem 5.26.

1. Let $g(t, \omega)$ be a smooth and compactly supported function on the cylinder T . It can be represented as Rf for a smooth and compactly supported function f on \mathbb{R}^2 if and only if g is even and satisfies the moment conditions.
2. The same statement holds for g and f in the Schwartz spaces of smooth functions decaying with their derivatives at infinity faster than any power of the independent variable.

The necessity of these conditions has already been shown. Let us provide a scheme of the proof of their sufficiency. One can make an educated guess of what the proof should be based upon—the projection-slice formula, what else? Indeed, if $g(t, \omega)$ were the Radon transform of a function $f(x)$ of one of the classes above, then the projection-slice formula would recover the Fourier transform of the function $f(x)$:

$$\tilde{f}(\sigma \omega) = \hat{g}(\sigma, \omega).$$

Now, given a function g of a class of the theorem, we can compute $\hat{g}(\sigma, \omega)$ and define the Fourier transform of the alleged function f as

$$\tilde{f}(\sigma \omega) := \hat{g}(\sigma, \omega). \quad (5.32)$$

Then, taking the inverse Fourier transform, we get that g is indeed the Radon transform of the resulting function f . Voila!

Well, the devil is in the details: How can we be sure that we get a function f of the required class (or indeed any function at all)? The standard theorems about the action of Fourier transforms (see Appendix B) show that we need to guarantee appropriate smoothness (or even analyticity in the case of the Paley–Wiener theorem) and some growth/decay estimates. Now, since g is of the needed class, we conclude that \hat{g} has the needed properties. Why would \tilde{f} not have them

then? Indeed, equation (5.32) defines function \tilde{f} in polar coordinates. So, why would smoothness and growth/decay properties not transfer when you change from polar to Cartesian coordinates, $\xi = \sigma\omega$? We thus check now whether you know planar analytic geometry. ☺

5.10.1 • Do you know your polar coordinates?

While the evenness condition, as we explained above, is easy to understand, the moment conditions, although easy to check when they are written, seem to be mysterious (how could one come up with them?). In fact, both conditions do have a rather simple interpretation, which goes back to the projection-slice theorem (what else??) again.

Consider a smooth function $F(x)$ on the plane. Then $F(x)$ defines in polar coordinates (r, θ) a smooth function $G(r, \theta) := F(r\theta)$. Let us now have an arbitrary smooth function $G(r, \theta)$ of $r \in \mathbb{R}$ and the unit vector $\theta \in S^1$. We wonder whether it defines a smooth function $F(r\theta) := G(r, \theta)$ on the plane. In other words, how are the types of smoothness in Cartesian and polar coordinates related?

Exercise 5.27.

1. Prove that such a smooth F exists if and only if G is even, $G(-r, -\theta) = G(r, \theta)$, and each expression

$$\frac{\partial^k g}{\partial r^k}(0, \theta), \quad k = 0, 1, 2, \dots,$$

extends to a homogeneous polynomial of degree k on the plane.

2. Show that the range conditions for R in the Fourier domain coincide with the conditions in 1.

The first part of this exercise should belong to multivariate calculus, but it somehow has escaped attention during the calculus reform.

5.10.2 • Back to the range

We have now provided sufficient information for the reader to reconstruct the sufficiency proof of the range description theorem (see [261, 349, 354, 559]).

The important implication of the existence of nontrivial range conditions (and even infinitely many of them) is that there exist many different left “inverse” operators $R^{(-1)}$ such that $R^{(-1)}R = I$. One can argue that if $g = Rf$, then all these left inverses should act the same on g . Although this is correct, the fact of life is that g will *always* be measured with errors, and thus will NOT belong to the range of R . Outside the range, though, different left inverses act differently.

5.11 ▪ Support (or “hole”) theorem

The very instructive proof of the following “hole” theorem, due to S. Helgason, can be found in [349].

Theorem 5.28. *Let K be a convex compact set on the plane \mathbb{R}^2 , and let a continuous function $f(x)$ decay at infinity faster than any power of $|x|$ (i.e., $|x|^k |f(x)|$ is bounded for any k). Then, if $\int_L f(x) dx = 0$ for any line L not intersecting K , then $f(x) = 0$ outside K . (In other words, the support of f is in K .)*

One can say that if f is “invisible” for all X-rays not touching K , then f is indeed zero outside K (i.e., its support is in K , which explains the name “support theorem”).

Remark 5.29.

- Since every bounded convex set is the intersection of balls containing that set, it is sufficient to prove the theorem for the case when K is a ball.
- It is interesting to note that if we assume that $f(x)$ decays as $|x|^{-k}$ for a fixed value of k , no matter how large, the statement of the theorem is no longer true, as the next exercise (which requires some knowledge of complex analysis) shows.
- One can easily construct examples showing that for nonconvex sets K the statement of the theorem is incorrect.

Exercise 5.30. Consider \mathbb{R}^2 as the complex plane \mathbb{C} , where $z = x + iy$. We then pick a large integer value of k and define the function $\phi(x, y)$, which is equal to z^{-k} when $z = x + iy$ is outside the unit disk at the origin, and is smooth everywhere (in particular, inside the disk). Prove that, for a sufficiently large k , the integral of this function along any line L not intersecting the disk is equal to zero.

5.12 ▪ Chapter’s final remarks and conclusions

- The reader has probably noticed already that “the projection-slice is the king.” Namely, all other properties—uniqueness of reconstructions, inversion formula, stability of reconstruction, and range conditions—follow from it. This is not surprising, since the formula recovers from the scan data the Fourier transform of the function in question. In many other tomographic techniques one strives to obtain analogues (exact or approximate, e.g., high frequency ones) of the projection-slice formula.
- Range conditions for the Radon transform, as we have seen, have two parts: evenness and moment conditions. It appears that the evenness part is easy, while the moment conditions seem to be mysterious at first glance. This is one of the instances where the standard Radon transform, being “too nice,” is misleading. Experience with less symmetric (attenuated and circular; see

Section 6.2 and Chapter 11) transforms shows that the situation there is essentially opposite: Some moment conditions (e.g., in TAT) can be easily written, but an analogue of the missing evenness condition is hard to find.

One can find some discussions and applications of the range conditions, for instance, in [198, 252, 253, 261, 303, 304, 349, 353, 391, 392, 453, 553, 559, 577, 620, 645, 646, 652, 678] for integral geometry and X-ray CT, in [12, 13, 199, 365, 450–452, 597, 599, 600, 636, 728, 729] for emission tomography and attenuated transforms, and in [5, 8, 9, 22, 441–443, 445, 448, 631, 632, 652] for thermoacoustic imaging and spherical mean operators.

- A very important observation concerns the locality issue. A reconstruction procedure is **local** if, in order to get the value of the image at a point x , it is sufficient to know the X-ray data only for lines passing infinitesimally close to the point x . Locality would allow, for instance, the so-called **region of interest (ROI)** reconstruction, when one uses only X-rays passing through the area of interest, thus significantly reducing the exposure. It follows immediately from the definition (5.14) that backprojection is a local operator. In order to get the backprojected image at a location x , one needs to have data only for X-rays passing exactly through x . However, one sees from the inversion formula (5.23) that presence of the nonlocal Hilbert transform there destroys locality. The resulting formula is **nonlocal**: In order to get the reconstruction in a small region U (or, indeed, at a single point) one still needs to irradiate the whole object.

The question arises of whether this is a defect of the particular inversion formula, or something deeper. We present here just a plausible argument that suggests that local inversion formulas do not exist in two dimensions (one can prove this claim rigorously; see, e.g., [252, 253]). Indeed, one could try a different filtration, which might possibly fix the nonlocality. Alas, this does not seem possible. Indeed, according to the stability estimates, after (or before) backprojection one needs to remove the extra one degree of smoothness that the function acquires (both R and $R^\#$ add a half-derivative each). One wants to have a local filtering operator that reduces smoothness by one degree. However, the famous theorem by J. Peetre [639] says that under very weak conditions on a linear operator acting on functions, its locality forces it to be a differential operator (at least in each bounded domain). Thus, our filtration should be a differential operator of order one. The rotational invariance property requires that it be rotationally invariant. And, oops, there are no rotationally invariant operators of order one! This is not the simplest argument and not the one usually employed, but the author could not resist the temptation to provide it, since it involves the beautiful Peetre theorem.

We will see later how the situation changes in higher dimensions, where it will depend on the parity of the dimension.

- We have mentioned integral geometry quite a few times and will do so even more in the following chapters. However, we cannot say that we have even shown the tip of the integral geometry iceberg. It is rather the tip-of-the-tip-of-the-tip. Not only do we not touch the transforms over curves, weighted transforms, Radon-type transforms on manifolds, the double fibration approach to the Radon transform, relations with the microlocal analysis, etc., which the reader can find, for instance, in [93, 94, 99, 100, 106, 108–110, 171, 173, 198, 204, 238, 250, 252–254, 261, 270, 272, 278, 301, 325, 326, 328, 349, 351, 353, 354, 392, 442, 455, 471–473, 492, 511, 512, 559, 620, 645, 646, 649, 651–653, 656, 657, 666, 668, 677, 678, 710, 716, 717, 736, 767, 770, 771, 775, 791], and references therein; but also we almost do not touch, except for a very brief mention in Chapter 8, the wonderful integral geometric techniques developed by I. Gelfand’s school (projective point of view at the Radon transform, transforms of differential forms, complex integral geometry, χ -operator, etc.). Regretfully, many of these techniques and results are not widely known in the tomography community. It is thus recommended that the reader checks out the corresponding literature [252–254, 261, 269, 270] (see also Chapter 8).
- Let us return to the stability and smoothing again. We recall the previously stated ansatz that the more smoothing is the operator, the more unstable (ill-conditioned) is its inversion. Let us now provide a little bit more detail for this claim.

Consider a bounded domain. We will assume that it is the n -dimensional torus $T = \mathbb{R}^n / \mathbb{Z}^n$. (We leave to the reader to figure out how the general bounded domain case follows from the torus one.¹¹) Suppose that we try to invert a linear operator A that is smoothing; i.e., it sends functions on the torus from L_2 to the Sobolev space H^s with $s > 0$. We can say that A “adds s derivatives to the level of smoothness of this function.” Then, as an operator from L_2 to L_2 it factors as follows:

$$L_2 \xrightarrow{A} H^s \hookrightarrow L_2,$$

where \hookrightarrow is the tautological **imbedding** of H^s into L_2 (i.e., the mapping that does not do anything to a function, just forgets its smoothness). Then both operators in this diagram are bounded in the corresponding spaces, and the operator $A : L_2 \hookrightarrow L_2$ is their composition. Let us look at the “trivial” imbedding operator $I := \hookrightarrow$. It is not that trivial, though. It is known (see details and definitions in Appendix Section D.3) that I belongs to the **Shatten–Neumann class** S_p with any $p > n/s$. As is explained in Section D.3, the class consists of the operators whose singular values are summable in degree p . Thus, the larger is the smoothing level s , and thus the smaller is

¹¹Tchebychev once was giving a lecture on optimal tailoring, which he started by saying, “Let us assume for simplicity that the human body has spherical shape...”

p , the more ill-conditioned is the inversion of I . Another important property of the Shatten–Neumann classes is that they are **operator ideals**. This means that if $B \in L(E, F)$ and $C \in S_p(F, G)$, then $CB \in S_p(E, G)$. Thus, we conclude that the operator A acting in L_2 belongs to $S_p(L_2)$, i.e., has the same level of ill-conditioning as the imbedding I .

Section D.4 then describes the technique of **regularized infinite determinants** available for these classes of operators. Although they are not used in this text, they are crucial for the Shatten–Neumann classes and thus are mentioned.

Chapter 6

Emission Tomography

As we have already discussed in the Introduction, in **emission tomography** one deals with an internal source of radiation, whose effects are detected on the boundary of the nontransparent object. The goal is to find the location and strength of the source.

The truth of the matter is that both X-ray transform of X-ray CT and PET and attenuated Radon transform of SPECT are merely reflections (or rather shadows or ghosts¹²) of a deeper mathematical object, the so-called **radiative transfer (transport) equation** (RTE). This equation also handles many other problems, such as optical tomography.

6.1 • Radiative transfer (transport) equation (RTE)

Let $\theta \in S^1$ be a unit vector on the plane, and $u(x, \theta)$ the density of the particles at x traveling with the unit speed in the direction θ . We assume here that this is a time independent quantity, a point of view that often needs to be abandoned in OT. Let us consider the rate of change (i.e., the directional derivative) of $u(x, \theta)$ in the direction θ , i.e., $\theta \cdot \nabla u(x, \theta)$. If the particles are not scattered or absorbed, and if there are no sources and sinks, then $\theta \cdot \nabla u(x, \theta) = 0$. Let us account for the possibility of all of these. This gives the following balance, which is the **stationary single speed transport equation**:

$$\theta \cdot \nabla u(x, \theta) + \mu(x)u(x, \theta) = \mu_s(x) \int_{S^1} \eta(x, \theta, \theta') u(x, \theta') d\theta' + f(x).$$

Here $\mu(x)$ is our familiar linear attenuation coefficient, which in fact accounts for two types of lost particles: the absorbed ones and the scattered away ones, i.e., $\mu(x) = \mu_a(x) + \mu_s(x)$. The function $\eta(x, \theta, \theta')$ (**scattering amplitude**) is the probability density that a particle incoming in direction θ' and scattered at x gets scattered in direction θ . Thus, the integral term accounts for all particles that get

¹²Recall Bishop Berkeley in 1734 calling infinitesimals “ghosts of departed quantities.”

scattered in direction θ . Finally, $f(x)$ is the source term, accounting for particles created at x going in direction θ . (Notice that it depends on the location x only; i.e., the source is omnidirectional.) It is often assumed that $\eta(x, \theta, \theta')$ depends on x and the angle between the two directions only: $\eta(x, \theta \cdot \theta')$. An even simpler version is that $\eta = b(x)\eta(\theta \cdot \theta')$, or even $\eta = b(x)$ (isotropic scattering).

It is easy to check that, in the absence of sources ($f = 0$) and scattering ($\eta = 0$), the incoming value of $u(\cdot, \theta)$ on the boundary and the outgoing value are related exactly by the familiar coefficient

$$e^{-\int_L^x a(y)dy}$$

and hence to the X-ray transform, as in Section 5.3. Thus, in CT we observe the boundary values of solutions of the transport equation when sources and scattering are absent.

If one neglects scatter, but keeps the source term, the RTE reduces to a simple ODE, whose solution results in the attenuated Radon transform. The recent advances in analytic understanding of this transform came about only after the researchers turned to the transport equation rather than trying to work with the transform itself.

6.2 • Attenuated X-ray transform and SPECT (single photon emission computed tomography)

In SPECT imaging, already rather common in hospitals, a patient is given a pharmaceutical labeled with a radionuclide, which emits γ -photons. The goal is to recover the distribution of the radiation sources function $f(x)$. We are dealing with $\mu(x)$, attenuation, and $f(x)$, sources distribution, and are looking for the unknown $f(x)$ now.

From a point x on beam L , out of $f(x)$ photons, only

$$f(x)e^{-\int_{L(x)}^x \mu(y)dy}$$

reach the detector. Here $L(x)$ is the segment along L from x to the detector (see Fig. 6.1). The total count of photons at the detector is then the **attenuated Radon transform** of f :

$$(T_\mu f)(L) := \int_L f(x)e^{-\int_{L_x}^x \mu(y)dy} dx. \quad (6.1)$$

Its inversion is the goal of SPECT.

In comparison with the Radon inversion, there are some obvious difficulties:

1. Even if the attenuation function $\mu(x)$ is known, the transform looks much more complicated than the usual (nonattenuated) X-ray transform.

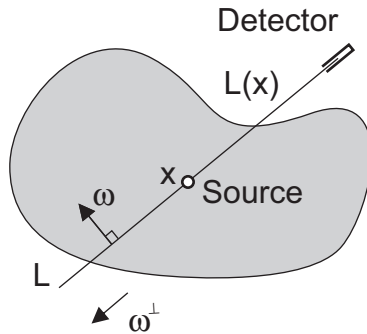


Figure 6.1. SPECT procedure.

2. The truth of the matter is that **both functions μ and f are unknown**. In principle, one solution is to run an X-ray scan to get the attenuation $\mu(x)$, which can then be used for reconstruction of $f(x)$ (not an easy task by itself) [51]. The question of whether and how one could recover both unknown functions simultaneously from the SPECT data alone is still being debated. See further discussion in Section 6.2.3.
3. To make things worse, the transform is very **nonlinear** with respect to the attenuation μ .

Remark 6.1. Notice that the factor $e^{-\int_{L_x} \mu(y) dy}$ represents the probability that a photon emitted at the location x in the direction of L_x will reach the detector (Fig. 6.1). This understanding is very useful in interpreting various formulas in emission tomography.

6.2.1 ■ The exponential Radon transform

The form of the attenuated transform (6.1) is rather complicated, so it had been assumed often that the **attenuation coefficient μ is constant and known**. Further iterative corrections were made then to account for variability of the attenuation (see, e.g., [133, 348, 458, 528]). It was also often assumed that the body of interest is **convex and of known shape**.

Exercise 6.2. Show that under the assumptions of constant attenuation and known convex shape of the object, the transform T_μ can be rewritten as follows:

$$(T_\mu f)(t, \omega) = v(x) \int_{x \cdot \omega = t} f(x) e^{\mu x \cdot \omega^\perp} dl,$$

where $v(x)$ is a known function (determined by the body's shape and attenuation coefficient μ) and ω^\perp is the 90° counterclockwise rotation of ω .

Thus, initially a lot of study was devoted to the **exponential X-ray transform**

$$(R_\mu f)(t, \omega) := \int_{x \cdot \omega = t} f(x) e^{\mu x \cdot \omega^\perp} dl, \quad (6.2)$$

which already offered many nontrivial mathematical problems (e.g., [12, 13, 133, 199, 223, 345–347, 450, 451, 455, 461, 528, 559, 590, 591, 599, 600, 689, 716, 717, 728, 729, 762, 763, 792]). And we know what to look for first, as given next.

Exercise 6.3. Establish an analogue of the projection-slice theorem for the exponential X-ray transform.¹³

After completing this exercise, one sees that the values of $R_\mu f$ uniquely determine the values of the 2D Fourier transform $\tilde{f}(\xi)$ of f on the **totally real**¹⁴ surface S_μ in \mathbb{C}^2 that consists of the points

$$\xi = \sigma\omega + i\mu\omega^\perp, \quad (6.3)$$

where σ is an arbitrary real number, ω is an arbitrary real unit vector, and μ is the given constant attenuation.

So, the question arises of whether one can reconstruct the function f from these values. Uniqueness of reconstruction for a compactly supported f follows from the Paley–Wiener theorem and uniqueness of analytic continuation. Reconstruction formulas, on the other hand, are somewhat tricky to get. Such formulas were obtained in [763], and, surprisingly, they did not use any values of $f(\sigma\omega + i\mu\omega^\perp)$ for $|\sigma|$ smaller than the attenuation coefficient μ .

What's going on? Why do we throw away the whole bunch of data?

One can try to proceed as follows: Start with the standard Fourier inversion formula

$$f(x) = \frac{1}{2\pi} \int_{\mathbb{R}^2} \tilde{f}(\xi) e^{ix \cdot \xi} d\xi.$$

Notice that the differential form integrated here is a piece of a holomorphic 2-form on \mathbb{C}^2 :

$$\Phi_x := \frac{1}{2\pi} \tilde{f}(z) e^{i(x_1 z_1 + x_2 z_2)} dz_1 \wedge dz_2.$$

Then one uses the Cauchy theorem to deform the integration surface from \mathbb{R}^2 to S_μ , and there you are!

Not so fast, though! One discovers immediately that S_μ is not simply connected, and thus cannot be deformed (not homological) to \mathbb{R}^2 . Indeed, it has a circular hole with its boundary circle $\{i\mu\omega^\perp\}$ lying in the imaginary space $i\mathbb{R}^2$. One could try to close this hole with the disk it bounds, but we do not have any

¹³Answer: $\tilde{f}(\sigma\omega + i\mu\omega^\perp) = \hat{g}(\sigma, \omega)$.

¹⁴A **totally real** surface has no tangent complex lines.

data on this patch. However, if the disk were analytic, i.e., belonged to a complex line in \mathbb{C}^2 , then the integral of Φ_x over it would be zero, no matter what the data was.¹⁵ Well, the disk lying in the imaginary space is NEVER analytic. However, it is amazing that one can cut a larger hole in S_μ , which can be closed with an analytic disk. Namely, the boundary of this larger hole consists of points $\sigma\omega + i\mu\omega^\perp$ such that $|\sigma| = \mu$.

Exercise 6.4. Check that this set is a flat circle, whose interior is a complex-analytic disk D .

Now, one can use surface-of-integration deformation to obtain an inversion formula. Notice that $\int_D \Phi_x = 0$, and so the data with $|\sigma| < \mu$ is not used. This, a direct calculation, leads to the Tretiak–Metz formula, analogous to (5.23):

$$f = \frac{1}{4\pi} R_{-\mu}^\# J_\mu (R_\mu f), \quad (6.4)$$

where

$$(R_{-\mu}^\# g)(x) = \int_{S^1} e^{-\mu x \cdot \omega^\perp} g(\omega, x \cdot \omega) d\omega$$

and J_μ is the operator that multiplies the Fourier transform by the filter

$$j(\sigma) = \begin{cases} |\sigma| & \text{when } |\sigma| > |\mu|, \\ 0 & \text{otherwise.} \end{cases}$$

A wide variety of inversion formulas was provided in [455]. In particular, one can write an inversion formula for the (seemingly unphysical) case when the attenuation depends on the direction, i.e., $\mu(\omega)$. As it turns out, this weird case is related to the 180-degree (or half-view) problem in SPECT [107, 591, 689], as well as to the so-called 3D slant hole SPECT [461, 792]. This just confirms the old adage that if the mathematical problem looks interesting, it must turn out to be useful for something. (One might have to wait for a long time, though.)

The range

The range description of the exponential X-ray transform was obtained in [450, 451]; see also [442]. We will not present it here, although it happens to be very interesting. In particular, it produces an unusual separate analyticity theorem [12, 452, 599, 600, 767] and an interesting infinite series of identities for $\sin x$ (!!)[450–452].

6.2.2 • The truly attenuated transform

For quite some time it was believed that the integral transform R_μ (see (6.1)) with such a complex functional weight could not be expected to have any explicit in-

¹⁵We would integrate a holomorphic 2-form over a complex line, which always gives zero.

version formulas.¹⁶ Even proving injectivity of this transformation took a long time; see [41, 220, 221, 512, 596]. However, such inversions were found at the end of 1990s and beginning of the 2000s independently (and in different ways) by Arbuzov, Bukhgeim, and Kazantsev [41] and by Novikov [596]. A Novikov-type formula can be written as follows:

$$f = \frac{1}{4\pi} \operatorname{Re} \operatorname{div} R_{-\mu}^{\#} (\omega e^{-b} H e^b g), \quad (6.5)$$

where H , as before, is the Hilbert transform; $b = 0.5(I + iH)R\mu$ (here R stands for the Radon transform); and $\mathbb{R}_{-\mu}^{\#}$ is the weighted backprojection

$$\mathbb{R}_{-\mu}^{\#} g(x) = \int_{\mathbb{S}^1} e^{-D\mu(x, \omega^\perp)} g(\omega, x \cdot \omega) d\omega.$$

See also [111, 221, 236, 323, 459, 460, 561] for various approaches to proving the inversion formula and its numerical implementations.

Later, complete range conditions were also found by Novikov [597]. (A partial set of conditions was found much earlier by Natterer; see [559] and references therein.)

Even before the inversion formulas were found, the attenuated transform was being successfully inverted by various combinations of approximate inversions and their iterative refinements (see, e.g., [133, 362, 458] and references therein). This shows that having an inversion formula is neither necessary nor sufficient for numerical inversion (such an upset for an analyst!).

6.2.3 ■ Simultaneous reconstruction of the attenuation and the source functions

Our discussion of inversion formulas for the attenuated X-ray transform assumed that the attenuation function $\mu(x)$ is known, while the goal is to recover the sources $f(x)$. This, in fact, is rather far from reality—the attenuation is also unknown. One of the solutions is to run both CT and SPECT (or PET) scans [51]. The former will determine the attenuation map, and then the latter will invert the attenuation transform. One can ask, however, whether one could recover both functions using just the SPECT data $R_{\mu} f$ provided by the scanner, although one might think first (and many people have) that this should be impossible, since “one cannot recover two functions, given just one function of the same number of variables.” **However, this claim is too broad to be correct.**

Exercise 6.5. *Provide a simple counterexample to this general claim. Namely, construct a left invertible linear operator that maps two functions on the segment $[0, 1]$ to a single function on the same interval. ☺*

¹⁶The only indication that there might be some chance was Natterer’s derivation of some explicit (albeit partial) range conditions [559].

The reason one might hope for simultaneous reconstruction is that the range of R_μ , as we have figured out, has infinite co-dimension and thus is very “small.” Therefore, it has a lot of space to “rotate” when μ changes. If the rotation is so significant that the ranges for different attenuations μ intersect only at zero, then one would be able to detect both μ and f .

It is known, for instance, that if the attenuation μ is constant, it can be found simultaneously with f from the data $R_\mu f$, unless f is a **radial function**; see [127, 128, 152, 365, 442, 728, 729] and references therein. In the recent years, results have started to appear showing that something similar holds for variable attenuation **in a generic situation**; see, e.g., [68, 135, 734]. Various generalizations of the attenuated transforms have also arisen, which explains the recent activity [56, 57, 636, 637, 695].

6.3 • PET (positron emission tomography)

PET [52] is similar to SPECT: A patient is given a pharmaceutical labeled by a radionuclide, and the goal is to recover the distribution $f(x)$ of the radiation sources. However, the difference is that the nuclide used in PET emits positrons rather than γ -photons. Emitted positrons immediately annihilate with electrons nearby and emit in exactly opposite directions simultaneous **pairs** of γ -photons. Detectors are located on both sides, and only simultaneous hits at opposite detectors are counted (see Fig. 6.2). Since arrivals at each of the two detectors are independent events, the probability that a pair of photons emitted at location x in opposite directions will reach both detectors is equal to

$$e^{-\int_{L_x^1}^\mu(y)dy} e^{-\int_{L_x^2}^\mu(y)dy} = e^{-\int_L^\mu(y)dy};$$

see Figure 6.3. Here L is the ray connecting two detectors, and L_x^j are its segments from the point x to the j th detector. Notice that the resulting expression on the

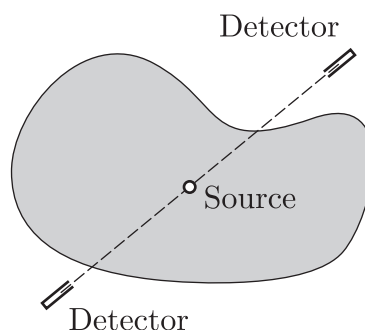


Figure 6.2. PET procedure.

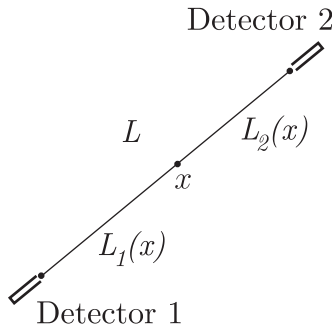


Figure 6.3. Two half-rays in PET.

right does not depend on the location x along L (although both factors on the left do). Thus, the data measured gives the expression

$$\int_L f(x) e^{-\int_L \mu(y) dy} dx = e^{-\int_L \mu(y) dy} \int_L f(x) dx.$$

Hence, if the attenuation $\mu(x)$ is known, the PET data provides, up to multiplication by the known factor $e^{-\int_L \mu(y) dy}$, the Radon transform $\int_L f(x) dx$ of $f(x)$. Thus, with a known attenuation, the mathematics of PET is equivalent to that of X-ray CT.

PET machines are very common in medical diagnostics. Unlike SPECT, they require very short-lived radioisotopes and thus need to be located close to particle accelerators (sometimes such accelerators are built within the medical facilities).

6.4 • Chapter's final remarks and conclusions

There are quite a few remarks to be made concerning the analytically difficult and beautiful area of SPECT and the associated attenuated Radon transform.

- The attenuated Radon (X-ray) transform in two dimensions is still an integral geometry object. In comparison with the regular X-ray transform, it has only some (positive) weights (depending upon the location and a line passing through it) in the integrals. Thus, one expects similar results, maybe not in terms of the proofs, but at least statements. This is indeed true, modulo some caveats.
- The first instance of such a caveat is the stability issue. It is not hard to show that stability holds essentially in the same spaces (in terms of their order) as for the X-ray transform (e.g., [559]). The problem is that the backprojection-type formulas require a weighted backprojection. Looking at the case of the exponential transform, we see that the weights grow exponentially and thus, on objects of sufficient size, cause numerical instabilities. In the constant attenuation case (i.e., for the exponential Radon transform),

there is a good solution. Namely, since we deal with **left** inverses, we have the freedom of choosing the one we like. And, lo and behold, a smart choice of a left inverse indeed exists (see [344, 718]). Regretfully, it seems like no one has come up with such a trick for the truly attenuated transform.

- In the next chapter we will discuss the very important issues of singularity detection, visibility, etc. Although mostly X-ray CT will be mentioned, it is not hard to show that similar conclusions also hold for the attenuated transform **with a smooth attenuation** [449]. A new feature arises, though, when the attenuation is nonsmooth (which is usually the case at tissue interfaces). One can expect new artifacts arising due to the attenuation jumps; those were studied in [401, 402].
- An interesting (and sometimes troublesome) distinction exists between the X-ray transform and its attenuated (and even exponential) version. Namely, the former does not notice the direction of the line of integration (and thus evenness range conditions arise), while the latter is indeed sensitive to the direction. The first hurdle this leads to is in obtaining range conditions, which have taken long time to figure out, even for the exponential transform [450–452] and especially for the fully attenuated one [559, 597].
- Here is the second hurdle coming from the direction-sensitivity of the attenuated transform. In the X-ray case, it is sufficient to rotate the projection only through 180 degrees, while this is not obvious at all in the attenuated case. One can prove that stable reconstruction from 180 (maybe an epsilon more) degrees should exist. It is interesting that this can be interpreted as having the full 360 degrees with attenuation depending on the angle (so that the data in inaccessible directions is attenuated to almost zero). This brings up the result of [455], where, for no practical reason at the time, inversion of the exponential (not the fully attenuated one) transform with angle-dependent attenuation was found. And indeed, 180 degree SPECT reconstructions in the case of constant attenuation have been developed [590, 591, 689, 690], although the author has the impression that some analytic understanding is still missing there. There is no such technique (except ART; see Section 9.2) to deal with the 180 degree problem for the fully attenuated transform.
- Another instance, where angle-dependent attenuation happens to be useful is the so-called 3D slant hole SPECT [792].
- The range conditions we have for the X-ray transform describe the (closed) range of the transform between two specific Hilbert function spaces. The range description obtained in [597] for the attenuated transform does not go that far. It would be interesting to find a pair of Banach spaces between which Novikov's condition will provide an exact range description.

- Some of the things done with the attenuated transform raise the hopes for treatment of more general **weighted (or generalized) Radon transforms**:

$$f(x) \mapsto \int_{x \cdot \omega = t} f(x) w(x, \omega) dx,$$

with a positive “nice” weight w . Indeed, some results, such as the local invertibility (i.e., on functions supported in a small neighborhood of a point) can be proven [108, 512]. Global uniqueness was shown, using microlocal analysis, when the weight w is analytic [109]. However, the famous Cormen example [106] shows that when w is a positive infinitely differentiable function, the transformation might indeed have a nontrivial kernel.

- Another feature distinguishing SPECT and PET from X-ray CT is that in fact the integral geometric model is not telling the whole truth here. Indeed, the integral model assumes that we have a steady flow of photons, which we observe for a time sufficient to accumulate the mean value of the number of particles arriving per unit of time. This value is exactly the line integral leading to the X-ray transform model. However, in emission tomography the sources are necessarily weak,¹⁷ the flow of photons becomes very sparse, and thus statistical noise arises. Then the Radon transform model describes only the (inaccessible) mean value of the counts. Here is the moment when statistical techniques have to kick in, and they indeed are widely used [133, 266]. The situation in homeland security applications is similar (if not worse) [813].
- Another issue, also due to the low levels of radiation in emission tomography, deals with the collimation. Using collimators, one drastically reduces the already low signal. On the other hand, without collimation one loses all directional information, which is crucial for inversion. The situation is similar in astronomy and is even more drastic for homeland security screening applications. A solution was found in using so-called **Compton cameras**. These types of detectors do not use collimation, but based on the Compton scattering effect they can provide, if not the exact incoming direction, at least a surface cone along which the particle came. Due to space limitations, we will not discuss Compton cameras further in this text. The reader is directed to publications [16, 17, 623, 722, 723, 765] and references therein.
- A lot of attention has been devoted to **intensity modulated radiation therapy treatment planning**, which aims at finding an “optimal” irradiation plan for a given cancer patient [119, 120]. We use the quotation marks here, since it is not quite clear what an optimal plan would be. Ideally, one would want to reach and eliminate the tumor, at the same time sparing all the healthy tissues around it. This is clearly impossible, since an X-ray

¹⁷Unless one is observing a nuclear reactor rather than a live patient.

beam cannot reach an internal tumor without passing through healthy tissue. Mathematically, the reflection of this difficulty is the following. One can argue [174, 175] that, while the SPECT problem is to solve an equation with the attenuated Radon transform, radiation treatment planning boils down to solving the equation with the dual operator, i.e. attenuated backprojection. The issue is that when solving this equation, trying to get the “ideal” plan, one unavoidably ends up having to use negative intensities of X-rays. This clearly does not make sense. Thus the problem of positivity arises: How well can one approximate the impossible ideal plan by using only nonnegative intensities [174, 175, 438]? Everything depends now upon what one means by “well.” The issue is clearly extremely important for clinical applications and is still being actively discussed; see, e.g., [119, 120, 151, 153, 156, 491, 644, 804] and references therein.

Chapter 7

Artifacts, Incomplete Data, Microlocal Analysis, and Such

While the previous chapters were devoted to the mathematics of several specific tomographic technologies, this one addresses some mathematical tools that are applicable across a variety of different tomographic modalities, both known and still under development (transmission and emission CT, some hybrid modalities, etc.). These tools belong to the category of so-called **microlocal analysis** and allow one to predict rather easily possible artifacts, stability issues, etc.

We start by discussing several common types of artifacts, although not all of them are susceptible to microlocal analysis.

7.1 • Some common artifacts

Reconstructed images can (and almost always do) display some distortions and/or features that are not present in the ideal image, so-called **artifacts**. It is important to recognize and, if possible, predict and alleviate appearance of these. In this section, we take a quick look at some most common artifacts.

Let us look at the phantom and its reconstruction in Fig. 7.1, which demonstrates a high quality reconstruction with no significant artifacts.

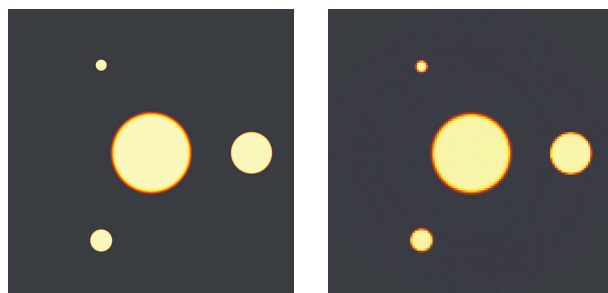


Figure 7.1. Full data: phantom (left) and its reconstruction (right).

7.1.1 • Insufficient number of lines in a projection

Insufficient sampling in the linear variable t (i.e., insufficient number of lines in a projection) can lead to the blurring artifact demonstrated in Fig. 7.2. One can understand this as follows: Insufficient linear sampling cannot resolve well higher frequencies, which are responsible for the sharpness of boundaries.

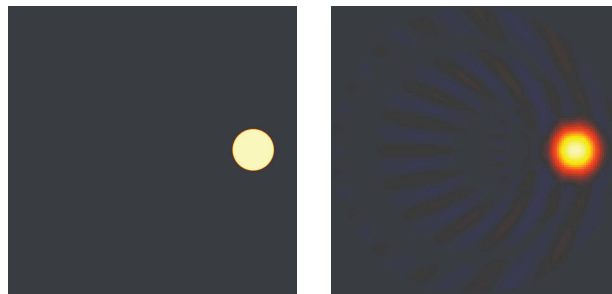


Figure 7.2. A disk phantom (left) and its reconstruction with an undersampling in t (right).

7.1.2 • Insufficient number of projections (angular undersampling)

The angular undersampling (insufficient number of projections) usually leads to the streak artifacts shown in Fig. 7.3.

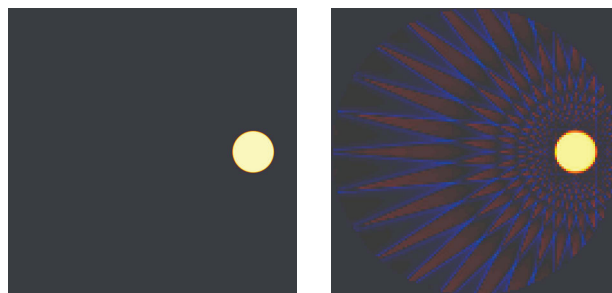


Figure 7.3. Reconstruction with too few (20) projections.

7.1.3 • Blurring due to limited data. “Invisible” singularities.

The “limited data” situation is very common in medical imaging, when some views either are inaccessible (e.g., obstructed by other body parts) or are preferably to be avoided (e.g., the spinal cord during X-ray study). In such cases, one can expect and indeed predict blurring away of some sharp details (tissue interfaces, blood vessels, etc.).

One of the most common situations is the **limited angle problem**, when only a particular angle of projections is available. Fig. 7.4 demonstrates the blurring artifacts, which are due to only 120° (instead of 180°) observation angle being available.

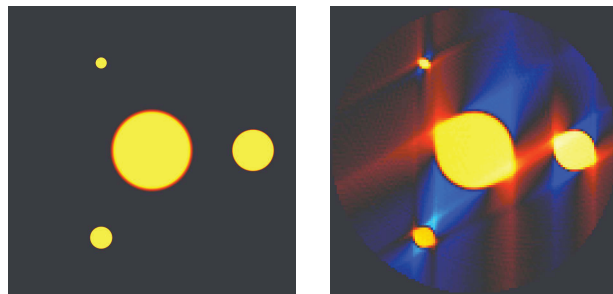


Figure 7.4. A phantom (left) and its reconstruction (right) with a 120 degree observation angle.

If one wants to avoid some region (e.g., spinal cord), this means that only rays not intersecting this part are used. This is the so-called **exterior problem**. The resulting blurring is demonstrated in Fig. 7.5.

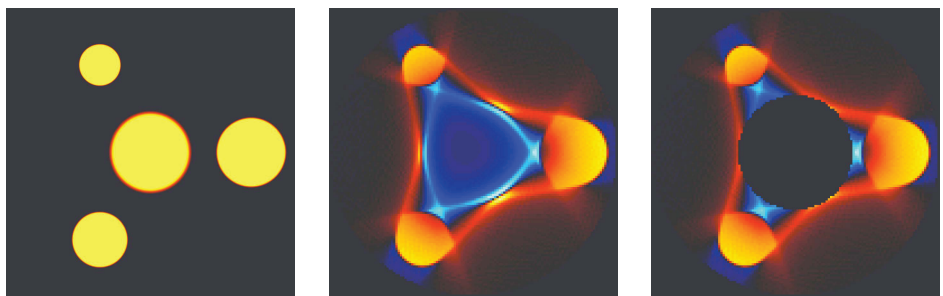


Figure 7.5. Exterior problem. A phantom (left), its exterior reconstruction (middle), and reconstruction showing the black central region that was avoided (right).

One can notice that apparently there is some rule about what gets blurred; it is not sheer madness. And one will be right: As we'll see in Section 7.3, the blurring can be predicted.

Exercise 7.1. Without reading forward, try to guess what the blurring rule is. ☺

Another frequent incomplete data problem is called in mathematics the **interior problem**, while the more common name used in practice is **region of interest (ROI) imaging**. In some sense, it is complementary to the exterior problem, since here one wants to use only the rays that do cross the region of interest (to reduce radiation damage, cost, and time). We will discuss this problem in more detail in Section 7.5.

Exercise 7.2. If you solved the previous exercise, try to predict on a simple example the blurring in the ROI problem. ☺

7.1.4 ■ Some other possible artifacts

We list below some other artifacts common in tomographic imaging (**mostly copied from http://en.wikipedia.org/wiki/X-ray_computed_tomography**; see also discussion of the important issues of artifacts in [142, 203, 357, 358, 361, 396, 559, 577] and essentially any book on tomography):

Streak artifact. Streaks are often seen around materials that block most X-rays, such as metal or bone. It can be caused by undersampling, motion, beam hardening (i.e., the proportion of lower energy photons dropping due to absorption), or scatter.

Partial volume effect. This appears as “blurring” over sharp edges (see examples above).

Ring artifact. Several “rings” appear within an image. Usually a mechanical artifact, due to a detector fault.

Noise artifact. This appears as graining on the image and is caused by a low **signal-to-noise ratio (SNR)**.

Motion artifact. These can introduce blurring and/or streaking caused by movement of the object being imaged.

Beam hardening. Low energy photons are absorbed more readily than higher energy ones. Thus, while traversing the body, the beam experiences a spectral shift to higher energies. This can give a “cupped” appearance to the image, creating the impression that there is more attenuation in the center of the object.

7.2 ■ Microlocal detection of singularities: Wavefront sets of distributions

In order to understand many aspects of tomography, particularly distortions due to limited data, one needs to learn at least the basics of what is called **microlocal analysis**. Here we introduce one of its main notions, which comes from taking one step further in the relation between the smoothness of a function and the decay of its Fourier transform (Appendix B). Namely, the Fourier transform allows one to check the smoothness at a point x_0 by going to the Fourier domain.

Exercise 7.3. *Prove that a function f is smooth near x_0 if and only if there exists a function $\phi \in C_0^\infty(\mathbb{R}^n)$ such that $\phi(x_0) \neq 0$ and $\widehat{(\phi f)}(\xi)$ decays at infinity faster than any power of $|\xi|$. In other words, for any $N > 0$, there is a constant C_N such that*

$$|\widehat{(\phi f)}(\xi)| \leq C_N(1 + |\xi|)^{-N}. \quad (7.1)$$

So, at the points where f is singular, no cut-off leads to fast decay of the Fourier transform. However, the decay (C.3) might be possible to achieve in at least some of the directions $\xi \in \mathbb{R}^n$. This leads to the following definition.

Definition 7.4. Let $x_0 \in \mathbb{R}^n$ and $\xi_0 \neq 0$, $\xi_0 \in \mathbb{R}^n$. The function f is said to be **microlocally smooth near (x_0, ξ_0)** , if there exists a function $\phi \in C_0^\infty(\mathbb{R}^n)$ such that $\phi(x_0) \neq 0$ and $\epsilon > 0$ such that for any $N > 0$ there is a constant C_N such that

$$|\widetilde{(\phi f)}(\xi)| \leq C_N(1 + |\xi|)^{-N} \quad (7.2)$$

holds for all ξ in the **conical neighborhood**

$$\left| \frac{\xi}{|\xi|} - \frac{\xi_0}{|\xi_0|} \right| < \epsilon$$

of the vector ξ_0 .

Definition 7.5. The **wavefront set** $WF(f)$ of function $f(x)$ consists of all points $(x_0, \xi_0) \in \mathbb{R}_x^n \times (\mathbb{R}_\xi^n \setminus \{0\})$ such that f is **not** microlocally smooth near (x_0, ξ_0) .

Exercise 7.6. Prove that $WF(f)$ is a closed conical (w.r.t. ξ) subset of $\mathbb{R}_x^n \times (\mathbb{R}_\xi^n \setminus \{0\})$.

Theorem 7.7. The projection onto the x -space of the wavefront set of f is the singular support of f . In other words, let $\pi : \mathbb{R}_x^n \times \mathbb{R}_\xi^n \rightarrow \mathbb{R}_x^n$ be the natural projection. Then $\pi(WF(f)) = \text{sing supp } f$.

Examples:

- $\text{sing supp}(\delta) = \{0\}$, while $WF(\delta) = \{0\} \times (\mathbb{R}^n \setminus 0)$.
- Let $(x, y) \in \mathbb{R}^{n_1+n_2}$ and $u(x) \in C^\infty(\mathbb{R}^{n_1})$. Consider the distribution

$$u(x) \times \delta(y) : \langle u \times \delta, w \rangle := \int w(x, 0) u(x) dx.$$

Then $WF(u \times \delta)$ consists of all pairs $((x, 0), (0, \eta))$ with $x \in \text{supp } u$ and $\eta \neq 0$. Here (ξ, η) is the dual variable to (x, y) .

- Let $S \subset \mathbb{R}^n$ be a smooth surface (of any dimension) and $u \in C^\infty(S)$. Consider the distribution

$$u \delta_S : \langle u \delta_S, \phi \rangle := \int_S u(x) \phi(x) dx.$$

Then $WF(u \delta_S)$ consists of all pairs (x, ξ) such that $x \in \text{supp } u$ and $\xi \neq 0$ is normal to S at the point x .

- If $S \subset \mathbb{R}^n$ is a smooth hypersurface and $f(x)$ is infinitely differentiable on both sides of S , but is not necessarily smooth through S , then $WF(f)$ may contain only the pairs (x, ξ) such that $x \in S$ and ξ is normal to S at the point x .

One can also introduce the notion of being microlocally in the Sobolev space H^s , as follows.

Definition 7.8. Let $x_0 \in \mathbb{R}^n$ and $\xi_0 \neq 0$, $\xi_0 \in \mathbb{R}^n$. The function f is said to be **microlocally in the Sobolev space H^s near (x_0, ξ_0)** if there exist a function $\phi \in C_0^\infty(\mathbb{R}^n)$ such that $\phi(x_0) \neq 0$ and $\epsilon > 0$ such that $(\phi f)(\xi) \in L^2(C_\epsilon, (1 + |\xi|^2)^s)$, where C_ϵ is the **conical neighborhood**

$$\left| \frac{\xi}{|\xi|} - \frac{\xi_0}{|\xi_0|} \right| < \epsilon$$

of the vector ξ_0 .

7.3 • Detection of singularities, stability, and incomplete data problems

The examples of incomplete data reconstructions shown above display blurring of some parts of the interfaces between different tissues, although in some of these cases uniqueness of reconstruction holds. What is the reason for such difficulty? Although the details are somewhat technical, the main ideas can be explained and used easily. Namely, as the discussion in Section 5.8 indicated, inversion of “smoothing” operators, i.e., operators that increase the level of smoothness of a function, is unstable. Moreover, the more smoothing is done, the less stable is the inversion. In particular, among the most unstable are inversions of operators that convert a nonsmooth function into an infinitely differentiable (or, even worse, analytic) one. In other words, the less trace of singularity remains in your data, the more unstable the inversion is. This is also true microlocally, in the sense that if an element of the wavefront set of a function does not lead to a wavefront vector appearing in the wavefront set of the transformed function, recovery of this original singularity is extremely unstable. Thus, if a piece of the wavefront set of a function (e.g., a piece of an interface) disappears after the transformation, this singularity (e.g., piece of interface) will be blurred. This leads to the following (not very precise so far) definition.

Definition 7.9. A singularity (wavefront set point (x_0, ξ_0)) of a function $f(x)$ is said to be **visible** (also called **audible**) if its presence leads to a singularity in the (Radon) transform of f , and **invisible** (**inaudible**) otherwise.

The question now arises of whether one can tell in advance which singularities are invisible. The answer is “yes.”

Let us start with the example of the Radon transform of the characteristic function of the unit disk centered at the origin. It is immediate that the Radon transform $g(t, \omega)$ of the characteristic function of such a disk is rotationally invariant (i.e., does not depend on ω); it is equal to zero when $|t| > 1$ and to $2\sqrt{1-t^2}$ when $|t| \leq 1$. Let us look at a fixed projection ω . Then the function g is analytic (in fact, equal to zero; see Fig. 7.6) till the line of integration touches the disk, and turns (with a jump of the derivative) into another analytic function, $2\sqrt{1-t^2}$, with the situation reversing itself when the line gets tangent to the disk again and leaves the disk at $t = -1$. What does this tell us? The boundary of the disk is where the singularities (jumps) of the characteristic function are located. When the line of integration touches the disk tangentially, the Radon transform has a singularity (not a discontinuity anymore, but a jump of the first derivative). However, when the line enters the disk, although it still crosses the jumps of the characteristic function, the result is actually analytic. In other words, in order to feel the jump, one has to have a line of integration touching it tangentially; otherwise, the jump singularity results in a smooth function.

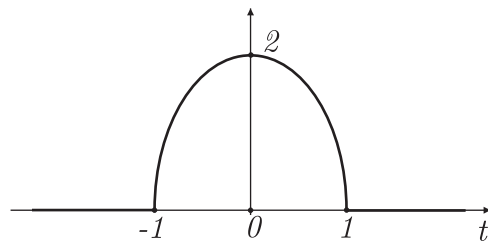


Figure 7.6. X-ray projection of the characteristic function of the unit disk at the origin.

This example indicates what happens in general. Namely, one can show [656] (see also [301, 668]) that a wavefront vector (x_0, ξ_0) in the tomogram $f(x)$ (see above and Appendix Section B.17) is visible in the Radon projection Rf only if there is an integration line available passing through x_0 and normal to ξ_0 . (In truth, to make the “if” into “iff,” the same should hold in a neighborhood of this wavefront vector; see the precise answer in [656].) This explains the blurring in the “limited data problems”: Whenever there is no ray that touches a part of an interface tangentially, then this part will blur during the reconstruction. Notice that this conclusion does not depend upon a particular method of reconstruction, and thus there is no way to beat the nature here (unless some extra information is available).

Similar “visibility” conditions are present in other tomographic techniques of integral geometry nature (SPECT, PET, TAT).

Exercise 7.10. Apply the test above to explain the blurring shown in our examples of limited angle and exterior reconstructions. (See Figures 7.4 and 7.5.)

7.4 • Local (high frequency) tomography—Sharpening singularities

In many instances, one would like to amplify (sharpen) singularities of the image, even if this renders the point values of the function useless. This is desirable, for instance, in geophysics, when one is often concentrating on finding the interfaces between different layers of rock, sand, etc. In medical imaging, one might want to see small blood vessels, which are barely (or not at all) visible on the regular tomograms. This is also what is often called in image processing **edge detection**. One could certainly try to start with the “honest” tomogram and then use image processing tools to sharpen the singularities present. In tomography, however, one might want to incorporate this kind of sharpening into the reconstruction algorithm, which presents various (e.g., computational) advantages.

The high frequency part of the image is responsible for the sharp details (see Appendix B). It is thus natural to try to strengthen the filter part of the filtered backprojection reconstruction in order to do the sharpening. In two dimensions, this can amount to replacing the filtration by Hilbert transform and the first derivative with just the second derivative. An example of such a “high frequency” reconstruction is shown in Fig. 7.7. One sees in this picture that the location of the singularities is correct (no singularities disappeared and no new ones appeared); only their strength is increased. This is an instance of a general theorem saying that the local tomogram operator is an elliptic pseudodifferential operator of a positive order and thus does not change the locations of singularities, but rather strengthens them [211, 214, 215, 449].

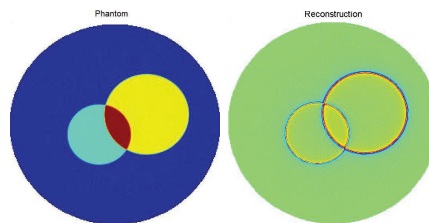


Figure 7.7. A *phantom* (left) and its local reconstruction (right). One sees the boundaries sharpened.

As far as the author knows, the first work of this kind was done in [778, 779] (where it was called **high frequency tomography**) and then fundamentally extended in [211, 214], where the name **local tomography** was coined (see also [208, 211, 214, 215, 449, 656, 657] for further details, discussion, and references).

If one wonders what the word “local” is doing here, we need to recall that the Radon transform inversion in two dimensions is a nonlocal transformation (Section 5.12), due to the presence of the Hilbert transform. Filtering with the second derivative, one obtains a local method. In other words, in order to construct a local tomogram near a point of interest, it is sufficient to use the Radon data for only the rays passing near this point (recall the ROI imaging).

Local tomography unavoidably makes the smooth details (i.e., point values) of the resulting tomogram incorrect. One sees this clearly in local tomographic reconstructions (see the works cited above and Fig. 7.7). In [211, 214], some corrections are implemented that make local reconstructions look more plausible to a doctor, although the truth of the matter is that the values are still wrong.

7.5 • Chapter's final remarks and conclusions

Probably the most important lesson to take away from this chapter is the “visibility” test in Section 7.3. Analogous tests also hold for several other types of tomography: SPECT, PET, MRI, TAT. Although justifying this rule is rather technical, it is very easy to apply.

Let us now collect here the important features of the most common limited data problems.

- Limited angle problem

Uniqueness

Proposition 7.11. *If X-ray data is available for an open set of angles $\omega \in S^1$, then any compactly supported function $f(x)$ is uniquely reconstructed.*

Indeed, according to the projection-slice theorem, the Fourier transform \tilde{f} of f is known for an open set (indeed, a cone) of vectors $\sigma\omega \in \mathbb{R}^2$. Since, due to the Paley–Wiener theorem, \tilde{f} is an entire function in \mathbb{C}^2 , it is uniquely determined by its values on any open subset of real vectors.

Stability

Here (as in all limited data problems, except maybe some of the hybrid methods, such as TAT¹⁸) one faces an unavoidable instability. Namely, as we have discussed in this chapter, some singularities will be “invisible” and thus necessarily blurred. For instance, any part of a tissue interface, whose normal vector ω is not among the available projections, will be blurred. To put it differently, as we have already discussed, to see the interface one needs to be able to touch it with X-rays tangentially.

This conclusion also means that in such a situation there is no hope for recovering stably not only the invisible parts of the interfaces, but also correct numerical values of the smooth features. (See also our discussion of the local tomography in Section 7.4.)

One should also note that the arising instability is of a very nasty kind, so neither Lipschitz nor Hölder stability is expected.

One of the approaches that have been tried is to use the range conditions to “complete” (i.e., extend to the full view) the limited angle

¹⁸Where “rays” can bend.

data. Alas, this should not work, since it does not remove the main provable instability obstruction, and it does not work. However, incorporating some a priori information (see, e.g., [25]) might stabilize the problem (sparse sensing is another example).

Inversion

The instability that we have just discussed removes the hopes of having good inversion formulas. However, location and strength of all visible singularities can be recovered easily. One can prove that just zero-filling the missing data (with some smoothing at junctions in order not to create artifact singularities) and using any full data inversion method will recover all visible singularities in the right places and with the right strengths. One should, however, be aware of what the visibility range is (which can be detected easily by the observation angle available).

Using a **local inversion** (i.e., a stronger high-pass filter) in this procedure would emphasize the visible singularities.

- **Exterior problem**

Uniqueness

The “hole” theorem, Theorem 5.28, provides uniqueness of reconstruction if the avoided region K is convex and the function to be reconstructed is decaying faster than algebraically at infinity (e.g., is compactly supported).

Stability

The situation with instability is the same as for the limited data problems: Only visible singularities are reconstructed correctly and stably, while the invisible ones are blurred, and smooth details are incorrect. The attempt to provide X-ray data for an extra shell inside K around the boundary does not stabilize the problem [490].

Inversion

The same can be said about inversion as for the limited view. E.g., zero-filling the missing data and using the full data inversion reconstructs the visible singularities. There are other approaches, e.g., using the singular value decomposition [654, 655].

As before, using a **local inversion** (i.e., a stronger high-pass filter) would emphasize the visible singularities.

- **Interior (region of interest (ROI)) problems**

Uniqueness

Uniqueness fails for ROI problems (see, e.g., [559]). So, do we go home? Does the work of many people working on ROI make no sense? We can recall here that we have already faced nonuniqueness

due to finiteness of the number of projections, and we discovered that if the number of projections is sufficiently high, one will lose only a very highly oscillatory (high frequency) part. Thus, CT does work. Here, due to complete visibility of singularities in the ROI (see the next paragraph), only smooth parts can be lost. All the interfaces will be preserved.

Stability

Well, any stability estimate would imply uniqueness. Thus, there is no stability, period. However, this extreme claim is not 100% correct, and as in the previous cases, some important features can be stably recovered. Indeed, one notices that in the ROI problems (when directions of X-rays are not restricted, the only requirement being that they cross the region of interest), **all singularities in the ROI are visible**. Indeed, zero-filling the missing exterior data and using any full data inversion, one recovers correctly and stably the location and strength of all singularities inside the ROI. Hence, tissue interfaces, blood vessels, etc., will be clearly visible. This settles the question of **inversion** as well.

Again, using a **local inversion** (i.e., a stronger high-pass filter) would emphasize the visible singularities.

Attenuated transform: All the considerations above, including the local reconstructions, also apply to the attenuated transform of SPECT and, modulo possible nonuniqueness as in ROI, to weighted transforms with a general positive smooth weight $w(t, \omega)$ [99, 449].

Reconstruction of visible singularities: Let us emphasize again that **all visible singularities can be reconstructed stably, with either the correct or emphasized strength. It is futile to try to reconstruct the invisible ones** (unless appropriate extra information is available (e.g., as in [25])).

Chapter 8

More about 3D Radon and X-ray Transforms

In this small chapter, we touch upon the 3D world of imaging. One can go to higher dimensions, but so far this seems to be further removed from medical applications. Moreover, after learning about the 2D and 3D situations, moving higher in dimension seems to create more technical, rather than ideological, hurdles. There are several significant differences between two and three dimensions, though, which warrant addressing the latter separately.

The important F. John's parametrization of the X-ray transform and the corresponding John's equation are also outlined. The author had Napoleonic plans of diving into more discussion of this matter, as well as of the closely related but going much further techniques developed in Gelfand's school. The latter opens marvelous vistas of integral geometry, mostly not known to (at least, not used by) researchers in tomography. Alas, it became clear quite quickly that this would require a separate book. And indeed, such books and surveys, written by experts, do exist; see [252, 253] and references therein. The reader is highly encouraged to read those. The effort it takes will pay off.

Essentially the same consideration applies to the currently booming field of fully 3D imaging [243], where the author only gives some references.

8.1 • 3D Radon transform

As we have already mentioned, in dimensions higher than two, the name Radon transform is reserved for the operator integrating functions over hyperplanes (thus, lines in two dimensions). Any hyperplane can be represented in the familiar way in polar coordinates by the equation $x \cdot \omega = t$ with a unit vector ω normal to the plane and a real number t as the (signed) distance from the origin to the plane. Thus, the formula for the Radon transform in three dimensions looks very much like that in two dimensions:

$$f(x) \mapsto g(t, \omega) := Rf(t, \omega) := \int_{x \cdot \omega = t} f(x) ds, \quad (t, \omega) \in \mathbb{R} \times S^2, \quad (8.1)$$

where ds now denotes the surface area measure.

The analogy with the 2D case raises hopes that the analysis can be very much similar as well. As it turns out, this is true (see, for instance, [252, 253, 261, 349, 354, 559, 577]). The similarity includes, in particular, the visibility of singularities, etc. We thus just provide a few sentences and formulas to indicate some differences.

The inversion formula looks as follows:

$$f = -\frac{1}{8\pi^2} R^\# \frac{d^2}{dt^2} (Rf). \quad (8.2)$$

One notices the filtered backprojection nature of the formula. An important difference from the 2D case is that the filtration is done with the second derivative instead of the composition of Hilbert transform and first derivative. This is a reflection of several related things:

- As we mentioned when studying the 2D case, the transforms of Radon type add to the smoothness level of a function “one half of a derivative” per each dimension of integration. Thus, when we integrate over planes, we add a single derivative. Backprojection adds another derivative, so the backprojected function would be two derivatives smoother than the original one (blurring). The second derivative removes this extra smoothness and de-blurs the image.
- This also shows that the stability estimate (5.28) that we had in two dimensions is replaced by

$$\frac{1}{C_{B,s}} \|Rf\|_{H^{s+1}} \leq \|f\|_{H^s} \leq C_{B,s} \|Rf\|_{H^{s+1}}. \quad (8.3)$$

- There is also an analogue of the ρ -filtered backprojection formula:

$$f = -\frac{1}{8\pi^2} \Delta R^\# (Rf), \quad (8.4)$$

where Δ is the 3D Laplace operator.

- A close look at the formulas (8.2) and especially (8.4) shows that

**Inversion of the 3D Radon transform is *local*
and thus can be done for ROI problems!**

Indeed, the backprojection is local (as in two dimensions), and both the second derivative with respect to t in (8.2) and the Laplace operator in (8.4) are local transformations.

This is a very significant departure from the 2D case, where all line integrals need to be used even if we are interested in only a small neighborhood of a point.

Exercise 8.1. Figure out why our ideological “proof” of 2D nonlocality, using Peetre’s theorem [639], does not work in three dimensions.

In general, there is a distinction between even and odd dimensions [252, 253, 261, 349, 354, 559, 577]:

**Inversion of the Radon transform in \mathbb{R}^n is local when n is odd
and cannot be done locally when n is even!**

8.2 ■ X-ray transform: Overdetermined parametrization and John’s equation

One way of parameterizing the X-ray transform in three dimensions (due to F. John [391, 392]) is the following. Let a and b be two 2D vectors. Representing \mathbb{R}^3 as $\mathbb{R}^2 \times \mathbb{R}$ and thus denoting $x \in \mathbb{R}^3$ as $x = (x', x_3)$, and correspondingly $f(x) = f(x', x_3)$, the John’s transform can be written as follows:

$$f(x) \rightarrow F(a, b) := \int_{-\infty}^{\infty} f(at + b, t) dt = \int_{-\infty}^{\infty} f(a_1 t + b_1, a_2 t + b_2, t) dt, \quad (8.5)$$

under appropriate decay conditions on the function $f(x)$ for the integral to converge.

Since a function of three variables is mapped to a function of four variables, one should expect an additional condition that the resulting function $F(a, b)$ must satisfy. And indeed, one can check that it satisfies the following **ultrahyperbolic John’s equation**:

$$\frac{\partial^2 F}{\partial_{a_1} \partial_{b_2}} = \frac{\partial^2 F}{\partial_{a_2} \partial_{b_1}}. \quad (8.6)$$

(After an appropriate rotation, in new coordinates $(u, v) \in \mathbb{R}^4$ the equation will look like $\Delta_u F = \Delta_v F$.)

Exercise 8.2.

1. Does (8.5) contain the whole X-ray transform of f ?
2. What does (8.6) tell us about the Fourier transform of the function F ?

Conversely, it can be shown [391, 392] that solutions of (8.6) can be represented as (8.5).

The Cauchy problem for (8.6) is ill-posed. However, there are some characteristic boundary value problems (**Goursat problem**) that can be solved. This, in particular, gives inversion of the John’s transform.

There is a natural generalization of (8.5)–(8.6) for the case of the k -plane transform in \mathbb{R}^n . In this case, one should assume in (8.5) that $t \in \mathbb{R}^k$, $b \in \mathbb{R}^{n-k}$, and a is an $(n-k) \times k$ matrix.

One can find details of the very interesting features of John's equation in, for instance, [198, 199, 252, 253, 270].

8.3 • Projectivization, χ -operator, and such

Here we will do the injustice of compressing into a superbrief section the important large area of integral geometry cultivated by I. M. Gelfand's school. The reader is urged to read the brief introductory/survey notes [269, 270, 680] and book [253], as well as more technical surveys and papers [95, 252, 254, 255, 257–261, 272, 285, 286, 288, 289, 678].

A few important things that need to be mentioned, at least in passing and with references, are the following:

- The Radon transform (unlike its sibling the Fourier transform) is amenable to a nice and extremely useful projective geometry interpretation [252, 259, 270].
- The John's equation happens to be equivalent to the condition of closedness of a very special differential form, produced by the so-called χ -operator [253, 269, 270, 304, 680].
- Integration of this form over appropriate cycles leads to inversion formulas (*ibid*).
- Due to closedness of the form, homologic cycles produce the same formula, which in the cycle coordinates might seem to be quite different. In particular, the Radon inversion formula turns out to be not just analogous, but in fact, equivalent, to the earlier inversion formula for the Minkowski–Funk transform [253, 270]. This is something not noticed by many researchers, including Radon, before (or even now). See other examples of such equivalence in [272] and [253, Chapter 5].
- The reach of this technique is much longer than problems with group invariance, e.g., to weighted integrations along arbitrary curves and surfaces [95, 254, 285, 286]. In particular, it should play a role in fully 3D imaging.

One should also consult with the book [620], especially its Chapters 3 and 4, for related considerations.

8.4 • Fully 3D X-ray CT

In the **fully 3D computed tomography (CT)** one usually strives to develop inversion formulas and algorithms for inverting the cone-beam X-ray transform with centers on a curve (e.g., a spiral). The questions of finding good formulas, uniqueness and stability of reconstruction, microlocal analysis, artifacts, etc., have been addressed in a large number of works. One can consult the Web site [243] for materials of the regular large conferences on the topic. In particular, the well-known

Grangeat (or Grangeat–Finch) and lately Katsevich formulas play a prominent role. See [577, Section 5.5], [142, Chapter 8], [361, Chapter 13], as well as a wealth of books and articles, such as [187, 188, 218, 219, 224, 294, 295, 403–408, 499, 613, 614, 658, 768, 792, 819].

Chapter 9

A Brief Overview of Numerical Methods

In this chapter, the author does not even attempt to provide any technical details. There is a vast and sophisticated literature on the subject, which cannot be presented in a short introductory text. Instead, the reader is given a brief laundry list of approaches to numerical inversion with pointers to some literature. The reader interested in numerical issues will be better served by reading the original papers and surveys written by experts; see [85, 86, 142, 153, 702, 799], [203, Chapters 11–13], [361, Chapters 8–13], [396, Chapters 3, 7], [168, Chapter 14], [557]¹⁹ [559, Chapter V], and [577, Chapter 5] for details and references.

There are quite a few different reconstruction techniques applied in X-ray CT and other CT modalities. We will list here some of the most common ones, dealing mostly with the 2D case.

9.1 • Analytic techniques

Here we list some common methods based upon the formulas the reader has met in this text:

- **Filtered backprojection** (FBP) techniques, based on formulas (5.23), (5.24), and (8.2) are extremely common.
- **Fourier inversion method**, using (5.12), was neglected for some time, but eventually was successfully implemented [629] (see also [559, Chapter V]).
- **Fourier series expansion** methods (e.g., **Cormack’s method**; see Section 5.9) have been used since Cormack’s original work. The first method proposed by Cormack was not very stable. However, further modifications overcame this problem.

Although we have discussed these formulas analytically, their numerical implementation involves nontrivial issues of appropriate discretization, sampling, speed

¹⁹This is a nice concise description of the details of several popular algorithms.

of calculations, etc. The reader is advised to turn, for instance, to [142, 203, 206, 207, 209, 210, 213, 361, 396, 557, 559, 577] for further details and references.

9.2 ■ Algebraic reconstruction techniques (ART)

One can represent the (discretized) Radon transform as a matrix, and thus the tomography problem becomes the problem of solving a very large (and ill-conditioned) system of linear equations. One thus could try any of the methods available for solving such systems, sometimes building in also some natural constraints, e.g., positivity of the function in question, which makes the problem very nonlinear. However, due to the size and ill-conditioned nature of the system, one does much better incorporating at least some analytic understanding about the transform (e.g., for preconditioning).

- Kaczmarz's²⁰ method [395] is an iterative method for solving systems of linear equations and thus has been used very extensively in CT, becoming a method of choice for many researchers; see, e.g., [559, 577].
- There have been numerous iterative numerical techniques introduced (the Kaczmarz method is just one of them) that treat Radon transform as a large linear system to be solved. Their common name is **algebraic reconstruction techniques (ART)** [142, 203, 361, 396, 559, 577].

9.3 ■ Optimization techniques

There is a large class of practically useful algorithms based on the optimization approach. Although in some sense they form a subclass of ART techniques, we devote a separate section to them.

In detail, given data g , one tries to find function f_{approx} that minimizes a functional

$$\|Rf_{approx} - g\| + F(f_{approx}),$$

where R is the forward operator, $\|\dots\|$ is an appropriate norm, and F is a functional penalizing the reconstruction for having undesirable properties (e.g., fast oscillations). This formulation contains, for example, various regularization techniques (with F being, say, the L_2 - or L_1 -norm of the gradient).

Depending on F , the problem can be linearizable (as in the quadratic optimization case) or fully nonlinear, in which case finding the minimum is computationally very expensive—so one uses computer clusters or graphic processing units (GPU's).

These techniques, despite the high computational costs and the necessity to avoid being stuck in local minima, are extremely important and widely used in various tomographic modalities.

²⁰Stefan Kaczmarz (March, 1895–September, 1939), a Polish mathematician, killed in the Katyn massacre among thousands of Polish officers.

The reader is referred to [33, 34, 48, 72, 98, 126–128, 142, 149, 152, 154, 201, 305, 338, 339, 357, 358, 361, 398, 431, 458, 554, 557, 559, 574, 577, 628, 650, 696, 702, 790, 799, 823]. Many of these books and surveys addressing the topic cover it for more general inverse problems than just tomography.

9.4 • Statistical techniques

As we have already discussed, in emission tomography and some homeland security applications, the photon statistics is very poor, which begs for statistical rather than integral-geometric techniques [715]. This has triggered quite a lot of activity in this direction; see, e.g., [40, 133, 189, 266, 470, 483, 782] and references therein. One can find discussion of the relevant maximum likelihood, expectation maximization (EM), and other methods in [577, Sections 3.2 and 5.3.2], [361, Chapter 6], [203, Chapter 16], [97, 142, 148, 383, 398, 751, 786], and [85, Chapter 17].

One can consider the statistical techniques as a particular instance of the iterative optimization methods described above. The peculiarity of the emission tomography case is that these (statistical) optimization methods are forced upon us by the very nature of the problem.

9.5 • Parametrix + ART

An interesting and often very useful combination of microlocal analysis and ART works as follows. It has been known for quite some time (e.g., see [10, 19, 99, 100, 109, 110, 191, 301, 325–328, 373, 449, 651, 656]) that transforms R of Radon type often belong to the class of the so-called **Fourier integral operators (FIO)**. This enables one, using the algebra of symbols, to easily write a “crude” inverse R^+ (called a **parametrix** for R) such that the composition R^+R can be represented as $L + r$, where L is an elliptic operator of order zero and r is a smoothing operator. Thus, applying a parametrix to the Radon-type data, one obtains a function with exactly the same singularities (wavefront set, and even Sobolev wavefront sets) as the true reconstruction, plus a smoother error term.

In some cases one can do even better, so that L is the identity operator, and thus one reconstructs the correct tomogram up to a smoother error.

Thus, the result can be either used as a tomographic image, where the structures are correct but the numerical values might not be, or used as preconditioner for an algebraic iterative method.

Finding the symbol of a parametrix usually requires only a simple algebraic computation. Moreover, this technique can be used even in the cases when exact reconstruction formulas are not known, not practical, or simply do not exist (as in ROI problems). See such examples in the literature cited above, as well as in [36, 458, 627, 647, 648].

One can say that the local tomography technique discussed before is one of the incarnations of the parametrix method, except that the resulting elliptic operator L has a positive order and thus amplifies the singularities.

As we cannot stop emphasizing, basics of microlocal analysis should be in the toolbox of any tomography researcher (as well as, clearly, any analyst).

The reader can find suggestions for reading on **microlocal analysis** (wavefronts, pseudodifferential operators, and FIOs) in Appendix E.

9.6 ▪ Some MATLAB® sources

MATLAB's imaging toolbox currently has the Radon transform and its inversion. However, a beginner would greatly benefit from writing her own codes—in MATLAB or any other programming language. And when your code works (and it will, just have patience), you'll have the great satisfaction of seeing a tomogram of your own creation!

Numerical methods with MATLAB were discussed on an introductory level by L. Kunyansky during the 2012 NSF-CBMS Conference on Mathematical Methods of Computed Tomography. This would be a good place to start. One can find the links to his codes and lecture slides at

<http://omega.uta.edu/~aktosun/cbms2012/links.html>.

C. Epstein's lectures on Mathematics of Medical Imaging also have a part devoted to MATLAB codes:

<http://www.math.upenn.edu/~cle/m584/matlab/ws2.html>.

See also some MATLAB sources on A. Faridani's page:

<http://people.oregonstate.edu/~faridana/preprints/preprints.html>.

A nice Image Reconstruction Toolbox for MATLAB, by J. Fessler, is available for free from

<http://web.eecs.umich.edu/~fessler/code/index.html>.

It can deal with X-ray CT, PET, SPECT, and MRI.

A more general MATLAB toolbox for solving inverse problems can be found on P. Hanson's page:

<http://www2.imm.dtu.dk/~pcha/AIRtools/>.

9.7 ▪ Numerical techniques for inverse problems

There are some books and surveys that address numerical problems for inverse problems in general, not necessarily of tomographic type. I can mention, for instance, [97, 148, 153–155, 164, 201, 305, 398, 415, 416, 696, 790, 799].

Chapter 10

MRI, EIT, OT, Elastography, UT

In this part, we mention in a very cursory manner several important modalities of medical imaging, which lead to challenging mathematical problems, often different from those considered previously in these lectures. These include the well-known magnetic resonance imaging (MRI), still developing electrical impedance tomography (EIT), optical tomography (OT), elastography, and the familiar but still promising new breakthroughs ultrasound tomography (UT). Consideration of any of these techniques in any detail would require a book by itself. We thus restrict ourselves to extremely brief introductions and literature references.

10.1 • MRI (magnetic resonance imaging)

In **magnetic resonance imaging** (also called **nuclear magnetic resonance (NMR) imaging**), in a crude approximation, one seeks to reconstruct the spatial distribution $f(x)$ of protons in tissues. This modality is based upon the so-called **nuclear magnetic resonance** effect. Namely, protons have spin (something like a rotational momentum vector), which, in the presence of a magnetic field H , rotates around the direction of the field with the frequency gH with a constant g (a phenomenon called Larmor precession). What is done in MRI is, in a simplified version, the following: A strong inhomogeneous magnetic field is created that looks like $H(x) = H_0 + \omega \cdot x$. Then resonances are observed on the frequency $g(H_0 + s)$ for some number s . The strength of this resonance is proportional to the integral

$$g = \int_{x \cdot \omega = t} f(x) dx,$$

which is exactly the 3D Radon (NOT X-ray!) transform of $f(x)$. Thus, the integral geometric techniques can be applied to invert it and find $f(x)$. The modality yields high quality images.

In other, more frequent, incarnations of the MRI technique, one might directly measure the Fourier transform of the tomogram, and thus the reconstruction boils down to Fourier inversion.

This simplified description does not do justice to the complexity of the MRI technique and its mathematical wealth, especially in its modern incarnations (such as, for instance, the functional MRI (fMRI)). We thus direct the interested reader to other books and surveys, e.g. [168, Chapter 4] and [203, Chapter 14] for a brief physics introduction and [96, 146, 332, 370] for extended physics background; brief mathematics description can be found in [577, Section 3.4] and more extended ones in [203, Chapter 14] and [202].

10.2 ▪ EIT (electrical impedance tomography)

In EIT, one strives to find the electrical conductivity function $\sigma(x)$ of a body Ω by attaching electrodes to its surface and by creating some currents and measuring the resulting boundary potentials (voltage drops), or, alternatively, creating voltage drops and measuring the resulting currents. Mathematically speaking, the problem can be described as follows:

$$\begin{cases} -\nabla \cdot \sigma(x) \nabla u(x) = 0 & \text{inside } \Omega, \\ u|_{\partial\Omega} = h, \\ \sigma \frac{\partial u}{\partial \nu}|_{\partial\Omega} = g. \end{cases}$$

Here $u(x)$ is the potential inside Ω . The first equation states the absence of free charges. Functions h and g are correspondingly the boundary voltage and current. Creating arbitrary h , one measures the resulting g and thus can access the whole operator $h \mapsto g$, which is called the **Dirichlet-to-Neumann map** and is often denoted Λ_σ . Here the subscript reminds us that the operator depends on the conductivity σ . We thus deal with the (highly nonlinear) mapping $\sigma \mapsto \Lambda_\sigma$. The EIT problem is to invert it.

Although EIT as an imaging method was suggested in [80–82, 356], its mathematical formulation goes back to earlier (and initially unpublished) work by A. Calderón [145] (see its reprint in [92]) and thus usually goes under the name of **Calderón’s problem**. Although Calderón himself obtained very important initial results, the breakthrough came in work by J. Sylvester and G. Uhlmann [748]. Since then, an avalanche of work devoted to this problem and its variations and applications has been produced, and the wealth of the issue has not been nearly exhausted yet. One can find the physics basics, current state of the art, applications, and open problems surveyed, e.g., in [65, 94, 113, 159, 160, 168, 385, 387, 577, 675, 676, 694, 698, 699, 769–771, 774, 775, 781, 786, 786].

The wealth of complex and beautiful mathematics produced by the EIT problem is nothing short of astonishing. One of the “unintended consequences” was discovery of **invisibility cloaks** [297, 298, 300, 773],²¹ rediscovered by physicists a few years later [183, 478–481, 640–642] and now being actively pursued technologically.

²¹See also [30, 423, 424, 530, 580, 581, 783, 784] and references therein for related mathematical studies.

EIT is a completely different creature from the imaging methods discussed above. Indeed, while all of the others deal with inverting a linear transformation of the unknown function (tomogram), EIT is significantly nonlinear. Another, probably even more important, difference is that those methods are all rather stable (do not react too badly to errors in data), while EIT is severely unstable. Specifically, the data one collects in EIT is infinitely smooth, or even analytic, while the function to be recovered is discontinuous (see the related discussion in Section 5.8). This high instability is shared by other methods (e.g., optical tomography) that strive to recover coefficients of an elliptic equation by observing some boundary data.

Thus, EIT presents a great challenge to mathematics. Even proving uniqueness of the solution was extremely hard and was resolved in several difficult celebrated papers (e.g., [50, 544, 748]), while the optimal result for the 3D case still remains elusive. One can refer to the works cited above in this section for further details.

Due to the high sensitivity and relatively low cost of EIT, there has been a lot of work done trying to bypass the low resolution/instability problem (see, e.g., [1, 49, 55, 58, 101, 114–118, 159, 165, 416, 421, 542, 731, 746, 774]). In particular, a variety of hybrid techniques (AET, MREIT, CDI, CDII) are being developed, some of which will be addressed in Sections 12.1 and 12.4.

10.2.1 • EIT and hyperbolic geometry

Although EIT is not a modality that can be treated fully in terms of integral geometry (which would have made it much easier to handle), integral geometry does enter the picture, and surprisingly, in a non-Euclidean setting! Indeed, after analysis done in [699] of the original algorithms of [80–82], it became clear that hyperbolic planar geometry might have something to do with them. Subsequently, it was shown [93, 94] that, linearizing the EIT problem near a constant conductivity, one arrives at an operator that is a composition of two explicitly presented operators. One of them is the **geodesic Radon transform** on the hyperbolic plane, and the other is the convolution, in the sense of hyperbolic harmonic analysis [353], with an explicitly provided radial function. Various inversions of the geodesic Radon transform on the hyperbolic plane are known [351, 492]. The inversion formula of [492] was numerically implemented in [238].²² This involved some complications in comparison with the Euclidean case. For instance, there are rigidity theorems that prevent one from obtaining a sufficiently fine mesh using orbits of discrete subgroups of the group of hyperbolic motions. Stability of this inversion is comparable with that of the regular 2D Radon inversion.

So, maybe the linearization did make the EIT problem stable? No luck here. We need to remember that there is one more component of the operator, a convo-

²²The reader is advised to use the Web version of [238], since, due to an editorial error, all pictures were not shown in the journal publication.

lution. A simple look at it shows that the deconvolution is hopelessly exponentially unstable. One cannot cheat Nature!²³

One can ask what triggers this relation with the hyperbolic geometry. Probably it occurs because the Laplace operator is quasi-invariant (and the Laplace equation is invariant) with respect to the Möbius transformations, a.k.a. rigid motions of the hyperbolic plane. Since this is not the case in dimensions higher than two, one might think that the trick does not work there. However, as was shown in [239], several applications of Euclidean integral-geometric transforms reduce the problem again to 2D hyperbolic integral geometry. We wish this helped! ☺

Another appearance of hyperbolic geometry in Calderón problem can be found in [388].

10.3 ■ Optical tomography (OT)

Optical tomography (OT), in its many variations being currently developed and used, is directed toward determining the optical parameters (absorption and scattering coefficients) of nontransparent biological tissues. To achieve this, a laser light is shined at the object, and the reflected and/or transmitted light is observed. From these observations one tries to reconstruct the internal optical parameters. One can use a red laser pointer to see that light does transmit through a human finger. However, one does not see any trace of a bone's being present inside. This indicates the difficulty of OT, which is similar to that faced by EIT. Namely, at a depth of several millimeters, due to multiple scattering, the photons essentially forget their recent travel history. Thus, internal location information disappears catastrophically fast. On the other hand, like the EIT, OT, if it works, provides a great diagnostic tool, since cancerous tissues display a very high optical contrast compared to the normal tissues. Thus the struggle for OT is very active. It already works well in clinics in eye scans and skin-level tomography (e.g., for melanoma detection). It is clear, though, that the nature of OT does not allow any reasonable resolution at depths measured in centimeters, unless significant changes in its physical setup are made. We will address some of these novel hybrid methods in Part III.

Mathematically, the difficulty with OT is very much similar to that with EIT. Namely, in diffusion approximation, one tries to reconstruct the diffusion and absorption coefficients $D(x)$ and $\mu(x)$ of the equation

$$-\nabla \cdot D \nabla u + \mu u = 0$$

from some boundary measurements of the solution. Why is this bad? Because elliptic equations do not propagate singularities, and thus a singular part of a coefficient, hidden inside the domain, will not lead to any singularity in the boundary data. As was discussed in Chapter 7, this is a bad omen, indicating an extremely high level of instability.

²³Although one can try, by changing the setup of the experiment, as we'll see in Part III.

The interested reader should look into the brief descriptions available, for instance, in [168, Chapters 11 and 14] and [577, Section 7.2] and then consult with the vast literature devoted to various incarnations of OT, e.g., [42–45, 48, 55, 233, 508, 509, 541, 693, 704, 705, 766, 789, 798] and references therein.

10.4 • Elastography

Mechanical, electrical, and optical properties of biological tissues, as the reader has already learned, carry important medical information, which various imaging methods try to recover. There is, however, a parameter that we have not encountered yet in this text, namely **stiffness**. It turns out that if one could “see” the stiffness of the internal tissues of a patient’s body, this would lead to some miracles of medical diagnostics. For instance, early detection of liver problems, now nearly impossible, would become quite feasible. Indeed, various liver diseases, even in early stages, lead to significant increases in stiffness. Analogously, cancerous growth is often 5–28 times stiffer than the surrounding healthy soft tissue. For the reader who is old enough to remember doctors who were still doing manual palpation, the stiffness was, among other things, what they were after. However, even the old doctors could not feel stiffness of the deep interior of the liver. **Elastography** strives to achieve what doctors tried but could not do: measure internal stiffness and strain. The idea is to actually let a machine do the (very gentle, gentler than a human would do) palpation and observe the outcomes. The mathematics here, unsurprisingly, boils down to inverse problems for the elasticity system. The interested reader is referred to [389, 518, 519, 521, 525, 527] and references therein.

Very promising novel hybrid versions of elastography, **MRE** and **sonoelastography**, will be mentioned in Section 12.4.

10.5 • Ultrasound imaging and tomography (UT)

Ultrasound imaging. This is the modality that everyone knows about, especially couples expecting children. The goal is to recover the internal distribution of the acoustic speed. It is done with hand-held devices, and one can easily guess that one is talking about reflection tomography, rather than transmission tomography as in most techniques previously considered in this text.

UT shares many features, problems, and approaches with reflection geophysics imaging. In particular, interfaces are mostly detected well, while smooth variations of the sound speed do not get reconstructed much. However, **transmission UT and combined transmission-reflection tomography** systems are being actively developed now and already produce impressive tomograms.

Unlike the integral geometric-type tomographic problems, UT poses a highly nonlinear problem. Although the so-called Born and Rytov approximations [46, 396, 413, 509, 541, 577] can sometimes be used to simplify the problem, in many cases one has to deal with full nonlinearity.

Discussion and analysis of various UT issues can be found, for instance, in [163, 165, 168, 178, 409, 427, 555, 555, 562, 565, 566, 568, 576–578].

Even the common clinical ultrasound scan images do display sharper images at depth than EIT and OT can possibly achieve (unless their technical setup is somehow changed or some additional stabilizing *a priori* information about the object of study is available). The reason for this is that in UT one deals with the recovery of a coefficient in the hyperbolic equation, namely a wave equation, but in OT and EIT, the equations are elliptic and do not propagate singularities. In UT the singularities usually do propagate to the boundary, where the measurements are done.

Chapter 11

Thermo-, Photo-, and Optoacoustic Tomography (TAT/PAT/OAT)

We start by providing a very brief overview of the TAT/PAT procedure. Surveys of the relevant physics and biology can be found, for instance, in [693, 793, 794, 798, 807].

In TAT (PAT), a short, wide pulse of radio-frequency electromagnetic (EM) wave (correspondingly, laser beam) irradiates a biological object (in the most common application, a human breast), causing a small level of heating in the interior. The resulting thermoelastic expansion generates a pressure wave that propagates through the object. The absorbed EM energy (and thus the initial pressure) is much higher in the cancerous cells than in healthy tissues (see the discussion of this effect in the above referenced works). Thus, the initial pressure $f(x)$ (**TAT image (tomogram)**) carries highly useful diagnostic information. So, how can one reconstruct this function?

The data for such a reconstruction is obtained by measuring time dependent pressure $p(x, t)$ using acoustic transducers. The transducers are placed along a surface S completely or partially surrounding the body (see Fig. 11.1). We will call S the **observation or acquisition surface**.

Thus, although the initial irradiation is electromagnetic, it triggers an acoustic signal, which is then used for reconstruction. As a result, high contrast is pro-

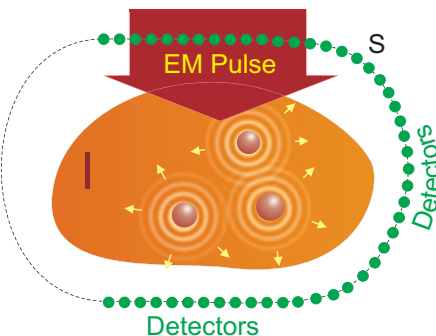


Figure 11.1. TAT/PAT procedure with a partially surrounding acquisition surface S .

duced by the EM irradiation (ultrasound alone would not produce good contrast in this case). On the other hand, good (submillimeter) resolution is achieved by using ultrasound measurements (the radio frequency EM waves are too long for high-resolution imaging). Thus, TAT, by using two types of waves, combines their advantages while eliminating their individual deficiencies.

The physical principle of energy transfer from electromagnetic to acoustic waves, upon which TAT/PAT is based, was discovered by Alexander Graham Bell in the 1880s [89, 90]. Its application to imaging of biological tissues was suggested a century later [121] and began to be developed as a medical imaging technique in the middle of 1990s [435–437, 606].

Some of the mathematical techniques that would become relevant for this imaging modality were originally developed starting in the 1990s for rather unrelated purposes of approximation theory, integral geometry, and sonar and radar (see [7, 10, 227, 445, 487] for references and reviews of the resulting developments). Physical, biological, and mathematical aspects of TAT/PAT are reviewed, for instance, in [7, 227, 228, 445, 620, 766, 789, 793, 798].

11.1 • Mathematical model

We describe here the mathematical model of the TAT procedure²⁴ and the mathematical problems that need to be addressed (which parallel our general tomography discussion in Section 3.2).

Let $c(x)$ denote the sound speed at a location x . The following mathematical model is commonly accepted as describing the propagating pressure wave $p(x, t)$ generated during the TAT procedure (see, e.g., [192, 750, 793, 794, 798, 805]):

$$\begin{cases} p_{tt} = c^2(x) \Delta_x p, & t \geq 0, x \in \mathbb{R}^3, \\ p(x, 0) = f(x), & p_t(x, 0) = 0. \end{cases} \quad (11.1)$$

Here $f(x)$ is the initial value of the acoustic pressure, whose density plot is the sought-after **TAT image (tomogram)**.

Although the basic wave equation model (11.1) stays the same, the kind of data collected by the scanner depends on the type of ultrasonic transducers used. We start by considering the historically first **point detectors**.

11.1.1 • Point detectors and the wave equation model

We assume here that the pressure $p(y, t)$ is measured by point-like, omnidirectional, broadband ultrasound transducers, located along an **observation (acquisition) surface** S . Here $y \in S$ denotes a detector location, and $t \geq 0$ is the time of the observation.

²⁴PAT strives to find biological features that are different from those in TAT [793, 798, 807]. However, this results in the same mathematical model, so we will refer here to TAT only. After PAT is completed, however, another step, so-called QPAT (quantitative photoacoustic tomography) is required, which will be discussed in Chapter 13.

Thus the (ideal) measured data provides the values of the pressure along the observation surface S . For a closed S , we denote by Ω the domain that it bounds (see Fig. 11.2 for the space-time geometry of (11.1)).

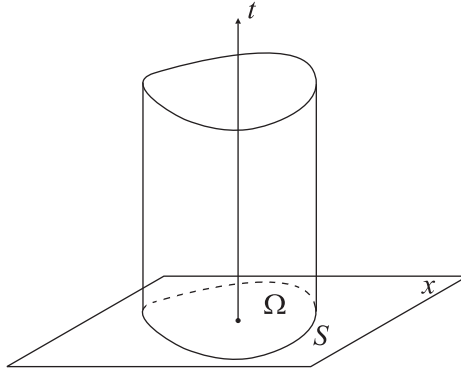


Figure 11.2. The observation surface S and the domain Ω containing the object to be imaged.

It is natural to assume that the (compact) support of $f(x)$ lies inside Ω . It is conceivable, though, that there are also some extraneous ultrasound sources in the lab, which would stretch the support of f outside Ω . We will see that some reconstruction algorithms are strongly influenced by such extraneous sources (and produce artifacts *inside* Ω), while some others do not react to this. Thus, the assumption that $\text{supp } f \subset \Omega$ sometimes becomes crucial for the validity of the reconstruction.

The data obtained by the point detectors located on a surface S is represented by the function

$$g(y, t) := p(y, t) \quad \text{for } y \in S, t \geq 0. \quad (11.2)$$

Incorporating it into the system (11.1), one gets

$$\begin{cases} p_{tt} = c^2(x) \Delta_x p, & t \geq 0, x \in \mathbb{R}^3, \\ p(x, 0) = f(x), & p_t(x, 0) = 0, \\ p|_S = g(y, t), & (y, t) \in S \times \mathbb{R}^+. \end{cases} \quad (11.3)$$

Thus, the goal in thermo-/photoacoustic tomography (TAT/PAT) is the following:

Find, using the data $g(y, t)$ on S , the initial value
 $f(x)$ at $t = 0$ of the solution $p(x, t)$ of (11.3).

We will denote by \mathcal{W} the forward operator

$$\mathcal{W} : f(x) \mapsto g(y, t), \quad (11.4)$$

where f and g are described in (11.3). Then the problem is, as in the tomographic modalities considered before, to **find a left inverse of this operator**.

Remark 11.1.

- The problem might seem ridiculous at first. Indeed, seemingly we are trying to find the initial data for a hyperbolic problem in a cylinder, using the boundary data. This is clearly impossible, since according to standard PDE theorems (e.g., [205]) these two types of data are almost completely independent (besides some matching condition at the boundary at the moment $t = 0$). This is, however, an incorrect impression, since we are dealing not with an initial-boundary value problem in a domain, but rather with an observation problem in the whole space. In other words, the surface S is not a physical boundary that prevents waves from propagation, but rather an observation surface that lets all waves through without affecting their propagation. We'll discuss this issue in more detail later.
- If a different type of detectors (e.g., planar, linear, circular) is used instead of point detectors, system (11.1) will still hold, while the measured data will be represented differently from (11.2). Namely, instead of point values of the pressure, some integral quantities will be obtained (see Section 11.1.4). This will correspondingly influence the reconstruction procedures.
- We can consider the same problem in the space \mathbb{R}^n of any dimension, not just in three dimensions. This is not merely a mathematical abstraction. Indeed, in the case of the so-called integrating line detectors (Section 11.1.4), one has to deal with the 2D version of the problem.

11.1.2 • Acoustically homogeneous media and spherical means

The problem is simpler (surprise, surprise!) if the medium being imaged is acoustically homogeneous; i.e., the sound speed $c(x)$ is now assumed to be equal to a constant, which can be taken to be equal to 1. In some situations, e.g., in breast imaging, this assumption is somewhat acceptable.²⁵ Then one deals with the constant coefficient wave equation problem

$$\begin{cases} p_{tt} = \Delta_x p, & t \geq 0, x \in \mathbb{R}^3, \\ p(x, 0) = f(x), & p_t(x, 0) = 0, \\ p|_S = g(y, t), & (y, t) \in S \times \mathbb{R}^+. \end{cases} \quad (11.5)$$

The well-known **Poisson–Kirchhoff formulas** (see [176, Chapter VI, Section 13.2, Formula (15)] or [205]) for the solution of the 3D wave equation give

$$p(x, t) = a \frac{\partial}{\partial t} (t(Mf)(x, t)), \quad (11.6)$$

where

$$(Mf)(x, r) := \frac{1}{4\pi} \int_{|y|=1} f(x + ry) dA(y) \quad (11.7)$$

²⁵It definitely is not acceptable when imaging a brain through the skull.

is the **spherical mean operator** applied to the function $f(x)$, dA is the standard area element on the unit sphere in \mathbb{R}^3 , and α is a constant.²⁶ One can deduce from this [10] that knowledge of the function $g(x, t)$ for $x \in S$ and all $t \geq 0$ is equivalent to knowing the spherical mean $Mf(x, t)$ of the function f for any center $x \in S$ and any radius $t \geq 0$. One thus arrives at the **spherical mean operator** $f \rightarrow Mf$, or, more precisely, its restriction to the points $x \in S$ only, which we will denote by \mathcal{M} :

$$\mathcal{M}f(x, t) := \frac{1}{4\pi} \int_{|y|=1} f(x + ty) dA(y), \quad x \in S, t \geq 0. \quad (11.8)$$

(A more telling, but more cumbersome, notation would be \mathcal{M}_S , which would indicate the set of centers S .)

Hence, in acoustically homogeneous media one can choose to work with the spherical mean operator rather than the wave equation (and many earlier works on TAT did just that).

The spherical mean operator \mathcal{M} resembles the Radon transform, except that the latter integrates functions over planes, while the former one, does so over spheres.²⁷ This analogy provides important intuition and frequently points toward correct directions of study. However, when the medium is acoustically inhomogeneous, and thus $c(x)$ is not constant, the relation between TAT and integral geometric transforms, such as the Radon transform or spherical mean, to a large extent breaks down, and thus one has to work with the wave equation directly.²⁸

In what follows, we will address both models of TAT (the PDE model and the integral geometry model) and thus will deal with both forward operators \mathcal{W} and \mathcal{M} .

11.1.3 • Mathematical problems of TAT

As it is discussed in section 3.2 for tomography in general, there is a standard laundry list of natural questions to ask about the TAT problem:

Sufficiency of the data: Is the data collected on the observation surface S sufficient for the unique reconstruction of the initial pressure $f(x)$ in (11.3)? In other words, is the kernel of the forward operator \mathcal{W} , or \mathcal{M} in the acoustically homogeneous case, zero? Or, to put it differently, for which sets $S \in \mathbb{R}^3$ does the data collected by transducers placed along S determine f

²⁶Versions in all dimensions are known; see (11.14) and (11.13). A significant difference exists between even and odd dimensions, which is related to the validity of Huygens' principle in odd dimensions starting with three [54, 176, 330]

²⁷In particular, when the centers of the spheres are sufficiently far from the object, the spheres can be approximated by planes, and thus standard 3D Radon inversion formulas can be applied. This in fact was done in the first TAT scanners.

²⁸Integral geometry does still apply, but only if one is interested in the propagation of singularities, where just the geometric rays (Section C.1) matter. It does not describe the full wave propagation, though.

uniquely? Yet another interpretation of this question is through observability of solutions of the wave equation on the set S : Does observation on S of a solution of the problem (11.1) determine the solution uniquely?

The choice of precise conditions on the function class, such as continuity, is often of no importance for the answer to the uniqueness question,²⁹ while behavior at infinity (e.g., compactness of support) is. So, without loss of generality, when discussing uniqueness, one can assume $f(x)$ in (11.5) to be infinitely differentiable.

Inversion formulas and algorithms. Here again one often works with smooth functions, in the end extending the formulas by continuity to a wider class.

Stability of reconstruction: If we can invert the transform and reconstruct f from the data g , how stable is the inversion?

Incomplete data artifacts: What happens if the data is “incomplete,” for instance if one can only partially surround the object by the observation surface?

Range descriptions: What is the range of the forward operator $\mathcal{W}: f \mapsto g$ that maps the unknown function f to the measured data g ? In other words, what is the space of all possible “ideal” data $g(t, y)$ collected on the surface S ? In the constant sound speed case, this is equivalent to the question of describing the range of the spherical mean operator \mathcal{M} in appropriate function spaces. As we already know, such ranges often have infinite codimensions, and the importance of knowing the range of Radon-type transforms for analyzing problems of tomography is also well known (Section 3.2). In TAT in particular, range descriptions are also closely related to the sound speed determination problem listed next (see Section 11.4.2 for a discussion of this connection).

Sound speed reconstruction. As the reader might expect, reconstruction procedures require knowing the sound speed $c(x)$. Thus, the problem arises of recovering $c(x)$ either from an additional scan or (preferably) from the same TAT data.

As we have seen, an analogous situation arises in SPECT, when one attempts to recover simultaneously the attenuation coefficient and the radiation source (see Section 6.2.3).

11.1.4 ■ Variations on the theme: Planar, linear, and circular integrating detectors

So far, we have assumed above the availability of point-like broadband transducers to measure the acoustic pressure $p(y, t)$ on a surface surrounding the object

²⁹It can sometimes be avoided using radial mollifiers; see Section A.3.

of interest. This leads to the mathematical model described by the system (11.3). In practice, the transducers cannot be made small enough, and the finite size of the transducers limits the resolution of the reconstructed images. In other words, the **detectors are integrated** in reality; i.e., they provide the integral of the pressure along the whole body of the detector. Researchers have been trying to design alternative acquisition schemes using receivers that are more realistic but still provide data sufficient for inversion. Such are 2D planar detectors [337, 625] and 1D linear and circular [138, 306, 340, 539, 818] integrating detectors.

We assume now that the sound speed $c(x)$ is constant and equal to 1.

Integrating planar detectors are made from a thin piezoelectric polymer film glued onto a flat substrate (e.g., [625]). Suppose that the object of interest is contained within the sphere of radius R . If the diameter of the planar detector is sufficiently large (see [625] for details), it can be assumed to be infinite. Let the detector plane be $\Pi(s, \omega)$, defined by the normal equation $x \cdot \omega = s$, where ω is the unit normal to the plane and s is the (signed) distance from the origin to the plane. While the propagation of acoustic waves is still modeled by (11.1), the measured data $g_{planar}(s, t, \omega)$ (up to a constant factor which we will, for simplicity, assume to be equal to 1) can be represented by the following integral:

$$g_{planar}(s, \omega, t) = \int_{\Pi(s, \omega)} p(x, t) dA(x).$$

Here $dA(x)$ is the surface measure on the plane. Obviously,

$$g_{planar}(s, \omega, 0) = \int_{\Pi(s, \omega)} p(x, 0) dA(x) = \int_{\Pi(s, \omega)} f(x) dA(x) \equiv F(s, \omega);$$

i.e., the value of g at $t = 0$ coincides with the integral $F(s, \omega)$ of the initial pressure $f(x)$ over the plane $\Pi(s, \omega)$ orthogonal to ω .

One can show [139, 337] that, for a fixed ω , function $g_{planar}(s, \omega, t)$ is the solution to the 1D wave equation

$$\frac{\partial^2 g}{\partial s^2} = \frac{\partial^2 g}{\partial t^2},$$

and thus

$$\begin{aligned} g_{planar}(s, \omega, t) &= \frac{1}{2} [g_{planar}(s, \omega, s-t) + g_{planar}(s, \omega, s+t)] \\ &= \frac{1}{2} [F(s+t, \omega) + F(s-t, \omega)]. \end{aligned}$$

Since the detector can be placed only outside the object, i.e., $s \geq R$, the term $F(s+t, \omega)$ vanishes, and one obtains

$$g_{planar}(s, \omega, t) = F(s-t, \omega).$$

In other words, by measuring $g_{planar}(s, \omega, t)$, one can obtain values of the planar integrals of $f(x)$. If, as proposed in [139, 337], one conducts measurements for all planes tangent to the upper half-sphere of radius R (i.e., $s = R$, $\omega \in S_+^2$), then the resulting data yields all values of the 3D Radon transform of $f(x)$. Now the reconstruction can be carried out using one of the many known inversion algorithms for the Radon transform (see [559] and Chapter 8).

Linear detectors are based on optical detection of an acoustic signal. Some of the proposed optical detection schemes utilize a thin straight optical fiber in combination with a Fabry–Perot interferometer [138, 306] as the sensitive element. Changes of acoustic pressure on the fiber change (proportionally) its length; this elongation, in turn, is detected by interferometer. A similar idea is used in [626]; in this work the role of a sensitive element is played by a laser beam passing through the water in which the object of interest is submerged, and thus the measurement does not perturb the acoustic wave. In both cases, the length of the sensitive element exceeds the size of the object, while the diameter of the fiber (or of the laser beam) can be made extremely small (see [625] for a detailed discussion), which removes restrictions on the resolution that one can achieve in the images.

Let us assume that the fiber (or laser beam) is aligned along the line

$$l(s_1, s_2, \omega_1, \omega_2) = \{x | x = s_1\omega_1 + s_2\omega_2 + s\omega\},$$

where vectors ω_1, ω_2 , and ω form an ortho-normal basis in \mathbb{R}^3 . Then the measured quantities $g_{linear}(s_1, s_2, \omega_1, \omega_2, t)$ are equal (up to a constant factor which, we will assume, equal 1) to the following line integral:

$$g_{linear}(s_1, s_2, \omega_1, \omega_2, t) = \int_{\mathbb{R}^1} p(s_1\omega_1 + s_2\omega_2 + s\omega, t) ds.$$

As in the case of planar detection, one can show [138, 306, 626] that for fixed vectors ω_1, ω_2 the measurements $g_{linear}(s_1, s_2, \omega_1, \omega_2, t)$ satisfy the 2D wave equation

$$\frac{\partial^2 g}{\partial s_1^2} + \frac{\partial^2 g}{\partial s_2^2} = \frac{\partial^2 g}{\partial t^2}.$$

The initial values $g_{linear}(s_1, s_2, \omega_1, \omega_2, 0)$ coincide with the line integrals of $f(x)$ along lines $l(s_1, s_2, \omega_1, \omega_2)$. Suppose one makes measurements for all values of $s_1(\tau), s_2(\tau)$ corresponding to a curve $\gamma = \{x | x = s_1(\tau)\omega_1 + s_2(\tau)\omega_2, \tau_0 \leq \tau \leq \tau_1\}$ lying in the plane spanned by ω_1, ω_2 . Then one can try to reconstruct the initial value of g from the values of g on γ . This problem is a 2D version of (11.3), and thus the known algorithms (see Section 11.4) are applicable.

In order to complete the reconstruction from data obtained using line detectors, the measurements should be repeated with different directions of ω . For each value of ω the 2D problem is solved; the solutions of these problems yield values of line integrals of $f(x)$. If this is done for all values of ω lying on a half circle, the set of the recovered line integrals provides the X-ray transform of $f(x)$. Now inversion of the X-ray transform finishes the job.

The use of circular integrating detectors was considered in [818]. Such a detector can be made out of optical fiber combined with an interferometer. In [818], a closed-form solution of the corresponding inverse problem was found. See also [539].

11.2 • Analysis of TAT: Acoustically homogeneous medium case

We address here the issues listed in Section 11.1.3 except for the reconstruction algorithms, which will be discussed in Section 11.4. We are assuming for now that the medium is acoustically homogeneous (the inhomogeneous case is addressed in Section 11.3). In other words, the sound speed $c(x)$ is equal to a constant, which will be assumed to be equal to 1.

11.2.1 • Uniqueness of reconstruction

We discuss here the most basic question: Given an acquisition surface S along which we distribute detectors, is the data $g(y, t)$ for $y \in S, t \geq 0$ (see (11.3)), sufficient for a unique reconstruction of the tomogram f ? We thus introduce the following definition.

Definition 11.2. A set S is said to be a **uniqueness set** if, when used as the acquisition surface, it provides sufficient data for unique reconstruction of the compactly supported tomogram f (i.e., the observed data g in (11.3) determines the function f uniquely). Otherwise, it is called a **nonuniqueness set**.

In other words, S is a uniqueness set if the forward operator \mathcal{W} (or, equivalently, \mathcal{M}) has zero kernel.

Thus, the task is to understand which observation sets S are uniqueness sets. Counting variables, one concludes that S should be a hypersurface in the ambient space (i.e., a surface in \mathbb{R}^3 or a curve in \mathbb{R}^2). As we will see below, there are some simple counterexamples and challenging open problems. Nevertheless, for all practical purposes, the uniqueness problem is positively resolved, and most surfaces S do provide uniqueness.

Assuming that $c(x) = 1$, let us recall the system (11.5), allowing an arbitrary dimension n of the space:

$$\begin{cases} p_{tt} = \Delta_x p, & t \geq 0, x \in \mathbb{R}^n, \\ p(x, 0) = f(x), & p_t(x, 0) = 0, \\ p|_S = g(y, t), & (y, t) \in S \times \mathbb{R}^+. \end{cases} \quad (11.9)$$

It is not hard to show (e.g., [10]) that uniqueness does not depend on the smoothness of f ; for simplicity the reader can assume that f is infinitely differentiable.³⁰

³⁰Indeed, if there is an example of nonuniqueness with a nonsmooth function f , one can convert it with a radial mollifier (see Appendix Section A.3) to get a smooth example.

On the other hand, compactness of support (or at least a sufficiently fast decay) is important in what follows.

Here is a very general (and at first glance, unexpected) statement about the nonuniqueness acquisition (observation) sets S [488] (see also [10] for the proof and further references).

Theorem 11.3. *If S is a nonuniqueness set, then there exists a nonzero harmonic polynomial Q , which vanishes on S .*

This theorem implies, in particular, that all “bad” (nonuniqueness) observation sets are algebraic, i.e., have a polynomial vanishing on them. Turning this statement around, we conclude that any set S that is a uniqueness set for harmonic polynomials is sufficient for unique TAT reconstruction. However, as we will see in Section 11.2.3, this does not mean practicality of the reconstruction.

The statement of Theorem 11.3 does not look obvious, but its proof, which the reader can find in [10, 445], is not hard and is indeed enlightening.

A standard result on Dirichlet boundary value problems (e.g., [176, 205]) says that any harmonic polynomial (and indeed, function) vanishing on the boundary of a bounded domain must vanish identically. Hence, Theorem 11.3 implies the following practically important conclusion.

Theorem 11.4 (see [10, 439]). *If the acquisition surface S is the boundary of a bounded domain Ω (i.e., a closed surface), then it is a uniqueness set. Thus, the observed data g in (11.9) uniquely determines the function $f \in L^2_{comp}(\mathbb{R}^n)$. (The statement holds even though f is not required to be supported inside S .)*

There is another useful explanation of why Theorem 11.4 holds true.³¹ Namely, if there is nonuniqueness, there exists a nonzero f such that $g(y, t) = 0$ for all $y \in S$ and t . This means that we can add, “for free,” homogeneous Dirichlet boundary conditions $p|_S = 0$ to (11.9). Now we have two different interpretations of the problem: as a nonobstructed wave propagation problem in the whole space, or as the Dirichlet boundary value problem in a cylinder. From the first point of view, since the solution p of (11.9) has compactly supported initial data, its energy is decaying inside any bounded domain, particularly inside Ω . See Appendix Section C.3 and [141, 197, 380, 638, 664, 776, 777] and references therein about local energy decay. On the other hand, under the second view, the standard PDE theorems [176] imply that the energy stays constant in Ω . Combination of the two conclusions means that p is zero in Ω for all times t and thus $f = 0$.

Remark 11.5. *This energy decay consideration also resolves the conundrum presented in Remark 11.1: The boundary data g did not seem to contain much information about the initial value f at all. As it is mentioned there, the key is that we are dealing*

³¹Although it requires somewhat stronger assumptions, or a more delicate proof than the one indicated here.

not with a boundary value, but rather with an observation problem, which allows for energy escape from Ω . This energy decay is exactly what makes TAT feasible.

The energy decay consideration can be extended to some classes of noncompactly supported functions f of the L^p classes, leading to the following result of [4].

Theorem 11.6 (after [4]). *Let S be the boundary of a bounded domain in \mathbb{R}^n , and $f \in L^p(\mathbb{R}^n)$. Then the following hold:*

1. *If $p \leq \frac{2n}{n-1}$ and the spherical mean of f over almost every sphere centered on S is equal to zero, then $f = 0$.*
2. *The previous statement fails when $p > \frac{2n}{n-1}$ and S is a sphere.*

In other words, a closed surface S is a uniqueness set for functions $f \in L^p(\mathbb{R}^n)$ when $p \leq \frac{2n}{n-1}$, and might fail to be so when $p > \frac{2n}{n-1}$.

This result shows that the assumption, if not necessarily of compactness of support of f , but at least of a sufficiently fast decay of f at infinity, is important for the uniqueness to hold.

What about **nonclosed observation (acquisition) sets S** then? Which ones provide enough data for uniqueness to hold?

Theorems 11.3 and 11.4 imply the following useful statement.

Theorem 11.7. *If a set S is not algebraic, or if it contains an open part of a closed analytic surface Γ , then it is a uniqueness set.*

Indeed, the first claim follows from Theorem 11.3. The second one works as follows: If an open subset of an analytic surface Γ is a nonuniqueness set, then by an analytic continuation-type argument (see [10]) one can show that the whole Γ is such a set. However, this would contradict Theorem 11.4.

After these positive claims, we are obliged to mention that examples of non-uniqueness surfaces do exist. Indeed, if S is a plane in three dimensions (or a line in two dimensions, or a hyperplane in arbitrary dimension) and $f(x)$ in (11.9) is odd with respect to S , then clearly the whole solution of (11.9) has the same parity and thus vanishes on S for all times t . This means that, if one places transducers on a planar S , they might register zero signals at all times, while the function f to be reconstructed is not zero. Thus, there is no uniqueness of reconstruction when S is a line/plane. On the other hand (see [176, 392]), if f is supported completely on one side of the plane (or line in two dimensions) S , it is uniquely recoverable from its spherical means centered on S , and thus from the observed data g . This one-sided placement is rather standard in TAT.

The question arises of what other “bad” (nonuniqueness) acquisition surfaces might be, besides lines/planes. This issue is resolved in two dimensions only. Namely, consider a set of N lines on the plane intersecting at a point and forming

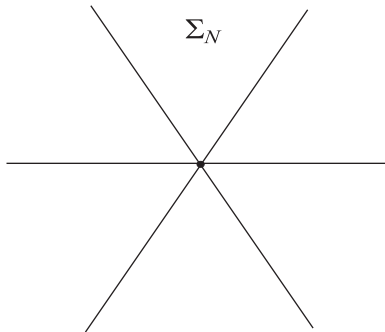


Figure 11.3. Coxeter cross of N lines.

at this point equal angles. We will call such a figure the **Coxeter cross** Σ_N (see Fig. 11.3).

Exercise 11.8. *Prove that there exist nonzero compactly supported functions that are odd simultaneously with respect to all lines in Σ_N . Thus, a Coxeter cross is also a nonuniqueness set.*

It takes more work to prove that if one adds a finite set to a Coxeter cross of lines, the resulting set S is still a nonuniqueness one. It was conjectured in [487] and proven in [10] that this is all that can happen to nonuniqueness sets.³²

Theorem 11.9 (see [10]). *A set S in the plane \mathbb{R}^2 is a nonuniqueness set for compactly supported functions f if and only if it belongs to the union $\Sigma_N \bigcup \Phi$ of a Coxeter cross Σ_N and a finite set of points Φ .*

Again, compactness of support is crucial for the proof provided in [10]. No other proof of this result is known at the moment. In particular, there is no proven analogue of Theorem 11.6 for nonclosed sets S (unless S is an open part of a closed analytic surface) or for functions very quickly (e.g., superexponentially) decaying at infinity but not having a compact support.

No n -dimensional (in particular, 3D) version of Theorem 11.9 has been proven. The following result has been conjectured [10], but never proven, although some partial advances in this direction have been made in [21, 225].

Conjecture 11.10. *A set S in \mathbb{R}^n is a nonuniqueness set for compactly supported functions f if and only if it belongs to the union $\Sigma \bigcup \Phi$, where Σ is the cone of zeros of a homogeneous (with respect to some point in \mathbb{R}^n) harmonic polynomial and Φ is an algebraic subset of \mathbb{R}^n of dimension at most $n - 2$ (see Fig. 11.4).*

³²A gap in the microlocal part of the proof in [10] was closed later in [736].

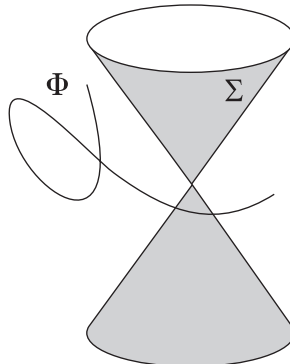


Figure 11.4. *The conjectured structure of a most general nonuniqueness set in three dimensions.*

Uniqueness and observation time

So far, we have addressed the question of uniqueness of reconstruction only under the nonpractical assumption of infinite observation time. There are, however, results that guarantee **uniqueness of reconstruction for a finite time of observation**. The general idea is that it is sufficient to observe for the time that it takes the geometric rays (see Appendix C) from the interior Ω of S to reach S . In the case when $c(x) = 1$, the rays are straight lines and are traversed with unit speed. This means that if D is the diameter of Ω (i.e., the maximal distance between two points in the closure of Ω), then after time $t = D$, all rays coming from Ω have left the domain. Thus, one hopes that waiting till time $t = D$ might be sufficient. In fact, due to the specific initial conditions in (11.3), namely, that the time derivative of the pressure is equal to zero at the initial moment, each singularity of f emanates two rays, and at least one of them will reach S in time not exceeding $D/2$. And indeed, the following result of [225, Theorem 2] holds.

Theorem 11.11 (see [225]). *If S is a smooth and closed surface bounding domain Ω and D is the diameter of Ω , then the TAT data on S collected for the time $0 \leq t \leq 0.5D$ uniquely determines f .*

Notice that a shorter collection time does not guarantee uniqueness. Indeed, if S is a sphere and the observation time is less than $0.5D$, due to the finite speed of propagation, no information from a neighborhood of the center can reach S during observation. Thus, values of f in this neighborhood cannot be reconstructed.

11.2.2 • Stability

The issue of stability has already been discussed for the case of Radon transform in Section 5.8. We thus direct the reader to that section for a general discussion and will try to give her a feeling of the general state of affairs with stability in TAT, referring to the literature (e.g., [8, 381, 445, 583, 622, 737]) for further exact details.

In the case of a constant sound speed and the acquisition surface completely surrounding the object, as we have mentioned before, the TAT problem can be

recast as an inversion of the spherical mean transform \mathcal{M} (see Section 11.1). Due to an analogy between the spheres centered on S and hyperplanes, one can expect that the Lipschitz stability of the inversion of the spherical mean operator \mathcal{M} is similar to that of the inversion of the Radon transform. This indeed is the case, as long as f is supported inside S , as has been shown in [622]. In the cases when closed-form inversion formulas are available (see Section 11.4.1), this stability can also be extracted from them. The same stability conclusion follows from the time reversal technique (Section 11.4.1). However, if the support of f reaches outside, reconstruction of the part of f that is outside is unstable (i.e., it is not even Hölder stable, due to the microlocal reasons explained in Section 11.2.3).

11.2.3 ■ Incomplete data

In the standard X-ray CT, incompleteness of data arises, for instance, if not all projection angles are accessible, or irradiation of certain regions is avoided, or in ROI (region of interest) imaging, only the ROI is irradiated.

It is not that clear what incomplete data means in TAT. Usually one says that one deals with **incomplete TAT data if the acquisition surface does not surround the object of imaging completely**. For instance, in breast imaging it is common that only a half-sphere arrangement of transducers is possible. We will see, however, that **in the case of acoustically inhomogeneous media, incomplete data effects in TAT can also arise due to trapping, even if the acquisition surface completely surrounds the object**. On the other hand, in inhomogeneous media it is sometimes possible to collect “full data” on a nonclosed observation surface (see Section 11.3.3).

The questions addressed here are as follows:

1. Is the collected “incomplete” data sufficient for **unique reconstruction?**
2. If yes, does the incompleteness of the data have any effect on **stability and quality of the reconstruction?**

Uniqueness of reconstruction with incomplete data

Uniqueness of reconstruction issues can be considered essentially resolved for incomplete data in TAT, at least in most situations of practical interest. We will briefly survey here some of the available results. In what follows, the acquisition surface S is not closed (otherwise the problem is considered to have complete data, and then uniqueness is already known).

Assuming that the medium is acoustically homogeneous, Theorem 11.7 contains some useful sufficient conditions on S that guarantee uniqueness. Microlocal results of [10, 498, 736], as well as the PDE approach of [225] further applied in [21] provide also some other conditions. We collect some of these in the following theorem.

Theorem 11.12. *Let S be a nonclosed acquisition surface in TAT. Each of the following conditions on S is sufficient for the uniqueness of reconstruction of any compactly supported function f from the TAT data collected on S :*

1. *Surface S is not algebraic (i.e., there is no nonzero polynomial vanishing on S).*
2. *Surface S is a uniqueness set for harmonic polynomials (i.e., there is no nonzero harmonic polynomial vanishing on S).*
3. *Surface S contains an open piece of a closed analytic surface Γ .*
4. *Surface S contains an open piece of an analytic surface Γ separating the space \mathbb{R}^n such that f is supported on one side of Γ .*
5. *For some point $y \in S$ the function f is supported on one side of the tangent plane T_y to S at y .*

For instance, if S is just a tiny nonalgebraic piece of a surface, data collected on S determines the tomogram f uniquely. However, one realizes that such data is unlikely to be useful for any practical reconstruction. Here the issue of stability of reconstruction kicks in, as will be discussed in the stability subsection further down.

“Visible” (“audible”) singularities

According to Appendix Section C.1, singularities (the points of the wavefront set $WF(f)$ of the function f in (11.3)) are transported with time along the bicharacteristics (C.2). Thus, in the x -space they are transported along the geometric rays. These rays may or may not reach the acquisition surface S , which triggers the introduction of the following notion.

Definition 11.13. *A phase space point (x_0, ξ_0) is said to be “visible” (sometimes the word “audible” is used instead) if the corresponding ray (see (C.2)) reaches the observation surface S in a finite time.*

A region $U \subset \mathbb{R}^n$ is said to be in the visibility zone if all points (x_0, ξ_0) with $x_0 \in U$ are visible.

Since in an acoustically homogeneous medium the rays are straight lines, the visibility test is similar to the X-ray CT case and is very simple. For example, the infinitesimal piece of a tissue interface at a point x is visible only if its normal line intersects the (possibly nonclosed) observation surface S .

Invisible singularities blur, the same way as in the X-ray CT (see Chapter 7).

Stability of reconstruction for incomplete data problems

In most examples discussed above, uniqueness of reconstruction held, but the images still got blurred. The question arises of whether the blurring of invisible parts is avoidable (after all, the uniqueness theorems seem to claim that “everything is

visible”). The answer to this is, in particular, the following result of [583], which is an analogue of similar statements in X-ray tomography.

Theorem 11.14 (after [583]). *If there are invisible points (x_0, ξ_0) in $\Omega \times (\mathbb{R}_\xi^n \setminus 0)$, then inversion of the forward operator \mathcal{W} is not Hölder stable in any Sobolev spaces. The singular values σ_j of \mathcal{W} in L^2 decay superalgebraically.*

Thus, having invisible singularities makes the reconstruction severely ill-posed. In particular, according to Remark 11.25 below, this theorem implies the following statement.

Corollary 11.15. *Reconstruction of the parts of $f(x)$ supported outside the closed observation surface S is unstable.*

On the other hand, we have the following result.

Theorem 11.16 (see [737]). *All visible singularities of f can be reconstructed with Lipschitz stability (in appropriate spaces).*

Such a reconstruction of visible singularities can be obtained in many ways, such as just by replacing the missing data by zeros (with some smoothing along the junctions with the known data, in order to avoid artifact singularities). However, there is no hope for stable recovery of the correct values of $f(x)$ if there are invisible singularities.

11.2.4 ■ Discussion of the visibility condition

In the constant speed case, the rays are straight, and thus the visibility condition has a simple test, given next.

Proposition 11.17 (see, e.g., [381, 810, 811]). *If the speed is constant, a point x_0 is in the visible region if and only if any line passing through x_0 intersects at least once the acquisition surface S (and thus a detector location).*

Figure 11.5 illustrates this statement. It shows a square phantom and its reconstruction from complete data and from the data collected on the half-circle S surrounding the left half of object. The parts of the interfaces where the normal to the interface does not cross S are blurred.

11.2.5 ■ Range conditions

In this section we address the problem of describing the ranges of the forward operators \mathcal{W} (see (11.4)) and \mathcal{M} (see (11.8)), the latter in the case of an acoustically homogeneous medium (i.e., for $c = \text{const}$). The ranges of these operators, similarly to the range of the Radon and X-ray transforms (see [559]), are of infinite

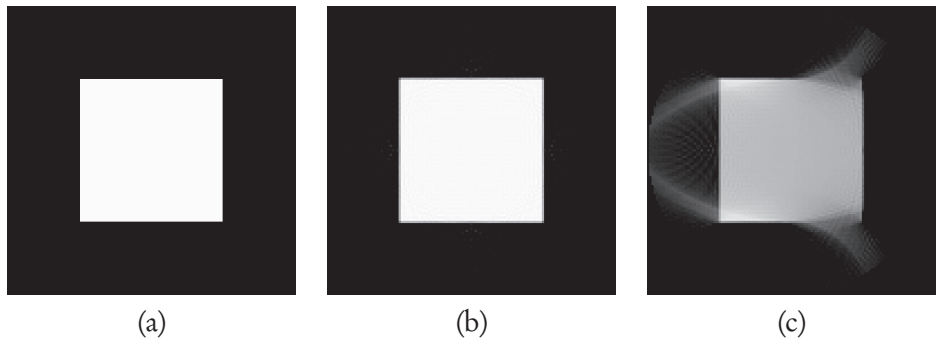


Figure 11.5. Reconstruction from incomplete data using a closed-form inversion formula in two dimensions; detectors are located on the left half-circle of radius 1.05: (a) phantom, (b) reconstruction from complete data, (c) reconstruction from incomplete data

co-dimensions. This means that ideal data g from a suitable function space has to satisfy infinitely many mandatory identities. Knowing the range is useful for many theoretical and practical purposes in various types of tomography (reconstruction algorithms, error corrections, incomplete data completion, etc.), and thus this topic has attracted a lot of attention (e.g., [253, 349, 559, 602, 620] and references therein).

As we will see in the next section, range descriptions in TAT are also intimately related to recovery of the unknown sound speed.

We recall (see Section 5.10) that for the standard Radon transform

$$f(x) \rightarrow g(t, \omega) = \int_{x \cdot \omega = t} f(x) dx, |\omega| = 1,$$

where f is assumed to be smooth and supported in the unit ball $B = \{x \mid |x| \leq 1\}$, the range conditions on $g(t, \omega)$ are the following:

1. *smoothness and support*: $g \in C_0^\infty([-1, 1] \times S)$, where S is the unit sphere of vectors ω ;
2. *evenness*: $g(-t, -\omega) = g(t, \omega)$;
3. *moment conditions*: for any integer $k \geq 0$, the k th moment

$$G_k(\omega) = \int_{-\infty}^{\infty} t^k g(t, \omega) dt$$

extends from the unit sphere S to a homogeneous polynomial of degree k in ω .

The seemingly “trivial” evenness condition is sometimes the hardest to generalize to other transforms of Radon type, while it is often easier to find analogues of the moment conditions. This is exactly what happens in TAT.

For the operators \mathcal{W}, \mathcal{M} in TAT, some sets of range conditions of moment type have been discovered over the years [10, 487, 631], but complete range descriptions have started to emerge only since 2006 [5, 7–9, 22, 226, 445].

Range descriptions for the more general operator \mathcal{W} are harder to obtain than for \mathcal{M} , and complete range descriptions are not known for even dimensions or for the case of the variable sound speed.

Let us address the case of the spherical mean operator \mathcal{M} first.

The range of the spherical mean operator \mathcal{M} .

The support and smoothness conditions are not hard to come up with, at least when S is a sphere. By choosing an appropriate length scale, we can assume that the sphere is of radius 1 and centered at the origin, and that the interior domain Ω is the unit ball $B = \{x \mid |x| = 1\}$. If f is smooth and supported inside B (i.e., $f \in C_0^\infty(B)$), then it is clear that the measured data satisfies the following.

Smoothness and support conditions:

$$g \in C_0^\infty(S \times [0, 2]). \quad (11.10)$$

An analogue of the moment conditions for $g(y, r) := \mathcal{M}f$ was implicitly present in [10, 487] and explicitly formulated as such in [631], as follows.

Moment conditions: for any integer $k \geq 0$, the moment

$$M_k(y) = \int_0^\infty r^{2k+d-1} g(y, r) dr \quad (11.11)$$

extends from S to a (in general, inhomogeneous) polynomial $Q_k(x)$ of degree at most $2k$.

These two types of conditions happen to be incomplete; i.e., infinitely many others exist. The Radon transform experience suggests that we look for an analogue of the evenness conditions. And indeed, a set of conditions called orthogonality conditions was found in [8, 22, 226].

Orthogonality conditions: Let $-\lambda_k^2$ be the eigenvalue of the Laplace operator Δ in B with zero Dirichlet conditions, and ψ_k be the corresponding eigenfunctions. Then the following orthogonality condition is satisfied:

$$\int_{S \times [0,2]} g(x, t) \partial_\nu \psi_\lambda(x) j_{n/2-1}(\lambda t) t^{n-1} dx dt = 0. \quad (11.12)$$

Here $j_p(z) = c_p z^{-p} J_p(z)$ is the so-called spherical Bessel function, and ∂_ν denotes the exterior normal derivative.

The range descriptions obtained in [8, 22, 226] demonstrated that these three types of conditions completely describe the range of the operator \mathcal{M} on functions $f \in C_0^\infty(B)$. At the same time, the results of [8, 226] showed that the moment conditions can be dropped in odd dimensions. It was then discovered in [5] that

the moment conditions can be dropped altogether in any dimension, since they follow from the other two types of conditions:

Theorem 11.18 (see [5]). *Let S be the unit sphere. A function $g(y, t)$ on the cylinder $S \times \mathbb{R}^+$ can be represented as $\mathcal{M}f$ for some $f \in C_0^\infty(B)$ if and only if it satisfies the above smoothness and support and orthogonality conditions (11.10), (11.12).*

The statement also holds in the finite smoothness case if one replaces the requirements by $f \in H_0^s(B)$ and $g \in H_0^{s+(n-1)/2}(S \times [0, 2])$.

The range of the forward operator \mathcal{M} has not been described when S is not a sphere, but, say, a convex smooth closed surface. The moment and orthogonality conditions hold for any S , and appropriate smoothness and support conditions can also be formulated, at least in the convex case. However, it has not been proven that they provide the complete range description.

It is quite possible that for nonspherical S the moment conditions might have to be included in the range description.

A different range description of **Fredholm alternative** type was developed in [622] (see also [228] for description of this result).

The range of the forward operator \mathcal{W} .

We recall that operator \mathcal{W} (see (11.4)) transforms the initial value f in (11.3) into the values g of the solution observed on S . There exist Kirchhoff–Poisson formulas representing the solution p , and thus $g = \mathcal{W}f$ in terms of the spherical means of f (i.e., in terms of $\mathcal{M}f$). However, translating the result of Theorem 11.18 into the language of \mathcal{W} is not straightforward, since in even dimensions these formulas are nonlocal [176, p. 682]:

$$\mathcal{W}f(y, t) = \frac{\sqrt{\pi}}{2\Gamma(n/2)} \left(\frac{1}{t} \frac{\partial}{\partial t} \right)^{(n-3)/2} t^{n-2} (\mathcal{M}f)(y, t) \quad \text{for odd } n, \quad (11.13)$$

and

$$\mathcal{W}f(y, t) = \frac{1}{\Gamma(n/2)} \left(\frac{1}{t} \frac{\partial}{\partial t} \right)^{(n-2)/2} \int_0^t \frac{r^{n-1} (\mathcal{M}f)(y, r)}{\sqrt{t^2 - r^2}} dr \quad \text{for even } n. \quad (11.14)$$

The nonlocality of the transformation for even dimensions reflects the absence of Huygens' principle (i.e., absence of sharp rear fronts of waves) in these dimensions [54, 176, 330]; it also causes difficulties in establishing the complete range descriptions. In particular, due to the integration in (11.14), $\mathcal{M}f(y, t)$ does not vanish for large times t anymore. One can try to use other known operators intertwining the two problems (see [8] and references therein), some of which do preserve vanishing for large values of t , but so far this has led only to very clumsy range descriptions.

However, for odd dimensions, the range description of \mathcal{W} can be obtained. In order to find it, given the TAT data $g(y, t)$, let us introduce an auxiliary time-reversed problem in the cylinder $B \times [0, 2]$:

$$\begin{cases} q_{tt} - \Delta q = 0 & \text{for } (x, t) \in B \times [0, 2], \\ q(x, 2) = q_t(x, 2) = 0 & \text{for } x \in B, \\ q(y, t) = g(y, t) & \text{for } (y, t) \in S \times [0, 2]. \end{cases} \quad (11.15)$$

We can now formulate the range description from [226, 228], as follows.

Theorem 11.19 (see [226, 228]). *For odd dimensions n and S being the unit sphere, a function $g \in C_0^\infty(S \times [0, 2])$ can be represented as $\mathcal{W}f$ for some $f \in C_0^\infty(B)$ if and only if the following condition is satisfied:*

The solution q of (11.15) satisfies $q_t(x, 0) = 0$ for all $x \in B$.

11.3 • Analysis of TAT: Acoustically inhomogeneous media

We have dealt so far with the case of an acoustically homogeneous medium, which in most cases is not the best approximation of real conditions. The situation when the medium is acoustically inhomogeneous is, expectably, trickier. We assume now that the sound speed $c(x)$ can vary but is strictly positive, $c(x) > c > 0$, and such that $c(x) - 1$ has compact support, i.e., $c(x) = 1$ for large x .

11.3.1 • Uniqueness of reconstruction

We start by presenting a uniqueness of reconstruction result in the case of non-trapping (see Appendix Section C.2) sound speeds.

Infinite observation time

If the speed is nontrapping (Section C.1), the local energy decay allows one to start solving the problem (11.3) from $t = \infty$, imposing zero conditions at $t = \infty$ and using the measured data g as the boundary conditions. This leads to recovery of the whole solution, and in particular its initial value $f(x)$. As a result, one obtains the following simple uniqueness result of [6].

Theorem 11.20 (after [6]). *If the speed $c(x)$ is smooth and nontrapping and the acquisition surface S is closed, then the TAT data $g(y, t)$ determines the tomogram $f(x)$ uniquely.*

Notice that the statement of the theorem holds even if the support of f is not completely inside of the acquisition surface S .

Here we again assume an (unrealistic) infinite observation time. This result can be improved significantly, as described next.

Finite observation time

As in the case of constant coefficients, if the sound speed is nontrapping, appropriately long finite observation time suffices for the uniqueness. Let us denote by $T(\Omega)$ the *supremum* of the time it takes the ray to reach S , over all rays originating in Ω . One sees $T(\Omega)$ as an analogue of the diameter D in the corresponding results for the acoustically homogeneous case.

In particular, if $c(x)$ is trapping, $T(\Omega)$ is infinite.

Theorem 11.21 (see [737]). *The data g measured till any time T larger than $T(\Omega)$ is sufficient for unique recovery of f .*

One expects that this result is not optimal, since in the constant speed case half of the time is sufficient. In fact, an analogue of this stronger result was also obtained in [737]. Since each wavefront vector (x, ξ) creates two rays (corresponding to ξ and $-\xi$), one suspects that it should be sufficient to wait until at least one of the two rays appears on the boundary. So, let us define $T_1(\Omega)$ as the minimal time by which at least one of each pair of rays from inside S reaches S . Then the following was proven in [737].

Theorem 11.22 (see [737]). *The data g measured till any time T larger than $T_1(\Omega)$ is sufficient for unique recovery of f .*

11.3.2 • Stability of reconstruction

In the case of **variable nontrapping sound speed** $c(x)$, integral geometry does not provide the complete picture of wave propagation,³³ and one needs to address the issue using, for instance, time reversal. In this case, stability follows from solving the wave equation in reverse time starting from $t = \infty$, as is done in [6]. In fact, **Lipschitz stability in this case holds for any observation time exceeding $T(\Omega)$** (see [737], where microlocal analysis is used to prove this result).

The bottom line is that **TAT reconstruction is as stable as Radon transform inversion, as long as the sound speed is nontrapping**.

However, **trapping speed does cause instability** [381]. Indeed, since some of the rays are trapped inside Ω , the information about some singularities never reaches S (no matter for how long one collects the data), and thus, as is shown in [583] (see also Section 5.8), the reconstruction is not even Hölder stable between any Sobolev spaces, and the singular values have superalgebraic decay.

11.3.3 • Incomplete data

As we have already mentioned, the notion of incomplete data in TAT becomes somewhat muddled when the acoustic speed is not constant. In particular, incom-

³³Although it does tell one how singularities of solutions propagate.

plete data effects in TAT can also arise due to trapping, even if the acquisition surface completely surrounds the object.

On the other hand, there is a silver lining that in inhomogeneous media it is sometimes possible to have stable reconstructions using the data collected on a nonclosed observation surface.

As in the corresponding section for the case of an acoustically homogeneous medium, we address the questions of **unique reconstruction** from limited data and **stability and quality of the reconstruction**.

Uniqueness of reconstruction

In the case of a variable sound speed, there still are uniqueness theorems for partial data [737, 742], e.g., the following.

Theorem 11.23 (see [737]). *Let S be an open part of the boundary $\partial\Omega$ of a strictly convex domain Ω , and let the smooth sound speed equal 1 outside Ω . Then the TAT data collected on S for a time $T > T(\Omega)$ uniquely determines any function $f \in H_0^1(\Omega)$ whose support does not reach the boundary.*

A modification of this result that does not require strict convexity is also available in [742].

While useful uniqueness of reconstruction results exist for incomplete data problems, all such problems are expected to show instability.

Visible singularities

As we know already, visibility of a singularity depends on whether at least one of two geometric rays corresponding to the wavefront vector reaches detectors. Namely, an analogue of Proposition 11.17 holds, with lines replaced by rays.

Proposition 11.24 (e.g., [381, 583, 737]). *A point x_0 is in the visible region if and only if for any $\xi_0 \neq 0$ at least one of the two geometric rays starting at (x_0, ξ_0) and at $(x_0, -\xi_0)$ (see (C.2)) intersects the acquisition surface S (and thus a detector location).*

An example of wave propagation through an inhomogeneous medium is presented in Fig. 11.6. Here the observation surface S consists of the two horizontal and the left vertical side of the square, leaving an open vertical “gate” on the right. We see how some rays bend, due to acoustic inhomogeneity, and leave through the opening on the right side of the square. Fig. 11.6(b) presents a flat phantom, whose wavefront set creates these escaping rays and thus is mostly invisible. Then Fig. 11.6(c)–(f) show the propagation of the corresponding wavefront.

Since the information about the horizontal boundaries of the phantom escapes, one does not expect to reconstruct it well. Fig. 11.7 shows two phantoms and their reconstructions from the partial data: (a)–(b) correspond to the vertical flat phantom, whose only invisible singularities are at its ends. One sees essentially good reconstruction, with a little bit of blurring at the endpoints. On

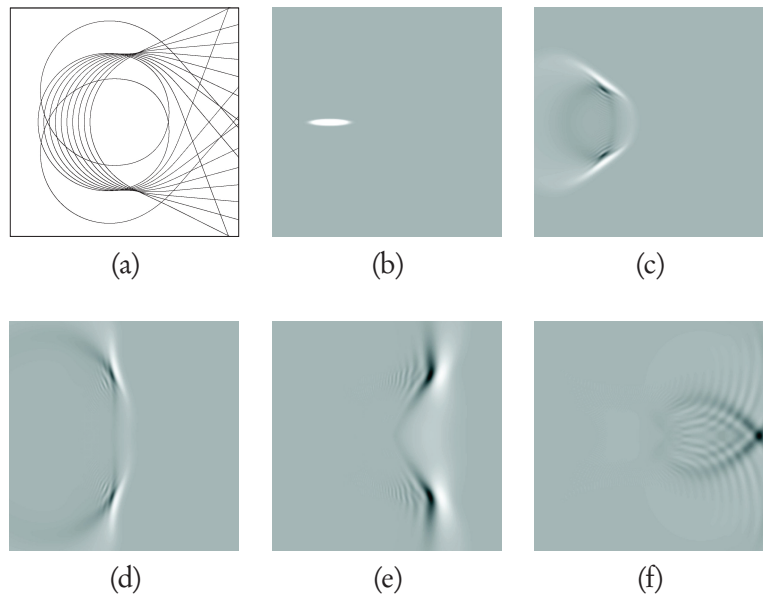


Figure 11.6. (a) Some rays starting along the interval $x \in [-0.7, -0.2]$ in the vertical directions escape on the right; (b) a flat phantom with “invisible wavefront”; (c)–(f) propagation of the flat front: most of the energy of the signal leaves the square domain through the “hole” on the right. [701]

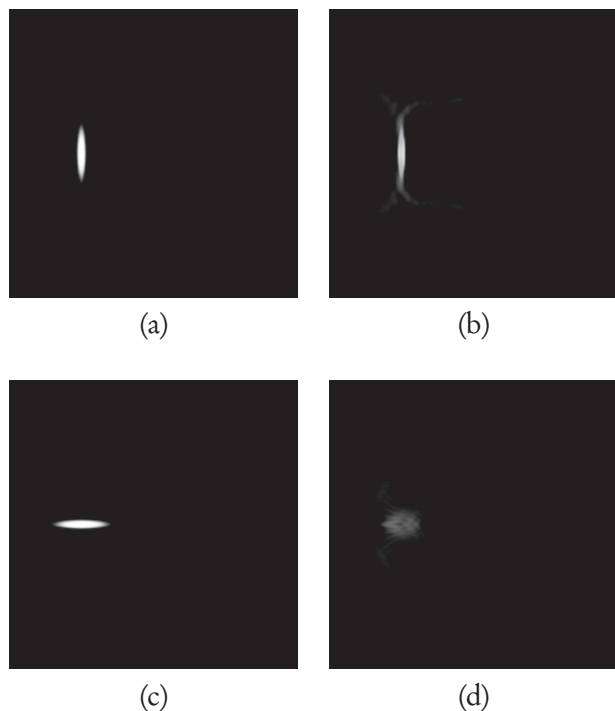


Figure 11.7. Reconstruction with the same sound speed as in Fig. 11.6: (a) phantom with strong vertical fronts, (b) its reconstruction; (c) phantom with strong horizontal fronts, (d) its reconstruction.

the other hand, reconstruction of the horizontal phantom with almost the whole wave front set invisible does not work.

Fig. 11.8 shows a more complex square phantom, whose singularities corresponding to the horizontal boundaries are invisible, while its vertical boundaries are fine. The invisible parts have been blurred away.

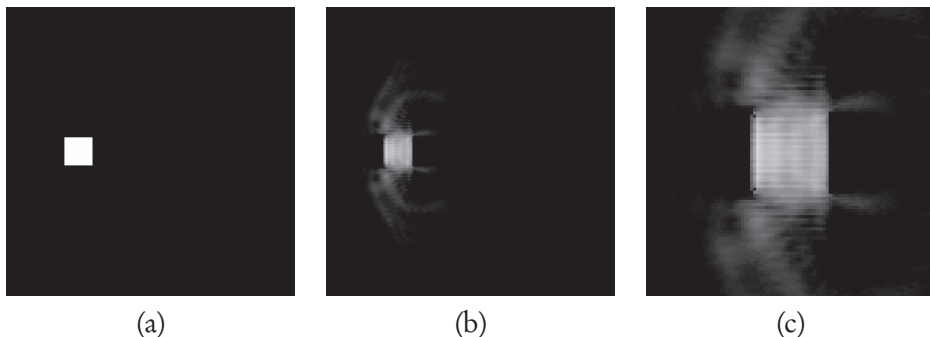


Figure 11.8. Reconstruction with the same sound speed as in Fig. 11.6: (a) phantom, (b) its reconstruction, (c) a magnified fragment of (b).

On the other hand, Fig. 11.11(a) in Section 11.4 shows the good news that one can reconstruct an image without blurring and with correct values, if the image is located in the visibility region. The reconstructed image in this figure is practically indistinguishable from the phantom shown in Figure 11.10(a).

Remark 11.25. Let S be a closed surface and x_0 a point outside of the convex hull of S . Then there exists a vector $\xi_0 \neq 0$ such that (x_0, ξ_0) is “invisible.” Thus, the visibility zone does not reach outside the closed acquisition surface S .

The reader should also notice another important difference between the acoustically homogeneous and inhomogeneous media. Namely, even if S surrounds the support of f completely, trapped rays (if any exist) will never find their way to S , which will lead, as we know by now, to instabilities and blurring of some interfaces. Thus, **presence of rays trapped inside the acquisition surface creates effects of incomplete data type**. This is exemplified in Fig. 11.9, with a square phantom and its reconstruction shown in the presence of a trapping (parabolic) speed. Notice that the square centered at the center of symmetry of the speed is reconstructed very well (see (d)), since none of the rays carrying its singularities is trapped.

11.3.4 • Range

As far as the author is aware, there are no complete range descriptions known for acoustically inhomogeneous media. Necessity of some of the range conditions

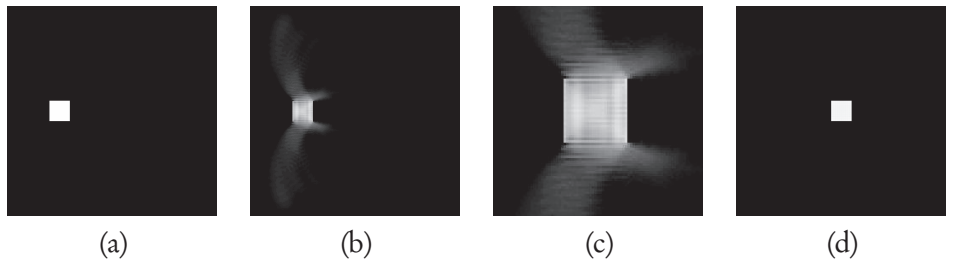


Figure 11.9. Reconstruction of a square phantom from full data in the presence of a trapping parabolic sound speed (the speed is radial with respect to the center of the picture): (a) an off-center phantom, (b) its reconstruction, (c) a magnified fragment of (b), (d) reconstruction of a centered square phantom.

described in section 11.2.5 also holds in the case of a variable speed, but sufficiency of the corresponding set of conditions is doubtful.

11.4 • Reconstruction methods in TAT/PAT

In this section we provide a brief overview of various reconstruction techniques being numerically implemented. Due to the speed of recent developments in this area, the section will be somewhat outdated at the moment of publication, so the reader is advised to follow the recent literature for updates.

We look at the situations of acoustically homogeneous and inhomogeneous media, as well as at closed and open observation surfaces.

11.4.1 • Full data (closed acquisition surfaces) for acoustically homogeneous media

We have already seen in section 11.1 that when the sound speed within the object is a known constant, the TAT problem can be reformulated in terms of inverting the (restricted) spherical means transform \mathcal{M} . Thus, we consider the problem of reconstructing a function $f(x)$ supported within the region bounded by a closed surface S from the known values of its spherical integrals $g(y, r)$ with centers on S :

$$g(y, r) = \int_{\mathbb{S}^{n-1}} f(y + r\omega) r^{n-1} d\omega, \quad y \in S, \quad (11.16)$$

where $d\omega$ is the standard measure on the unit sphere.

Closed-form inversion formulas

Closed-form inversion formulas play a special role in tomography. They provide better theoretical understanding of the problem and frequently serve as starting points for the development of efficient reconstruction algorithms. A well-known example of the use of explicit inversion formulas is the celebrated filtered back-projection (FBP) formula in X-ray CT (see (5.23)).

The very existence of closed-form inversion formulas for TAT was long in doubt, till the first such formulas were obtained in odd dimensions in [225], under the assumption that the acquisition surface S is a sphere. Suppose that the function $f(x)$ is supported within a ball of radius R and that the detectors are located on the surface $S = \partial B$ of this ball. Then some of the formulas obtained in [225] read as follows:

$$f(x) = -\frac{1}{8\pi^2 R} \Delta_x \int_{\partial B} \frac{g(y, |y-x|)}{|y-x|} dA(y), \quad (11.17)$$

$$f(x) = -\frac{1}{8\pi^2 R} \int_{\partial B} \left(\frac{1}{r} \frac{\partial^2}{\partial r^2} g(y, r) \right) \Big|_{r=|y-x|} dA(y), \quad (11.18)$$

$$f(x) = -\frac{1}{8\pi^2 R} \int_{\partial B} \left(\frac{1}{r} \frac{\partial}{\partial r} \left(r \frac{\partial}{\partial r} \frac{g(y, r)}{r} \right) \right) \Big|_{r=|y-x|} dA(y), \quad (11.19)$$

where $dA(y)$ is the surface measure on ∂B and g represents the values of the spherical integrals (11.16).

These formulas are of the FBP type. Indeed, differentiation with respect to r in (11.18) and (11.19) and the Laplace operator in (11.17) represent the filtration, while the (weighted) integrals correspond to the backprojection, i.e., integration over the set of spheres passing through the point of interest x and centered on S .

The so-called universal backprojection formula in three dimensions was described in [806]. It is also valid for the cylindrical and plane acquisition surfaces; see Section 11.4.4. In our notation, this formula takes the form

$$f(x) = \frac{1}{8\pi^2} \operatorname{div} \int_{\partial B} n(y) \left(\frac{1}{r} \frac{\partial}{\partial r} \frac{g(y, r)}{r} \right) \Big|_{r=|y-x|} dA(y) \quad (11.20)$$

or, equivalently,

$$f(x) = -\frac{1}{8\pi^2} \int_{\partial B} \frac{\partial}{\partial n} \left(\frac{1}{r} \frac{\partial}{\partial r} \frac{g(y, r)}{r} \right) \Big|_{r=|y-x|} dA(y), \quad (11.21)$$

where $n(y)$ is the exterior normal vector to ∂B .

A family of inversion formulas valid in \mathbb{R}^n for arbitrary $n \geq 2$ was found in [462]:

$$f(x) = \frac{1}{4(2\pi)^{n-1}} \operatorname{div} \int_{\partial B} n(y) b(y, |x-y|) dA(y), \quad (11.22)$$

where

$$h(y, t) = \int_{\mathbb{R}^+} Y(\lambda t) \left[\int_0^{2R} J(\lambda r) g(y, r) dr - J(\lambda t) \int_0^{2R} Y(\lambda r) g(y, r) dr \right] \lambda^{2n-3} d\lambda, \quad (11.23)$$

$$J(t) = \frac{J_{n/2-1}(t)}{t^{n/2-1}}, \quad Y(t) = \frac{Y_{n/2-1}(t)}{t^{n/2-1}}, \quad (11.24)$$

and $J_{n/2-1}(t)$ and $Y_{n/2-1}(t)$ are respectively the Bessel and Neumann functions of order $n/2-1$. In three dimensions, $J(t)$ and $Y(t)$ are simply $t^{-1} \sin t$ and $t^{-1} \cos t$, and formulas (11.22) and (11.23) reduce to (11.21).

In two dimensions, equation (11.23) also can be simplified [7], which results in the formula

$$f(x) = \frac{1}{2\pi^2} \operatorname{div} \int_{\partial B} n(y) \left[\int_0^{2R} g(y, r) \frac{1}{r^2 - |x-y|^2} dr \right] dl(y), \quad (11.25)$$

where ∂B now stands for the circle of radius R and $dl(y)$ is the standard arc length.

A different set of closed-form inversion formulas applicable in even dimensions was found in [222]. Formula (11.25) can be compared to the following inversion formulas from [222]:

$$f(x) = \frac{1}{2\pi R} \Delta \int_{\partial B} \int_0^{2R} g(y, r) \log(r^2 - |x-y|^2) dr dl(y) \quad (11.26)$$

or

$$f(x) = \frac{1}{2\pi R} \int_{\partial B} \int_0^{2R} \frac{\partial}{\partial r} \left(r \frac{\partial}{\partial r} \frac{g(y, r)}{r} \right) \log(r^2 - |x-y|^2) dr dl(y). \quad (11.27)$$

Finally, a unified family of inversion formulas was derived in [582]. In our notation, it has the following form:

$$f(x) = -\frac{4}{\pi R} \int_{\partial B} \left(\frac{\partial}{\partial t} K_n(y, t) \right) \Big|_{t=|x-y|} \frac{\langle y-x, y-\xi \rangle}{|x-y|} dA(y), \quad (11.28)$$

$$K_n(y, t) = -\frac{1}{16(2\pi)^{n-2}} \int_{\mathbb{R}^+} \lambda^{2n-3} Y(\lambda t) \left(\int_{\mathbb{R}^+} J(\lambda r) g(y, r) dr \right) d\lambda,$$

where ∂B is the surface of a ball in \mathbb{R}^n of radius R , functions J and Y are as in (11.24), and ξ is an arbitrary fixed vector. In particular, in three dimensions

$$J(t) = \sqrt{\frac{2}{\pi}} \frac{\sin t}{t}, \quad Y(t) = \sqrt{\frac{2}{\pi}} \frac{\cos t}{t},$$

and, after simple calculation, the above inversion formula reduces to

$$f(x) = -\frac{1}{8\pi^2 R} \int_{\partial B} \left(\frac{\partial}{\partial r} \frac{1}{r} \frac{\partial}{\partial r} \frac{g(y, r)}{r} \right) \Bigg|_{r=|x-y|} \frac{\langle y-x, y-\xi \rangle}{|x-y|} dA(y). \quad (11.29)$$

Different choices of vector ξ in the above formula result in different inversion formulas. For example, if ξ is set to zero, the ratio $\frac{\langle y-x, y-\xi \rangle}{|x-y|}$ equals $R \cos \alpha$, where α is the angle between the exterior normal $n(y)$ and the vector $y-x$; when combined with the derivative in t , this factor produces the normal derivative, and the inversion formula (11.29) reduces to (11.21). On the other hand, the choice of $\xi = x$ in (11.29) leads to

$$f(x) = -\frac{1}{8\pi^2 R} \int_{\partial B} \left(r \frac{\partial}{\partial r} \frac{1}{r} \frac{\partial}{\partial r} \frac{g(y, r)}{r} \right) \Bigg|_{r=|x-y|} dA(y),$$

which is reminiscent of formulas (11.17)–(11.19).

More about FBP formulas

Closed-form FBP formulas are very valuable and are often used in practice. They usually lead to much faster algorithms than do the algebraic reconstruction techniques. In TAT, however, they suffer from several limitations, which we briefly address now.

- Such formulas are known for acoustically homogeneous media only.
- Even for acoustically homogeneous media, they have been discovered for very special observation surfaces: spheres, cylinders, planes, cubes, and lately ellipsoids [222, 225, 340, 342, 462, 571, 582]. There is a strong doubt that such formulas can be derived for other smooth surfaces (in fact, even their existence for a sphere came as a surprise). One can find in [443, 462] some discussion (due to L. Kunyansky) of why having such formulas might require significant symmetry from the surface.
- One can show [7, 582] that formulas (11.17) through (11.20) are not equivalent on nonperfect data: The results will differ if these formulas are applied to a function that does not belong to the range of the spherical mean transform \mathcal{M} . This is not surprising, due to our discussion of left inverses in Section 5.7.2. More surprising is the next observation.

- The FBP formulas assume that the function in question is supported inside the observation surface. How significant is this assumption? In particular, if the function has a nonzero part outside, does this influence its reconstruction *inside*? It is interesting to notice that **all FBP formulas we have checked can lead to incorrect reconstruction of the function inside the observation surface if the support of the function reaches outside.** Moreover, **different formulas lead to different incorrect reconstructions inside!** It is not known whether one can write a FBP formula without this deficiency.

Parametrix approaches

Some of the earlier noniterative reconstruction techniques [435–437] were of approximate nature. For example, by approximating the integration spheres by their tangent planes at the point of reconstruction and by applying one of the known inversion formulas for the classical Radon transform, one can reconstruct an approximation to the image. Due to the evenness symmetry in the classical Radon projections (see Section 5.10), the normals to the integration planes need only fill a half of a unit sphere, in order to make possible the reconstruction from an open measurement surface. A more sophisticated approach is represented by the so-called straightening methods [627, 647, 648] based on the approximate reconstruction of the classical Radon projections from the values of the spherical mean transform $\mathcal{M}f$ of the function $f(x)$ in question. These methods yield not a true inversion, but rather what is called in microlocal analysis a **parametrix**. Application of a parametrix reproduces the function f with a smoother error term. In other words, the locations (and often the sizes) of jumps across sharp material interfaces, as well as the whole wavefront set $WF(f)$, are reconstructed correctly, while the accuracy of the lower spatial frequencies cannot be guaranteed. Sometimes, the reconstructed function has a more general form Af , where A is an elliptic pseudodifferential operator [378, 719] of order zero. In this case, the sizes of the jumps across the interfaces might be altered.

Unlike the approximations resulting from the discretization of the exact inversion formulas (in the situations when such formulas are known), the parametrix approximations do not converge when the discretization of the data is refined and the noise is eliminated. Parametrix reconstructions can be either accepted as approximate images, where the singularities are preserved while the smooth details are distorted, or used as starting points for iterative algorithms.

These methods are closely related to the general scheme proposed in [99] for the inversion of the generalized Radon transform with integration over curved manifolds. It reduces the problem to a Fredholm integral equation of the second kind, which is well suited for numerical solution. Such an approach amounts to using a parametrix method as an efficient preconditioner for an iterative solver; the convergence of such iterations is much faster than that of unpreconditioned algebraic iterative methods.

Series solutions for spherical geometry

Probably the first inversion procedures for closed acquisition surfaces were described in [592, 593] for circular (in two dimensions) and spherical (in three dimensions) surfaces. These solutions used expansions into spherical harmonics, followed by equating coefficients of the corresponding Fourier series. In particular, the 2D algorithm of [592] deals with detectors located on a circle of radius R as the observation curve. One starts with the Fourier decomposition of f and g in angular variables:

$$\begin{aligned} f(x) &= \sum_{-\infty}^{\infty} f_k(\rho) e^{ik\varphi}, \quad x = (\rho \cos(\varphi), \rho \sin(\varphi)), \\ g(y(\theta), r) &= \sum_{-\infty}^{\infty} g_k(r) e^{ik\theta}, \quad y(\theta) = (R \cos(\theta), R \sin(\theta)). \end{aligned} \quad (11.30)$$

It was shown in [592] that Fourier coefficients $f_k(\rho)$ can be recovered from the known coefficients $g_k(r)$ as follows:

$$f_k(\rho) = \mathcal{H}_m \left(\frac{1}{J_k(\lambda|R|)} \mathcal{H}_0 \left[\frac{g_k(r)}{2\pi r} \right] \right)$$

where

$$(\mathcal{H}_m u)(s) = 2\pi \int_0^\infty u(t) J_m(st) t dt$$

is the Hankel transform and $J_m(t)$ is the Bessel function. This method requires division of the Hankel transform of the measured data by the Bessel functions J_k , which have infinitely many zeros. Theoretically, there is no problem. Indeed, the range conditions (Section 5.10) on the exact data g imply that the Hankel transform $\mathcal{H}_0[(2\pi r)^{-1} g_k(r)]$ has zeros that cancel those in the denominator. However, since the measured data always contain errors, the exact cancellation does not happen, and one needs a sophisticated regularization scheme to guarantee that the error remains bounded.

This difficulty can be avoided (see, e.g., [445]) by replacing the Bessel function J_0 in the inner Hankel transform by the Hankel function $H_0^{(1)}$, which yields a formula for $f_k(\rho)$ without instability.³⁴

This derivation can be repeated in three dimensions, with the exponentials $e^{ik\theta}$ replaced by the spherical harmonics, and with cylindrical Bessel functions replaced by their spherical counterparts. By doing this, one arrives at the Fourier series method of [593] (see also [805]).

Eigenfunction expansions for a general geometry

The above spherical harmonics expansion method relies upon separation of variables and thus spherical geometry of the observation surface. A different series expansions approach was proposed in [463]. Theoretically, it works for arbitrary

³⁴A different way of avoiding divisions by zero was found in [340].

closed observation surfaces, but it is practical probably only for those where the spectrum and eigenfunctions of the Dirichlet Laplacian in the interior are known explicitly. These include, in particular, spheres, half-spheres, cylinders, cubes, and parallelepipeds, as well as crystallographic domains.

We denote by λ_m^2 and $u_m(x)$ the eigenvalues and an ortho-normal basis of eigenfunctions of the Dirichlet Laplacian $-\Delta$ in the interior Ω of a closed surface S :

$$\begin{aligned}\Delta u_m(x) + \lambda_m^2 u_m(x) &= 0, & x \in \Omega, \Omega \subseteq \mathbb{R}^n, \\ u_m(x) &= 0, & x \in S, \\ \|u_m\|_2^2 &\equiv \int_{\Omega} |u_m(x)|^2 dx = 1.\end{aligned}\quad (11.31)$$

As before, one needs to reconstruct a compactly supported function $f(x)$ from the known values of its spherical integrals $g(y, r)$ from (11.16) centered on S . Function $u_m(x)$ admits the **Helmholtz representation**

$$u_m(x) = \int_S \Phi_{\lambda_m}(|x - y|) \frac{\partial}{\partial n} u_m(y) ds(y), \quad x \in \Omega, \quad (11.32)$$

where $\Phi_{\lambda_m}(|x - y|)$ is a free-space Green's function of the Helmholtz equation (11.31) and n is the exterior normal to S .

Function $f(x)$ can be expanded into the series

$$f(x) = \sum_{m=0}^{\infty} \alpha_m u_m(x), \quad \text{where } \alpha_m = \int_{\Omega} u_m(x) f(x) dx. \quad (11.33)$$

Substituting (11.32) into (11.33), one arrives at a reconstruction formula for α_m (and thus for $f(x)$):

$$\alpha_m = \int_{\Omega} u_m(x) f(x) dx = \int_S I(y, \lambda_m) \frac{\partial}{\partial n} u_m(y) dA(x), \quad (11.34)$$

where

$$I(y, \lambda) = \int_{\Omega} \Phi_{\lambda}(|x - y|) f(x) dx = \int_0^{\text{diam } \Omega} g(y, r) \Phi_{\lambda}(r) dr. \quad (11.35)$$

This method is computationally efficient when the eigenvalues and eigenfunctions are known explicitly and a fast summation formula for the series (11.33) is available. This is the case when the acquisition surface S is a surface of a cube and thus the eigenfunctions are products of sine functions. The resulting 3D reconstruction algorithm is extremely fast and precise (see [463]).

This technique has an interesting property. Namely, if the support of the source $f(x)$ extends outside Ω , the algorithm still yields theoretically exact reconstruction of $f(x)$ inside Ω . Indeed, the value of the expression (11.32) for all x

lying outside Ω is zero. Thus, values of $f(x)$ outside Ω are multiplied by zero and do not affect further computation in any way. This feature is shared by the time reversal method (see the corresponding paragraph in Section 11.4.1). As we have already seen, no known closed-form FBP-type reconstruction formulas have this property. In other words, when using such methods, presence of a source outside the measurement surface can render the FBP reconstruction within Ω incorrect.

The reason for this difference is that all currently known closed-form FBP-type formulas rely (implicitly or explicitly) on the assumption that the wave propagates outside S in the whole free space and has no sources outside. On the other hand, the eigenfunction expansion method and the time reversal rely only upon the time decay of the wave inside S , which is not influenced by f having a part outside S .

Algebraic iterative algorithms

Iterative algebraic techniques are among the favorite tomographic methods of reconstruction and have been used in CT for quite a while [559]. They amount to discretizing the equation relating the measured data with the unknown source, followed by iterative solution of the resulting linear system. Iterative algebraic reconstruction algorithms frequently produce better images than those obtained by other methods. However, they are notoriously slow. In TAT, they have been used very successfully, including for reconstructions with partial data [33, 34, 140]; see Section 11.4.4.

Time reversal

This powerful method will be discussed in the next section, since it handles inhomogeneous media as easily as homogeneous ones.

11.4.2 • Full data (closed acquisition surfaces) for acoustically inhomogeneous media

The reconstruction formulas and algorithms described in the previous section work under the assumption that the sound speed within the region of interest is constant. This assumption, however, is not always realistic—for example, if the region of interest contains both soft tissues and bones, the sound speed will vary significantly. Experiments with numerical and physical phantoms show [381, 390] that if acoustic inhomogeneities are not taken into account, the reconstructed image can be severely distorted. Not only could the numerical values be reconstructed incorrectly, but so would the material interface locations and discontinuity magnitudes.

We review below some of the reconstruction methods that work in acoustically inhomogeneous media. We will assume that the sound speed $c(x)$ is known, smooth, positive, constant for large x , and nontrapping. In practice, a transmission ultrasound scan can be used to reconstruct $c(x)$ prior to thermoacoustic reconstruction, as is done in [390].

FBP formulas and parametrices

It appears that there are no closed-form inversion formulas known when the sound speed is variable. However, parametrix approaches are still available.

Eigenfunction expansions

While variable sound speed makes the methods of expansions into spherical harmonics unfeasible, the eigenfunction expansion technique survives (at least theoretically).

An “inversion formula” that reconstructs the initial value $f(x)$ of the solution of the wave equation from values on the measuring surface S can be easily obtained using time reversal and Duhamel’s principle [6]. We will not repeat it here, but rather describe its consequences for the eigenfunction expansion technique.

Consider in Ω the operator $A = -c^2(x)\Delta$ with zero Dirichlet conditions on the boundary $S = \partial\Omega$. This operator is self-adjoint if considered in the weighted space $L^2(\Omega; c^{-2}(x))$. Let us denote by E the operator of harmonic extension, which transforms a function ϕ on S to a harmonic function on Ω which coincides with ϕ on S .

The function $f(x)$ can be expanded inside Ω into an $L^2(B)$ -convergent series:

$$f(x) = \sum_k f_k \psi_k(x). \quad (11.36)$$

One can show that under the nontrapping condition, the Fourier coefficients f_k can be recovered from the data g in (11.3), using one of the following formulas:

$$\begin{aligned} f_k &= \lambda_k^{-2} g_k(0) - \lambda_k^{-3} \int_0^\infty \sin(\lambda_k t) g_k''(t) dt, \\ f_k &= \lambda_k^{-2} g_k(0) + \lambda_k^{-2} \int_0^\infty \cos(\lambda_k t) g_k'(t) dt, \text{ or} \\ f_k &= -\lambda_k^{-1} \int_0^\infty \sin(\lambda_k t) g_k(t) dt = -\lambda_k^{-1} \int_0^\infty \int_S \sin(\lambda_k t) g(x, t) \overline{\frac{\partial \psi_k}{\partial n}(x)} dx dt, \end{aligned} \quad (11.37)$$

where

$$g_k(t) = \int_S g(x, t) \overline{\frac{\partial \psi_k}{\partial n}(x)} dx.$$

One notices that this is a generalization to the case of variable sound speed of the expansion method of [463] discussed in Section 11.4.1. Unlike the algorithm of [463], this method does not use the whole space Green’s function for A (which is in this case unknown). However, computation of a large set of eigenfunctions and eigenvalues followed by the summation of the series (11.36) at the nodes of the computational grid may turn out to be too time-consuming. Thus, numerical feasibility of this technique is still untested.

Time reversal

Let us assume temporarily that the sound speed c is constant and the spatial dimension is odd. Then Huygens' principle guarantees that the sound wave will leave the region of interest Ω in time $T = c/(\text{diam } \Omega)$, so that $p(x, t) = 0$ for all $x \in \Omega$ and $t \geq T$. Now one can solve the wave equation back in time from $t = T$ to $t = 0$ in the domain $\Omega \times [T, 0]$, with zero initial conditions at T and boundary conditions on S provided by the data g collected by the detectors. Then the value of the solution at $t = 0$ will coincide with the initial condition $f(x)$ that one seeks to reconstruct. Such a solution of the wave equation is easily obtained numerically by finite difference techniques [306, 381]. The required number of floating point operations is actually lower than that of methods based on discretized inversion formulas ($\mathcal{O}(m^4)$ for time reversal on a grid $m \times m \times m$ in three dimensions versus $\mathcal{O}(m^5)$ for inversion formulas), which makes this method quite competitive even in the case of constant sound speed.

Most importantly, however, the method is also applicable if the sound speed $c(x)$ is variable and/or the spatial dimension is even. In these cases, the Huygens' principle does not hold, and thus the solution to the direct problem will not vanish within $\partial\Omega$ in finite time. However, the solution inside Ω will decay with time. Under the nontrapping condition, as shown in (C.3) (see [197, 776, 777]), the time decay is exponential in odd dimensions but only algebraic in even dimensions. Although, in order to obtain theoretically exact reconstruction, one would have to start the time reversal at $T = \infty$, numerical experiments (e.g., [381]) and theoretical estimates [380] show that in practice it is sufficient to start at values of T for which the signal becomes small enough, and to approximate the unknown value of $p(x, T)$ by zero. This works [137, 306, 381, 430, 809, 822] even in two dimensions (where decay is the slowest) and in inhomogeneous media. However, when trapping occurs, the “invisible” parts blur away (see Section 11.2.3 for the discussion).

A significantly more sophisticated version of time reversal was introduced and analyzed in [737]. It employs a smarter cut-off at time T , which takes into account the collected data. Amazingly, it leads to an equation with a contraction operator and thus can be improved quickly by iterations. This technique has been very successfully used recently [650].

One should notice that time reversal is a well-known and frequently employed technique in acoustics; see, e.g., [83, 229–232].

ART

Algebraic reconstruction techniques (ART) are still methods of choice in many cases, especially when analysis is lacking or gets too complicated for implementation. Since the scope of this text is mostly analytic, the reader is directed to numerous recent works (e.g., [154, 382, 431, 628, 650, 795, 797] and references therein) devoted to these techniques.

Remark 11.26. *It is important to mention that the ART, time reversal, and eigenfunction expansions do not suffer from the deficiencies of FBP formulas. Namely, they*

all work for inhomogeneous media, arbitrary shape of the (closed) observation surface, and the reconstruction inside the domain does not suffer from the support of $f(x)$ extending to its exterior [381, 445, 448].

Sound speed reconstruction

Unsurprisingly, all inversion procedures outlined in Section 11.4.2 rely upon the knowledge of the sound speed $c(x)$. Although often, e.g., in breast imaging, the medium is assumed to be acoustically homogeneous, this is not a good assumption in many other cases. It has been observed (e.g., [381, 390]) that replacing even slightly varying sound speed with its average value might significantly distort the image; not only the numerical values, but also the shapes of interfaces between the tissues will be reconstructed incorrectly. Thus, the question of estimating $c(x)$ correctly becomes important. One possible approach [390] is to use an additional transmission ultrasound scan to reconstruct the speed beforehand.

The question arises of whether one could determine the sound speed $c(x)$ and the tomogram $f(x)$ (assuming that f is not zero) simultaneously from the TAT data.³⁵

At the first glance, this seems to be an unreasonably ambitious project. Indeed, if we denote the forward operator \mathcal{W} by \mathcal{W}_c , to indicate its dependence on the sound speed $c(x)$, then the problem becomes, given the data g , to find both c and f from the equality

$$\mathcal{W}_c f = g. \quad (11.38)$$

Let us recall, though, that a similar situation arises in the SPECT emission tomograph, where the role of the sound speed is played by the unknown attenuation. As we discussed in Section 6.2.3, having the range of the forward operator of infinite co-dimension raises the possibility of such simultaneous reconstruction. It is known, for instance, that in SPECT the attenuation can be recovered for a “generic” f . Thus, the problem of recovering the sound speed from the TAT data is closely related to the range descriptions.

Numerical inversions using algebraic iterative techniques (e.g., [815, 820]) show that recovering both c and f might indeed be possible (at least, generically).

Not that much is known at the moment about this problem. Direct usage of range conditions attempted in [381] has led only to extremely weak and practically rather useless results so far. A revealing relation to the transmission eigenvalue problem well known in inverse problems (see, e.g., [143, 144, 163, 167, 415, 610, 747] and references therein) was recently discovered by D. Finch. Unfortunately, the needed transmission eigenvalue problem still remains unresolved (see partial results in [367–369, 584]). However, one can derive from this relation the

³⁵In fact, one needs only to determine $c(x)$ (without knowing f), since then the inversion procedures of Section 11.4 would apply to recovering f . However, experience shows that simultaneous reconstruction of both functions works better numerically. There is also numerical evidence that trying to recover $c(x)$ and $f(x)$ simultaneously improves reconstruction of the source f , even if the quality of the sound speed reconstruction is inferior.

following result (still not very useful in TAT) regarding uniqueness of the reconstruction of the sound speed, due to the works of M. Agranovsky and D. Finch (both apparently unpublished).

Theorem 11.27. *If two speeds satisfy the inequality $c_1(x) \geq c_2(x)$ for all $x \in \Omega$ and produce for some functions f_1, f_2 the same nonzero TAT data g (i.e., $\mathcal{W}c_1f_1 = g, \mathcal{W}c_2f_2 = g$), then $c_1(x) = c_2(x)$.*

It is known [387, Corollary 8.2.3] that if a function $f(x)$ is such that $\Delta f(x) \neq 0$ and for two acoustic speeds $c_1(x)$ and $c_2(x)$ it produces the same TAT data g , then $c_1 = c_2$.

Some partial results on numerical methods, uniqueness, and (in)stability of the speed reconstruction have been obtained recently in [367–369, 381, 390, 417, 427, 584, 598, 737, 820]. It is clear that the problem of finding the sound speed from the TAT data still requires significant analysis.

11.4.3 • Some numerical considerations and examples

In the constant speed case, discretization of the FBP formulas leads to accurate and efficient reconstruction algorithms. The 3D case is especially simple: Computation of derivatives in the formulas (11.17)–(11.21) and (11.29) can be easily done, for instance by using finite differences; this is followed by the backprojection (described by the integral over ∂B), which requires prescribing quadrature weights for quadrature nodes that coincide with the positions of the detectors.

The backprojection step is stable; the differentiation is a mildly unstable operation.

The sensitivity to noise in measurements across the various FBP formulas above seems to be roughly the same. It is very similar to that of the standard FBP algorithm of classical X-ray tomography.

In two dimensions, the implementation is just a little bit harder: The filtration step in formulas (11.25)–(11.27) can be reduced to computing two Hilbert transforms (see [445]), which, in turn, can be easily done in the frequency domain.

The number of floating point operations (flops) required by such algorithms is determined by the slowest backprojection step. In three dimensions, if the number of detectors is m^2 and the size of the reconstruction grid is $m \times m \times m$, the backprojection step (and the whole algorithm) will require $O(m^5)$ flops. In practical terms this amounts to several hours of computations on a single processor computer for a grid of size $129 \times 129 \times 129$.

In two dimensions, the operation count is just $O(m^3)$. As discussed in Section 11.1.4, the 2D problem needs to be solved when integrating line detectors are used. In this situation, the 2D problem needs to be solved m times in order to reconstruct the image, which raises the total operation count to $O(m^4)$ flops.

Fig. 11.10 shows three examples of simulated reconstruction using formula (11.25). The phantom we use (Fig. 11.10(a)) is a linear combination of several characteristic functions of disks and ellipses. Panel (b) illustrates the image recon-

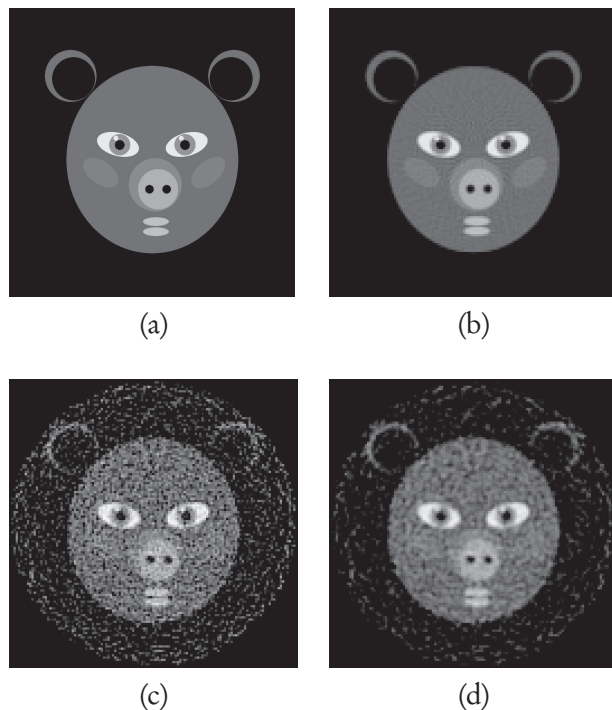


Figure 11.10. Example of a reconstruction using formula (11.25): (a) phantom, (b) reconstruction from accurate data, (c) reconstruction from data contaminated with 15% noise, (d) reconstruction from noisy data with additional smoothing.

struction within the unit circle from 257 equi-spaced projections each containing 129 spherical integrals. The detectors were placed on a concentric circle of radius 1.05. The image shown in Fig. 11.10(c) corresponds to the reconstruction from the simulated noisy data that were obtained by adding to projections values of a random variable scaled so that the L^2 intensity of the noise was 15% of the intensity of the signal. Finally, Fig. 11.10(d) shows how application of a smoothing filter (in the frequency domain) suppresses the noise; it also somewhat blurs the edges in the image.

11.4.4 • Reconstructions with partial (incomplete) data

Reconstruction formulas and algorithms of the previous sections work under the assumption that the acoustic signal is measured by detectors covering a closed surface S that completely surrounds the object of interest. However, in many practical applications of TAT, detectors can be placed only on a certain part of a surrounding surface. Such is the case, for example, when TAT is used for breast screening—one of the most promising applications of this modality. Thus, one needs methods and algorithms capable of accurate reconstruction of images from partial (incomplete) data, i.e., from the measurements made on open surfaces (or open curves in two dimensions). Regretfully, most inversion techniques that we

have discussed are based (explicitly or implicitly) on some sort of the Green's formula, Helmholtz representation, or eigenfunction decomposition for closed surfaces, and thus they cannot be extended to the case of partial data. Below we list various available options, although this topic still needs further development.

Remark 11.28. *Special cases of open acquisition surfaces are a plane or an infinite cylinder, for which exact inversion formulas are known. Of course, the plane or a cylinder would have to be truncated in any practical situation. The resulting acquisition geometry will not satisfy the visibility condition, and material interfaces whose normals do not intersect the acquisition surface will be blurred.*

Presence of invisible singularities

Even the case of an acoustically homogeneous medium is quite challenging if reconstruction needs to be done from partial data (i.e., when the acquisition surface S is not closed). As was discussed in Section 11.2.3, if the detectors are located around the object in such a way that the “visibility” condition is not satisfied, stable accurate reconstruction is impossible: The invisible interfaces will be smoothed out in the reconstructed image. Moreover, the values in smooth regions will also be incorrect. Only the visible singularities will be recovered correctly.

No invisible singularities

The situation changes when the whole object is in the visibility region. Then, if uniqueness of the reconstruction holds (see Section 11.3.3), the natural expectation is that there should be a stable way to recover the whole tomogram (as with the inversion of the classic Radon transform) [622, 737]. There are different ways to approach this issue, although this is an area that still needs a lot of work. We thus address briefly some approaches, as follows.

ART: Iterative algebraic techniques (see section 11.4.1) were among the first methods successfully used for reconstruction from surfaces only partially surrounding the object (e.g., [33, 34, 628]). Such methods are very slow. For example, reconstructions in [33] required the use of a cluster of computers and took 100 iterations to converge.

Parametrix-type reconstructions from partial data in homogeneous media were proposed in [36]. A couple of different parametrix-type algorithms were also proposed in [628]. They are based on applying one of the exact inversion formulas for full circular acquisition to the available partial data, with zero-filled missing data and some correction factors. Namely, since the missing data is replaced by zeros, each line passing through a node of the reconstruction grid will be tangent either to one or to two circles of integration. Therefore some directions during the backprojection step will be represented twice, and some only once. This, in turn, will cause some interfaces to appear twice stronger than they should be. The use of weight factors was proposed in [628] in order to partially compensate for this distortion. In particular, smooth weight factors (depending

on a reconstruction point) are assigned to each detector in such a way that the total weight for each direction is exactly one. This method is not exact; the error is described by a certain smoothing operator. However, the singularities (or jumps) in the image will be reconstructed correctly. As shown by numerical examples, such a correction significantly improves the reconstruction visually. Moreover, iterative refinement was proposed to further improve the image, and it is shown to work well in numerical experiments.

Some approaches for acoustically homogeneous media: Returning to noniterative techniques, one should mention an interesting attempt made in [631, 632] to generate the missing data using the moment range conditions for \mathcal{M} (see Section 5.10). The resulting algorithm, however, does not seem to recover the values well, although, as expected, it reconstructs all visible singularities.

An accurate 2D noniterative algorithm for reconstruction from data measured on an open curve S was proposed in [464]. It is based on precomputing approximations of plane waves in the region of interest Ω by the single layer potentials of the form

$$\int_S Z(\lambda|y-x|)\rho(y)dl(y),$$

where $\rho(y)$ is the density of the potential, which needs to be chosen appropriately, $dl(y)$ is the standard arc length, and $Z(t)$ is either the Bessel function $J_0(t)$ or the Neumann function $Y_0(t)$. Namely, for a fixed ξ one numerically finds the densities $\rho_{\xi,J}(y)$ and $\rho_{\xi,Y}(y)$ of the potentials

$$W_J(x, \rho_{\xi,J}) = \int_S J_0(\lambda|y-x|)\rho_{\xi,J}(y)dl(y), \quad (11.39)$$

$$W_Y(x, \rho_{\xi,Y}) = \int_S Y_0(\lambda|y-x|)\rho_{\xi,Y}(y)dl(y), \quad (11.40)$$

where $\lambda = |\xi|$, such that

$$W_J(x, \rho_{\xi,J}) + W_Y(x, \rho_{\xi,Y}) \approx \exp(-i\xi \cdot x) \quad \text{for all } x \in \Omega. \quad (11.41)$$

Obtaining such approximations is nontrivial. One can show that exact equality in (11.41) cannot be achieved, due to different behavior at infinity of the plane wave and the approximating single-layer potentials. However, as shown by numerical examples in [464], if each point in Ω is visible from S , very accurate *approximations* can be obtained, while keeping the densities $\rho_{\xi,J}$ and $\rho_{\xi,Y}$ under certain control.

Once the densities $\rho_{\xi,J}$ and $\rho_{\xi,Y}$ have been found for all ξ , the function $f(x)$ can be easily reconstructed. Indeed, for the Fourier transform $\hat{f}(\xi)$ of $f(x)$,

$$\hat{f}(\xi) = \frac{1}{2\pi} \int_{\Omega} f(x) \exp(-i\xi \cdot x) dx,$$

one obtains, using (11.41),

$$\begin{aligned} \hat{f}(\xi) &\approx \frac{1}{2\pi} \int_{\Omega} f(x) [W_J(x, \rho_{\xi,J}) + W_Y(x, \rho_{\xi,Y})] dx \\ &= \frac{1}{2\pi} \int_S \left[\int_{\Omega} f(x) J_0(\lambda|y-x|) dx \right] \rho_{\xi,J}(y) dl(y) \\ &\quad + \frac{1}{2\pi} \int_S \left[\int_{\Omega} f(x) Y_0(\lambda|y-x|) dx \right] \rho_{\xi,Y}(y) dl(y), \end{aligned} \quad (11.42)$$

where the inner integrals are computed from the data g :

$$\int_{\Omega} f(x) J_0(\lambda|y-x|) dx = \int_{R^+} g(y, r) J_0(\lambda r) dr, \quad (11.43)$$

$$\int_{\Omega} f(x) Y_0(\lambda|y-x|) dx = \int_{R^+} g(y, r) Y_0(\lambda r) dr. \quad (11.44)$$

Formula (11.42), in combination with (11.43) and (11.44), yields values of $\hat{f}(\xi)$ for arbitrary ξ . Now $f(x)$ can be recovered by numerically inverting the Fourier transform, or by a reduction to a FBP inversion [559] of the regular Radon transform.

The most expensive part of the algorithm, which is computing the densities $\rho_{\xi,J}$ and $\rho_{\xi,Y}$, needs to be done only once for a given acquisition surface. Thus, for a scanner with a fixed S , the resulting densities can be precomputed once and for all. The actual reconstruction part then becomes extremely fast.

Examples of reconstructions from incomplete data using this technique of [464] are shown in Fig. 11.11. The images were reconstructed within the unit square $[-1, 1] \times [-1, 1]$, while the detectors were placed on the part of the concentric circle of radius 1.3 lying to the left of line $x_1 = 1$. We used the same phantom as in Fig. 11.10(a); the reconstruction from the data with 15% noise added is shown in Fig. 11.11(b); panel (c) demonstrates the results of applying an additional smoothing filter to reduce the effects of noise in the data.

Acoustically inhomogeneous media

The problem of numerical reconstruction in TAT from the data measured on open surfaces in the presence of a known variable sound speed currently remains

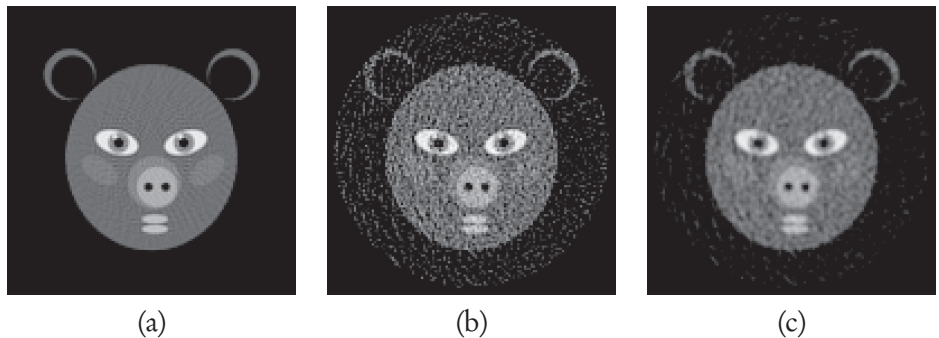


Figure 11.11. Examples of reconstruction from incomplete data using the technique of [464]. Detectors are located on the circular arc of radius 1.3 lying to the left of the line $x_1 = 1$. (a) Reconstruction from accurate data, (b) reconstruction from the data with added 15% noise, (c) reconstruction from noisy data with an additional smoothing filter.

largely open (except successful but computationally expensive ART attempts). One of the difficulties was discussed in Section 11.2.3: Even if the sound speed $c(x)$ is nontrapping, it can happen that some of the characteristics escape from the region of interest to infinity without intersecting the open measuring surface. Then stable reconstruction of the corresponding interfaces will become impossible. It should be possible, however, to develop stable reconstruction algorithms in the case when the whole object of interest is located in the visible zone.

The generalization of the method of [464] (see the previous subsection) to the case of variable sound speed is so far problematic, since this algorithm is based on the knowledge of the open space Green's function for the Helmholtz equation. In the case of a nonconstant $c(x)$, this Green's function is position-dependent, and its numerical computation is likely to be prohibitively time-consuming.

A promising approach to this problem, currently under development, is to use time reversal with the missing data replaced by zeros, or maybe by a more clever extension (e.g., using the range conditions, as in [631, 632]). This would produce an initial approximation to $f(x)$, which one can try to refine by fixed-point iterations; however, the pertinent questions concerning such an algorithm remain open.

An interesting technique of using a reverberant cavity enclosing the target to compensate for the missing data is described in [179, 468].

11.5 • Chapter's final remarks and conclusions

We list here some unresolved issues in the mathematics of TAT/PAT, as well as some developments that were not addressed in the main text.

1. The issue of uniqueness acquisition sets S (i.e., such that transducers distributed along S provide sufficient information for TAT reconstruction) can be considered to be resolved, for most practical purposes. However, there

remain significant unresolved theoretical questions. One of them consists of proving an analogue of Theorem 11.9 for noncompactly supported functions with a sufficiently fast (e.g., superexponential) decay at infinity. The original (and the only known) proof of this theorem uses microlocal techniques [10, 736] that significantly rely upon the compactness of support. However, one hopes that the condition of a sufficiently fast decay should suffice for this result. In particular, there is no proven analogue of Theorem 11.6 for nonclosed sets S (unless S is an open part of a closed analytic surface).

Techniques developed in [225] (see also [21] for their further use in TAT) might provide the right approach.

This also relates to the still unresolved situation in dimensions three and higher. Namely, one would like to prove Conjecture 11.10.

2. Concerning the inversion methods, one notices that closed-form formulas are known only for spherical, ellipsoidal, cylindrical, and planar smooth acquisition surfaces. The question arises of whether closed-form inversion formulas could be found for any other smooth closed surface. It is the belief of the author that the answer to this question is negative.

Another feature of the known closed-form formulas that was mentioned before is that they do not work correctly if the support of the function $f(x)$ in question lies partially outside the acquisition surface. Time reversal, ART, and eigenfunction expansion methods do not suffer from this deficiency. The question arises of whether one could find closed-form formulas that reconstruct the function inside S correctly, despite its having part of its support outside. Again, the author believes that the answer is negative.

3. The complete range description of the forward operator \mathcal{W} in even dimensions is still unknown. It is also not clear whether one can obtain complete range descriptions for nonspherical observation sets S or for a variable sound speed. The moment and orthogonality conditions do hold in the case of a constant speed and arbitrary closed surface, but they do not provide a complete description of the range. For acoustically inhomogeneous media, an analogue of orthogonality conditions exists, but it also does not describe the range completely.
4. The problem of unique determination of the sound speed from TAT data is still largely open.
5. In the standard X-ray CT, as well as in SPECT, the so-called **local tomography** technique [214, 449] is often very useful. It allows one to emphasize singularities (e.g., tissue interfaces) of the reconstruction in a stable way. This holds even in the case of incomplete data, when the invisible parts will be lost. An analogue of local tomography can be easily implemented in

TAT, for instance, by introducing an additional high-pass filter in the FBP-type formulas.

6. The mathematical analysis of TAT presented in the text did not take into account the issue of modeling and compensating for the **acoustic attenuation**. This subject is currently actively discussed (see, e.g., [29, 137, 432, 545, 633]), but probably cannot be considered completely resolved.
7. **Quantitative PAT (QPAT)**. This chapter was centered on finding the initial pressure $f(x)$. This pressure is proportional to the initial energy deposition, which, in turn, is related to the optical parameters (attenuation and scattering coefficients) of the tissue. These parameters are in fact the ones we would like to recover. QPAT addresses the issue of recovering them from the energy deposition found in PAT. This is a highly nontrivial issue (see, e.g., [62, 73, 75, 76, 76, 181, 182, 182, 505, 669, 671, 672, 752, 815]). It will also be touched upon in Chapter 13.
8. The TAT technique discussed in this chapter uses **active interrogation** of the medium. There is a discussion in the literature of a **passive version of TAT**, where no irradiation of the target is involved [630].

Chapter 12

Ultrasound Modulation in EIT and OT

We have already briefly discussed the promising electrical impedance and optical tomography methods (see Chapter 10). As we noticed there, these inexpensive and high contrast imaging techniques suffer from high instability and low resolution. The reason is that both photons in OT and currents in EIT “forget” the details of their traveled paths by the time they reach the observation boundary and contribute to the signal. The idea of ultrasound modulation is to try to attach to the boundary measurements an additional mark, which would indicate some internal location. Namely, one focuses an ultrasound (US) beam at a chosen internal location x . Due to the US irradiation, optical and electrical properties of the tissue at the point x will be slightly affected. This should leave a signature on the optical or electrical impedance measurement conducted at the boundary. Thus, one gets some “internal information”—a boundary signal depending on the internal location x . Since this is exactly the type of information that is lost in the standard EIT and OT procedures, the hope is that such ultrasound modulation (or internal information in general) might make the reconstructions much stabler.

We refer the reader to Chapter 13 for more details on the problems with internal information, while here we concentrate on the cases of ultrasound modulated EIT (acousto-electric tomography, AET) and ultrasound modulated optical tomography (UMOT).

Remark 12.1. *There are some obvious difficulties with ultrasound modulation:*

- *Good focusing can be done in a known acoustic medium, which is usually not what we have. One thus mostly assumes acoustic homogeneity.*
- *Even if the medium is acoustically homogeneous, the quality of focusing that one can practically achieve is far from the desirable one. This is where the idea of synthetic focusing kicks in (see Section 12.2).*

12.1 ▪ AET (acousto-electric tomography)

It has been known for some time that ultrasound irradiation of soft tissues modifies the tissues' electrical and optical properties (**acousto-electric effect** [475, 476, 693]). It was thus a natural step to decide to send an ultrasound beam that focuses on some internal location x and thus modifies (by a multiplicative factor close to 1) the electrical conductivity $\sigma(x)$ at this location (see Fig. 12.1). This might lead to a detectable perturbation of the boundary EIT measurements, and, what is crucial, one will know where the perturbation came from—from the point x . Then one may scan the focused beam throughout the whole object and get hopefully sufficient information for a stable reconstruction. This idea of AET was suggested and tried by a direct measurement in [821]. It was shown there that a detectable (albeit rather small) signal does exist. However, no reconstruction was done at that time. In the next few years, the topic started developing fast [26, 27, 31, 112, 149, 247, 249, 422, 446, 447, 467, 469, 821], often with the researchers being unaware of the original work [821]. Let us briefly describe the current state of affairs in AET (although by the time of publication, the situation will definitely have changed).

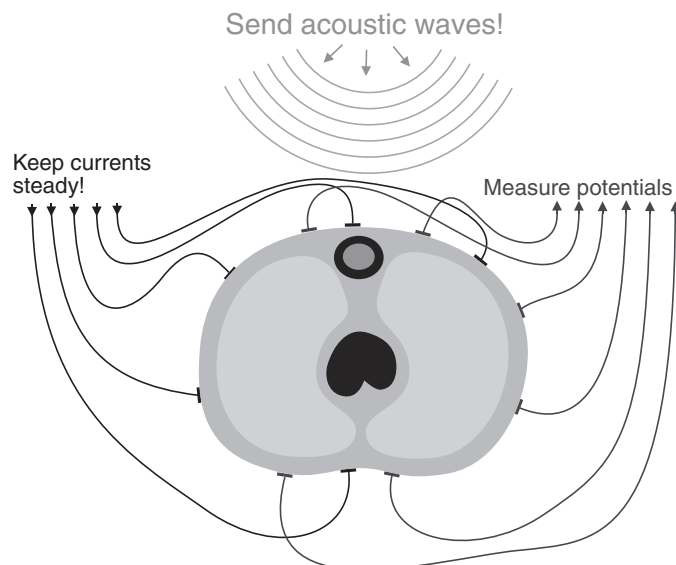


Figure 12.1. The AET procedure: Electrical boundary measurements are done concurrently with scanning the object with ultrasound.

The following observation was made experimentally and justified theoretically [475, 476, 821]: The acousto-electric effect, although detectable, is very small. This allows one to safely linearize the problem.³⁶

³⁶The reconstructions that we present later in this section were done with the fully nonlinear forward computation, but with the reconstruction using linearization. The pictures clearly show that the linearization did not introduce any noticeable artifacts.

Another smallness assumption was used in many works: the ability of sharp focusing at a given location (i.e., creating a delta-type ultrasound pulse). Such perfect focusing is clearly impossible (see the discussion in the book [363] devoted to this issue). Still, let us assume for the time being that sufficiently good focusing is possible and return to this discussion in Section 12.2. This allows one to use “small volume inclusion” asymptotics, as in [26, 27, 149, 150], where such asymptotics play a major role. This is, however, overkill, and in [446, 447] only smallness of the acousto-electric effect is needed; no perfect focusing is required (see Section 12.2).

In all these works the authors discovered that some interior quantities can be stably recovered from the ultrasound modulated measurements if perfect focusing (in particular, small volume asymptotics) is possible. For instance, if $u_1(x), u_2(x)$ are the (unknown) potentials created by two boundary current setups, then one can recover the values

$$\sigma(x)\nabla u_1(x) \cdot \nabla u_2(x)$$

for any interior point x , where $u \cdot v$ denotes the inner product of two vectors. In particular, the quantity $\sigma(x)|\nabla u(x)|^2$ can be recovered.

It was shown that such values, if recovered from measurements, lead to locally unique and stable reconstruction of the conductivity σ [112, 149, 446, 447, 456]. Essentially, one can prove that the Fréchet derivative of the mapping

$$\sigma \mapsto \text{values of } F(\sigma, u_i, \nabla u_i) := \sigma(x)|\nabla u(x)|^2$$

(in appropriate function spaces) is an injective semi-Fredholm operator (see Chapter 13).

A variety of inversion procedures has been introduced and in most cases tested on numerical phantoms: those involving numerical optimization [27, 149], those reduced to solving well-posed hyperbolic problems [60], or those that lead to solving transport equations or Poisson-type elliptic equations [446, 447].

In most cases one can achieve wonderful quality reconstructions; e.g., see Fig. 12.2, where the method of [447] is used, which reduces to solving a Poisson equation to determine the conductivity.

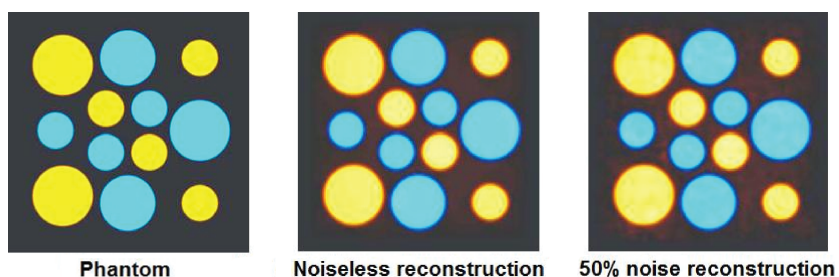


Figure 12.2. An example of AET reconstruction. [447]

Looking at the reconstruction with noise in Fig. 12.2, one should feel cheated. Indeed, how can one get such a good reconstruction with the data contaminated by 50% noise? The answer will be given in Section 12.2.

Remark 12.2.

- *There is a well-known significant technical difference between the 2D and 3D situations. Namely, a lot of analysis and reconstruction depends upon one's ability to create a boundary current (or several) such that the internal current does not vanish (correspondingly, the internal currents are linearly independent). Since the internal conductivity is unknown, this is not a simple question at all. This is known to be possible in two dimensions [14] and in general impossible in dimension three and higher [474].*
- *Using a hyperbolic approach (which usually requires only a single current pattern) does lead to reconstructions, but due to propagation of singularities, it creates some streak artifacts.*
- *In three dimensions, one can sometimes (e.g., near constant conductivity) get away with using two current patterns, which leads to solving slice-by-slice the 2D Poisson equation. Due to 2D ellipticity, there are no singularity propagation artifacts. However, the wavefront vectors orthogonal to the slices are not captured, which leads to tiny (but often noticeable) blurring of the horizontal (i.e., parallel to the slices) interfaces [447].*
- *Using three currents under some independence condition (achievable near constant conductivity) leads to solving the 3D Poisson equation with no wavefront vectors lost and high quality overall reconstruction [447].*
- *Analysis shows [78, 456] that in general the number of currents required for achieving full ellipticity is higher than the dimension of the space.*

Currently, the mathematics of AET, albeit just a few years old, is already rather successful. The mathematics usually lags behind in such topics. Surprisingly, the situation is different in this case, and experimental implementation of the AET still faces difficulties, due to the difficulty of acquiring good SNR.

Another combination of ultrasound and EIT is suggested in [249]. Here one again creates currents through the interior of the body of interest. These currents lead to a small inhomogeneous heating of the tissues, and thus to thermoelastic expansion. Then the TAT procedure, using the microphones surrounding the body, reconstructs a local functional $F(\sigma(x), u(x), \nabla u(x))$, after which one of the previously mentioned procedures of reconstruction can be applied.

12.2 • Synthetic focusing

As we have mentioned, perfect US focusing is not feasible [363]. It is, however, assumed in most mathematical work on AET, especially when using the small volume asymptotics. As was explained in [446] and then confirmed in [447], this is

avoidable. Indeed, the delta-functions (idealized perfectly focused beams), form a function “basis.” One could try to produce another, practically feasible, set of ultrasound waves which also forms a basis. Then, using the smallness of the acousto-electric effect, and thus linearity, one could mathematically process the data obtained from that basis of waves and “synthetically focus” them by changing the basis to the one of delta-functions.

We now list several examples of possible bases [446]:

- Using large planar broad-band transducers, one could generate a set of monochromatic planar waves with arbitrary wave vectors, and then the synthetic focusing would be just applying the inverse Fourier transform. The practical feasibility of this option is not yet clear.
- Using point-like omnidirectional transducers, one could generate thin spherical shell waves. Then, lo and behold, the synthetic focusing would boil down to inversion of a restricted spherical mean transform, and thus any of the standard TAT inversions would do it. This is the option of [447]. The hurdle seems to be that it is much easier to create a short N-shaped spherical wave (Fig. 12.3), than a δ -shaped spherical shell wave. We’ll see below that this “hurdle” turns out to be a blessing.



Figure 12.3. An N-shaped pulse.

- Instead of spherical shell waves, one could also use monochromatic spherical waves for scanning [443, 446, 447]. Using such waves has the advantage that the resulting boundary measurement will oscillate with US frequency. Hence, temporal Fourier transform enables one to selectively pick up this frequency, thus reducing the effects of the noise.
- One could create narrow “pencil beams,” as is done in [798]. Then synthetic focusing could be approximated with the inversion of the standard X-ray transform. This option has been tried and still struggles with the impossibility of creating a truly homogeneous pencil US beam of sufficient length [363].

Let us compare on a numerical example the application of physical and synthetic focusing to noiseless image reconstruction in AET. We simulated numerically a square domain, with the electrical currents equal to 1 on the left and right

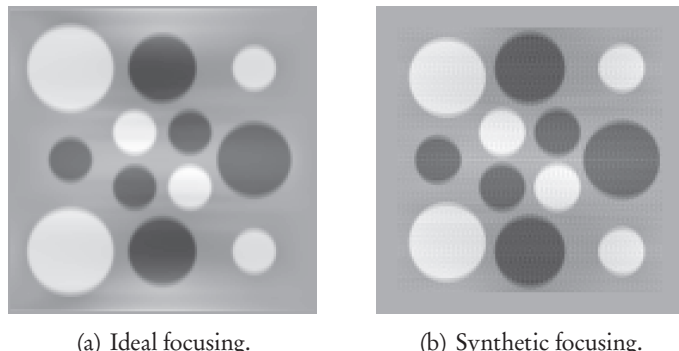


Figure 12.4. Comparison of AET reconstructions using ideal focusing (a) versus synthetic focusing (of spherical pulse waves) (b) [446].

sides of the square and 0 on the top and the bottom. The conductivity $\sigma(x)$ that we used in our experiments was close to 1; the density plot of the logarithm $\log \sigma(x)$ is shown in Figure 12.2(a). In this figure the yellow circles correspond to the value $\log \sigma(x) = 0.05$, the blue ones represent the value of $\log \sigma(x) = -0.05$, and the gray background depicts $\log \sigma(x) = 0$. The simulated electric potential was “measured” on the whole boundary of the square.

As mentioned previously, Figure 12.2(b) presents the result of AET reconstruction from simulated measurements corresponding to perfectly focused US modulation. For convenience, we repeat this image in Figure 12.4(a). The AET reconstruction of the same phantom, obtained by using synthetic measurements, is shown in Figure 12.4(b). In this example we modeled the perturbations of electric potential on the boundary caused by the spherical pulse waves with the centers on a circle surrounding our square domain. A total of 300 transducers and 800 different radii of outgoing spherical pulses per transducer were simulated. The reconstruction shown in Figure 12.4(b) was computed by using synthetic focusing to obtain $l(x, y)$ and then by reconstructing conductivity $\sigma(x)$. (Again, the methods for reconstructing σ from l will be discussed elsewhere.) As before, no noise was added to the simulated measurements. The reconstructed image is clearly as good as the one obtained using perfectly focused US modulation (12.4(a)).

We can now disclose the secret of the impossibly sharp reconstruction with 50% noise shown in Fig. 12.2. The trick is that it was done using the synthetic focusing that uses thin N-shaped spherical waves, with consecutive TAT inversion for the synthetic focusing. The presence of the N-shape happens to take care of the filtration step in TAT inversion. What remains to do is only the backprojection, which is a smoothing operator, removing most of the noise.³⁷ After that, an elliptic (Poisson-type) equation was solved to recover the conductivity.

³⁷If we could indeed produce and use δ -shaped pulses, the reconstruction would work but would be very unlikely to survive a 50%, or even much weaker, noise.

12.3 • Ultrasound modulated optical tomography (UMOT)

The idea of scanning an object with focused US, which we applied in AET, can be tried with optical tomography (OT) as well. The goal is the same: to drastically improve the resolution of OT (which is dismal at a centimeter depth and deeper). Since OT, like EIT, is a cheap, safe, and high contrast modality, achieving this goal, and thus adding high resolution, would make it an invaluable diagnostic tool.

In comparison with AET, the situation with **UMOT** is reversed: There is an extensive body of experimental research (see [798] and references therein), but the first glimpses on the mathematics of UMOT are just appearing [15, 77, 549, 550], and even the mathematical model is not completely settled down yet.

The setup of this modality is as follows: One sends a beam of (coherent or incoherent) laser light through the body of interest and observes at the boundary the intensity and speckle patterns of the outgoing light. The features to recover are the internal distributions of the absorption and scattering coefficients.

The contrast in optical properties of cancerous and healthy locations is often huge. However, diffused photons, when they reach a detector after multiple scattering, lose any memory about the locations that they went through. This leads to dismal resolution at a centimeter's depth (although good pictures can be obtained at skin depth with various incarnations of OT, e.g., in widely used in ophthalmology OCT (**optical coherence tomography**)).

The idea of UMOT is to scan the body with focused US, concurrently with taking OT measurements. One thus acquires some interior (i.e., location dependent) information, which hopefully can stabilize the problem. According to the physics and biomedical engineering literature (e.g., [411, 482, 798]), when using coherent light and measuring the US frequency Fourier component of the outgoing speckle pattern, one can practically recover the values of the following functional at an interior location x :

$$G(x, d)A^2(x)I(x).$$

Here A is the applied US power (assumed to be known), I is the light intensity, d is the detector position on the boundary, and $G(x, d)$ is the “probability that a photon emitted at the location x will reach the detector at the location d .” In other words, $G(x, d)$ is a Green's function of the diffusion equation

$$-\nabla D(x)\nabla I(x) + \mu_a(x)I(x) = 0$$

inside the domain of the interest. There was some ambiguity concerning what boundary condition the Green's function satisfies. (As was shown in [457], this is irrelevant for stabilizing the problem.) It was assumed in [15] that the correct boundary conditions are those that correspond to the optical impedance at the boundary of the object. Under this condition and with the perfect focusing assumption, a reconstruction algorithm was applied that showed sufficiently sharp internal reconstructions of the absorption coefficient μ_a (see Fig. 12.5). The image sharpness, however, looks lower than in the AET case. This is to be expected,

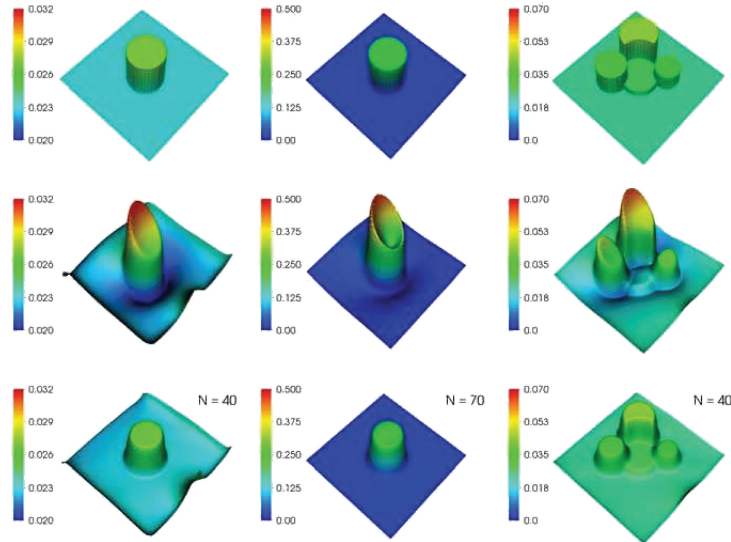


Figure 12.5. UMOT reconstructions: Top row—the phantoms; middle row—initial run of the algorithms; bottom row—reconstructions after 40 iterations (see [15]).

as will be explained in Chapter 13. It was also shown in [15]³⁸ that the formally computed Fréchet derivative of the forward mapping is a semi-Fredholm operator in natural function spaces. However, injectivity of this derivative was not shown. Thus there are so far no local injectivity results (some probably could be obtained using the technique of [457]).

Some controversy also surrounds the usage of coherent light. It is claimed in the engineering literature [798] that the signal from US modulation in the case of incoherent light has thus far been undetectable. However, there already are some mathematical studies of UMOT using incoherent light [77].

Synthetic focusing in UMOT is also possible. However, while the spherical waves should still be able to do the job, the use of planar waves and the consequent inversion of the Fourier transform seems to be not an option here, due to the presence of the *square* of the acoustic power $A(x)$ in the measured functional.

One of the UMOT reconstruction methods, suggested in [484] (see also the description of this work in [798]), appears to be, in fact, synthetic focusing. Indeed, the authors of [484] employed the observation that the focusing was imperfect: The focal zone of the ultrasonic waves was 2 mm across and 20 mm in length, which made it a better approximation to a segment rather than a point. As far as we understand the procedure of [484], by shifting and rotating the focusing area, an approximation to the X-ray transform of the kernel $l(x, y)$ (as before, with respect to the variable x) was obtained. Then standard X-ray inversion formulas were used to recover the kernel l , which was treated as the image.

³⁸See also the acknowledgments of the author's contribution there.

12.4 • Chapter's final remarks and conclusions

- **Other hybrid variations of EIT: MREIT, CDI, CDII.**

It has been found that the very unstable EIT problem can be stabilized if, during an EIT scan, one simultaneously runs an MRI scan. This can be done in different ways. The two well developed approaches are MREIT [708, 803] and CDI/CDII [546–548]. In both cases, one obtains the values inside the object of some function of the unknown conductivity and current(s). We cannot discuss these very interesting and mathematically deep methods in any detail, although they will be parts of a general discussion of the methods that provide some interior information in Chapter 13.

- **Hybrid variations of elastography: Magnetic resonance elastography (MRE), sonoelastography.**

The situation here is somewhat similar to the MREIT/CDI in the previous bullet section. Namely, during an elastography experiment, one would like to observe the wavefront propagation inside the body, to gather some “internal information.” There are two approaches being developed (and already going commercial): magnetic resonance elastography (MRE) [62, 62, 506, 523, 543, 709] and sonoelastography [245, 389, 521, 522, 525]. In the first, an MRI scan is used, while the second uses ultrasound. Again, we cannot include any details here, and recommend that the reader look at the texts mentioned above and the references in them.

- **SAR (synthetic aperture radar)**

SAR does not fall into the framework of hybrid methods. The reason it is featured here is its close connections with the techniques of the spherical mean Radon transforms, which were prominent in TAT (Chapter 11). This, as well as many other interesting mathematical problems arising in SAR, can be found in the very nice surveys [157, 158].

Chapter 13

Inverse Problems with Interior Information

As we have already noticed, many hybrid problems remove the instability of single-mode problems (such as EIT, OT) by being able to produce the *internal* values of a function of the unknown parameters of the problem (electrical conductivity, absorption coefficient, current, voltage, etc.). This is a clear break with the main deficiency of the unstable methods—that all the data is collected at the boundary, and some information has a hard time getting to the boundary. One can thus hope that by obtaining such “insider information,” one could possibly get a more stable reconstruction.³⁹

Before going into this discussion, let us introduce one more example of such a problem, which is extremely important and actively studied currently [62, 73, 75, 76, 76, 181, 182, 182, 505, 669, 671, 672, 752, 815]: the so-called **quantitative photoacoustic tomography (QPAT)**, previously mentioned in passing.

When the PAT inversion procedure is completed, one obtains the initial pressure $f(x)$ (Chapter 11), which in turn is proportional to the distribution of the electromagnetic energy absorbed. One can argue that this boils down to having in our hands the function

$$\Gamma(x)\mu(x)u(x),$$

where $\Gamma(x)$ is the so-called Grüneisen parameter, which we will assume to be constant (or at least known)⁴⁰ and thus neglect. Here $\mu(x)$ is the light absorption parameter (it is indeed the quantity we are after), and $u(x)$ is the **unknown** light intensity inside the object. This is our “internal information,” from which we need to reconstruct the optical parameter $\mu(x)$ (and preferably also the scattering coefficient). Many other hybrid methods (CDI, AET, OT, MREIT) also provide the interior values of some functionals of the form

$$F(\sigma(x), u_i(x), \nabla u_i(x)). \quad (13.1)$$

They all make the formerly unstable problems stable.⁴¹

³⁹In this case, fortunately, trading insider information does not put you in jail, even in inverse crime jail. ☺

⁴⁰Which is not entirely true, sorry.

⁴¹In (13.1) we use the EIT notation; thus $\sigma(x)$ is the conductivity and $u_j(x)$ are the interior potentials (assuming that several experiments are done).

What is going on? Is there any (hopefully simple) reason, besides the hand-waving we produced before, for this to happen? The answer is a “yes” [456, 457], as we will try to indicate in this chapter.

Let us sketch our approach. Suppose we want to recover the values of the conductivity function $\sigma(x)$ (or some other parameters of interest) inside a bounded domain from the data (13.1). This means solving the nonlinear equation $A\sigma = F$, where $A : \sigma \mapsto F$ is the forward operator producing the interior data F . Would solving this equation be stable in the sense of some appropriate norms? The natural approach is to take the Fréchet derivative dA of A , if it exists in an appropriate Banach function space, and consider the stability of solving the linearized equation $dA\sigma = g$ first. What we would like to get is the continuous left invertibility of the operator dA . The second best thing would be to realize that dA is **Fredholm**, or at least (more realistically) a **left semi-Fredholm operator** (see Appendix D). This would tell us that, modulo possibly having a finite-dimensional kernel, the solution of the problem is stable.

Now, how could one get a left semi-Fredholmity statement? As one can see from Appendix D, the left semi-Fredholm property is equivalent to the existence of a **left regularizer** B such that $BdA = I + C$, with a compact operator C . How can one hope to construct an “inverse modulo compact operator”? If dA happens to be an elliptic **pseudodifferential operator** (Ψ DO) in a bounded domain, the Ψ DO technique does exactly this.

We thus have the following program:

1. Prove Fréchet differentiability.
2. Find out whether dA is a Ψ DO.
3. Check whether dA is elliptic in some sense (see the discussion later on in this chapter of what this means).
4. If yes, it has a (left) parametrix and thus is (semi-)Fredholm.
5. If not, maybe one can add more measurements to have an (overdetermined now) operator dA that is elliptic.
6. If successful, prove that dA indeed has a zero kernel (rather than a finite-dimensional one).
7. If successful, use an appropriate inverse function theorem to prove **local nonlinear uniqueness**⁴² for the operator A .

The first five steps work smoothly in all hybrid problems with internal information that we have tried.

The sixth step, proving absence of the kernel, is always much harder (and we believe does not hold as generally as the first five steps do). It is believable, though,

⁴²Global uniqueness results are much harder and cannot be handled in this simple way.

that “generically” (in the space of media parameters) the Fréchet derivative should have no kernel. This is discussed in Section 13.3.

Finally, even with the first six steps working out, going from the linearized to local nonlinear uniqueness is nontrivial. Indeed, experience with these problems shows that, unfortunately, the spaces where Fréchet differentiability is proven do not match those where Fredholmity holds. Thus, the standard (infinite-dimensional) calculus inverse/implicit function theorem does not apply, and one probably has to resort to much more sophisticated versions, such as those from [374, 375, 540, 551, 586, 587, 609, 735]. This has been done in at least one situation in [537].

Let us look at step 2. Why in the world would you expect the differential to be a Ψ DO? The reasoning (rather than a rigorous proof) is the following. If we recall Peetre’s theorem [639], which we have invoked before, then the criterion for a linear operator A to be a differential operator is **locality**; i.e., the support of Af should never exceed the support of f . Analogously, the criterion for an operator being a Ψ DO is **pseudolocality**: The **singular support** of Af should never exceed the **singular support** of f . In other words, the operator A should not create singularities where there were none originally. Let us now look at our operator $A : \sigma(x) \mapsto F(\sigma(x), u(x), \nabla u(x))$, ignoring its nonlinearity. (Remember that our considerations are hand-waving anyway.) Here in all our examples $\sigma(x)$ is a coefficient of an elliptic equation, and $u(x)$ is its solution. Wherever the coefficient $\sigma(x)$ is smooth, due to ellipticity, the solution $u(x)$ is smooth as well. If now the external function $F(\cdot, \cdot, \cdot)$ is smooth, we have the pseudolocality property, at least for our nonlinear operator.

Before going into some detail, to avoid misunderstanding, it is worth mentioning what the program above can try to achieve and what it cannot.

There are quite a few recent works (e.g., [61, 66, 67, 422, 456, 457, 537, 546–548]) where some individual cases of problems with internal information are considered in great detail. Reconstruction procedures, uniqueness (at least local) theorems, stability estimates, etc., were established. These are usually technically challenging tasks, and what is described below does not replace any of these achievements. What it does, though (besides being very simple) is the following:

- It quickly determines whether the interior information that one has is expected to stabilize the problem.
- If the answer is “yes,” it immediately shows which are the correct spaces where the stability estimates should hold. (E.g., recoveries of the absorption coefficient and of the diffusion coefficient naturally come out with different stability estimates.) Thus, you know in advance what the optimal estimate should look like.
- If the answer is “no,” often you can easily determine whether several additional measurements can help out, and what the requirements for these measurements would be.

Again, the difficult analysis is still needed to actually prove the estimates (in particular, establishing the linearized uniqueness) and to then derive nonlinear results. It is much better to do this, though, when one knows what the right answer should be.

13.1 ▪ The QPAT example worked out (well, sketched)

Here we sketch the results of the steps of the program described above, when applied to QPAT. The details of calculations [456, 457] are very simple and easy to recover.

Let us recall that in QPAT (at least in diffusion approximation) one strives to recover the coefficients of the diffusion equation boundary value problem:

$$\begin{cases} -\nabla \cdot (e^{\sigma(x)} \nabla u(x)) + e^{\gamma(x)} u(x) = 0 & \text{in a nice bounded domain } \Omega, \\ u|_{\partial\Omega} = f(x). \end{cases} \quad (13.2)$$

Here it is more convenient for us to use the log-diffusion coefficient $\sigma(x)$ instead of the diffusion coefficient $D(x) = e^{\sigma(x)}$. The same goes for the log-absorption coefficient $\gamma(x)$.

The data in hand is the function

$$F(x) := e^{\gamma(x)} u(x)$$

inside the domain.

In order to make the considerations simpler, we assume that $\sigma(x)$ is known near the boundary.

We allow σ to belong to $L^\infty(\Omega)$, being equal to 0 in a given shell near the boundary. We assume that $\gamma \in H^1(\Omega)$ also vanishes near the boundary.

Suspecting that a single measurement might not be enough, we leave the freedom of imposing a number of different boundary data $f_j(x)$, $j = 1, \dots, k$, and the corresponding solutions $u_j(x)$, and thus also the data $F_j(x)$. Let us start with just two (after all, we do have two unknowns, don't we?) and consider the vector operator $\mathbf{F} = (F_1, F_2)^t$. One can prove [456, Lemma 2.1] that the mapping $(\sigma, \gamma) \mapsto \mathbf{F}$ is Fréchet differentiable in appropriate spaces at any pair of smooth functions (σ_0, γ_0) . After that, the Fréchet derivative can be found easily by a formal expansion, such as $\sigma = \sigma_0 + \delta\sigma + O(|\delta\sigma|^2)$, etc. This results in a matrix PDO with the principal symbol

$$A(x, \xi) = \begin{pmatrix} \frac{i\xi \cdot \nabla u_0^1}{|\xi|^2} & u_0^1 \\ \frac{i\xi \cdot \nabla u_0^2}{|\xi|^2} & u_0^2 \end{pmatrix}. \quad (13.3)$$

Is it elliptic (and if yes, in what sense)? One notion of ellipticity (**Petrovsky ellipticity**) of a square system requires that the determinant of the matrix that contains

only the highest order terms of the symbol not vanish for nonzero real vectors ξ . Immediate calculation shows that this condition requires that

$$\xi \cdot (u_0^1 \nabla u_0^2 - u_0^2 \nabla u_0^1) \neq 0.$$

Well, there is always a vector ξ that is orthogonal to some value of the vector field in the parentheses above. No luck, no ellipticity. This, however, suggests that maybe, having more pairs of vector fields like that, we can have enough of them so that no vector can be orthogonal to all of them simultaneously.

We thus assume $2n$ measurements $(F_{1,1} F_{1,2}), \dots, (F_{n,1} F_{n,2})$ such that at each point the n vector fields $(u_0^{k,1} \nabla u_0^{k,2} - u_0^{k,2} \nabla u_0^{k,1})$, $k = 1, \dots, n$, span the whole space (plane in two dimensions).

In this case, the $(2n) \times 2$ matrix operator

$$A(x, \xi) = \begin{pmatrix} \frac{i\xi \cdot \nabla u_0^1}{|\xi|^2} & u_0^1 \\ \frac{i\xi \cdot \nabla u_0^2}{|\xi|^2} & u_0^2 \\ \cdots & \cdots \\ \frac{i\xi \cdot \nabla u_0^{2n-1}}{|\xi|^2} & u_0^{2n-1} \\ \frac{i\xi \cdot \nabla u_0^{2n}}{|\xi|^2} & u_0^{2n} \end{pmatrix} \quad (13.4)$$

is elliptic in the so-called **Douglis–Nirenberg sense** [3, 322, 489, 730]. This involves, in comparison to the Petrovsky sense, a more sophisticated choice of what the “highest order terms” are. Namely, for an $(2n) \times 2$ operator matrix $A_{i,j}$, this means a choice of parameters (s_1, \dots, s_n) and (t_1, t_2) such that the order of each $A_{i,j}$ does not exceed $t_j - s_i$ and such that when one leaves in the symbol of the operator $A_{i,j}$ only terms of exactly that order, the resulting $(2n) \times 2$ matrix will have no kernel for any $\xi \neq 0$.

In our current situation, the correct choices are $s = (1, 1, \dots, 1)$ and $t = (0, 1)$. The resulting ellipticity immediately allows one to construct a left parametrix (see [456]) and to conclude that the correct spaces between which one has the Fredholm property are $(\sigma, \gamma) \in L_2 \oplus H^1$ and $\mathbf{F} \in (H^1)^{2n}$. Notice that, when solving the inverse problem, we expect the loss of one derivative in the diffusion coefficient recovery and no loss in the absorption coefficient.

The appearance of overdetermined problems comes very naturally here and triggers the use of the well-developed theory of such overdetermined elliptic boundary value problems [194, 322, 730, 733].

13.2 • Other examples

Other examples of inverse problems with internal information can be handled as easily as QPAT, and this was done in [456, 457]. We briefly list which functionals were studied there:

- $e^{\gamma(x)}u(x)$ —QPAT;
- $e^{\sigma(x)}|\nabla u(x)|^p$, $p \in (0, 2]$ —AET when $p = 2$, CDI when $p = 1$;
- $G(x, d)A(x)u(x)$, where G is an appropriate Green's function (see Section 12.3)—UMOT;
- more general functionals of the type $F(\sigma(x), u(x), \nabla u(x))$ —..., well, just in case. ☺

The corresponding symbol computations, similar to those for QPAT above, can be done in all these cases. For instance, they yield lesser stability in UMOT than in AET, which explains the stronger blurring in UMOT reconstructions.

We want to emphasize again that this ability to do a quick “back of the envelope” check only suggests what the correct results and sufficient experimental setups might be. It does not diminish at all the numerous recent works that require hard analysis [27, 31, 59, 61, 62, 64, 66, 67, 69, 71, 74, 78, 79, 149, 447, 537].

Another comment is that we have avoided coming near the boundary, as we assume the parameters to be known there. This was just a simplification assumption, in order not to get too much into technicalities. The known theory of overdetermined boundary value problems (see the references provided above) should allow one to improve the results, going all the way to the boundary. For instance, such an extension of [456] was done in [63]. See also [537].

13.3 • Generic linearized uniqueness

The pseudodifferential Fréchet derivatives dA , discussed above, might have finite-dimensional kernels. To finish proving linearized uniqueness and stability (rather than just (semi-)Fredholmity), one needs to eliminate the possibility of existence of a nonzero kernel. The claim in this section (justified in [457], as well as in some special cases in [76]) is that “generically” with respect to the parameters of the operator (such as conductivity, diffusion coefficient, absorption coefficient, etc.) the derivative dA has zero kernel. This is done by pursuing the following scheme: One notices analytic dependence of the operator on its parameters, discovers a set of values of the parameters where dA can be checked to be left invertible, and then uses the facts from the analytic (semi-)Fredholm theory (Appendix D) to conclude that the operator is left invertible on an open dense set of parameters.

The word “generic” can be understood in various meanings, for instance in the sense of the Baire category. A stronger version is “on an open and dense set.” An even stronger (and the most useful) possibility is “outside of a proper analytic subset.” In the case of tomographic problems with internal information, the latter, stronger meaning should apply. However, the standard technique of Ψ DOs with smooth symbols used in [457] restricts the strength of the result, limiting it to only the “open and dense set” option. Using less demanding finite smoothness symbols calculus (e.g., *à la* [756]) should allow one to upgrade to the strongest version of genericity.

Appendix A

Notation

A.1 • Sets, vectors, etc.

The set of real numbers will be denoted by \mathbb{R} , while $\mathbb{C}, \mathbb{Z}, \mathbb{Z}^+, \mathbb{N}$ will denote the sets of complex numbers, integers, nonnegative integers, and natural numbers, respectively.

We will be dealing with the n -dimensional Euclidian vector space \mathbb{R}^n , points of which are denoted as $x = (x_1, \dots, x_n)$. We denote by $|x| = \sqrt{x_1^2 + \dots + x_n^2}$ the length of x , and by $\langle x \rangle$ the function $(1+|x|^2)^{1/2}$. The behavior of these two expressions is very much comparable (e.g., they have the same asymptotics at infinity), with the important difference that $|x|$ vanishes at the origin, while $\langle x \rangle$ does not have any zeros.

A set $X \subset \mathbb{R}^n$ is said to be **open** if it contains any of its points $x_0 \in X$ with a **neighborhood**, i.e., with a small ball $|x - x_0| < r$. When we say a **domain** $X \subset \mathbb{R}^n$, this will always mean an open set.

Complements of open sets are **closed**. The **closure** \overline{X} of a set X is the smallest closed set containing X .

A set $X \subset \mathbb{R}^n$ is **compact** if it is bounded (i.e., contained in a finite ball $\{|x| < R\}$) and closed. We will use the notation $K \Subset X$ to show that K is a **compact** subset of X (in particular, when X is open, the set K cannot reach the boundary of X).

A.2 • Multi-index notation and derivatives

A vector with nonnegative integer coordinates $\alpha = (\alpha_1, \dots, \alpha_n) \in (\mathbb{Z}^+)^n$ is said to be a **multi-index**. We will use the following notation:

$$\begin{aligned} \alpha + \beta &= (\alpha_1 + \beta_1, \dots, \alpha_n + \beta_n) \quad \text{for multi-indices } \alpha, \beta, \\ \alpha! &= \alpha_1! \dots \alpha_n!, \quad |\alpha| = \sum \alpha_j, \\ x^\alpha &= x_1^{\alpha_1} \dots x_n^{\alpha_n} \quad \text{for } x \in \mathbb{R}^n. \end{aligned} \tag{A.1}$$

We will also use the notation

$$D_j = \frac{1}{i} \frac{\partial}{\partial x_j}, \quad \partial_j = \frac{\partial}{\partial x_j}, \quad D^\alpha = D_1^{\alpha_1} D_2^{\alpha_2} \dots D_n^{\alpha_n}, \quad \partial^\alpha = \frac{\partial^{|\alpha|}}{\partial_1^{\alpha_1} \partial_2^{\alpha_2} \dots \partial_n^{\alpha_n}},$$

and

$$\langle D \rangle = (1 + D_1^2 + \cdots + D_n^2)^{1/2}.$$

The meaning of the last expression is not that clear, but we will use only $\langle D \rangle^N$ for an EVEN natural number N , when the expression is well defined.

The following **multinomial theorem** is not hard to prove and is often useful,

$$(x_1 + \cdots + x_n)^m = \sum_{|\alpha|=m} \frac{m!}{\alpha!} x^\alpha,$$

as is the (formal) Taylor theorem,

$$f(x+h) = \sum_{\alpha \geq 0} \frac{h^\alpha}{\alpha!} \partial^\alpha f(x).$$

A.3 • Some useful functions

Let Y be a subset of \mathbb{R}^n . The **characteristic function** χ_Y of this set is $\chi_Y(x) = 1$ if $x \in Y$, and $\chi_Y(x) = 0$ otherwise.

The **Heaviside function** of one variable is

$$H(x) = \begin{cases} 1 & \text{when } x \geq 0, \\ 0 & \text{when } x < 0. \end{cases}$$

In particular, $H = \chi_{\mathbb{R}^+}$.

The **box function** is

$$\Pi(x) := \chi_{[-0.5, 0.5]}(x) = \begin{cases} 1 & \text{when } |x| \leq 0.5, \\ 0 & \text{otherwise.} \end{cases}$$

Exercise A.1. Express the box function in terms of the Heaviside function.

Exercise A.2. The **B-splines** $\Pi_n(x)$ are defined as $\Pi_n(x) = \underbrace{\Pi(x) * \cdots * \Pi(x)}_{n \text{ times}}$

1. Find and graph $\Pi_1(x)$, $\Pi_2(x)$, and $\Pi_3(x)$.

2. Determine the support of $\Pi_n(x)$.

The **Gaussian function** in one variable:

$$G(x) = e^{-\frac{|x|^2}{2}}.$$

In \mathbb{R}^n , one can define the Gaussian function by the same formula, and for $x = (x_1, \dots, x_n)$ one has $G(x) = \prod_{j=1}^n G(x_j)$.

The **cardinal sine function**, or $sinc(x)$:

$$sinc(x) = \begin{cases} \frac{\sin x}{x} & \text{when } x \neq 0, \\ 1 & \text{when } x = 0. \end{cases}$$

The **normal density** with the mean $\mu = (\mu_1, \dots, \mu_n)$ and standard deviation $\sigma > 0$:

$$\frac{1}{(\sigma\sqrt{2\pi})^n} e^{-\frac{|x-\mu|^2}{2\sigma^2}}.$$

We will call a **mollifier** any function $\rho(x)$ in \mathbb{R}^n that has the following properties:

1. ρ is infinitely differentiable.
2. $\rho \geq 0$.
3. $\rho(x) > 0$ for $|x| < 1$
4. $\rho(x) = 0$ for $|x| \geq 1$.
5. $\int \rho(x) dx = 1$.

Such a function can be defined explicitly:

$$\rho(x) = \begin{cases} e^{(|x|^2 - 1)^{-1}} & \text{when } |x| < 1, \\ 0 & \text{otherwise,} \end{cases}$$

where $c > 0$ is chosen in such a way that the integral of ρ is equal to 1.

Given a mollifier ρ , we introduce for any $\epsilon > 0$ the squeezed version of the mollifier as follows:

$$\rho_\epsilon(x) = \epsilon^{-n} \rho\left(\frac{x}{\epsilon}\right).$$

A.4 • Radon transform

S^1 is the circle of unit vectors ω . $T = \mathbb{R} \times S^1$ is the cylinder of points (t, ω) labeling the lines: $x \cdot \omega = t$. In fact, points (t, ω) and $(-t, -\omega)$ need to be identified, which turns T into the (infinitely wide) Möbius strip (this can be ignored in the future).

Ω is the unit disk $|x| < 1$ on the plane. We will often assume that our objects are inside Ω .

Functions $f(x)$ to be recovered will be either defined in the whole space or supported only inside Ω . The common spaces needed will be $L_2(\mathbb{R}^2)$ of square integrable functions on the plane with the inner product

$$(f_1, f_2) = \int_{\mathbb{R}^2} f_1(x) \overline{f_2(x)} dx,$$

similar space $L_2(T)$ on the cylinder with

$$(g_1, g_2) = \int_T g_1(t, \omega) \overline{g_2(t, \omega)} d\omega dt,$$

and the **Schwartz space** \mathcal{S} of infinitely differentiable functions on the plane, which decay with all their derivatives faster than any power of $|x|$ at infinity: For any α and $N > 0$

$$\left| \frac{\partial^\alpha f(x)}{\partial x^\alpha} \right| \leq C_{\alpha, N} \langle x \rangle^{-N}.$$

Analogous Schwartz space $\mathcal{S}(T)$ can be defined on the cylinder T , where decay is understood with respect to the linear variable t . We will also denote by $C_0^\infty(\mathbb{R}^2)$ the space of smooth compactly supported functions on the plane, and a similar space $C_0^\infty(T)$ on T .

A.5 • Some linear algebra

Space $H = \mathbb{C}^n$ of vectors $f = (f^1, \dots, f^n)$ with complex components.

Hermitian metric (dot product) in this space $(f, g) = \sum f^i \overline{g^i}$. (Notice the complex conjugation!!)

Norm (length) on this space $\|f\|^2 = (f, f) = \sum |f^i|^2$.

Identity matrix $I = (\delta_{ij})$ such that $Ig = g$ for all g .

Matrix $A = (a_{ij})$. Its **adjoint** $A^* = (\overline{a_{ji}})$; i.e.,

$$(Af, g) = (f, A^*g).$$

Definition A.3. Matrix A is **Hermitian** if $A^* = A$ (or equivalently $a_{ij} = \overline{a_{ji}}$).

This means that $(Af, g) = (f, Ag)$ for any two vectors f and g (which can be taken as an equivalent definition).

Theorem A.4. Every Hermitian matrix A has an ortho-normal basis of eigenvectors f_j ($j = 1, \dots, n$) such that $Af_j = \lambda_j f_j$ with real eigenvalues λ_j . In this basis we have $A = \text{diag}(\lambda_1, \dots, \lambda_n)$.

Lemma A.5. For any matrix B , matrices B^*B and BB^* are Hermitian (simple check).

Definition A.6. Matrix F is **isometric** if $\|Fg\| = \|g\|$ for all vectors g , or equivalently $(Fg, Fg) = (g, g)$.

Lemma A.7. If F is isometric, then $F^*F = I$ (this is also true for rectangular matrices).

Exercise A.8. Prove Lemma A.7.

The conclusion is that if you have established isometric property $\|Fg\| = \|g\|$ for a square matrix, then you invert F for free: $F^{-1} = F^*$. If the matrix is not square, you still get a left inverse.

Definition A.9. Let e_k , $k = 1, \dots, n$, be any ortho-normal basis in H ; then for any

vector f we determine its Fourier coefficients as

$$f_k = (f, e_k). \quad (\text{A.2})$$

Mapping f into the set of its Fourier coefficients $\{f_k\}$ is usually called **Fourier analysis**.

Theorem A.10 (Fourier synthesis). *For any vector f*

$$f = \sum f_k e_k. \quad (\text{A.3})$$

Remark A.11. *If the basis vectors e_k are not ortho-normal, but merely orthogonal, then, keeping (A.2), one has to modify (A.3) as follows:*

$$f = \sum \frac{f_k}{\|e_k\|^2} e_k.$$

Exercise A.12. *Prove the statement of this remark.*

Corollary A.13.

$$\|f\|^2 = \sum \frac{|f_k|^2}{\|e_k\|^2}.$$

Exercise A.14. *Prove the corollary.*

Appendix B

Brief Notes on the Fourier Transform and Harmonic Analysis

B.1 • Harmonic analysis

We will try to provide here a cartoon of an idea that plays a crucial role in all branches of mathematics and physics. It is what is called **harmonic (or Fourier) analysis**. To put it in the crudest way, the idea of harmonic analysis says

“If your problem has symmetries, use them!”

Below, we will specify this in a simple linear algebra setting.

The reader might enjoy reading the wonderful historical survey “Harmonic analysis as exploitation of symmetry” by Mackey [502].

Let A be an $n \times n$ matrix, and e be its eigenvector corresponding to the eigenvalue λ :

$$Ae = \lambda e.$$

Theorem B.1. *Assume that λ is a simple eigenvalue, i.e., that it has unique (up to a scalar multiple) eigenvector e . Let the matrix B commute with A . Then e must be an eigenvector of B as well.*

Exercise B.2. *Prove this theorem.*

Corollary B.3. *If A has a basis of eigenvectors and all the eigenvalues are simple, then any matrix B that commutes with A is diagonal in this basis.*

We can now formulate an instance of the idea of harmonic analysis:

If you study a linear operator B that commutes with an operator A with simple spectrum, then choosing the basis of eigenvectors of A diagonalizes (and thus simplifies) B .

Remark B.4. *Notice that when λ is not simple (i.e., has multiplicity), the conclusion is incorrect: While Be is still an eigenvector that corresponds to λ , it does not*

have to be proportional to e . In other words, B can “move around” the eigenvectors corresponding to the same eigenvalue λ of A .

Example B.5. Let $A = \text{diag}(2, 2, 3)$, i.e.,

$$A = \begin{pmatrix} 2 & 0 & 0 \\ 0 & 2 & 0 \\ 0 & 0 & 3 \end{pmatrix};$$

then any matrix B of the form

$$B = \begin{pmatrix} * & * & 0 \\ * & * & 0 \\ 0 & 0 & * \end{pmatrix}$$

(where stars denote arbitrary numbers) commutes with A but is not necessarily diagonal. The reason is the multiplicity of $\lambda = 2$. ■

This problem of multiplicity (which is rather common) can be alleviated by the following observation, which gives a more general harmonic analysis principle.

Theorem B.6. Let A_1, \dots, A_m be $n \times n$ matrices, and e_1, \dots, e_n be a basis such that all its vectors are eigenvectors of all the matrices A_j (i.e., $A_j e_i = \lambda_{ij} e_i$). Assume that for each two of these vectors there is a matrix among A_j whose eigenvalues corresponding to these two vectors are distinct. Let B be a matrix that commutes with all matrices A_j . Then B is diagonal in the basis $\{e_i\}$.

Exercise B.7. Prove this theorem.

Exercise B.8. Let

$$A_1 = \begin{pmatrix} 2 & 0 & 0 \\ 0 & 2 & 0 \\ 0 & 0 & 3 \end{pmatrix}, \quad A_2 = \begin{pmatrix} 3 & 0 & 0 \\ 0 & -5 & 0 \\ 0 & 0 & 3 \end{pmatrix}.$$

1. Show that these matrices satisfy the conditions of the above theorem and thus that any B commuting with both of them is diagonal.
2. In this example, matrices A_j commute with each other. Does that always have to be the case under the conditions of Theorem B.6 above?

Now we extend somewhat the idea of harmonic analysis in the linear algebra setting:

If you study a linear operator B , which commutes with a family of operators A_j satisfying the conditions of Theorem B.6, then choosing the basis of joint eigenvectors of A_j diagonalizes B .

As the main body of the book shows, these ideas provide important guidance in analysis of tomographic problems.

Remark B.9. We have discussed here only what is called **commutative harmonic analysis** [331], i.e., when the symmetries of the problem commute with each other. There is a whole beautiful (and complex) world of **noncommutative harmonic analysis** (see, e.g., [87, 265, 366, 420, 426, 433, 502, 754, 787, 788] and references therein), which we will not touch here. In fact, the spherical harmonic expansion in dimension 3 and higher comes from that noncommutative world [706, 741], as do most other familiar special functions [420, 787, 788].

B.2 • Fourier series expansions

Although we consider here only functions of one variable, the considerations can be easily extended to Fourier series for periodic functions in several variables (e.g., [741]).

Space (infinite-dimensional) $H = L_2[-\pi/h, \pi/h]$ of functions $f(x)$ on $[-\pi/h, \pi/h]$, whose square $|f(x)|^2$ is integrable.

Hermitian metric (analogue of the dot-product) on this space

$$(f, g) = \int_{-\pi/h}^{\pi/h} f(x) \overline{g(x)} dx, \quad \|f\|^2 = \int_{-\pi/h}^{\pi/h} |f(x)|^2 dx.$$

(See [426, Sections 32, 33].)

Consider the sequence of functions $e_k = \frac{1}{\sqrt{2\pi}} e^{ikhx}$, $k = 0, \pm 1, \pm 2, \dots$

Lemma B.10.

$$(e_k, e_j) = \frac{1}{h} \delta_{ij},$$

where $\delta_{ij} = \begin{cases} 1 & \text{when } i = j, \\ 0 & \text{otherwise,} \end{cases}$ is the Kronecker's delta.

Exercise B.11. Prove the lemma.

Theorem B.12. Functions

$$\sqrt{\frac{h}{2\pi}} e^{ikhx}, \quad k = 0, \pm 1, \pm 2, \dots,$$

form an ortho-normal basis of $L_2[-\pi/h, \pi/h]$.

Orthogonality and normalization have just been proven. Completeness (i.e., that there is no function orthogonal to all these exponents) is proven in Fourier analysis books (e.g., [426, Section 34]).

Definition B.13. For any function $f(x) \in L_2[-\pi/b, \pi/b]$ its **Fourier coefficients** are defined as

$$\hat{f}(k) = \left(f, \frac{1}{\sqrt{2\pi} e^{ikbx}} \right) = \frac{1}{\sqrt{2\pi}} \int_{-\pi/b}^{\pi/b} f(x) e^{-ikbx} dx. \quad (\text{B.1})$$

Fourier analysis: Take a function $f(x) \in L_2[-\pi/b, \pi/b]$ and produce its Fourier coefficients $\hat{f}(k)$.

Fourier synthesis (Fourier series expansion): For any $f(x) \in L_2[-\pi/b, \pi/b]$

$$f(x) = \frac{b}{\sqrt{2\pi}} \sum_{k=-\infty}^{\infty} \hat{f}(k) e^{ikbx}. \quad (\text{B.2})$$

The series converges in L_2 .

Fourier series expansion represents any function $f(x)$ on $[-\pi/b, \pi/b]$, or alternatively any $2\pi/b$ -periodic function on \mathbb{R} , as a sum of harmonic oscillations (sinusoidal waves).

Theorem B.14 (Plancherel's or Parseval's).

$$\int_{-\pi/b}^{\pi/b} |f(x)|^2 dx = b \sum |f_k|^2.$$

B.3 ▪ Properties of Fourier series expansions

Remark B.15. All functions e^{ikbx} with integer k are $\frac{2\pi}{b}$ -periodic. Hence, it is natural to consider the sum in (B.2) as a $\frac{2\pi}{b}$ -periodic function too.

Considering the function $f(x)$ as $\frac{2\pi}{b}$ -periodic, we can talk about its values on the whole axis.

Exercise B.16. Prove that the Fourier coefficients of a $\frac{2\pi}{b}$ -periodic function $f(x)$ can be computed as

$$\hat{f}(k) = \frac{1}{\sqrt{2\pi}} \int_a^{a+2\pi/b} f(x) e^{-ikbx} dx$$

for any value of a .

Remark B.17. Convergence in (B.2) in general does not hold in the pointwise sense but as L_2 -convergence (i.e., in an average sense).

Namely, the following convergence results hold.

Theorem B.18 (see, e.g., [426, Section 34]). If $f \in L_2[-\pi/b, \pi/b]$ and $f_N(x)$ is the N th partial sum of (B.2), then

$$\int_{-\pi/b}^{\pi/b} |f(x) - f_N(x)|^2 dx \xrightarrow[N \rightarrow \infty]{} 0.$$

Theorem B.19 (e.g., [426, Sections 15–17], [760, Chapter 1, Section 10]).

1. If $f(x) \in C[-\pi/b, \pi/b]$, has bounded first derivative, and is periodic (i.e., $f(-\pi/b) = f(\pi/b)$), then

$$\lim_{N \rightarrow \infty} f_N(x) = f(x)$$

for all $x \in [-\pi/b, \pi/b]$.

2. If $f(x)$ is as in the first part of the theorem, except for a finite number of finite discontinuities, then

$$\lim_{N \rightarrow \infty} f_N(x) = \begin{cases} \frac{f(x+0) + f(x-0)}{2} & \text{when } x \in (-\pi/b, \pi/b), \\ \frac{f(-\pi/b+0) + f(\pi/b-0)}{2} & \text{when } x = \pm\pi/b. \end{cases}$$

B.4 • Smoothness of $f(x) \Leftrightarrow$ decay of Fourier coefficients f_k

In the theorem below, the word “periodic” applied to a function f on $[-\frac{\pi}{b}, \frac{\pi}{b}]$ means $f(-\frac{\pi}{b}) = f(\frac{\pi}{b})$.

Theorem B.20.

1. If $f(x)$ is continuous (in fact, $f \in L_1$ suffices), then

$$|\hat{f}(k)| \leq \text{const.}$$

2. If $f(x)$ is periodic and has a continuous first derivative, then

$$|\hat{f}(k)| \leq \frac{\text{const}}{|k|} \quad \text{for } k \neq 0.$$

3. If $f(x)$ has n continuous derivatives and the first $n-1$ of them are periodic, then

$$|\hat{f}(k)| \leq \frac{\text{const}}{|k|^n} \quad \text{for } k \neq 0.$$

4. If

$$|\hat{f}(k)| \leq \frac{\text{const}}{|k|^\alpha} \quad \text{for some } \alpha > 1 \text{ and } k \neq 0,$$

then $f(x)$ is continuous and periodic.

5. If

$$|\widehat{f}(k)| \leq \frac{\text{const}}{|k|^\alpha} \quad \text{for some } \alpha > 2 \text{ and } k \neq 0,$$

then $f(x)$ is continuous, periodic, and once continuously differentiable.

Exercise B.21. Prove this theorem.

Exercise B.22. Find necessary and sufficient conditions on the Fourier coefficients for a function $f(x)$ to be real.

Exercise B.23. Find the Fourier coefficients of the function $f(x) = x$ on $[-\pi, \pi]$.

Exercise B.24. Let on $[-\pi, \pi]$

$$f(x) = \begin{cases} x + \pi & \text{on } [-\pi, 0], \\ -x + \pi & \text{on } [0, \pi]. \end{cases}$$

Find the Fourier coefficients.

B.5 • Relations with shifts and derivatives

Functions on $[-\frac{\pi}{b}, \frac{\pi}{b}]$ will be extended $\frac{2\pi}{b}$ -periodically to \mathbb{R} . Then we can shift (translate) them:

$$(T_t f)(x) := f(x + t).$$

Exercise B.25.

1. Prove that for functions $e_k = e^{ikbx}$ one has $(T_t e_k)(x) = \lambda_{k,t} e_k(x)$ for some constant $\lambda_{k,t}$. Find $\lambda_{k,t}$.
2. Prove that if a continuous function $e(x)$ on \mathbb{R} satisfies $T_t e = \lambda_t e$ for all $t \in \mathbb{R}$ and some numbers λ_t , then $e(x) = C e^{\mu x}$ for some $\mu \in \mathbb{C}$ and a constant C . Prove that if such an $e(x)$ is $\frac{2\pi}{b}$ -periodic, then $e(x) = C e_k(x)$ for some $k \in \mathbb{Z}$. These statements are not necessarily true if e is discontinuous.
3. Let B be a linear operator acting on functions of x such that B commutes with shifts (i.e., $B T_t = T_t B$ for all $t \in \mathbb{R}$). If $B e_k$ is continuous, then $B e_k = \beta_k e_k$ for some constant β_k , which is called the **Fourier multiplier** corresponding to B . In other words, B is diagonal in the basis $\{e_k\}$.
4. Prove that $\frac{d^l}{dx^l}$ commutes with T_t for any t , and find the corresponding Fourier multipliers.
5. Check when the operator of multiplication by a given function $g(x)$ commutes with the shifts.

So, if there is a linear transformation B commuting with all shifts T_t , then it has exponents as eigenvectors; i.e., $Be_k = \beta_k e_k$ for some numbers β_k depending on B . In particular, the action of B on any function f is easy to write down in terms of the Fourier expansion: If $f(x) = \sum_k f_k e_k$, then $Bf = \sum_k \beta_k f_k e_k$. The common examples of such operations are differentiation and convolution (considered in the next section).

B.6 ■ Product-convolution relations

Definition B.26. Convolution $f * g$ of two $\frac{2\pi}{h}$ -periodic functions (say, belonging to $L_1[-\pi/h, \pi/h]$) is defined as

$$f * g(x) = \int_{-\frac{\pi}{h}}^{\frac{\pi}{h}} f(y)g(x-y)dy.$$

Exercise B.27.

1. Prove that convolution is commutative.
2. Prove that in the definition of convolution one can integrate over an arbitrary segment of the length of the period.
3. Prove that (under appropriate smoothness conditions)

$$\frac{d}{dx}(f * g) = \left(\frac{df}{dx} * g \right) = \left(f * \frac{dg}{dx} \right).$$

4. Prove that convolution commutes with shifts:

$$T_t(f * g) = (T_t f * g).$$

5. Prove that $(f * g)_k = \sqrt{2\pi} f_k g_k$.

B.7 ■ Convolution on \mathbb{R}^n

Definition B.28. The convolution of two (sufficiently fast decaying, so the integral converges) functions on \mathbb{R}^n is

$$(f * g)(x) = \int_{\mathbb{R}^n} f(y)g(x-y)dy.$$

Exercise B.29. Prove the following properties of convolution:

1. **Linearity:** $f(x) * (a g_1(x) + b g_2(x)) = a(f * g_1) + b(f * g_2)$.
2. **Commutativity:** $f * g = g * f$.

3. *Commuting with shifts:* If $(T_a f)(x) := f(x+a)$, then $f * (T_a g) = T_a(f * g)$.
4. *Commuting with differentiation:* If $f \in L^1_{loc}(\mathbb{R}^n)$ and g is smooth and compactly supported, then $f * g$ is smooth and $\frac{d^l}{dx^l}(f * g) = (f * \frac{d^l g}{dx^l})$.
5. *Convolution operation has no unity;* i.e., there is no function $i(x)$ such that $i * f = f$ for all functions f . (Make reasonable assumptions on the functions f in order for this to make sense.) (If you know distributions [264, 745], there is a distribution, namely Dirac's δ -function, with this property.)

One can make the following statement (converse to statement 3 of Exercise B.30) precise.

“Theorem”: Any linear operator A mapping functions of $x \in \mathbb{R}^n$ into functions of $x \in \mathbb{R}^n$ and commuting with shifts, i.e., $AT_a = T_a A$ for all $a \in \mathbb{R}^n$, is a convolution; i.e., $Af = f * g$ for some g .

B.8 ▪ Fourier transform (FT)

Definition B.30. Fourier transform of a function $f(x)$ on \mathbb{R} is defined as

$$(\mathcal{F}f)(\xi) = \hat{f}(\xi) := \int_{-\infty}^{\infty} f(x) e^{-i\xi x} dx. \quad (\text{B.3})$$

In \mathbb{R}^n ,

$$\hat{f}(\xi) = \int e^{-ix \cdot \xi} f(x) dx,$$

where $x \cdot \xi = x_1 \xi_1 + x_2 \xi_2 + \cdots + x_n \xi_n$.

This is well defined when $f(x)$ decays sufficiently fast, e.g., $f \in L_1(\mathbb{R}^n)$. If $f \in L_2(\mathbb{R}^n)$, then the definition should be carefully adjusted (e.g., [741]).

Theorem B.31 (Plancherel's theorem/Parseval's identity). The following identity holds:

$$\int_{\mathbb{R}^n} |f(x)|^2 dx = (2\pi)^{-n} \int_{\mathbb{R}^n} |\hat{f}(\xi)|^2 d\xi. \quad (\text{B.4})$$

In other words, operator $(2\pi)^{-n/2} \mathcal{F} : L_2(\mathbb{R}^n) \rightarrow L_2(\mathbb{R}^n)$ is isometric.

Exercise B.32.

1. Prove that the adjoint operator to \mathcal{F} is given by

$$(\mathcal{F}^* g)(x) = \int_{\mathbb{R}^n} g(\xi) e^{i\xi \cdot x} d\xi. \quad (\text{B.5})$$

2. Prove that $(2\pi)^{-n}\mathcal{F}^*$ is inverse to \mathcal{F} . Hint: Use the isometric property of $(2\pi)^{-n/2}\mathcal{F}$.

We thus get the **Fourier inversion formula**:

$$f(x) = \frac{1}{(2\pi)^n} \int_{\mathbb{R}^n} \hat{f}(\xi) e^{i\xi \cdot x} d\xi. \quad (\text{B.6})$$

Exercise B.33. Show that this inversion formula for $n = 1$ can be obtained formally as a limit when $h \rightarrow 0$ from (B.2).

Remark B.34. The Fourier inversion is almost the same as the direct Fourier transform; one needs only to flip the sign of the independent variable and introduce the constant factor $(2\pi)^{-n}$:

$$(\mathcal{F}^{-1}g)(x) = (2\pi)^{-n}(\mathcal{F}g)(-x).$$

FT $f \mapsto \hat{f}$ provides **Fourier analysis** of a function, i.e., finds the amplitudes with which different oscillating exponents enter the function. Fourier inversion $\hat{f} \mapsto f$ provides **Fourier synthesis**, synthesizing the function back from these amplitudes.

B.9 • Properties of the FT

Exercise B.35. Prove the following properties of the FT in \mathbb{R}^n :

1. **Dilation invariance:** Let $f_r(x) = f(rx)$. Then $\widehat{f}_r(\xi) = r^{-n} \widehat{f}(r^{-1}\xi)$.
2. **Homogeneity preservation:** If $f(x)$ is homogeneous of order a , then its Fourier transform $\widehat{f}(\xi)$ is homogeneous of order $-a - n$, where n is the number of independent variables.
3. **Shift invariance:** $\widehat{T_y f}(\xi) = e^{i\xi \cdot y} \widehat{f}(\xi)$.
4. **Rotational invariance:** If A is a rotation in \mathbb{R}^n , then $\widehat{f(Ax)}(\xi) = \widehat{f(x)}(A\xi)$. (The formula is somewhat more complicated when A is an arbitrary invertible linear transformation, not necessarily a rotation (orthogonal matrix). Work this case out.)
5. $\widehat{\frac{\partial^{|a|} f}{dx^\alpha}}(\xi) = (i\xi)^\alpha \widehat{f}(\xi)$, where $(\xi)^\alpha = (\xi_1)^{\alpha_1} (\xi_2)^{\alpha_2} \dots (\xi_n)^{\alpha_n}$.
6. Find a formula for $\widehat{x^l f}(\xi)$ in terms of $\widehat{f}(\xi)$. (Hint: Use the previous question and the remark above.)

7. Show that the following relation between convolution and FT holds:

$$\widehat{f * g} = \widehat{f} \widehat{g}.$$

8. Analogously, $\widehat{f g} = \frac{1}{(2\pi)^n} \widehat{f} * \widehat{g}$.

9. Parseval identity: $\int f \widehat{g} dx = \int \widehat{f} g dx$.

B.10 • FT of some common functions

Exercise B.36. Find the FT of the box function.

Exercise B.37.

1. Check that the Gaussian $G(x)$ satisfies the differential equation

$$\frac{dG}{dx} + xG = 0.$$

2. Prove that the FT of the Gaussian satisfies the same equation:

$$\frac{d\widehat{G}}{d\xi} + \xi \widehat{G} = 0. \quad (\text{B.7})$$

3. Prove that the FT of the Gaussian is the Gaussian (with an extra constant factor):

$$\widehat{G}(\xi) = \sqrt{2\pi} e^{-\frac{\xi^2}{2}}.$$

Hint: Use (B.7) and Plancherel's theorem.

B.11 • The Paley–Wiener theorem

Several versions of the **Paley–Wiener theorem**, which describe Fourier transforms of various classes of functions, are combined here ($\Im \xi$ denotes the imaginary part of a complex vector ξ) as follows.

Theorem B.38.

1. FT $\widehat{f}(\xi)$ of a function $f \in C_0^\infty(\mathbb{R}^n)$ supported in the ball $\{x \mid |x| \leq A\}$ is an entire function in \mathbb{C}^n and satisfies for any $N > 0$ the estimate

$$|\widehat{f}(\xi)| \leq C_N (1 + |\xi|)^{-N} e^{A|\Im \xi|}. \quad (\text{B.8})$$

The converse statement also holds: Any entire function with such estimates is the FT of a smooth function supported in that ball.

2. FT $\hat{f}(\xi)$ of a function $f \in L_2(\mathbb{R}^n)$ supported in the ball $\{x \mid |x| \leq A\}$ is an entire function in \mathbb{C}^n , which is square integrable along \mathbb{R}^n and satisfies in \mathbb{C}^n the estimate

$$|\hat{f}(\xi)| \leq C e^{A|\xi|}. \quad (\text{B.9})$$

The converse statement also holds.

3. A function f belongs to the Schwartz class $\mathcal{S}(\mathbb{R}^n)$ if and only if its FT $\hat{f}(\xi)$ belongs to the Schwartz class.

B.12 • Smoothness and decay of the FT

As for the Fourier series, smoothness of a function is tied to the decay of its FT (although exact theorems must be stated rather carefully). We give an example.

Exercise B.39. Prove the following:

1. If $f \in L_1(\mathbb{R})$, then \hat{f} is bounded (in fact, even continuous and tending to zero at infinity).
2. If $f, f' \in L_1(\mathbb{R})$, then $|\hat{f}(\xi)| \leq C(1 + |\xi|)^{-1}$.
3. If $f, f', f'', \dots, f^{(n)} \in L_1(\mathbb{R})$, then $|\hat{f}(\xi)| \leq C(1 + |\xi|)^{-n}$.
4. If $|\hat{f}(\xi)| \leq C(1 + |\xi|)^{-\alpha}$, $\alpha > 1$, then f is bounded and continuous.
5. If $|\hat{f}(\xi)| \leq C(1 + |\xi|)^{-\alpha}$, $\alpha > 2$, then f has a bounded and continuous derivative.
6. If, for a function f on \mathbb{R}^n , $|\hat{f}(\xi)| \leq C_N(1 + |\xi|)^{-N}$ for all $N > 0$ (i.e., \hat{f} decays faster than any power), then $f \in C^\infty(\mathbb{R}^n)$.

B.13 • Smoothing

If one can guarantee fast decay of the FT of a function, then the function is smooth. This is the basis of standard smoothing procedures. Namely, suppose that function $f(x)$ is not smooth (e.g., $f \in L_2(\mathbb{R})$ only). Assume that we have another function $w(x)$ whose FT \widehat{w} is smooth and fast decaying (for instance, even supported on a finite interval). Then, taking convolution $f * w$, we get a smooth function. The reason is that $\widehat{f * w}$ coincides (up to a constant factor) with $\widehat{f} \widehat{w}$, which decays due to the decay of \widehat{w} . In other words, multiplication of \widehat{f} by \widehat{w} “filters out” high frequencies ξ , making the original function smoother. This is why \widehat{w} is often called a **filter**, or a **window function** (the window that allows certain frequencies through), while w is called a **mollifier**. There are quite a few window functions used in practice. The simplest one is the box function $\Pi(\xi)$ (the rectangular window). It has the disadvantage that it is not continuous; hence after the

convolution the function will not decay quickly, and one has to deal with long “tails.” One also uses Gaussian filters, where the window function is the Gaussian $G_a(\xi) = \exp(-a\xi^2)$. There are many more commonly used filters.

Can one make the smoothed (**mollified**) function $f * w$ close to the original one? We cannot make it equal to f , since there is no identity element for the convolution. So, the question is whether one can find an approximate identity under the convolution, i.e., a sequence of functions w_n such that $w_n * f \rightarrow f$ for a reasonable class of functions f and a reasonable notion of convergence. This can be done. The simplest way of constructing approximate identities is the following.

Theorem B.40. *Let $w(x)$ be smooth, supported on $[-1, 1]$, and such that*

$$\int_{\mathbb{R}} w(x) = 1.$$

*Define $w_n(x) = nw(nx)$. Then for any continuous function $f(x)$ on \mathbb{R} the convolutions $f_n = w_n * f$ converge when $n \rightarrow \infty$ to f , where convergence is uniform on any finite interval.*

Analogous statements hold for different classes of functions, for instance for L_1 -functions (then convergence also needs to be understood in the L_1 -sense).

B.14 • Sobolev spaces

The relations between the smoothness of a function and the decay of its FT are seen best in the **Sobolev spaces** of functions.

Definition B.41 (Sobolev spaces of a positive integer order). *Let $k \geq 0$ be an integer. A function f belongs to the Sobolev space $H^k(\mathbb{R}^n)$ if $D^\alpha f \in L^2(\mathbb{R}^n)$ for any $|\alpha| \leq k$ and*

$$\|f\|_{H^k}^2 := \int_{\mathbb{R}^n} \sum_{|\alpha| \leq k} |D^\alpha f(x)|^2 dx.$$

Here the derivatives $D^\alpha f$ are understood in the distributional sense.

The following statement can be proven using the properties of the FT.

Theorem B.42. *$f \in H^k(\mathbb{R}^n)$ if and only if*

$$\int_{\mathbb{R}^n} |\widehat{f}(\xi)|^2 \langle \xi \rangle^{2k} d\xi < \infty$$

(here $\langle \xi \rangle = (1 + |\xi|^2)^{1/2}$). The norm $\|f\|_{H^k}$ is equivalent to

$$\left(\int_{\mathbb{R}^n} |\widehat{f}(\xi)|^2 \langle \xi \rangle^{2k} d\xi \right)^{1/2}.$$

Now one can define Sobolev spaces of arbitrary (not necessarily integer and positive) order, as follows.

Definition B.43. A function f belongs to the Sobolev space $H^s(\mathbb{R}^n)$, $s \in \mathbb{R}$, if

$$\int_{\mathbb{R}^n} |\widehat{f}(\xi)|^2 \langle \xi \rangle^{2s} d\xi < \infty.$$

The norm is defined as

$$\|f\|_{H^s}^2 := \int_{\mathbb{R}^n} |\widehat{f}(\xi)|^2 \langle \xi \rangle^{2s} d\xi.$$

B.15 • Sampling

Let $f(x)$ be a function on \mathbb{R} . Sampling of f consists of evaluating this function at a sequence of points $\{x_j\}_{j=-\infty}^{\infty}$ (for example, $x_j = jh$ with a fixed step h). The questions that arise are: Can the function be uniquely recovered from these values? If not, how precisely can it be recovered?

It is clear that in general one cannot recover an arbitrary smooth function from its values at a discrete set of points, since one can create an arbitrarily smooth function that is zero at any of these points and yet not entirely zero (Fig. B.1).

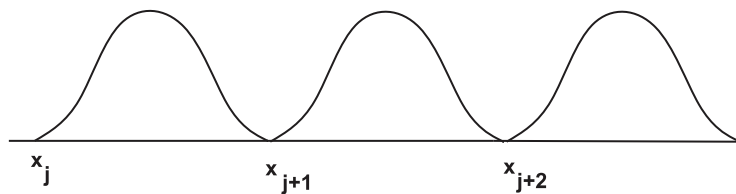


Figure B.1. A function “invisible” at the given sequence of points.

Here is the important idea of sampling: In order for a nonzero function to be zero at a sequence jh , its Fourier transform must contain sufficiently high frequencies (otherwise the function does not change fast enough to be zero at two consecutive points and nonzero in between). This rule of thumb is made precise by the following Nyquist condition and sampling theorem.

Proposition B.44. If $h > \pi/b$, then there exist nonzero b -band-limited functions that vanish at the points $\{jh\}$. In other words, a b -band-limited function in general cannot be determined from its values at the points $\{jh\}$ with $h > \pi/b$.

Proof. This is done by constructing an example. Let $b > \pi/b$, and hence $c = b - \pi/b > 0$. Consider any smooth (infinite differentiable) function $\zeta(\xi)$ supported in $[-c, c]$, and define $\psi(x) = \mathcal{F}^{-1}(\zeta)$. Then $\psi(x)$ is c -band-limited (since $\hat{\psi} = \zeta$), and $\psi(x)$ decays faster than any power of x . The Paley–Wiener theorem claims that ψ is analytically extendable for the whole complex plane \mathbb{C} and satisfies there the estimate

$$|\psi(z)| \leq \text{const } e^c |\operatorname{Im} z|.$$

Now let $f(x) = \sin(\pi x/b)\psi(x)$. Then $f \in L_2(\mathbb{R})$, extends analytically to the complex plane, and satisfies the inequality

$$|f(z)| = |\sin(\pi z/b)| |\psi(z)| \leq \text{const } e^{\frac{\pi}{b}} |\operatorname{Im} z| e^c |\operatorname{Im} z| = \text{const } e^b |\operatorname{Im} z|. \quad (\text{B.10})$$

We have used here the Euler's formula for the sine function:

$$\sin z = \sin(x + iy) = \frac{1}{2} (e^{ix-y} - e^{-ix+y}),$$

which implies right away that

$$|\sin z| \leq e^{|y|} = e^{|\operatorname{Im} z|}.$$

Now the Paley–Wiener theorem and (B.10) imply that f is b -band-limited. Since its values at all points kh with integer k are zeros, looking at these values cannot help one distinguish $f(x)$ from zero.

The conclusion is that in order to be able to reconstruct a b -band-limited function, one needs to sample it with at least the step size $h = \pi/b$.

Definition B.45. Condition

$$h \leq \frac{\pi}{b} \quad (\text{B.11})$$

is called the **Nyquist condition**. A function sampled with a larger step is said to be **undersampled**, and one sampled with a smaller step is **oversampled**.

The question arises of whether the Nyquist condition is sufficient. The answer is given by the following famous **sampling theorem** (see, e.g., [559] for its proof).

Theorem B.46 (Whittacker, Kotel'nikov, and Shannon). Let $h \leq \frac{\pi}{b}$. Then the following hold:

1. Any b -band-limited function $f(x)$ can be recovered from its values at the points kh as follows:

$$f(x) = \sum_k f(kh) \sin c \left(\frac{\pi}{b} (x - kh) \right). \quad (\text{B.12})$$

The series converges as a series of functions in $L_2(\mathbb{R})$.

2. The FT of f can be obtained as follows:

$$\widehat{f}(\xi) = \frac{h}{\sqrt{2\pi}} \sum_k f(kh) e^{-ikh\xi}. \quad (\text{B.13})$$

3. If g is another b -band-limited function, then

$$\int_{-\infty}^{\infty} f(x) \overline{g(x)} dx = h \sum_k f(kh) \overline{g(kh)}. \quad (\text{B.14})$$

Exercise B.47. Look at the example of the cardinal sine function, its zeros, and its FT. Why does it not provide a counterexample to Theorem B.47 when $h = \pi/b$?

When $f \in L_2$, the series (B.12) converges in the L_2 -sense:

$$\left\| f - \sum_{|k| \leq N} f(kh) \sin c \left(\frac{\pi}{h}(x - kh) \right) \right\|^2 \leq C \sum_{|k| > N} |f(kh)|^2 \xrightarrow[N \rightarrow \infty]{} 0.$$

This, however, is not such a fast convergence. In the case when the function is oversampled, i.e., $h < \pi/b$, one can significantly improve the speed of convergence. One can find the proof of the next theorem in [559].

Theorem B.48. Let f be b -band-limited, $h < \pi/b$, and γ be a smooth function such that $\gamma(x) = 0$ for $|x| > 1$ and $\int \gamma(x) dx = (2\pi)^{-1/2}$. Then

$$f(x) = \sum_k f(kh) \widehat{\gamma} \left(\left(\frac{\pi}{h} - b \right) (x - kh) \right) \sin c \left(\frac{\pi}{h} (x - kh) \right). \quad (\text{B.15})$$

Remark B.49. Notice that, due to the smoothness of γ , function $\widehat{\gamma}(x)$ decays at infinity very fast (faster than any power of $|x|$). This improves the convergence of the series significantly.

Exercise B.50. Write MATLAB scripts that evaluate the sums of 10, 20, and 30 terms of the Fourier series of the functions $f(x) = x$ and

$$g(x) = \begin{cases} x + \pi & \text{on } [-\pi, 0], \\ -x + \pi & \text{on } [0, \pi], \end{cases}$$

on $[-\pi, \pi]$. Graph them against the graphs of the original functions. Do you observe any phenomena discussed before? Do both functions display them?

B.16 • Mellin transform

The positive half-axis $\mathbb{R}^+ = \{x \in \mathbb{R} \mid x > 0\}$ is a group with respect to multiplication. The simple transform $t \in \mathbb{R}^+ \mapsto x = \ln t \in \mathbb{R}$ establishes an isomorphism

between the half-line \mathbb{R}^+ as a group with respect to multiplication and the real axis \mathbb{R} with respect to addition. Thus, there is a transform on functions defined on the positive half-axis that corresponds to the FT on the whole axis. This is the **Mellin transform**.

Exercise B.51.

1. Derive the formulas for the direct and inverse Mellin transforms on \mathbb{R}^+ by changing variables $x \mapsto t = e^x$ in the FT on \mathbb{R} .
2. Derive the Plancherel and Paley–Wiener-type theorems for the Mellin transform.

It is now clear that just as the FT diagonalizes shift invariant linear operators, its Mellin counterpart does the same for dilation invariant ones. Here by dilation one means the transformation $x \mapsto ax$ of \mathbb{R}^+ for some $a > 0$.

B.17 • Wavefront sets of distributions

Let $u(x)$ be a distribution on \mathbb{R}^n . We remind the reader of the notion of the **wavefront set** $WF(u)$ of u . This set carries detailed information on singularities of $u(x)$ and plays a crucial role in contemporary analysis, PDEs, as well as tomography.

Definition B.52. *Distribution $u(x)$ is said to be **microlocally smooth near a point** (x_0, ξ_0) , where $x_0, \xi_0 \in \mathbb{R}^n$ and $\xi_0 \neq 0$, if there is a smooth “cut-off” function $\phi(x)$ such that $\phi(x_0) \neq 0$ and such that the FT $\widehat{\phi u}(\xi)$ of the function $\phi(x)u(x)$ decays faster than any power $|\xi|^{-N}$ when $|\xi| \rightarrow \infty$, in directions that are close to the direction of ξ_0 .⁴⁴*

The **wavefront set** $WF(u) \subset \mathbb{R}_x^n \times (\mathbb{R}_\xi^n \setminus 0)$ of u consists of all pairs (x_0, ξ_0) such that u is not microlocally smooth near (x_0, ξ_0) .

In other words, if $(x_0, \xi_0) \in WF(u)$, then u is not smooth near x_0 , and the direction of ξ_0 indicates why it is not: The FT does not decay well in this direction. For instance, if $u(x)$ consists of two smooth pieces connected nonsmoothly across a smooth interface Σ , then $WF(u)$ can contain only pairs (x, ξ) such that $x \in \Sigma$ and ξ is normal to Σ at x .

⁴⁴We remind the reader that if this FT decays that way in all directions, then $u(x)$ is smooth (infinitely differentiable) near the point x_0 .

Appendix C

Geometric Rays, Trapping, Energy Decay

We provide here a brief account on energy decay of solutions of the wave equation. One can find more information and references on this well-studied topic in [141, 197, 638, 776, 777].

In what follows below, we are dealing with the wave equation problem in the whole space with a smooth sound speed $c(x)$:

$$\begin{cases} p_{tt} = c^2(x) \Delta_x p, & t \geq 0, x \in \mathbb{R}^n, \\ p(x, 0) = f(x), & p_t(x, 0) = 0. \end{cases} \quad (\text{C.1})$$

C.1 • Geometric rays

Let us consider the Hamiltonian system in $\mathbb{R}_{x,\xi}^{2n}$ with the Hamiltonian $H = \frac{c^2(x)}{2} |\xi|^2$:

$$\begin{cases} x'_t = \frac{\partial H}{\partial \xi} = c^2(x) \xi, \\ \xi'_t = -\frac{\partial H}{\partial x} = -\frac{1}{2} \nabla(c^2(x)) |\xi|^2, \\ x|_{t=0} = x_0, \quad \xi|_{t=0} = \xi_0. \end{cases} \quad (\text{C.2})$$

The solutions of this system are called **bicharacteristics**, and their projections into \mathbb{R}_x^n are **rays** (or **geometric rays**).

It is known (e.g., [378]) that singularities of solutions of the wave equation are carried by geometric rays. More precisely, the wavefront sets of solutions propagate with time along the bicharacteristics introduced above. This is a particular instance of a more general fact that applies to general PDEs and can be found in [378, 719]. As a result, if after time T all the rays leave the domain Ω of interest, the solution becomes smooth (infinitely differentiable) inside Ω .

C.2 ▪ Trapping

An important phenomenon called **trapping** can occur in the case of a variable speed. To introduce the so-called **nontrapping condition** on the sound speed $c(x)$ in \mathbb{R}^n , we have the following definition.

Definition C.1. *The sound speed $c(x)$ satisfies the **nontrapping condition** if all rays with $\xi_0 \neq 0$ tend to infinity when $t \rightarrow \infty$. If this condition is not satisfied, the rays that do not tend to infinity are called **trapped**.*

A simple example, where quite a few rays are trapped, is the radial parabolic sound speed $c(x) = c|x|^2$.

C.3 ▪ Local energy decay

We next recall the (already mentioned) notion of so-called **local energy decay**, which is important for understanding the nontrapping conditions in TAT.

Assuming that the initial data $f(x)$ from (11.1) is compactly supported and that the smooth speed $c(x)$ is nontrapping, one can provide so-called **local energy decay estimates** [197, 638, 776, 777]. Namely, in any bounded domain Ω , the solution $p(x, t)$ of (11.1) satisfies, for a sufficiently large T_0 and for any (k, m) , the estimate

$$\left| \frac{\partial^{k+|m|}}{\partial_t^k \partial_x^m} \right| \leq C_{k,m} v_k(t) \|f\|_{L^2} \quad \text{for } x \in \Omega, t > T_0. \quad (\text{C.3})$$

Here $v_k(t) = t^{-n+1-k}$ for even n , and $v_k(t) = e^{-\delta t}$ for odd n and some $\delta > 0$. Any value T_0 larger than the diameter of Ω works in this estimate.

Appendix D

Some Classes of Linear Operators and Operator Functions

We provide here a very brief overview of some main definitions and properties of Fredholm, semi-Fredholm, and Shatten-von Neumann classes of operators and operator-valued functions.

A more detailed surveys of (semi-)Fredholm operators can be found in [279, 400, 434, 816], and of the corresponding operator-functions in [816].

Shatten-von Neumann operator classes and the regularized determinants are discussed in detail in [195, 280, 720].

D.1 • Some notation concerning linear operators

Let E and F be Banach spaces. We denote by $L(E, F)$ the space of all bounded linear operators $A : E \rightarrow F$ equipped with the operator norm. When $E = F$, we use the notation $L(E) := L(E, E)$. The identity operator in E is denoted as I_E (we also write id or I when the domain of the mapping is clear from the context).

We denote by $GL(E) \subset L(E)$ the group of invertible bounded linear operators acting in E , and by $C(E, F) \subset L(E, F)$ the space of compact linear operators acting from E to F ($C(E)$ is used instead of $C(E, E)$).

For a linear operator A acting from E to F we denote by $Ran A$, $Ker A$, $Coker A$, and $rank A$ correspondingly the range, the kernel, the co-kernel and the rank of A :

$$\begin{aligned} Ran A &= \{y \in F \mid y = Ax, \text{ for some } x \in E\} \subset F, \\ Ker A &= \{x \in E \mid Ax = 0\} \subset E, \\ Coker A &= \{f \in F^* \mid f(Ax) = 0 \text{ for all } x \in E\} \subset F^*, \\ rank A &= \dim Ran A. \end{aligned}$$

D.2 • Fredholm and semi-Fredholm operators. Fredholm index.

Details about the topic sketched in this section can be found, for instance, in [279, 400, 434, 816] and [440, Chapter 1].

Definition D.1. An operator $A \in L(E, F)$ is said to be a **Fredholm operator**⁴⁵ if

- $\dim \text{Ker } A < \infty$;
- $\text{Ran } A$ is closed;
- $\dim \text{Coker } A < \infty$.

In this case

$$\text{ind}(A) := \dim \text{Ker } A - \dim \text{Coker } A$$

is said to be the **index** of A .

The set of Fredholm operators acting from E into F will be denoted $\Phi(E, F) \subset L(E, F)$ ($\Phi(E) := \Phi(E, E)$). The set $\Phi^n(E, F)$ consists of Fredholm operators of index n . So, $\Phi = \bigcup_{n \in \mathbb{Z}} \Phi^n$. We also use the notation

$$S_p \Phi(E) := \{A \in \Phi(E) \mid \dim \text{Ker } A \geq p\} \quad (\text{D.1})$$

and

$$CS_p \Phi(E) = \{A \in \Phi(E) \mid \dim \text{Coker } A \geq p\} \quad (\text{D.2})$$

The next result collects some standard properties of the Fredholm operators and their indexes.

Theorem D.2.

1. Each of the sets Φ^n (and thus the whole Φ) is open in the operator norm topology.
2. Index ind is a continuous (and thus locally constant) function on $\Phi(E, F)$.
3. $\text{ind}(AB) = \text{ind}(A) + \text{ind}(B)$.
4. $A \in \Phi(E)$ if and only if $A^* \in \Phi(E^*)$; further, $\text{ind}(A^*) = -\text{ind}(A)$.
5. If $A \in \Phi(E, F)$ and $B \in C(E, F)$, then $(A + B) \in \Phi(E, F)$ and $\text{ind}(A + B) = \text{ind}(A)$.
6. The set $\Phi^0(E, F)$ consists of the sums $A + B$, where $A \in L(E, F)$ is invertible and $B \in C(E, F)$.
7. An operator $A \in L(E, F)$ is Fredholm if and only if there exists an operator $B \in L(F, E)$ (called the **regularizer** of A) such that $AB - I$ and $BA - I$ are compact operators.
8. An operator $A \in L(E, F)$ is a Fredholm operator of index zero (i.e., $A \in \Phi^0(E, F)$) if and only if it has an invertible regularizer.

⁴⁵Sometimes the name **Noether operator** is used.

Theorem D.2 in particular claims that any Fredholm operator of zero index can be perturbed by a compact (or even finite-dimensional) operator to an invertible one.

The last two statements of this theorem are important for the discussion in Chapter 13. Indeed, as we see there, in tomography one can sometimes easily construct a two-sided or one-sided parametrix of a (pseudo-)differential operator arising in the problem. This means that it is an inverse (one-sided inverse) of the operator in question, **modulo smoothing operators**, which happen to be **compact**. This immediately implies that Fredholm and semi-Fredholm operators enter the game.

The following facts are also often useful.

Lemma D.3.

1. *The functions $\dim \text{Ker } A$ and $\text{co-dim Ran } A$ are upper semicontinuous on $\Phi(E, F)$.*
2. *Let $A_0 \in \Phi(E, F)$, and let M be a closed subspace of finite codimension in E such that $M \cap \text{Ker } A = \{0\}$. Then for all operators A in a neighborhood of A_0 one has $M \cap \text{Ker } A = \{0\}$.*

A wider class is formed by the so-called **semi-Fredholm operators**.

Definition D.4. *The class $\Phi_+(E, F)$ (resp., $\Phi_-(E, F)$) consists of all continuous linear operators from E to F with closed range and finite-dimensional kernel (correspondingly, co-kernel).*

Under the additional condition that the range (resp., the kernel) is a complemented subspace in F (in E), one obtains the class $\Phi_l(E, F)$ (resp., $\Phi_r(E, F)$).

In the Hilbert case $\Phi_+(E, F) = \Phi_l(E, F)$ and $\Phi_-(E, F) = \Phi_r(E, F)$.

The names used are correspondingly left semi-Fredholm operator and right semi-Fredholm operators.

The names chosen are explained by the following result.

Lemma D.5. *An operator $A \in L(E, F)$ belongs to $\Phi_l(E, F)$ if and only if there exists an operator $B \in L(F, E)$ (called **left regularizer** of A) such that the operator $BA - I$ is compact.*

*Similarly, an operator $A \in L(E, F)$ belongs to $\Phi_r(E, F)$ if and only if there exists an operator $B \in L(F, E)$ (called **right regularizer** of A) such that the operator $AB - I$ is compact.*

D.3 • Schatten–von Neumann classes

Detailed information on the topics of this section can be found in [195, 280, 720].

We assume here that we are dealing with operators in a separable Hilbert space H . Let $A \in C(H)$ be a compact linear operator in H . For any such operator, we denote by $\lambda_1(A) \geq \lambda_2(A) \geq \dots$ its eigenvalues counted in nonincreasing order with

their multiplicity. The operator A^*A is a nonnegative compact operator, and let $(A^*A)^{1/2}$ be its nonnegative square root.

Definition D.6. Let j be a nonnegative integer. The j th singular value (or the j th s-number) of A is

$$s_j(A) = \lambda_j((A^*A)^{1/2}). \quad (\text{D.3})$$

The importance of singular values is underscored by their following alternative descriptions.

Theorem D.7.

1. $s_j(A) = \min_{\dim M=j-1} \max_{x \neq 0, x \perp M} \frac{\|Ax\|}{\|x\|}$.
2. $s_j(A) = \min\{\|A - K\| \mid K \in L(H), \operatorname{rank} K \leq j-1\}$.
3. There exist (finite or infinite) ortho-normal sequences of vectors $\{\phi_j\}$ and $\{\psi_j\}$ such that

$$Ax = \sum_j s_j(A)(x, \psi_j)\phi_j \quad \text{for any } x \in H. \quad (\text{D.4})$$

We are now ready to introduce the celebrated Schatten–von Neumann classes of compact operators [195, 280, 720].

Definition D.8. Let $p \in [1, \infty]$. The Schatten–von Neumann classes $\mathcal{S}_p(H)$ consist of all compact linear operators A in H such that the sequence of the singular values $s_j(A)$ belongs to l_p ; i.e.,

$$\|A\|_p := \left(\sum_j s_j^p(A) \right)^{1/p} < \infty \quad \text{when } p < \infty.$$

For $p = \infty$, the norm naturally becomes $\max s_j(A)$, which coincides with the operator norm $\|A\|$ and thus $\mathcal{S}_\infty(H) = C(H)$.

The class \mathcal{S}_p is a Banach space with respect to the norm $\|A\|_p$. When $p_1 < p_2$, the space \mathcal{S}_{p_1} is continuously embedded into \mathcal{S}_{p_2} .

The class $\mathcal{S}_1(H)$ consists of **trace class operators**, while $\mathcal{S}_2(H)$ consists of **Hilbert–Schmidt operators**.

The classes \mathcal{S}_p are **operator ideals**; i.e., if $A \in \mathcal{S}_p(H)$ and $B \in L(H)$, then $AB \in \mathcal{S}_p(H)$ and $BA \in \mathcal{S}_p(H)$.

In a similar manner, one can introduce **Schatten–von Neumann classes** for compact operators acting between two Hilbert spaces.

The following example is instructive and useful for this text.

Consider the Sobolev space $H^s(\mathbb{T})$ of functions on the torus $\mathbb{T} = \mathbb{R}^n / \mathbb{Z}^n$. It consists of all functions $f(x) = \sum_{\gamma \in \mathbb{Z}^n} f_\gamma e^{2\pi i \gamma \cdot x}$ such that

$$\|f\|_s^2 = \sum (1 + |\gamma|)^{2s} |f_\gamma|^2 < \infty.$$

Theorem D.9. Let $s > 0$. The natural embedding operator from $H^s(\mathbb{T})$ into $L_2(\mathbb{T})$ belongs to the class $\mathcal{S}_p(H^s(\mathbb{T}), L_2(\mathbb{T}))$ for $p > \frac{n}{s}$.

A similar statement holds also on other compact manifolds, not just on the torus. The torus is chosen here due to the simplicity of the proof for this case.

Notice that this is the result that explains why inversion of a smoothing operator is unstable (ill-conditioned). This ill-conditioning gets worse when the degree of smoothing grows. See Section 7.3 for the related tomography discussion.

D.4 • Regularized determinants

See the details about what follows in [195, 280, 720].

Although we are not using this information explicitly in this book, consideration of Shatten–von Neumann operator ideals would not be complete without brief mention of the regularized determinants technique.

Definition D.10. Let p be a positive integer and $A \in \mathcal{S}_p(H)$. We define the **regularized determinant** of the operator $I - A$ as follows:

$$\det_p(I - A) := \prod_j \left((1 - \lambda_j(A)) \exp \left(\sum_{k=1}^{p-1} k^{-1} \lambda_j^k(A) \right) \right). \quad (\text{D.5})$$

If $A \in \mathcal{S}_r(H)$ for some noninteger r , the regularized determinant $\det_p(I - A)$ is defined for any $p > r$.

The following result collects the main properties of regularized determinants.

Theorem D.11.

1. If $r \leq p$, then the determinant $\det_p(I - A)$ is analytic as a complex-valued function on the complex Banach space $\mathcal{S}_p(H)$.

2. If $p - 1 \leq r \leq p$, then

$$|\det_p(I - A)| \leq C e^{C \|A\|_r^r},$$

where the constant C depends only on p and r .

3. If $p \geq 2$ and $r \leq p - 1$, then for $A \in \mathcal{S}_r(H)$ one has

$$\det_p(I - A) = e^{(p-1)^{-1} \operatorname{tr}(A^{p-1})} \det_{p-1}(I - A).$$

4. If $p - 1 \leq r \leq p$ and $A \in \mathcal{S}_r(H)$, then the operator-valued function $\det_p(I - A)(I - A)^{-1}$ (a priori defined only when $1 \notin \sigma(A)$), is analytic on the whole Banach space $\mathcal{S}_r(H)$ and satisfies the estimate

$$\|\det_p(I - A)(I - A)^{-1}\| \leq e^{C(\|A\|_r^r + 1)}$$

for some constant C depending on p and r .

D.5 ▪ Analytic Fredholm operator functions

In this section, we briefly present some basic facts about holomorphic Fredholm operator functions. Most of the proofs and relevant references can be found in [816], and partly in [440, Chapter 1].

D.5.1 ▪ Some notions from the several complex variables theory

In Chapter 13, we use operator-valued functions analytically depending on a multidimensional (or even infinitely-dimensional) complex parameter. In addition to open sets in complex Banach spaces, we also encounter sometimes a nice class of complex domains/manifolds/analytic sets, the so-called **Stein manifolds**. In particular, the so-called **Oka's principle** holds for these manifolds, which essentially says that “everything that can be done topologically can be done analytically” (e.g., topologically trivial vector bundles are automatically analytically trivial). One can find this and other basic notions and results of the several complex variables theory in many books, such as [296, 329, 376, 504].

Definition D.12. *A complex analytic, countable at infinity, manifold X is called a Stein manifold if the following hold:*

1. *It is holomorphically convex (i.e., the holomorphic convex hull of any compact subset of X is compact).*
2. *It is holomorphically separable (i.e., for any two distinct points $x, y \in X$ there is a holomorphic function f on X with the property that $f(x) \neq f(y)$).*
3. *For any point $x_0 \in X$ there is a set of holomorphic functions on X forming local coordinates in a neighborhood of x_0 .*

There are several frequently encountered cases, when X is Stein, including these:

- Any 1D domain $X \subset \mathbb{C}$ is Stein. Thus, when dealing with functions of one variable, one should not worry about satisfying the Stein properties.
- Any direct product of 1D domains $U_1 \times U_2 \times \dots \times U_n \subset \mathbb{C}^n$ is Stein.
- Any analytic submanifold of \mathbb{C}^n (or even a finite-dimensional analytic submanifold of an infinite-dimensional complex Banach space) is Stein.

Definition D.13. *A subset X of an analytic manifold M is said to be an analytic set if it can be locally described as the set of common zeros of several analytic functions. If (locally) one such function suffices, the set is called a principal analytic one.*

D.5.2 ■ Analytic Fredholm operator functions

Let $A(z)$, $z \in X$, be an analytic function on the analytic manifold X with values in the set $\Phi(E)$ of Fredholm operators in a complex Banach space E . We are interested in the sets of points $z \in X$, where the kernel of $A(z)$ is nontrivial (the **spectrum of the operator function** $A(\cdot)$) and where the co-kernel is nontrivial (**co-spectrum**). In order to do this, instead of working with particular operator functions, let us turn to the sets $S_p\Phi(E)$ and $CS_p\Phi(E)$ (see (D.1) and (D.2)).

Theorem D.14.

1. *The set $S_p\Phi(E)$ is an analytic subset of $\Phi(E)$.*
2. *The same is true for $CS_p\Phi(E)$.*
3. *In particular, the set $\Phi^{(0)}(E) \setminus GL(E)$ is a principal analytic subset in $\Phi^{(0)}(E)$.*

Now, let $A(z)$, $z \in X$, be a Fredholm-valued analytic function on analytic manifold X .

We define a scale of its spectra (co-spectra) as follows.

Definition D.15.

- $S_p(A(\cdot)) := \{z \in X \mid A(z) \in S_p\Phi(E)\} = A^{-1}(S_p\Phi(E)) = \{z \in X \mid \dim \text{Ker}A(z) \geq p\}.$
- $CS_p(A(\cdot)) := \{z \in X \mid A(z) \in CS_p\Phi(E)\} = A^{-1}(CS_p\Phi(E)) = \{z \in X \mid \dim \text{Coker}A(z) \geq p\}.$

Corollary D.16.

- $S_p(A(\cdot))$ and $CS_p(A(\cdot))$ are analytic subsets of X .
- If the values $A(z)$ are of zero index, then $S_1(A(\cdot)) = CS_1(A(\cdot))$ is a principal analytic subset of X .

The following result follows from [816, Theorem 4.6].

Theorem D.17. *Let $f : X \rightarrow \Phi_l(E, F)$ be an analytic mapping such that for some $x_0 \in X$ the operator $f(x_0)$ has zero kernel. Then $f(x)$ has zero kernel for any x outside of a proper analytic subset of X .*

Appendix E

Recommended Books and Surveys

Disclaimer: There are many other good sources besides the ones mentioned below. The choices made reflect the author’s personal knowledge and/or preferences.

Fourier series

See [760] for one dimension and [741] for any dimension.

Fourier transform

A nice introduction to the Fourier transform, distributions, and microlocal analysis is [745]. Several books by E. Stein provide Fourier analysis theory on different levels (e.g., [740] and the classic [741]). Körner’s book [426] is a wonderful collection of essays, proofs, historical accounts, etc., concerning Fourier analysis. Hörmander’s volume [377] is a comprehensive (albeit very technical) account of Fourier analysis. Natterer’s classical book [559] shows how Fourier analysis works in tomography.

Harmonic analysis

A wonderful historical survey is “Harmonic analysis as exploitation of symmetry” by G. Mackey [502]. See also [331, 426, 706, 740] concerning mostly commutative harmonic analysis, and [265, 366, 420, 433, 754, 787, 788] for the non-commutative version (which we left behind the scenes in this text).

Sampling

See [559, Chapter III] as well as [206–210, 213].

Microlocal analysis—Wavefront sets, pseudodifferential operators, integral Fourier operators

Gentle introductions include [588, 745]. For textbooks and lecture notes, see [240, 241, 526, 719, 753]. More advanced material can be found in [131, 301, 302, 328, 377–379, 692, 764].

Integral geometry and the Radon transform

Introductory texts of Radon transform and integral geometry are [261, 349, 817]. More advanced material is given in [198, 252, 290, 353, 354, 392, 651, 684, 710]. For integral geometry in relation to tomography, see [442, 453, 559, 577, 602, 620].

Video lectures and slides on inverse problems and tomography

See [444, 560, 786, 786].

Tomography

An outdated, but still very useful collection of **nontechnical surveys of physics, mathematics, and challenges of various types of medical imaging** is [168]. See also [142, 707, 711, 712, 725, 726].

Undergraduate texts include [203, 217]; **classical texts with an applied tilt** are [123, 186, 358, 396]; and **classical texts on analysis of tomography** include [396, 559, 577, 726]. Maybe not classical, but still worth noting in this last category are [203, 208, 442, 511, 649, 657].

For specific techniques, see the following: **emission tomography** [52, 133, 221, 357, 361, 442, 559, 577]; **EIT (electrical impedance tomography)** [113, 159, 160, 675, 676, 781]; **MREIT, CDI, CDII (hybrid versions of EIT)** [65, 546–548, 708, 803]; **thermo-/photoacoustics** [7, 28, 226, 445, 448, 630, 634, 732, 739, 766, 789, 798]; **hybrid methods** [47, 61, 443, 444, 456, 457, 739, 775, 786]; **radar and sonar** [157, 158, 573, 589]; **electron and cryo-electron imaging** [237, 601, 721]; **statistical techniques** [148, 383, 398, 751].

Radiation therapy planning

See [119, 120, 151, 153].

Inverse problems for PDEs

See [147, 386, 387, 392, 410, 477, 542, 579, 659, 694, 759, 769].

Invisibility cloaking

See [478, 481, 773].

Collections of articles on inverse problems and tomography

Among the many, start with [65, 92, 105, 120, 132, 153, 164, 168, 237, 251, 277, 295, 357, 359, 360, 362, 383, 477, 602, 660, 661, 700, 701, 766, 771, 775, 789, 793, 799, 823].

Bibliography

- [1] J.-F. P. J. Abascal, W. R. B. Lionheart, S. R. Arridge, M. Schweiger, D. Atkinson, D. S. Holder, Electrical impedance tomography in anisotropic media with known eigenvectors, *Inverse Problems*, **27** (2011), 065004.
- [2] R. A. Adams, *Sobolev Spaces*, Academic Press, New York, 1975.
- [3] S. Agmon, A. Douglis, L. Nirenberg, Estimates near the boundary for solutions of elliptic partial differential equations satisfying general boundary conditions. I, *Comm. Pure Appl. Math.*, **12** (1959), pp. 623–727; II, *Comm. Pure Appl. Math.*, **17** (1964), pp. 35–92.
- [4] M. Agranovsky, C. Berenstein, P. Kuchment, Approximation by spherical waves in L^p -spaces, *J. Geom. Anal.*, **6** (1996), pp. 365–383.
- [5] M. Agranovsky, D. Finch, P. Kuchment, Range conditions for a spherical mean transform, *Inverse Problems Imaging*, **3** (2009), pp. 373–338.
- [6] M. Agranovsky and P. Kuchment, Uniqueness of reconstruction and an inversion procedure for thermoacoustic and photoacoustic tomography with variable sound speed, *Inverse Problems*, **23** (2007), pp. 2089–2102.
- [7] M. Agranovsky, P. Kuchment, L. Kunyansky, On reconstruction formulas and algorithms for the thermoacoustic and photoacoustic tomography, in [793, pp. 89–101].
- [8] M. Agranovsky, P. Kuchment, E. T. Quinto, Range descriptions for the spherical mean Radon transform, *J. Funct. Anal.*, **248** (2007), pp. 344–386.
- [9] M. Agranovsky and L. Nguyen, Range conditions for a spherical mean transform and global extension of solutions of Darboux equation, *J. Anal. Math.*, **112** (2011), pp. 351–367.
- [10] M. Agranovsky and E. T. Quinto, Injectivity sets for the Radon transform over circles and complete systems of radial functions, *J. Funct. Anal.* **139** (1996), pp. 383–414.
- [11] M. L. Agranovsky, V. V. Volchkov, L. Zalcman, Conical uniqueness sets for the spherical Radon transform, *Bull. London Math. So.*, **31** (1999), pp. 363–372.
- [12] V. Aguilar, L. Ehrenpreis, P. Kuchment, Range conditions for the exponential Radon transform, *J. Anal. Math.*, **68** (1996), pp. 1–13.
- [13] V. Aguilar and P. Kuchment, Range conditions for the multidimensional exponential X-ray transform, *Inverse Problems*, **11** (1995), pp. 977–982.
- [14] G. Alessandrini and V. Nesi, Univalent σ -harmonic mappings, *Arch. Ration. Mech. Anal.*, **158** (2001), pp. 155–171.

- [15] M. Allmaras and W. Bangerth, Reconstructions in ultrasound modulated optical tomography, *J. Inverse Ill-Posed Problems*, **19** (2011), pp. 801–823.
- [16] M. Allmaras, W. Charlton, A. Ciabatti, Y. Hristova, P. Kuchment, A. Olson, J. Ragusa, *Detecting small low emission sources—Case studies*, preprint, arXiv:1309.5974, 2013.
- [17] M. Allmaras, D. Darrow, Y. Hristova, G. Kanschat, P. Kuchment, Detecting small low emission radiating sources, *Inverse Problems Imaging*, **7** (2013), pp. 47–79.
- [18] G. Ambartsoumian, Inversion of the V-line Radon transform in a disc and its applications in imaging, *Comput. Math. Appl.*, **64** (2012), pp. 260–265.
- [19] G. Ambartsoumian, J. Boman, V. P. Krishnan, E. T. Quinto, Microlocal analysis of an ultrasound transform with circular source and receiver trajectories, in [661, pp. 45–58].
- [20] G. Ambartsoumian, R. Gouia-Zarrad, M. A. Lewis, Inversion of the circular Radon transform on an annulus, *Inverse Problems*, **26** (2010), 105015.
- [21] G. Ambartsoumian and P. Kuchment, On the injectivity of the circular Radon transform, *Inverse Problems*, **21** (2005), pp. 473–485.
- [22] G. Ambartsoumian and P. Kuchment, A range description for the planar circular Radon transform, *SIAM J. Math. Anal.*, **38** (2006), pp. 681–692.
- [23] G. Ambartsoumian and L. Kunyansky, *Exterior/interior problem for the circular means transform with applications to intravascular imaging*, arXiv:1308.6016, 2013.
- [24] G. Ambartsoumian and S. Moon, A series formula for inversion of a V-line Radon transform in a disc, *Comput. Math. Appl.*, to appear.
- [25] G. Ambartsoumian and M. Xie, Tomographic reconstruction of nodular images from incomplete data. Application of mathematics in technical and natural sciences, in *Proceedings of the AIP Conference*, 1301, Amer. Inst. Phys., Melville, NY, 2010, pp. 167–174.
- [26] H. Ammari, *An Introduction to Mathematics of Emerging Biomedical Imaging*, Springer-Verlag, Berlin, 2008.
- [27] H. Ammari, E. Bonnetier, Y. Capdeboscq, M. Tanter, M. Fink, Electrical impedance tomography by elastic deformation, *SIAM J. Appl. Math.*, **68** (2008), pp. 557–573.
- [28] H. Ammari, E. Bossy, V. Jugnon, H. Kang, Mathematical modeling in photoacoustic imaging of small absorbers, *SIAM Rev.*, **52** (2010), pp. 677–695.
- [29] H. Ammari, E. Bretin, V. Jugnon, A. Wahab, Photo-acoustic imaging for attenuating acoustic media, in *Mathematical Modeling in Biomedical Imaging II*, Lecture Notes Math. **2035**, Springer-Verlag, Berlin, 2011, pp. 57–84.
- [30] H. Ammari, G. Ciraolo, H. Kang, H. Lee, G. Milton, Spectral theory of a Neumann-Poincaré-type operator and analysis of cloaking due to anomalous localized resonance, *Arch. Ration. Mech. Anal.*, **208** (2013), pp. 667–692.
- [31] H. Ammari, J. Garnier, W. Jing, Resolution and stability analysis in acousto-electric imaging, *Inverse Problems*, **28** (2012), 084005.
- [32] M. A. Anastasio, J. Zhang, D. Modgil, P. J. La Rivière, Application of inverse source concepts to photoacoustic tomography, *Inverse Problems*, **23** (2007), pp. S21–S35.

- [33] M. Anastasio, J. Zhang, X. Pan, Y. Zou, G. Ku, L. V. Wang, Half-time image reconstruction in thermoacoustic tomography, *IEEE Trans. Med. Imaging*, **24** (2005), pp. 199–210.
- [34] M. A. Anastasio, J. Zhang, E. Y. Sidky, Z. Zou, X. Dan, X. Pan, Feasibility of half-data image reconstruction in 3-D reflectivity tomography with a spherical aperture, *IEEE Trans. Med. Imaging*, **24** (2005), pp. 1100–1112.
- [35] L.-E. Andersson, On the determination of a function from spherical averages, *SIAM J. Math. Anal.*, **19** (1988), pp. 214–232.
- [36] V. Andreev, D. Popov, et al, Image reconstruction in 3D optoacoustic tomography system with hemispherical transducer array, *Proc. SPIE*, **4618** (2002), pp. 137–145.
- [37] Yu. E. Anikonov and I. Shneiberg, Radon transform with variable attenuation, *Dokl. Akad. Nauk SSSR*, **316** (1991), pp. 93–95; English translation in *Soviet. Math. Dokl.*
- [38] Y. A. Antipov, R. Estrada, B. Rubin, Method of analytic continuation for the inverse spherical mean transform in constant curvature spaces, *J. Anal. Math.*, **118** (2012), pp. 623–656.
- [39] Y. A. Antipov and B. Rubin, A generalization of the Mader-Helgason inversion formulas for Radon transforms, *Trans. Amer. Math. Soc.*, **364** (2012), pp. 6479–6493.
- [40] D. Applegate, J. Reeds, S. Scheinberg, L. Shepp, P. Shor, Some problems in probabilistic tomography, *Teor. Veroyatnost. i Primenen.*, **41** (1996), pp. 323–335; translation in *Theory Probab. Appl.*, **41** (1996), pp. 199–209.
- [41] E. V. Arbuzov, A. L. Bukhgeim, and S. G. Kazantsev, Two-dimensional tomography problems and the theory of A-analytic functions, *Siberian Adv. Math.*, **8** (1998), pp. 1–20.
- [42] S. R. Arridge, Methods in diffuse optical imaging, *Philos. Trans. R. Soc. Lond. Ser. A Math. Phys. Eng. Sci.*, **369** (2011), pp. 4558–4576.
- [43] S. R. Arridge, Optical tomography in medical imaging, *Inverse Problems*, **15** (1999), pp. R41–R93.
- [44] S. R. Arridge and J. C. Hebden, Optical imaging in medicine II: Modelling and reconstruction, *Phys. Med. Biol.*, **42** (1997), pp. 841–853.
- [45] S. R. Arridge, V. Kolehmainen, M. J. Schweiger, Reconstruction and regularisation in optical tomography, in [153, pp. 1–18].
- [46] S. R. Arridge, S. Moskow, J. C. Schotland, Inverse Born series for the Calderon problem, *Inverse Problems*, **28** (2012), 035003.
- [47] S. R. Arridge and O. Scherzer, Imaging from coupled physics, *Inverse Problems*, **28** (2012), 080201.
- [48] S. R. Arridge and M. Schweiger, A general framework for iterative reconstruction algorithms in optical tomography, using a finite element method. Computational radiology and imaging (Minneapolis, MN, 1997), *IMA Vol. Math. Appl.* **110**, Springer, New York, 1999, pp. 45–70.
- [49] K. Astala, J. Mueller, L. Päivärinta, A. Perämäki, S. Siltanen, Direct electrical impedance tomography for nonsmooth conductivities, *Inverse Problems Imaging*, **5** (2011), pp. 531–549.
- [50] K. Astala and L. Päivärinta, Calderón’s inverse conductivity problem in the plane, *Ann. Math.*, **163** (2006), pp. 265–299.

- [51] D. L. Bailey, B. F. Hutton, and P. J. Walker, Improved SPECT using simultaneous emission and transmission tomography, *J. Nuclear Med.*, **28** (1987), pp. 844–851.
- [52] D. L. Bailey, D. W. Townsend, P. E. Valk, M. N. Maisey, *Positron Emission Tomography: Basic Sciences*, Springer-Verlag, Secaucus, NJ, 2005.
- [53] T. N. Bailey and R. J. Baston (Editors), *Twistors in Mathematics and Physics*, London Mathematical Society Lecture Note Series **156**, Cambridge University Press, Cambridge, UK, 1990.
- [54] B. B. Baker, *The Mathematical Theory of Huygens' Principle*, AMS, Providence, RI, 2003.
- [55] G. Bal, Optical tomography for small volume absorbing inclusions, *Inverse Problems*, **19** (2003), pp. 371–386.
- [56] G. Bal, On the attenuated Radon transform with full and partial measurements, *Inverse Problems*, **20** (2004), pp. 399–418.
- [57] G. Bal, Ray transforms in hyperbolic geometry, *J. Math. Pures Appl. (9)*, **84** (2005), pp. 1362–1392.
- [58] G. Bal, Reconstructions in impedance and optical tomography with singular interfaces, *Inverse Problems*, **21** (2005), pp. 113–131.
- [59] G. Bal, Inverse transport theory and applications, *Inverse Problems*, **25** (2009), 053001.
- [60] G. Bal, Cauchy Problem for Ultrasound Modulated EIT, *Anal. Partial Differential Equations*, **6** (2013), pp. 751–775.
- [61] G. Bal, Hybrid inverse problems and internal functionals, in [775, pp. 325–368].
- [62] G. Bal, Explicit Reconstructions in QPAT, QTAT, TE, and MRE, arXiv:1202.3117.
- [63] G. Bal, Hybrid Inverse Problems and Redundant Systems of Partial Differential Equations, arXiv:1210.0265.
- [64] G. Bal, E. Bonnetier, F. Monard, F. Triki, Inverse Diffusion from Knowledge of Power Densities, *Inverse Problems Imaging*, **7** (2013), pp. 353–375.
- [65] G. Bal, D. Finch, P. Kuchment, P. Stefanov, G. Uhlmann (Editors), *Tomography and Inverse Transport Theory*, AMS, Providence, RI, 2011.
- [66] G. Bal, C. Guo, F. Monard, Linearized Internal Functionals for Anisotropic Conductivities, arXiv:1302.3354.
- [67] G. Bal, C. Guo, F. Monard, Inverse Anisotropic Conductivity from Internal Current Densities, arXiv:1303.6665.
- [68] G. Bal and A. Jollivet, Combined source and attenuation reconstructions in SPECT, in [65, pp. 13–27].
- [69] G. Bal, A. Jollivet, V. Jugnon, Inverse transport theory of photoacoustics, *Inverse Problems*, **26** (2010), 025011.
- [70] G. Bal and P. Moireau, Fast numerical inversion of the attenuated Radon transform with full and partial measurements, *Inverse Problems*, **20** (2004), pp. 1137–1164.
- [71] G. Bal and S. Moskow, Local Inversions in Ultrasound Modulated Optical Tomography, arXiv:1303.5178.

- [72] G. Bal, W. Naetar, O. Scherzer, The Levenberga Marquardt iteration for numerical inversion of the power density operator, *J. Inverse Ill-Posed Problems*, **21** (2013), pp. 265–280.
- [73] G. Bal and K. Ren, Multiple-source quantitative photoacoustic tomography in a diffusive regime, *Inverse Problems*, **27** (2011), 075003.
- [74] G. Bal and K. Ren, Non-uniqueness result for a hybrid inverse problem, in [65, pp. 29–38].
- [75] G. Bal and K. Ren, On multi-spectral quantitative photoacoustic tomography in diffusive regime, *Inverse Problems*, **28** (2012), 025010.
- [76] G. Bal, K. Ren, G. Uhlmann, T. Zhou, Quantitative thermo-acoustics and related problems. *Inverse Problems*, **27** (2011), 055007.
- [77] G. Bal and J. C. Schotland, Inverse scattering and acousto-optic imaging, *Phys. Rev. Lett.*, **104** (2010), 043902.
- [78] G. Bal and G. Uhlmann, Inverse diffusion theory of photoacoustics, *Inverse Problems*, **26** (2010), 085010.
- [79] G. Bal and G. Uhlmann, Reconstructions for some coupled-physics inverse problems, *Appl. Math. Lett.*, **25** (2012), pp. 1030–1033.
- [80] D. C. Barber and B. H. Brown, Applied potential tomography, *J. Phys. E*, **17** (1984), pp. 723–733.
- [81] D. C. Barber and B. H. Brown, Recent developments in applied potential tomography—APT, in *Information Processing in Medical Imaging*, Nijhoff, Amsterdam, 1986, pp. 106–121.
- [82] D. C. Barber and B. H. Brown, Progress in electrical impedance tomography, in *Inverse Problems in Partial Differential Equations*, SIAM, Philadelphia, 1990, pp. 151–164.
- [83] C. Bardos, A mathematical and deterministic analysis of the time-reversal mirror, in [771, pp. 381–400].
- [84] A. Barnett, C. Gordon, P. Perry, A. Uribe (Editors), *Spectral Geometry*, AMS, Providence, RI, 2012.
- [85] H. H. Barrett and K. J. Myers, *Foundations of Imaging Science*, Wiley Interscience, New York, 2004.
- [86] H. H. Barrett and W. Swindell, *Radiological Imaging: The Theory of Image Formation, Detection, and Processing*, Academic Press, New York, 1981.
- [87] A. O. Barut and R. Raczka, *Theory of Group Representations and Applications*, second edition, World Scientific Publishing, Singapore, 1986.
- [88] R. Baston and M. Eastwood, *The Penrose Transform. Its Interaction with Representation Theory*, Oxford Mathematical Monographs, Oxford Science Publications, Clarendon Press, Oxford University Press, New York, 1989.
- [89] A. G. Bell, On the production and reproduction of sound by light, *Am. J. Sci.*, **20** (1880), pp. 305–324.
- [90] A. G. Bell, Production of sound by radiant energy, *Manufacturer and Builder*, **13** (1881), 156.
- [91] S. Bellini, M. Piacentini, C. Caffario, P. Rocca, Compensation of tissue absorption in emission tomography, *IEEE Trans. ASSP*, **27** (1979), pp. 213–218.

- [92] A. Bellow, E. Kenig, P. Malliavin (Editors), *Selected papers of Alberto P. Calderón*, with commentary. AMS, Providence, RI, 2008.
- [93] C. Berenstein and E. Casadio Tarabusi, The inverse conductivity problem and the hyperbolic X-ray transform, in [277, pp. 39–44].
- [94] C. A. Berenstein and E. Casadio Tarabusi, Integral geometry in hyperbolic spaces and electrical impedance tomography, *SIAM J. Appl. Math.*, **56** (1996), pp. 755–764.
- [95] J. Bernstein and S. Gindikin, Notes on integral geometry for manifolds of curves, *Amer. Math. Soc. Transl. (2)*, **210** (2003), pp. 57–80.
- [96] M. A. Bernstein, K. F. King, X. J. Zhou, *Handbook of MRI Pulse Sequences*, Elsevier, New York, 2004.
- [97] M. Bertero and P. Boccacci, *Introduction to Inverse Problems in Imaging*, Institute of Physics Publishing, Bristol, Philadelphia, 1998.
- [98] M. Bertero, H. Lantéri, L. Zanni, Iterative image reconstruction: A point of view, in [153, pp. 37–54].
- [99] G. Beylkin, The inversion problem and applications of the generalized Radon transform, *Comm. Pure Appl. Math.*, **37** (1984), pp. 579–599.
- [100] G. Beylkin, Inversion and applications of the generalized Radon transform, in [277, pp. 70–80].
- [101] J. Bikowski, K. Knudsen, J. L. Mueller, Direct numerical reconstruction of conductivities in three dimensions using scattering transforms, *Inverse Problems*, **27** (2011), 015002.
- [102] B. L. Biondi, *3D Seismic Imaging*, Soc. Explor. Geophysics, 2006.
- [103] S. S. Blume, *Insight and Industry: On the Dynamics of Technological Change in Medicine*, MIT Press, Cambridge, MA, 1992.
- [104] H. Bockwinkel, On the propagation of light in a biaxial crystal about a midpoint of oscillation, *Verh. Konink Acad. V. Wet. Wissen. Natur.*, **14** (1906), 636.
- [105] H. M. J. Boffin, D. Steeghs, J. Cuypers (Editors), *Astrotomography: Indirect Imaging Methods in Observational Astronomy*, Springer-Verlag, Berlin, 2001.
- [106] J. Boman, An example of nonuniqueness for a generalized Radon transform, *J. Anal. Math.*, **61** (1993), pp. 395–401.
- [107] J. Boman, On stable inversion of the attenuated Radon transform with half data, in *Integral Geometry and Tomography*, Contemp. Math. **405**, Amer. Math. Soc., Providence, RI, 2006, pp. 19–26.
- [108] J. Boman, A local uniqueness theorem for weighted Radon transforms, *Inverse Problems Imaging*, **4** (2010), pp. 631–637.
- [109] J. Boman and E. T. Quinto, Support theorems for real analytic Radon transforms, *Duke Math. J.*, **55** (1987), pp. 943–948.
- [110] J. Boman and E.T. Quinto, Support theorems for real-analytic Radon transforms on line complexes in three-space, *Trans. Amer. Math. Soc.*, **335** (1993), pp. 877–890.
- [111] J. Boman and J.-O. Strömberg, Novikov’s inversion formula for the attenuated Radon transform—A new approach, *J. Geom. Anal.*, **14** (2004), pp. 185–198.

- [112] E. Bonnetier and F. Triki, A stability result for electric impedance tomography by elastic perturbation, Presentation at the workshop “Inverse Problems: Theory and Applications,” November 12th, 2010, MSRI, Berkeley, CA.
- [113] L. Borcea, Electrical impedance tomography, *Inverse Problems*, **18** (2002), pp R99–R136.
- [114] L. Borcea, J. G. Berryman, G. C. Papanicolaou, High contrast impedance tomography, *Inverse Problems*, **12** (1996), pp 1–24.
- [115] L. Borcea, V. Druskin, F. Guevara Vasquez, Electrical impedance tomography with resistor networks, *Inverse Problems*, **24** (2008), 035013.
- [116] L. Borcea, V. Druskin, A. V. Mamonov, Circular resistor networks for electrical impedance tomography with partial boundary measurements, *Inverse Problems*, **26** (2010), 045010.
- [117] L. Borcea, V. Druskin, A. V. Mamonov, F. Guevara Vasquez, Pyramidal resistor networks for electrical impedance tomography with partial boundary measurements, *Inverse Problems*, **26** (2010), 105009.
- [118] L. Borcea, G. C. Papanicolaou, Network approximation for transport properties of high contrast materials, *SIAM J. Appl. Math.*, **58** (1998), pp. 501–539.
- [119] C. Börgers, The radiation therapy planning problem, in [120, pp. 1–16].
- [120] C. Börgers and F. Natterer (Editors), *Computational Radiology and Imaging. Therapy and Diagnostics*, Springer-Verlag, New York, 1999.
- [121] T. Bowen, Radiation-induced thermoacoustic soft tissue imaging, *Proc. IEEE Ultrasonics Symposium*, **2** (1981), pp. 817–822.
- [122] R. N. Bracewell, Strip integration in radio astronomy, *Australian J. Phys.*, **9** (1956), pp. 198–217.
- [123] R. N. Bracewell, *Two-Dimensional Imaging*, Prentice-Hall, Englewood Cliffs, NJ, 1995.
- [124] R. N. Bracewell and A. C. Riddle, Inversion of fan-beam scans in radio astronomy, *Astrophys. J.*, **150** (1967), pp. 427–434.
- [125] T. P. Branson, G. Olafsson, H. Schlichtkrull, A bundle-valued Radon transform with applications to invariant wave equations, *Quart. J. Math. Oxford*, **45** (1994), pp. 429–461.
- [126] A.V. Bronnikov, Approximate reconstruction of attenuation map in SPECT imaging, *IEEE Trans. Nuclear Sci.*, **42** (1993), pp. 1483–1488.
- [127] A. V. Bronnikov, Numerical solution of the identification problem for the attenuated Radon transform, *Inverse Problems*, **15** (1999), pp. 1315–1324.
- [128] A. V. Bronnikov and A. Kema, Reconstruction of attenuation map using discrete consistency conditions, *IEEE Trans. Med. Imaging*, **19** (2000), pp. 451–462.
- [129] R. Brooks, C. Gordon, P. Perry (Editors), *Geometry of the Spectrum*, AMS, Providence, RI, 1994.
- [130] G. L. Brownell, A history of positron imaging, Presentation given in celebration of the 50th year of services by the author to the Massachusetts General Hospital on October 15th, 1999; online version at <http://www.petdiagnostik.ch/de/informationen-fuer-fachpersonen/a-history-of-positron-imaging/index.php>.

- [131] J. Brüning and V. W. Guillemin (Editors), *Mathematics Past and Present. Fourier Integral Operators*, Springer-Verlag, Berlin, 1994.
- [132] R. L. Bryant, V. Guillemin, S. Helgason, R. O. Wells (Editors), *Integral Geometry*, Contemp. Math. **63**, AMS, Providence, RI, 1987.
- [133] T. F. Budinger, G. T. Gullberg, R. H. Huseman, Emission computed tomography, in [357, pp. 147–246].
- [134] A. L. Bukhgeim, Inversion formulas in inverse problems, a supplement to M. M. Lavrent'ev and L. Ya. Savel'ev, “Linear Operators and Ill-posed Problems”, Nauka, Moscow, 1995; Translated from the Russian, Consultants Bureau, New York.
- [135] A. L. Bukhgeim, Inverse gravimetry approach to attenuated tomography, in [65, pp. 49–63].
- [136] B. Bukovics, Biography of Johann Radon, in [277, pp. 13–18].
- [137] P. Burgholzer, H. Grün, M. Haltmeier, R. Nuster, G. Paltauf, Compensation of Acoustic Attenuation for High-Resolution Photoacoustic Imaging with Line Detectors Using Time Reversal, in Proc. SPIE 6437–75, SPIE, Bellingham, WA, 2007.
- [138] P. Burgholzer, C. Hofer, G. J. Matt, G. Paltauf, M. Haltmeier, O. Scherzer, Thermoacoustic tomography using a fiber-based Fabry-Perot interferometer as an integrating line detector, Proc. SPIE 6086, SPIE, Bellingham, WA, 2006, pp. 434–442.
- [139] P. Burgholzer, C. Hofer, G. Paltauf, M. Haltmeier, O. Scherzer, Thermoacoustic tomography with integrating area and line detectors, *IEEE Trans. Ultrasonics, Ferroelectrics, and Frequency Control*, **52** (2005), pp. 1577–1583.
- [140] P. Burgholzer, G. J. Matt, G. Paltauf, M. Haltmeier, Exact and approximate imaging methods for photoacoustic tomography using an arbitrary detection surface, *Phys. Rev. E*, **75** (2007), 046706.
- [141] N. Burq, Décroissance de l'énergie locale de l'équation des ondes pour le problème extérieur et absence de résonance au voisinage du réel, *Acta Math.*, **180** (1998), pp. 1–29.
- [142] T. M. Buzug, *Computed Tomography*, Springer-Verlag, Berlin, 2008.
- [143] F. Cakoni, D. Gintides, H. Haddar, The existence of an infinite discrete set of transmission eigenvalues, *SIAM J. Math. Anal.*, **42** (2010), pp. 237–255.
- [144] F. Cakoni and H. Haddar, Transmission eigenvalues in inverse scattering theory, in [775, pp. 529–580].
- [145] A. Calderón, On an inverse boundary value problem, *Seminar on Numerical Analysis and Its Applications to Continuum Physics*, Soc. Brasileira de Matemática, Rio de Janeiro, Brazil, 1980, pp. 65–73.
- [146] P. Callaghan, *Principles of Nuclear Magnetic Resonance Microscopy*, Oxford University Press, London, 1994.
- [147] D. Calvetti and E. Somersalo, *Computational Mathematical Modeling: An Integrated Approach Across Scales*, Math. Model. Comput. **17**, SIAM, Philadelphia, 2013.
- [148] D. Calvetti and E. Somersalo, *Introduction to Bayesian Scientific Computing. Ten Lectures on Subjective Computing*, Springer, New York, 2007.

- [149] Y. Capdeboscq, J. Fehrenbach, F. de Gournay, O. Kavian, Imaging by modification: Numerical reconstruction of local conductivities from corresponding power density measurements, *SIAM J. Imaging Sci.*, **2** (2009), pp. 1003–1030.
- [150] Y. Capdeboscq and M. Vogelius, A general representation formula for boundary voltage perturbations caused by internal conductivity inhomogeneities of low volume fraction, *Math. Model. Numer. Anal.*, **37** (2003), pp. 159–173.
- [151] Y. Censor, Mathematical aspects of radiation therapy treatment planning: Continuous inversion versus full discretization and optimization versus feasibility, in *Computational Radiology and Imaging* (Minneapolis, MN, 1997), IMA Vol. Math. Appl. **110**, Springer, New York, 1999, pp. 101–112.
- [152] Y. Censor, D. E. Gustafson, A. Lent, H. Tuy, A new approach to the emission computerized tomography problem: Simultaneous calculation of attenuation and activity coefficients, *IEEE Trans. Nuclear Sci.*, **26** (1979), pp. 2775–2779.
- [153] Y. Censor, M. Jiang, A. K. Louis (Editors), *Mathematical Methods in Biomedical Imaging and Intensity-Modulated Radiation Therapy (IMRT). Including papers from the workshop held in Pisa, October 15–19, 2007*, Centro di Ricerca Matematica Ennio De Giorgi (CRM) Series **7**, Edizioni della Normale, Pisa, 2008.
- [154] Y. Censor and A. Segal, Iterative projection methods in biomedical inverse problems, in [153, pp. 65–96].
- [155] K. Chadan, D. Colton, L. Päivärinta, W. Rundell, *An Introduction to Inverse Scattering and Inverse Spectral Problems*, SIAM Monogr. Math. Model. Comput. **2**, SIAM, Philadelphia, 1997.
- [156] W. Chen, G. T. Herman, Y. Censor, Algorithms for satisfying dose-volume constraints in intensity-modulated radiation therapy, in [153, pp. 97–106].
- [157] M. Cheney, A mathematical tutorial on synthetic aperture radar, *SIAM Rev.*, **43** (2001), pp. 301–312.
- [158] M. Cheney and B. Borden, *Fundamentals of Radar Imaging*, CBMS-NSF Roy. Conf. Ser. Appl. Math. **79**, SIAM, Philadelphia, 2009.
- [159] M. Cheney, D. Isaacson, J. C. Newell, Electrical impedance tomography, *SIAM Rev.*, **41** (1999), pp. 85–101.
- [160] B. Cipra, Shocking images from RPI, *SIAM News*, **27** (1994), pp. 14–15.
- [161] C. Clason and M. V. Klibanov, The quasi-reversibility method for thermoacoustic tomography in a heterogeneous medium, *SIAM J. Sci. Comput.*, **30** (2007), pp. 1–23.
- [162] R. R. Coifman, Y. Shkolnisky, F. J. Sigworth, A. Singer, Graph Laplacian tomography from unknown random projections, *IEEE Trans. Image Process.*, **17** (2008), pp. 1891–1899.
- [163] D. Colton, Inverse acoustic and electromagnetic scattering theory, in [771, pp. 67–110].
- [164] D. Colton, R. Ewing, W. Rundell (Editors), *Inverse Problems in Partial Differential Equations*, SIAM, Philadelphia, 1990.
- [165] D. Colton and R. Kress, *Inverse Acoustic and Electromagnetic Scattering Theory*, second edition, Appl. Math. Sci. **93**, Springer-Verlag, Berlin, 1998.

- [166] D. Colton and P. Monk, Mathematical methods in microwave medical imaging, in [120, pp. 137–156].
- [167] D. Colton, L. Päivärinta, J. Sylvester, The interior transmission problem, *Inverse Problems Imaging*, **1** (2007), pp. 13–28.
- [168] Committee on the Mathematics and Physics of Emerging Dynamic Biomedical Imaging, *Mathematics and Physics of Emerging Biomedical Imaging*, National Academies Press, Washington, DC, 1996.
- [169] A. M. Cormack and G. N. Hounsfield, *Allan M. Cormack—Biographical*, notes submitted after receiving Nobel Prize, 1979; available online at http://www.nobelprize.org/nobel_prizes/medicine/laureates/1979/cormack-bio.html.
- [170] A. M. Cormack and G. N. Hounsfield, *Godfrey N. Hounsfield—Biographical*, notes submitted after receiving the Nobel Prize, 1979; available online at http://nobelprize.org/nobel_prizes/medicine/laureates/1979/hounsfield-autobio.html.
- [171] A. Cormack, The Radon transform on a family of curves in the plane, *Proc. Amer. Math. Soc.*, **83** (1981), pp. 325–330.
- [172] A. M. Cormack, My connection with the Radon transform, in [277, pp. 32–35].
- [173] A. Cormack and E.T. Quinto, A Radon transform on spheres through the origin in \mathbb{R}^n and applications to the Darboux equation, *Trans. Amer. Math. Soc.*, **260** (1986), pp. 575–581.
- [174] A. Cormack and E.T. Quinto, A problem in radiotherapy: Questions of non-negativity, *Internat. J. Imaging Systems Tech.*, **1** (1989), pp. 120–124.
- [175] A. Cormack and E.T. Quinto, *The Mathematics and Physics of Radiation Dose Planning*, Contemp. Math. **113**, AMS, Providence, RI, 1990.
- [176] R. Courant and D. Hilbert, *Methods of Mathematical Physics, Volume II: Partial Differential Equations*, Interscience, New York, 1962.
- [177] B. Cox, *Laser-Tissue Interactions*, lecture notes, 2012; available online at http://www.ucl.ac.uk/medphys/staff/people/bcox/bens_lecture_notes.
- [178] B. Cox, *Acoustics for Ultrasound Imaging*, lecture notes, 2013; available online at http://www.ucl.ac.uk/medphys/staff/people/bcox/bens_lecture_notes.
- [179] B. T. Cox, S. R. Arridge, P. C. Beard, Photoacoustic tomography with a limited-aperture planar sensor and a reverberant cavity, *Inverse Problems*, **23** (2007), S95–S112.
- [180] B. T. Cox, S. R. Arridge, P. C. Beard, Estimating chromophore distributions from multi-wavelength photoacoustic images, *J. Opt. Soc. Amer. A*, **26** (2009), pp. 443–455.
- [181] B. T. Cox, J. G. Laufer, P. C. Beard. The challenges for quantitative photoacoustic imaging, *Proc. SPIE*, **7177** (2009), 717713.
- [182] B. Cox, T. Tarvainen, S. Arridge, Multiple illumination quantitative photoacoustic tomography using transport and diffusion models, in [65, pp. 1–13].
- [183] S. Cummer, B.-I. Popa, D. Schurig, D. Smith, J. Pendry, Full-wave simulations of electromagnetic cloaking structures, *Phys. Rev. E*, **74** (2006), 036621.
- [184] K. Datchev and H. Hezari, Inverse problems in spectral geometry, in [775, pp. 455–486].

- [185] M. E. Davison, The ill-conditioned nature of the limited angle tomography problem, *SIAM J. Appl. Math.*, **43** (1983), pp. 428–448.
- [186] S. R. Deans, *The Radon Transform and Some of Its Applications*, Wiley-Interscience, New York, 1983.
- [187] M. Defrise and X. Liu, A fast rebinning algorithm for 3D positron emission tomography using John's equation, *Inverse Problems*, **15** (1999), pp. 1047–1066.
- [188] M. Defrise, D. W. Townsend, R. Clack, Three-dimensional image reconstruction from complete projections, *Phys. Med. Biol.*, **34** (1989), pp. 573–587.
- [189] A. P. Dempster, N. M. Laird, D. B. Rubin, Maximum likelihood from incomplete data via the EM algorithm, *J. Roy. Statist. Soc. B*, **39** (1977), pp. 1–38.
- [190] A. Dermanis, A. Grun, F. Sanso (Editors), *Geometric Methods for the Analysis of Data in the Earth Sciences*, Springer, Berlin, 2000.
- [191] A. J. Devaney and G. Beylkin, Diffraction tomography using arbitrary transmitter and receiver surfaces, *Ultrasonic Imaging*, **6** (1984), pp. 181–193.
- [192] G. J. Diebold, T. Sun, M. I. Khan, Photoacoustic monopole radiation in one, two, and three dimensions, *Phys. Rev. Lett.*, **67** (1991), pp. 3384–3387.
- [193] T. Dolby and G. Alker, *Origins and Development of Medical Imaging*, Southern Illinois University Press, Carbondale, IL, 1997.
- [194] P. I. Dudnikov and S. N. Samborski, Linear overdetermined systems of partial differential equations. Initial and initial-boundary value problems, in *Partial Differential Equations*, Encyclopaedia Math. Sci. **65**, Springer, Berlin, Vol. VIII, 1996, pp. 1–86.
- [195] N. Dunford and J. T. Schwartz, *Linear Operators. Part II: Spectral Theory. Self Adjoint Operators in Hilbert Space*, Interscience Publishers, John Wiley & Sons, New York, London, 1963.
- [196] D. E. Edmunds and W. D. Evans, *Spectral Theory and Differential Operators*, Oxford University Press, New York, 1987.
- [197] Yu. V. Egorov and M. A. Shubin, *Partial Differential Equations I*, Encyclopaedia Math. Sci. **30**, Springer-Verlag, Berlin, 1992, pp. 1–259.
- [198] L. Ehrenpreis, *The Universality of the Radon Transform*, Oxford University Press, London, 2003.
- [199] L. Ehrenpreis, P. Kuchment, A. Panchenko, The exponential X-ray transform and Fritz John's equation. I. Range description, in *Analysis, Geometry, Number Theory: The Mathematics of Leon Ehrenpreis (Philadelphia, PA, 1998)*, Contemp. Math. **251**, AMS, Providence, RI, 2000, pp. 173–188.
- [200] P. Elbau, O. Scherzer, R. Schulze, Reconstruction formulas for photoacoustic sectional imaging, *Inverse Problems*, **28** (2012), 045004.
- [201] H. W. Engl, M. Hanke, A. Neubauer, *Regularization of Inverse Problems*, Kluwer, Dordrecht, The Netherlands, 1996.
- [202] C. Epstein, Introduction to magnetic resonance imaging for mathematicians, *Ann. Inst. Fourier*, **54** (2004), pp. 1697–1716.

- [203] C. Epstein, *Introduction to the Mathematics of Medical Imaging*, Second edition, SIAM, Philadelphia, 2008.
- [204] C. L. Epstein and B. Kleiner, Spherical means in annular regions, *Comm. Pure Appl. Math.*, **46** (1993), pp. 441–451.
- [205] L. Evans, *Partial Differential Equations*, AMS, Providence, RI, 1998.
- [206] A. Faridani, An application of a multidimensional sampling theorem to computed tomography, in *Integral Geometry and Tomography (Arcata, CA, 1989)*, Contemp. Math. **113**, AMS, Providence, RI, 1990, pp. 65–80.
- [207] A. Faridani, A generalized sampling theorem for locally compact Abelian groups, *Math. Comp.*, **63** (1994), pp. 307–327.
- [208] A. Faridani, Introduction to the mathematics of computed tomography, in [771, pp. 1–46].
- [209] A. Faridani, Sampling theory and parallel-beam tomography, in *Sampling, Wavelets, and Tomography*, Appl. Numer. Harmon. Anal., Birkhäuser Boston, Boston, MA, 2004, pp. 225–254.
- [210] A. Faridani, Fan-beam tomography and sampling theory, *The Radon Transform, Inverse Problems, and Tomography*, Proc. Sympos. Appl. Math. **63**, AMS, Providence, RI, 2006, pp. 43–66.
- [211] A. Faridani, D. V. Finch, E. L. Ritman, K. Smith, Local tomography II, *SIAM J. Appl. Math.*, **57** (1997), pp. 1095–1127.
- [212] A. Faridani, F. Keinert, E. L. Ritman, K. T. Smith, Local and global tomography, in *Signal Processing, Part II*, Springer, New York, 1990, pp. 241–256.
- [213] A. Faridani and E. L. Ritman, High-resolution computed tomography from efficient sampling, *Inverse Problems*, **16** (2000), pp. 635–650.
- [214] A. Faridani, E. L. Ritman, K. T. Smith, Local tomography, *SIAM J. Appl. Math.*, **52** (1992), pp. 459–484.
- [215] A. Faridani, E. L. Ritman, K. T. Smith, Examples of local tomography, *SIAM J. Appl. Math.*, **52** (1992), pp. 1193–1198.
- [216] J. A. Fawcett, Inversion of n -dimensional spherical averages, *SIAM J. Appl. Math.*, **45** (1985), pp. 336–341.
- [217] T. G. Feeman, *The Mathematics of Medical Imaging: A Beginners Guide*, Springer Undergrad. Texts Math. Tech., Springer-Verlag, Berlin, 2009.
- [218] R. Felea and E. T. Quinto, The microlocal properties of the local 3-D SPECT operator, *SIAM J. Math. Anal.*, **43** (2011), pp. 1145–1157.
- [219] D. V. Finch, Cone beam reconstruction with sources on a curve, *SIAM J. Appl. Math.*, **45** (1985), pp. 665–673.
- [220] D. V. Finch, Uniqueness for the attenuated x-ray transform in the physical range, *Inverse Problems*, **2** (1986), pp. 197–203.
- [221] D. Finch, The attenuated X-ray transform: Recent developments, in [771, pp. 47–66].
- [222] D. Finch, M. Haltmeier, Rakesh, Inversion of spherical means and the wave equation in even dimensions, *SIAM J. Appl. Math.*, **68** (2007), pp. 392–412.

- [223] D. V. Finch and A. Hertle, The exponential Radon transform, in [132, pp. 67–74].
- [224] D. V. Finch, I.-R. Lan, G. Uhlmann, Microlocal analysis of the restricted x-ray transform with sources on a curve, in *Inside Out: Inverse Problems and Applications*, G. Uhlmann, ed., Math. Sci. Res. Inst. Publ. **47**, Cambridge University Press, Cambridge, UK, 2003, pp. 193–218.
- [225] D. Finch, S. K. Patch, Rakesh, Determining a function from its mean values over a family of spheres, *SIAM J. Math. Anal.*, **35** (2004), pp. 1213–1240.
- [226] D. Finch and Rakesh, The range of the spherical mean value operator for functions supported in a ball, *Inverse Problems*, **22** (2006), pp. 923–938.
- [227] D. Finch and Rakesh, Recovering a function from its spherical mean values in two and three dimensions, in [793, Chapter 7].
- [228] D. Finch and Rakesh, The spherical mean value operator with centers on a sphere, *Inverse Problems*, **23** (2007), pp. S37–S50.
- [229] M. Fink, Time-reversal of ultrasonic fields—Part I: Basic principles, *IEEE Trans. Ultrasonic Ferroelectr. Freq. Control*, **39** (1992), pp. 555–567.
- [230] M. Fink, Time-reversed acoustics, *Scientific American*, (1999), pp. 91–97.
- [231] M. Fink, Time-reversed acoustics, *J. Phys. Conf. Ser.*, **118** (2008), 012001.
- [232] M. Fink and C. Prada, Acoustic time-reversal mirrors, *Inverse Problems*, **17** (2001), R1.
- [233] L. Florescu, V. A. Markel, J. C. Schotland, Inversion formulas for the broken-ray Radon transform, *Inverse Problems*, **27** (2011), 025002.
- [234] A. S. Fokas, Applied mathematics and the imaging of the brain, *Bull. Greek Math. Soc.*, **47** (2003), pp. 3–18.
- [235] A. S. Fokas and V. Marinakis, The mathematics of the imaging techniques of MEG, CT, PET and SPECT, *Internat. J. Bifur. Chaos Appl. Sci. Engrg.*, **16** (2006), pp. 1671–1687.
- [236] A. S. Fokas and L.-Y. Sung, Generalized Fourier transforms, their nonlinearization and the imaging of the brain, *Not. Amer. Math. Soc.*, **52** (2005), pp. 1178–1192.
- [237] J. Frank (Editor), *Electron Tomography*, Plenum Press, New York, 1992.
- [238] B. Fridman, P. Kuchment, K. Lancaster, S. Lissianoi, M. Mogilevsky, D. Ma, I. Ponomarev, V. Papanicolaou, Numerical harmonic analysis on the hyperbolic plane, *Appl. Anal.*, **76** (2000), pp. 351–362; see figures omitted from the original online at <http://www.math.tamu.edu/~kuchment/hypnum.pdf>.
- [239] B. Fridman, P. Kuchment, D. Ma, V. Papanicolaou, Solution of the linearized conductivity problem in the half space via integral geometry, in *Voronezh Winter Mathematical Schools*, P. Kuchment (Editor), Amer. Math. Soc. Transl. Ser. 2 **184**, AMS, Providence, RI, 1998, pp. 85–95.
- [240] L. Friedlander, *Introduction to Microlocal Analysis*, course site with linked teacher notes, <http://math.arizona.edu/~friedlan/micro.htm>.
- [241] F. G. Friedlander and M. Joshi, *Introduction to the Theory of Distributions*, Cambridge University Press, Cambridge, UK, 1999.

- [242] B. Frigyik, P. Stefanov, G. Uhlmann, The X-ray transform for a generic family of curves and weights, *J. Geom. Anal.*, **18** (2008), pp. 81–97.
- [243] *Fully 3D* 2013, Website for the 2013 Conference on Fully Three-Dimensional Image Reconstruction in Radiology and Nuclear Medicine, fully3d.org.
- [244] P. Funk, Über eine geometrische Anwendung der Abelschen Integralgleichung, *Math. Ann.*, **77** (1915), pp. 129–135.
- [245] L. Gao, K. J. Parker, S. K. Alam, Sonoelasticity imaging: Theory and experimental verification, *J. Acoust. Soc. Amer.*, **97** (1995), pp. 3875–3880.
- [246] R. J. Gardner, *Geometric Tomography*, Cambridge University Press, Cambridge, UK, 2006.
- [247] H. A. J. Garnier and W. Jing, Resolution and Stability Analysis in Acousto-electric Imaging, *Inverse Problems*, **28** (2012), 084005.
- [248] J. Gasqui and H. Goldschmidt, *Radon Transforms and the Rigidity of the Grassmannians*, Princeton University Press, Princeton, NJ, 2004.
- [249] B. Gebauer and O. Scherzer, Impedance-acoustic tomography, *SIAM J. Appl. Math.*, **69** (2009), pp. 565–576.
- [250] I. M. Gelfand, Integral geometry and its relation to the theory of group representations, *Russ. Math. Surv.*, **15** (1960), pp. 143–151.
- [251] I. M. Gelfand and S. G. Gindikin (Editors), *Mathematical Problems of Tomography*, Transl. Math. Monogr. **81**, Math. Monogr., AMS, Providence, RI, 1990.
- [252] I. Gelfand, S. Gindikin, M. Graev, Integral geometry in affine and projective spaces. *J. Sov. Math.*, **18** (1980), pp. 39–167.
- [253] I. Gelfand, S. Gindikin, M. Graev, *Selected Topics in Integral Geometry*, Transl. Math. Monogr. **220**, AMS, Providence, RI, 2003.
- [254] I. M. Gelfand, S. G. Gindikin, Z. Ya. Shapiro, A local problem of integral geometry, *Funct. Anal. Appl.*, **13** (1979), pp. 87–102.
- [255] I. M. Gelfand and A. B. Goncharov, Reconstruction of a compactly supported function from its integrals on lines intersecting a set of points in a space, *Dokl. Akad. Nauk SSSR*, **290** (1986), pp. 1037–1040.
- [256] I. M. Gelfand and M. I. Graev, An application of the horospheres method to the spectral analysis of functions in real and imaginary Lobachevsky space, *Trudi Mosk. Math. Soc.*, **11** (1962), pp. 243–308.
- [257] I. M. Gelfand and M. I. Graev, *The Geometry of Homogeneous Spaces, Group Representations in Homogeneous Spaces and Questions in Integral Geometry Related to Them*, Amer. Math. Soc. Transl. **37**, AMS, Providence, RI, 1964.
- [258] I. M. Gelfand and M. I. Graev, Complexes of k -dimensional planes in the space C^n and Plancherels' formula for the group $GL(n, \mathbb{C})$, *Soviet Math. Dokl.*, **9** (1968), pp. 394–398.
- [259] I. M. Gelfand, M. I. Graev, V. S. Retakh, General hypergeometric systems of equations and series of hypergeometric type, *Uspekhi Mat. Nauk*, **47** (1992), pp. 3–82, 235 (in Russian); English translation in *Russian Math. Surveys*, **47** (1992), pp. 1–88.

- [260] I. M. Gelfand, M. I. Graev, Z. Ya. Shapiro, Integral geometry on k -dimensional planes, *Funct. Anal. Appl.*, 1 (1967), pp. 14–27.
- [261] I. Gelfand, M. Graev, N. Vilenkin, *Generalized Functions, v. 5: Integral Geometry and Representation Theory*, Academic Press, New York, 1965.
- [262] I. M. Gelfand and M. A. Naimark, Unitary representations of the Lorentz group, *Izv. Acad. Nauk SSSR Ser. Mat.*, 11 (1947), pp. 411–504.
- [263] I. M. Gelfand and M. A. Naimark, *Unitarnye predstavleniya klassicheskikh grupp* [Unitary Representations of the Classical Groups] Trudy Mat. Inst. Steklov. 36, Izdat. Nauk SSSR, Moscow-Leningrad, 1950 (in Russian); *Unitäre Darstellungen der Klassischen Gruppen*, Akademie-Verlag, Berlin, 1957 (in German).
- [264] I. Gelfand and G. Shilov, *Generalized Functions*, Academic Press, New York, 1964.
- [265] I. M. Gelfand and N. Ya. Vilenkin, *Generalized Functions. Vol. 4. Applications of Harmonic Analysis*, Academic Press, New York, London, 1964.
- [266] S. Geman and D. McClure, Statistical methods for tomographic image reconstruction, *Bull. Intl. Statist. Inst.*, 52 (1987), pp. 5–21.
- [267] *Geometric Tomography*, Web page, <http://www.geometrictomography.com/>.
- [268] S. G. Gindikin, Integral geometry and twistors, in *Twistor Geometry and Nonlinear Systems (Primorsko, 1980)*, Lecture Notes in Math. 970, Springer, Berlin, New York, 1982, pp. 2–42.
- [269] S. Gindikin, Integral geometry as geometry and as analysis, in [132, pp. 75–108].
- [270] S. Gindikin, Some notes on Radon transform and integral geometry, *Monatsch. Math.*, 113 (1992), pp. 23–32; reprinted in [277, pp. 293–300].
- [271] S. Gindikin, The Radon transform from the cohomological point of view, in [277, pp. 123–128].
- [272] S. Gindikin, Integral geometry on real quadrics, in *Lie groups and Lie algebras: E. B. Dynkin's Seminar*, Amer. Math. Soc. Transl. Ser. 2 169, AMS, Providence, RI, 1995, pp. 23–31.
- [273] S. Gindikin, *Applied Problems of Radon Transform*, AMS, Providence, RI, 1995.
- [274] S. G. Gindikin and F. I. Karpelevich, A problem of integral geometry, *Selecta Math. Sov.*, 1 (1981), pp. 160–184.
- [275] S. G. Gindikin and G. M. Khenkin, The Penrose transform and complex integral geometry, in *Current Problems in Mathematics*, 17 (1981), pp. 57–111, 220 1981; Akad. Nauk SSSR, Vsesoyuz. Inst. Nauchn. i Tekhn. Informatsii, Moscow, 1981 (in Russian).
- [276] S. G. Gindikin and G. M. Khenkin, Complex integral geometry and Penrose transformation for solutions of Maxwell equations, *Teoret. Mat. Fiz.*, 43 (1980), pp. 18–31 (in Russian).
- [277] S. Gindikin and P. Michor (Editors), *75 Years of the Radon Transform*, International Press, Boston, 1994.
- [278] S. Gindikin, J. Reeds, L. Shepp, Spherical tomography and spherical integral geometry, in [659, pp. 83–92].
- [279] I. C. Gohberg and M. G. Krein, The basic propositions on defect numbers, root numbers and indices of linear operators, *Trans. Amer. Math. Soc.* (2), 13 (1960), pp. 185–264; translated from *Uspekhi Mat. Nauk.*, 12 (1957), pp. 43–118.

- [280] I. C. Gohberg and M. G. Krein, *Introduction to the Theory of Linear Nonselfadjoint Operators*, AMS, Providence, RI, 1969.
- [281] S. V. Goldin, *Seismic Traveltime Inversion*, Society of Exploration Geophysicists, Tulsa, OK, 1986.
- [282] A. B. Goncharov, Integral geometry and three-dimensional reconstruction of arbitrarily oriented identical particles from electron micrographs, *Soviet Phys. Cryst.*, **32** (1987), pp. 663–666 (in Russian); translated from *Kristallografiya*, **32** (1987), pp. 1131–1136.
- [283] A. B. Goncharov, Integral geometry and three-dimensional reconstruction of randomly oriented identical particles from their electron micrographs, *Acta Appl. Math.*, **11** (1988), pp. 199–211.
- [284] A. B. Goncharov, Methods of integral geometry and recovering a function with compact support from its projections in unknown directions, *Acta Appl. Math.*, **11** (1988), pp. 213–222.
- [285] A. B. Goncharov, Integral geometry on families of surfaces in the space, *J. Geom. Phys.*, **5** (1988), pp. 571–593.
- [286] A. B. Goncharov, Integral geometry on families of k -dimensional submanifolds, *Funkt. Anal. i Prilozhen.*, **23** (1990), pp. 11–23, 96; English translation in *Funct. Anal. Appl.*, **23** (1990), pp. 178–189.
- [287] A. B. Goncharov, Three-dimensional reconstruction of arbitrarily arranged identical particles given their projections, in *Mathematical Problems of Tomography*, Transl. Math. Monogr. **81**, AMS, Providence, RI, 1990, pp. 67–96.
- [288] A. B. Goncharov, Admissible double bundles, in [277, pp. 129–152].
- [289] A. B. Goncharov, Differential equations and integral geometry, *Adv. Math.*, **131** (1997), pp. 279–343.
- [290] F. B. Gonzalez, *Notes on Integral Geometry and Harmonic Analysis*, COE Lecture Note 24, Kyushu University, Fukuoka, Japan, 2010, http://gcoe-mi.jp/english/publish_list/pub_inner/id:2/cid:12.
- [291] F. Gonzalez and T. Kakehi, Pfaffian systems and the range of the Radon transforms on affine Grassmann manifolds, *Math. Ann.*, **326** (2003), pp. 237–273.
- [292] F. Gonzalez and T. Kakehi, Invariant differential operators and the range of the matrix Radon transform, *J. Funct. Anal.*, **241** (2006), pp. 232–267.
- [293] C. Gordon, D. Webb, S. Wolpert, One cannot hear the shape of a drum, *Bull. Amer. Math. Soc.*, **27** (1992), pp. 134–138.
- [294] P. Grangeat, Mathematical framework of cone beam 3D reconstruction via the first derivative of the Radon transform, in [362, pp. 66–97].
- [295] P. Grangeat and J.-L. Amans (Editors), *Three-Dimensional Image Reconstruction in Radiology and Nuclear Medicine*, Springer, New York, 1996.
- [296] H. Grauert and R. Remmert, *Theory of Stein Spaces* (Translated from the German by Alan Huckleberry), Classics in Math., Springer-Verlag, Berlin, 2004.
- [297] A. Greenleaf, Y. Kurylev, M. Lassas, G. Uhlmann, Full-wave invisibility of active devices at all frequencies, *Comm. Math. Phys.*, **275** (2007), pp. 749–789.

- [298] A. Greenleaf, Y. Kurylev, M. Lassas, G. Uhlmann, Electromagnetic wormholes via handlebody constructions, *Comm. Math. Phys.*, **281** (2008), pp. 369–385.
- [299] A. Greenleaf, Y. Kurylev, Yaroslav, M. Lassas, G. Uhlmann, Invisibility and inverse problems, *Bull. Amer. Math. Soc. (N.S.)*, **46** (2009), pp. 55–97.
- [300] A. Greenleaf, M. Lassas, G. Uhlmann, Anisotropic conductivities that cannot be detected in EIT, *Physiolog. Meas.* (special issue on impedance tomography), **24** (2003), pp. 413–420.
- [301] A. Greenleaf and G. Uhlmann, Microlocal techniques in integral geometry, in *Integral Geometry and Tomography (Arcata, CA, 1989)*, Contemp. Math. **113**, AMS, Providence, RI, 1990, pp. 121–135.
- [302] A. Grigis, J. Sjöstrand, *Microlocal Analysis for Differential Operators: An Introduction*, London Mathematical Society Lecture Note Series, Cambridge University Press, Cambridge, UK, 1994.
- [303] E. L. Grinberg, Euclidean Radon transform: Ranges and restrictions, in [132, pp. 109–133].
- [304] E. L. Grinberg, That kappa operator: Gelfand–Graev–Shapiro inversion and Radon transform on isotropic planes, in [659, 93–104].
- [305] C. W. Groetsch, *Inverse Problems in Mathematical Sciences*, Vieweg-Verlag, Braunschweig, Wiesbaden, Germany, 1984.
- [306] H. Grün, M. Haltmeier, G. Paltauf, P. Burgholzer, *Photoacoustic Tomography Using a Fiber Based Fabry–Perot Interferometer as an Integrating Line Detector and Image Reconstruction by Nodel-based Time Reversal Method*, Proc. SPIE **6631**, Bellingham, WA, 2007.
- [307] F. A. Grünbaum, A study of Fourier space methods for “limited angle” image reconstruction, *Numer. Funct. Anal. Optim.*, **2** (1980), pp. 31–42.
- [308] F. A. Grünbaum, Reconstruction with arbitrary directions: Dimensions two and three, in *Mathematical Aspects of Computerized Tomography (Oberwolfach, 1980)*, Lecture Notes in Med. Inform. **8**, Springer, Berlin, 1981, pp. 112–126.
- [309] F. A. Grünbaum, The limited angle reconstruction problem, in *Computed Tomography (Cincinnati, Ohio, 1982)*, Proc. Sympos. Appl. Math. **27**, AMS, Providence, RI, 1982, pp. 43–61.
- [310] F. A. Grünbaum, The limited angle problem in tomography and some related mathematical problems, *Bifurcation Theory, Mechanics, and Physics*, Math. Appl., Reidel, Dordrecht, The Netherlands, 1983, pp. 317–329.
- [311] F. A. Grünbaum, Some mathematical problems suggested by limited angle tomography, in *Inverse Problems (New York, 1983)*, SIAM-AMS Proc. **14**, AMS, Providence, RI, 1984, pp. 65–77.
- [312] F. A. Grünbaum, Diffuse tomography: A refined model, in *Mathematical Methods in Tomography (Oberwolfach, 1990)*, Lecture Notes in Math. **1497**, Springer, Berlin, 1991, pp. 106–111.
- [313] F. A. Grünbaum, An inverse problem in transport theory: Diffuse tomography, in *Invariant Imbedding and Inverse Problems (Albuquerque, NM, 1990)*, SIAM, Philadelphia, PA, 1992, pp. 209–215.
- [314] F. A. Grünbaum, Diffuse tomography as a source of challenging nonlinear inverse problems for a general class of networks, *Modern Signal Processing*, Math. Sci. Res. Inst. Publ. **46**, Cambridge University Press, Cambridge, UK, 2004, pp. 137–146.

- [315] F. A. Grünbaum, Backprojections in tomography, spherical functions and addition formulas: A few challenges, in *Inverse Problems, Image Analysis, and Medical Imaging (New Orleans, LA, 2001)*, Contemp. Math. **313**, AMS, Providence, RI, 2002, pp. 143–152.
- [316] F. A. Grünbaum, A nonlinear inverse problem inspired by three-dimensional diffuse tomography, *Inverse Problems*, **17** (2001), pp. 1907–1922.
- [317] F. A. Grünbaum and L. F. Matusevich, Explicit inversion formulas for a model in diffuse tomography, *Adv. in Appl. Math.*, **29** (2002), pp. 172–183.
- [318] F. A. Grünbaum and L. F. Matusevich, A network tomography problem related to the hypercube, in *Partial Differential Equations and Inverse Problems*, Contemp. Math. **362**, AMS, Providence, RI, 2004, pp. 189–197.
- [319] F. A. Grünbaum and S. K. Patch, How many parameters can one solve for in diffuse tomography? in *Inverse Problems in Wave Propagation (Minneapolis, MN, 1995)*, IMA Vol. Math. Appl. **90**, Springer, New York, 1997, pp. 219–235.
- [320] F. A. Grünbaum and S. K. Patch, The use of Grassmann identities for inversion of a general model in diffuse tomography, in *Inverse problems in Mathematical Physics (Saariselkä, 1992)*, Lecture Notes in Phys. **422**, Springer, Berlin, 1993, pp. 29–48.
- [321] F. A. Grünbaum and J. P. Zubelli, Diffuse tomography: Computational aspects of the isotropic case, *Inverse Problems*, **8** (1992), pp. 421–433.
- [322] I. S. Gudovič and S. G. Krein, Boundary value problems for overdetermined systems of partial differential equations, *Differencial'nye Uravnenija i Primenen.*, **9** (1974), pp. 1–145 (in Russian).
- [323] J.-P. Guillement, F. Jauberteau, L. Kunyansky, R. Novikov, R. Trebessen, On SPECT imaging based on an exact formula for the nonuniform attenuation correction, *Inverse Problems*, **18** (2002), pp. L11–L19.
- [324] J.-P. Guillement and R. Novikov, A noise property analysis of single-photon emission computed tomography data, *Inverse Problems*, **20** (2004), pp. 175–198.
- [325] V. Guillemin, Fourier integral operators from the Radon transform point of view, *Proc. Sympos. Pure Math.*, **27** (1975), pp. 297–300.
- [326] V. Guillemin, On some results of Gelfand in integral geometry, *Proc. Sympos. in Pure Math.*, **43** (1985), pp. 149–155.
- [327] V. Guillemin, Perspectives in integral geometry, in [132, 35–150].
- [328] V. Guillemin and S. Sternberg, *Geometric Asymptotics*, AMS, Providence, RI, 1977.
- [329] R. C. Gunning and H. Rossi, *Analytic Functions of Several Complex Variables*, AMS Chelsea Publishing, Providence, RI, 2009.
- [330] P. Günther, *Huygens' Principle and Hyperbolic Equations*, Academic Press, Boston, 1988.
- [331] V. P. Gurarii, Group methods in commutative harmonic analysis, *Commutative Harmonic Analysis*, II, Encyclopaedia Math. Sci. **25**, Springer, Berlin, 1998, pp. 1–325.
- [332] E. M. Haacke, R. W. Brown, M. R. Thompson, R. Venkatesan, *Magnetic Resonance Imaging: Physical Principles and Sequence Design*, Wiley–Liss, New York, 1999.

- [333] R. Hadani and A. Singer, Representation theoretic patterns in three dimensional cryo-electron microscopy II—The class averaging problem, *Found. Comput. Math.*, **11** (2011), pp. 589–616.
- [334] R. Hadani and A. Singer, Representation theoretic patterns in three dimensional cryo-electron microscopy I—The intrinsic reconstitution algorithm, *Ann. Math.*, **174** (2011), pp. 1219–1241.
- [335] O. H. Hald and J. R. McLaughlin, *Inverse nodal problems: Finding the potential from nodal lines*, *Mem. Amer. Math. Soc.*, **119** (1996), no. 572.
- [336] O. H. Hald and J. R. McLaughlin, Inverse problems: Recovery of BV coefficients from nodes, *Inverse Problems*, **14** (1998), pp. 245–273.
- [337] M. Haltmeier, P. Burgholzer, G. Paltauf, O. Scherzer, Thermoacoustic computed tomography with large planar receivers, *Inverse Problems*, **20** (2004), pp. 1663–1673.
- [338] M. Haltmeier, R. Kowar, A. Leit  o, O. Scherzer, Kaczmarz methods for regularizing nonlinear ill-posed equations. II. Applications, *Inverse Problems Imaging*, **1** (2007), pp. 507–523.
- [339] M. Haltmeier, A. Leit  o, O. Scherzer, Kaczmarz methods for regularizing nonlinear ill-posed equations. I. Convergence analysis, *Inverse Problems Imaging*, **1** (2007), pp. 289–298.
- [340] M. Haltmeier, O. Scherzer, P. Burgholzer, R. Nuster, G. Paltauf, Thermoacoustic tomography and the circular Radon transform: Exact inversion formula, *Math. Models Methods Appl. Sci.*, **17** (2007), pp. 635–655.
- [341] M. Haltmeier, O. Scherzer, P. Burgholzer, G. Paltauf, Thermoacoustic computed tomography with large planar receivers, *Inverse Problems*, **20** (2004), pp. 1663–1673.
- [342] M. Haltmeier, T. Schuster, O. Scherzer, Filtered backprojection for thermoacoustic computed tomography in spherical geometry, *Math. Methods Appl. Sci.*, **28** (2005), pp. 1919–1937.
- [343] B. Handwerk, *King Tut Not Murdered Violently, CT Scans Show*, National Geographic News, March 8, 2005; online at http://news.nationalgeographic.com/news/2005/030308_050308_kingtutmurder.html.
- [344] W. G. Hawkins, P. K. Leichner, N. C. Yang, The circular harmonic transform for SPECT reconstruction and boundary conditions on the Fourier transform of the sinogram, *IEEE Trans. Med. Imag.*, **7** (1988), pp. 135–148.
- [345] I. Hazou and D. Solmon, Inversion of the exponential Radon transform I, Analysis, *Math. Methods Appl. Sci.*, **10** (1988), pp. 561–574.
- [346] I. Hazou and D. Solmon, Inversion of the exponential Radon transform II, Numerics, *Math. Methods Appl. Sci.*, **13** (1990), pp. 205–218.
- [347] I. Hazou and D. Solmon, Filtered-backprojection and the exponential Radon transform, *Math. Anal. Appl.*, **141** (1989), pp. 109–119.
- [348] U. Heike, Single-photon emission computed tomography by inverting the attenuated Radon transform with least-squares collocation, *Inverse Problems*, **2** (1986), pp. 307–330.
- [349] S. Helgason, *The Radon Transform*, Birkh  user, Basel, 1980.
- [350] S. Helgason, Some results on Radon transforms, Huygens' principle and X-ray transforms, in [132, 151–178].

- [351] S. Helgason, The totally-geodesic Radon transform on constant curvature spaces, *Contemp. Math.*, **113** (1990), pp. 141–149.
- [352] S. Helgason, Comment, in [277, p. 31].
- [353] S. Helgason, *Groups and Geometric Analysis*, AMS, Providence, RI, 2000.
- [354] S. Helgason, *Integral Geometry and Radon Transforms*, Springer, New York, 2011.
- [355] S. Helgason, Some personal remarks on the Radon transform, in [661, pp. 3–19].
- [356] R. P. Henderson and J. G. Webster, An impedance camera for spatially specific measurements of the thorax, *IEEE Trans. Biomed. Eng.*, **25** (1978), pp. 250–254.
- [357] G. Herman (Editor), *Image Reconstruction from Projections*, Topics in Appl. Phys. **32**, Springer-Verlag, Berlin, New York, 1979.
- [358] G. Herman, *Image Reconstruction from Projections: The Fundamentals of Computerized Tomography*, Academic Press, New York, 1980.
- [359] G. T. Herman and A. Kuba (Editors), *Discrete Tomography: Foundations, Algorithms, and Applications* (Applied and Numerical Harmonic Analysis), Birkhauser, Boston, 1999.
- [360] G. T. Herman and A. Kuba (Editors), *Advances in Discrete Tomography and Its Applications* (Applied and Numerical Harmonic Analysis), Birkhauser, Boston, 2007.
- [361] G. Herman, *Fundamentals of Computerized Tomography*, Springer-Verlag, Berlin, 2009 (an updated version of [358]).
- [362] G. T. Herman, A. K. Louis, F. Natterer (Editors), *Mathematical Methods in Tomography*, Lecture Notes in Math. **1497**, Springer, New York, 1991.
- [363] H. E. Hernandez-Figueroa, M. Zamboni-Rached, E. Recami (Editors), *Localized Waves*, IEEE Press, J. Wiley & Sons, Hoboken, NJ, 2008.
- [364] A. Hertle, On the injectivity of the attenuated Radon transform, *Proc. Amer. Math. Soc.*, **92** (1984), pp. 201–205.
- [365] A. Hertle, The identification problem for the constantly attenuated Radon transform, *Math. Z.*, **197** (1988), pp. 13–19.
- [366] E. Hewitt and K. A. Ross, *Abstract Harmonic Analysis. Vol. I. Structure of Topological Groups, Integration Theory, Group Representations*, Second edition, Grundlehren Math. Wiss. **115**, Springer-Verlag, Berlin, New York, 1979; *Vol. II: Structure and Analysis for Compact Groups. Analysis on Locally Compact Abelian Groups*, Grundlehren Math. Wiss. **152**, Springer-Verlag, New York, Berlin, 1970.
- [367] K. Hickmann, *Unique Determination of Acoustic Properties from Thermoacoustic Data*, Ph.D. Thesis, Department of Mathematics, Oregon State University, Corvallis, OR, 2010.
- [368] K. Hickmann, The interior transmission spectrum in one dimension, *Inverse Problems*, **28** (2012), 115007.
- [369] K. Hickmann, Interior transmission eigenvalue problem with refractive index having C2-transition to the background medium, *Appl. Anal.*, **91** (2012), pp. 1675–1690.
- [370] W. S. Hinshaw and A. H. Lent, An introduction to NMR imaging: From the Bloch equation to the imaging equation, *Proc. IEEE*, **71** (1983), pp. 338–350.

- [371] E. Hlawka, On the work of Professor Fritz John, in [277, pp. 36–38].
- [372] B. Holtzmann Kevles, *Naked to the Bone: Medical Imaging in the Twentieth Century*, Rutgers University Press, New Brunswick, NJ, 1997.
- [373] M. de Hoop, Microlocal analysis of seismic inverse scattering, in [771, pp. 219–2916].
- [374] L. Hörmander, *Implicit Function Theorems*, Lectures at Stanford University, Summer Quarter, 1977.
- [375] L. Hörmander, On the Nash-Moser implicit function theorem, *Ann. Acad. Sci. Fenn. Ser. A I Math.*, **10** (1985), pp. 255–259.
- [376] L. Hörmander, *An Introduction to Complex Analysis in Several Variables*, North-Holland, Amsterdam, 1990.
- [377] L. Hörmander, *The Analysis of Linear Partial Differential Operators I: Distribution Theory and Fourier Analysis*, Second edition, Springer-Verlag, Berlin, 2003.
- [378] L. Hörmander, *The Analysis of Linear Partial Differential Operators II*, Springer-Verlag, Berlin 1983; *The Analysis of Linear Partial Differential Operators III*, Springer-Verlag, Berlin, 1985; *The Analysis of Linear Partial Differential Operators IV*, Corrected edition, Springer-Verlag, Berlin, 1994.
- [379] L. Hörmander, Fourier integral operators, I, *Acta Math.*, **127** (1971), pp. 79–183 (can also be found in [131]).
- [380] Y. Hristova, Time reversal in thermoacoustic tomography: Error estimate, *Inverse Problems*, **25** (2009), pp. 1–14.
- [381] Y. Hristova, P. Kuchment, L. Nguyen, On reconstruction and time reversal in thermoacoustic tomography in homogeneous and non-homogeneous acoustic media, *Inverse Problems*, **24** (2008), 055006.
- [382] C. Huang, K. Wang, L. Nie, L.V. Wang, M. A. Anastasio, Full-wave iterative image reconstruction in photoacoustic tomography with acoustically inhomogeneous media, *IEEE Trans. Med. Imaging*, **32** (2013), pp. 1097–1110.
- [383] J. Idier (Editor), *Bayesian Approach to Inverse Problems*, John Wiley & Sons, Hoboken, NJ, 2008.
- [384] ImPACT Group, *A brief history of CT*, <http://www.impactscan.org/CThistory.htm>.
- [385] D. Isaacson and M. Cheney, Current problems in impedance imaging, in *Inverse Problems in Partial Differential Equations*, SIAM, Philadelphia, 1990, pp. 141–149.
- [386] V. Isakov, *Inverse Source Problems*, AMS, New York, 1990.
- [387] V. Isakov, *Inverse Problems for Partial Differential Equations*, Second edition, Springer-Verlag, Berlin, 2005.
- [388] H. Isozaki and G. Uhlmann, Hyperbolic geometry and local Dirichlet-Neumann map, *Adv. Math.*, **188** (2004), pp. 294–314.
- [389] L. Ji, J. McLaughlin, D. Renzi, J.-R. Yoon, Interior elastodynamics inverse problems: Shear wave speed reconstruction in transient elastography, *Inverse Problems*, **19** (2003), pp. s1–s29.
- [390] X. Jin and L. V Wang, Thermoacoustic tomography with correction for acoustic speed variations, *Phys. Med. Biol.*, **51** (2006), pp. 6437–6448.

- [391] F. John, The ultrahyperbolic differential equation with four independent variables, *Duke Math. J.*, **4** (1938), pp. 300–322; reprinted in [277, pp. 301–323].
- [392] F. John, *Plane Waves and Spherical Means Applied to Partial Differential Equations*, Dover, New York, 1971.
- [393] F. John, Reminiscences, in [277, pp. 29–30].
- [394] M. Kac, Can one hear the shape of a drum?, *Amer. Math. Monthly*, **73** (1966), pp. 1–23.
- [395] S. Kaczmarz, Angenaherte Auflösung von Systemen linearer Gleichungen, *Bull. Acad. Polon. Sci. Lett.*, **A35** (1937), pp. 355–357.
- [396] A. C. Kak and M. Slaney, *Principles of Computerized Tomographic Imaging*, SIAM, Philadelphia, 2001.
- [397] Y. E. Karpeshina and J. R. McLaughlin, Two methods of solution of the three-dimensional inverse nodal problem, *Séminaire sur les Équations aux Dérivées Partielles*, 1997–1998, Exp. No. I, École Polytechnique, Palaiseau, France, 1998.
- [398] J. Karpio and E. Somersalo, *Statistical and Computational Inverse Problems*, Springer, New York, 2005.
- [399] J. Kastner, *Conference on Industrial Computed Tomography (ICT) 2012: Proceedings*, Shaker Verlag, Aachen, Germany, 2012.
- [400] T. Kato, *Perturbation Theory for Linear Operators*, Springer-Verlag, Berlin, 1980.
- [401] A. I. Katsevich, Local tomography for the generalized Radon transform, *SIAM J. Appl. Math.*, **57** (1997), pp. 1128–1162.
- [402] A. Katsevich, Local tomography with nonsmooth attenuation, *Trans. Amer. Math. Soc.*, **351** (1999), pp. 1947–1974.
- [403] A. Katsevich, Cone beam local tomography, *SIAM J. Appl. Math.*, **59** (1999), pp. 2224–2246.
- [404] A. Katsevich, Microlocal analysis of an FBP algorithm for truncated spiral cone beam data, *J. Fourier Anal. Appl.*, **8** (2002), pp. 407–425.
- [405] A. Katsevich, Theoretically exact filtered backprojection-type inversion algorithm for spiral CT, *SIAM J. Appl. Math.*, **62** (2002), pp. 2012–2026.
- [406] A. Katsevich, A general scheme for constructing inversion algorithms for cone beam CT, *Int. J. Math. Math. Sci.*, **21** (2003), pp. 1305–1321.
- [407] A. Katsevich, An improved exact filtered backprojection algorithm for spiral computed tomography, *Adv. Appl. Math.*, **32** (2004), pp. 681–697.
- [408] A. Katsevich and G. Lauritsch, Filtered backprojection algorithms for spiral cone beam CT, *Sampling, Wavelets, and Tomography*, Appl. Numer. Harmon. Anal., Birkhäuser Boston, Boston, MA, 2004, pp. 255–287.
- [409] A. Katsevich and F. Natterer, Ultrasound tomography with sources on a line, in [153, pp. 201–209].
- [410] J. B. Keller, Inverse problems, *Amer. Math. Monthly*, **83** (1976), pp. 107–118.
- [411] M. Kempe, M. Larionov, D. Zaslavsky, A. Z. Genack, Acousto-optic tomography with multiply scattered light, *J. Opt. Soc. Am. A*, **14** (1997), pp. 1151–1158.

- [412] C. E. Kenig, J. Sjöstrand, G. Uhlmann, The Calderón problem with partial data, *Ann. of Math.* (2), **165** (2007), pp. 567–591.
- [413] K. Kilgore, S. Moskow, J. C. Schotland, Inverse Born series for scalar waves, *J. Comput. Math.*, **30** (2012), pp. 601–614.
- [414] A. Kirsch, *An Introduction to the Mathematical Theory of Inverse Problems*, Springer-Verlag, New York, 1996.
- [415] A. Kirsch, On the existence of transmission eigenvalues, *Inverse Problems Imaging*, **3** (2009), pp. 155–172.
- [416] A. Kirsch and N. Grinberg, *The Factorization Method for Inverse Problems*, Oxford University Press, London, 2008.
- [417] A. Kirsch and O. Scherzer, Simultaneous reconstructions of absorption density and wave speed with photoacoustic measurements, *SIAM J. Appl. Math.*, **72** (2012), pp. 1508–1523.
- [418] M. V. Klibanov, Thermoacoustic tomography with an arbitrary elliptic operator, *Inverse Problems*, **29** (2013), 025014.
- [419] M. V. Klibanov, A. V. Kuzhuget, S. I. Kabanikhin, D. V. Nechaev, A new version of the quasi-reversibility method for the thermoacoustic tomography and a coefficient inverse problem, *Appl. Anal.*, **87** (2008), pp. 1227–1254.
- [420] A. U. Klimyk and N. Ya. Vilenkin, Representations of Lie groups and special functions, *Representation Theory and Noncommutative Harmonic Analysis*, II, Encyclopedia Math. Sci. **59**, Springer, Berlin, 1995, pp. 137–259.
- [421] K. Knudsen, M. Lassas, J. L. Mueller, S. Siltanen, D-bar method for electrical impedance tomography with discontinuous conductivities, *SIAM J. Appl. Math.*, **67** (2007), pp. 893–913.
- [422] I. Kocyigit, Acousto-electric tomography and CGO solutions with internal data, *Inverse Problems*, **28** (2012), 125004.
- [423] R. V. Kohn, D. Onofrei, M. S. Vogelius, M. I. Weinstein, Cloaking via change of variables for the Helmholtz equation, *Comm. Pure Appl. Math.*, **63** (2010), pp. 973–1016.
- [424] R. V. Kohn, H. Shen, M. S. Vogelius, M. I. Weinstein, Cloaking via change of variables in electric impedance tomography, *Inverse Problems*, **24** (2008), 015016.
- [425] B. I. Korenblum and S. I. Tetel'baum, A. A. Tyutin, About one scheme of tomography, *Bulletin of the Institutes of Higher Education-Radiophysics (Izvestiya Vysshikh Uchebnykh Zavedenii-Radiofizika)*, **1** (1958), pp. 151–157.
- [426] T. W. Körner, *Fourier Analysis*, Cambridge University Press, Cambridge, UK, 1989.
- [427] R. Kowar, Estimation of the density, the wave speed and the acoustic impedance function in ultrasound imaging, *Inverse Problems*, **21** (2005), pp. 93–112.
- [428] R. Kowar, Integral equation models for thermoacoustic imaging of acoustic dissipative tissue, *Inverse Problems*, **26** (2010), 095005.
- [429] R. Kowar, *Some Inverse Problems and Their Applications*, Habilitationsschrift, Universität Innsbruck, Austria, 2011.
- [430] R. Kowar, *On time reversal in photoacoustic tomography for tissue similar to water*, arXiv:1308.0498, 2013.

- [431] R. Kowar and O. Scherzer, Convergence analysis of a Landweber-Kaczmarz method for solving nonlinear ill-posed problems, *Ill-Posed and Inverse Problems*, VSP, Zeist, 2002, pp. 253–270.
- [432] R. Kowar, O. Scherzer, X. Bonnefond, Causality analysis of frequency dependent wave attenuation, *Math. Methods Appl. Sci.*, **34** (2011), pp. 108–124.
- [433] S. G. Krantz, *Explorations in Harmonic Analysis, With Applications to Complex Function Theory and the Heisenberg Group*, Birkhäuser, Boston, MA, 2009.
- [434] S. G. Krein, *Linear Equations in a Banach Space*, Birkhäuser, Boston, 1982.
- [435] R. A. Kruger, K. K. Kopecky, A. M. Aisen, D. R. Reinecke, G. A. Kruger, W. L. Kiser, Jr., Thermoacoustic CT with radio waves: A medical imaging paradigm, *Radiology*, **211** (1999), pp. 275–278.
- [436] R. A. Kruger, P. Liu, Y. R. Fang, C. R. Appledorn, Photoacoustic ultrasound (PAUS) reconstruction tomography, *Med. Phys.*, **22** (1995), pp. 1605–1609.
- [437] R. A. Kruger, D. R. Reinecke, G. A. Kruger, Thermoacoustic computed tomography, *Med. Phys.*, **26** (1999), pp. 1832–1837.
- [438] P. Kuchment, On positivity problems for the Radon transform and some related transforms, *Contemp. Math.*, **140** (1993), pp. 87–95.
- [439] P. Kuchment, *unpublished*, 1993.
- [440] P. Kuchment, *Floquet Theory for Partial Differential Equations*, Birkhäuser, Boston, 1993.
- [441] P. Kuchment, On inversion and range characterization of one transform arising in emission tomography, in [277, pp. 240–248].
- [442] P. Kuchment, Generalized transforms of Radon type and their applications, in [602, pp. 67–91].
- [443] P. Kuchment, Mathematics of hybrid imaging. A brief review, in [691, pp. 183–208].
- [444] P. Kuchment, *Some Hybrid Imaging Modalities*, slides from a 2011 talk, available online at <http://aipc.tamu.edu/speakers/kuchment.pdf>.
- [445] P. Kuchment and L. Kunyansky, Mathematics of thermoacoustic tomography, *European J. Appl. Math.*, **19** (2008), pp. 191–224.
- [446] P. Kuchment and L. Kunyansky, Synthetic focusing in ultrasound modulated tomography, *Inverse Problems and Imaging*, **4** (2010), pp. 665–673.
- [447] P. Kuchment and L. Kunyansky, 2D and 3D reconstructions in acousto-electric tomography, *Inverse Problems*, **27** (2011), 055013.
- [448] P. Kuchment and L. Kunyansky, Mathematics of thermoacoustic and photoacoustic tomography, in [701, pp. 817–866].
- [449] P. Kuchment, K. Lancaster, L. Mogilevskaya, On local tomography, *Inverse Problems*, **11** (1995), pp. 571–589.
- [450] P. Kuchment and S. Lvin, Paley-Wiener theorem for exponential Radon transform, *Acta Appl. Math.*, **18** (1990), pp. 251–260.

- [451] P. Kuchment and S. Lvin, The range of the exponential Radon transform, *Soviet Math. Dokl.*, **42** (1991), pp. 183–184.
- [452] P. Kuchment and S. Lvin, Identities for $\sin(x)$ that came from medical imaging, *Amer. Math. Monthly*, **120** (2013), pp. 609–621.
- [453] P. Kuchment and E. T. Quinto, Some problems of integral geometry arising in tomography, in [198, Chapter XI].
- [454] P. Kuchment and O. Scherzer, *Mathematical Methods in Photoacoustic Imaging*, Encyclopedia Appl. Comput. Math., Springer-Verlag, Berlin, to appear.
- [455] P. Kuchment and I. Shneiberg, Some inversion formulas in the single photon emission tomography, *Appl. Anal.*, **53** (1994), pp. 221–231.
- [456] P. Kuchment and D. Steinhauer, Stabilizing inverse problems by internal data, *Inverse Problems*, **28** (2012), 4007.
- [457] P. Kuchment and D. Steinhauer, Stabilizing inverse problems by internal data. II. Non-local internal data. Generic linearized uniqueness, in preparation.
- [458] L. A. Kunyansky, Generalized and attenuated Radon transforms: Restorative approach to the numerical inversion, *Inverse Problems*, **8** (1992), pp. 809–819.
- [459] L. A. Kunyansky, Analytic reconstruction algorithms in emission tomography with variable attenuation, *J. Comput. Methods Sci. Engrg.*, **1** (2001), pp. 267–286.
- [460] L. A. Kunynasky, A new SPECT reconstruction algorithm based on the Novikov explicit inversion formula, *Inverse Problems*, **17** (2001), pp. 293–306.
- [461] L. Kunyansky, Inversion of the 3D exponential parallel-beam transform and the Radon transform with angle-dependent attenuation, *Inverse Problems*, **20** (2004), pp. 1455–1478.
- [462] L. Kunyansky, Explicit inversion formulae for the spherical mean Radon transform, *Inverse Problems*, **23** (2007), pp. 737–783.
- [463] L. Kunyansky, A series solution and a fast algorithm for the inversion of the spherical mean Radon transform, *Inverse Problems*, **23** (2007), pp. S11–S20.
- [464] L. Kunyansky, Thermoacoustic tomography with detectors on an open curve: An efficient reconstruction algorithm, *Inverse Problems*, **24** (2008), 055021.
- [465] L. Kunyansky, Reconstruction of a function from its spherical (circular) means with the centers lying on the surface of certain polygons and polyhedra, *Inverse Problems*, **27** (2011), 025012.
- [466] L. Kunyansky, Fast reconstruction algorithms for the thermoacoustic tomography in certain domains with cylindrical or spherical symmetries, *Inverse Problems Imaging*, **6** (2012), pp. 111–131.
- [467] L. Kunyansky, A mathematical model and inversion procedure for magneto-acousto-electric tomography, *Inverse Problems*, **28** (2012), 035002.
- [468] L. Kunyansky, B. Holman, B. T. Cox, *Photoacoustic tomography in rectangular reflecting cavity*, arXiv:1308.1421.
- [469] L. Kunyansky and P. Kuchment, Synthetic focusing in acousto-electric tomography, in *Oberwolfach Report No. 18/2010*, DOI: 10.4171/OWR/2010/18, Proceedings of the Workshop on Mathematics and Algorithms in Tomography, 2010, pp. 44–47.

- [470] A. Kuruc, Probability measure estimation using “weak” loss functions in positron emission tomography, in [659, pp. 125–142].
- [471] A. Kurusa, The Radon transform on hyperbolic space, *Geom. Dedicata*, **40** (1991), pp. 325–339.
- [472] A. Kurusa, The invertibility of the Radon transform on abstract rotational manifolds of real type, *Math. Scand.*, **70** (1992), pp. 112–126.
- [473] A. Kurusa, Support theorems for totally geodesic Radon transforms on constant curvature spaces, *Proc. Amer. Math. Soc.*, **122** (1994), pp. 429–435.
- [474] R. S. Laugesen, Injectivity can fail for higher-dimensional harmonic extensions, *Complex Var. Theory Appl.*, **28** (1996), pp. 357–369.
- [475] B. Lavandier, J. Jossinet, D. Cathignol, Quantitative assessment of ultrasound-induced resistance change in saline solution, *Med. Biol. Engrg. Comput.*, **38** (2000), pp. 150–155.
- [476] B. Lavandier, J. Jossinet, D. Cathignol, Experimental measurement of the acousto-electric interaction signal in saline solution, *Ultrasonics*, **38** (2000), pp. 929–936.
- [477] M. M. Lavrentév (Editor), *Computerized Tomography*, VSP, Utrecht, 1995.
- [478] U. Leonhardt, Optical conformal mapping, *Science*, **312** (2006), pp. 1777–1780.
- [479] U. Leonhardt, Notes on conformal invisibility devices, *New J. Phys.*, **8** (2006), p. 118.
- [480] U. Leonhardt, topic web page, *Invisibility*, <http://www.st-andrews.ac.uk/~ulf/invisibility.html>.
- [481] U. Leonhardt and T. Philbin, *Geometry and Light: The Science of Invisibility*, Dover, New York, 2010.
- [482] W. Leutz and G. Maret, Ultrasonic modulation of multiply scattered light, *Phys. B*, **204** (1995), pp. 14–19.
- [483] E. Levitan and G.T. Herman, A maximum a posteriori probability expectation maximization algorithm for image reconstruction in emission tomography, *IEEE Trans. Med. Imag.*, **6** (1987), pp. 185–192.
- [484] J. Li and L.-H. Wang, Methods for parallel-detection-based ultrasound-modulated optical tomography, *Appl. Optics*, **41** (2002), pp. 2079–2084.
- [485] K. Lin, J. McLaughlin, D. Renzi, A. Thomas, Shear wave speed recovery in sonoelastography using crawling wave data, *J. Acoust. Soc. Amer.*, **128** (2010), pp. 88–97.
- [486] V. Ya. Lin and A. Pinkus, Fundamentality of ridge functions, *J. Approx. Theory*, **75** (1993), pp. 295–311.
- [487] V. Lin and A. Pinkus, Approximation of multivariate functions. in *Advances in Computational Mathematics*, H. P. Dikshit and C. A. Micchelli (Editors), World Scientific Publishing, River Edge, NJ, 1994, pp. 1–9.
- [488] V. Lin and N. Zobin, *unpublished*, 1993.
- [489] J. L. Lions and E. Magenes, *Non-Homogeneous Boundary Value Problems and Applications*, vol. 1, Springer-Verlag, Berlin, Heidelberg, New York, 1972.

- [490] S. Lissianoi, On stability estimates in the exterior problem for the Radon transform, in [659, pp. 143–148].
- [491] S. Lissianoi, *Some Problems of Tomography and Radiation Therapy*, Ph.D. Dissertation, Mathematics Department, Wichita State University, Kansas, 1996.
- [492] S. Lissianoi and I. Ponomarev, On the inversion of the geodesic Radon transform on the hyperbolic plane, *Inverse Problems*, **13** (1997), pp. 1053–1062.
- [493] B. F. Logan, The uncertainty principle in reconstructing functions from projections, *Duke Math. J.*, **42** (1975), pp. 661–706.
- [494] A. K. Louis, Nonuniqueness in inverse Radon problems: The frequency distribution of the ghosts, *Math. Z.*, **185** (1984), pp. 429–440.
- [495] A. K. Louis, Orthogonal function series expansions and the null space of the Radon transform, *SIAM J. Math. Anal.*, **15** (1984), pp. 621–633.
- [496] A. K. Louis, Incomplete data problems in x-ray computerized tomography I. Singular value decomposition of the limited angle transform, *Numer. Math.*, **48** (1986), pp. 251–262.
- [497] A. K. Louis, Medical imaging: State of the art and future development, *Inverse Problems*, **8** (1992), pp. 709–738.
- [498] A. K. Louis and E. T. Quinto, Local tomographic methods in sonar, in *Surveys on Solution Methods for Inverse Problems*, Springer, Vienna, 2000, pp. 147–154.
- [499] A. K. Louis and T. Weber, Image reconstruction and image analysis in tomography: Fan beam and 3D cone beam, in [153, pp. 211–230].
- [500] S. Lvin, Data correction and restoration in emission tomography, in [659, pp. 149–155].
- [501] P. Maass, The interior Radon transform, *SIAM J. Appl. Math.*, **52** (1992), pp. 710–724.
- [502] G. W. Mackey, Harmonic analysis as exploitation of symmetry—A historical survey, *Bull. Amer. Math. Soc.*, **3** (1980), pp. 543–698.
- [503] W. R. Madych, Approximate reconstruction from circular and spherical mean Radon transform data, in [661, pp. 155–166].
- [504] B. Malgrange, *Lectures on the Theory of Functions of Several Complex Variables*, Tata Institute of Fundamental Research Lectures on Mathematics and Physics 13, Tata Institute of Fundamental Research, Bombay, 1984.
- [505] A. V. Mamonov and K. Ren, *Quantitative photoacoustic imaging in radiative transport regime*, arXiv:1207.4664
- [506] A. Manduca, T. E. Oliphant, M. A. Dresner, J. L. Mahowald, S. A. Kruse, E. Amromin, J. P. Felmlee, J. F. Greenleaf, R. L. Ehman, Magnetic resonance elastography: Non-invasive mapping of tissue elasticity, *Med. Image Anal.*, **5** (2001), pp. 237–254.
- [507] R. Marabini, G. T. Herman, J. M. Carazo, Fully three-dimensional reconstruction in electron microscopy, in [120, pp. 251–281].
- [508] V. A. Markel and J. C. Schotland, Inverse problem in optical diffusion tomography. I. Fourier-Laplace inversion formulas, *J. Opt. Soc. Amer. A*, **18** (2001), pp. 1336–1347.
- [509] V. A. Markel and J. C. Schotland, On the convergence of the Born series in optical tomography with diffuse light, *Inverse Problems*, **23** (2007), pp. 1445–1465.

- [510] A. Markoe, Fourier inversion of the attenuated X-ray transform, *SIAM J. Math. Anal.*, **15** (1984), pp. 718–722.
- [511] A. Markoe, *Analytic Tomography*, Cambridge University Press, Cambridge, UK, 2006.
- [512] A. Markoe and E. T. Quinto, An elementary proof of local invertibility for generalized and attenuated Radon transforms, *SIAM J. Math. Anal.*, **16** (1985), pp. 1114–1119.
- [513] A. Martinez, *An Introduction to Semiclassical and Microlocal Analysis*, Springer-Verlag, Berlin, 2002.
- [514] J. Mattson and M. Simon, *The Pioneers of NMR and Magnetic Resonance in Medicine, The Story of MRI*, Bar-Ilan University Press, Ramat Gan, Israel, 1996.
- [515] V. Maz'ya, *Sobolev Spaces*, Springer-Verlag, Berlin, 2011.
- [516] J. R. McLaughlin, Inverse spectral theory using nodal points as data—A uniqueness result, *J. Differential Equations*, **73** (1988), pp. 354–362.
- [517] J. R. McLaughlin, Determination of a radially symmetric speed of sound from transmission eigenvalues, *Inverse Problems in Mathematical Physics* (Saariselkä, 1992), Lecture Notes in Phys. **422**, Springer, Berlin, 1993, pp. 148–156.
- [518] J. R. McLaughlin, *Interior Elastodynamics Inverse Problems*, tutorial slides from IPAM 2003, http://www.ipam.ucla.edu/publications/invtut/invtut_3728.pdf.
- [519] J. R. McLaughlin, *Imaging Shear Stiffness Tissue Properties Using Inverse Methods When Measurements Are Time Dependent*, lecture slides from a talk in Austin, 2005, <http://www.iprpi.rpi.edu/Austin2005.pdf>.
- [520] J. R. McLaughlin and P. L. Polyakov, On the uniqueness of a spherically symmetric speed of sound from transmission eigenvalues, *J. Differential Equations*, **107** (1994), pp. 351–382.
- [521] J. McLaughlin and D. Renzi, Shear wave speed recovery in transient elastography and supersonic imaging using propagating fronts, *Inverse Problems*, **22** (2006), pp. 681–706.
- [522] J. McLaughlin, D. Renzi, K. Parker, Z. Wu, Shear wave speed recovery using moving interference patterns obtained in sonoelastography experiments, *J. Acoust. Soc. Am.*, **121** (2007), pp. 2438–2446.
- [523] J. McLaughlin, D. Renzi, J.-R. Yoon, R. L. Ehman, Variance controlled shear stiffness images for MRE data, in *Biomedical Imaging: Nano to Macro, 2006 (3rd IEEE International Symposium on)*, IEEE Press, Piscataway, NJ, 2007, pp. 960–963.
- [524] J. R. McLaughlin, P. E. Sacks, M. Somasundaram, Inverse scattering in acoustic media using interior transmission eigenvalues, in *Inverse Problems in Wave Propagation (Minneapolis, MN, 1995)*, IMA Vol. Math. Appl. **90**, Springer, New York, 1997, pp. 357–374.
- [525] J. R. McLaughlin and J.-R. Yoon, Unique identifiability of elastic parameters from time-dependent interior displacement measurement, *Inverse Problems*, **20** (2004), pp. 25–45.
- [526] R. B. Melrose and G. Uhlmann, *An Introduction to Microlocal Analysis*, book manuscript, available online at <http://math.mit.edu/~rbm/books/imaast.pdf>.
- [527] E. B. Mendelson, J. Chen, P. Karstaedt, Assessing tissue stiffness may boost breast imaging specificity, *Diagnostic Imaging*, **31** (2009), pp. 15–17.

- [528] C. Mennesier, F. Noo, R. Clackdoyle, G. Bal, L. Desbat, Attenuation correction in SPECT using consistency conditions for the exponential ray transform, *Phys. Med. Biol.*, **44** (1999), pp. 2483–2510.
- [529] D. Miller, M. Oristaglio, G. Beylkin, A new slant on seismic imaging: Migration and integral geometry, *Geophys.*, **52** (1987), pp. 943–964.
- [530] G. W. Milton and N.-A. P. Nicorovici, On the cloaking effects associated with anomalous localized resonance, *Proc. R. Soc. Lond. Ser. A Math. Phys. Eng. Sci.*, **462** (2006), pp. 3027–3059.
- [531] H. Minkowski, About bodies of constant width, *Math. Sbornik*, **25** (1904), pp. 505–508 (in Russian); *Über die Körper kostanter Breite*, Collected Works, II, Teubner, Leipzig, 1911, pp. 277–279.
- [532] A. Mohammad-Djafari, A variational Bayesian algorithm for inverse problem of computed tomography, in [153, pp. 231–252].
- [533] A. Moloisane and I. Ganchev, *Internet Tomography: An Introduction to Concepts, Techniques, Tools and Applications*, Cambridge Scholars Publishing, Newcastle upon Tyne, UK, 2013.
- [534] F. Monard, *Taming Unstable Inverse Problems*, Ph.D. Thesis, Columbia University, New York, 2012.
- [535] F. Monard and G. Bal, Inverse anisotropic diffusion from power density measurements in two dimensions, *Inverse Problems*, **28** (2012), 084001.
- [536] F. Monard and G. Bal, Inverse anisotropic conductivity from power densities in dimension 3, *SIAM J. Imaging Sci.*, **6** (2013), pp. 32–55.
- [537] C. Montaldo and P. Stefanov, *Stability of coupled-physics inverse problems with internal measurements*, preprint arXiv:1306.1978, 2013.
- [538] S. Moon, *On the determination of a function from an elliptical Radon transform*, preprint, arXiv:1302.4396.
- [539] S. Moon, *Properties of Some Integral Transforms Arising in Tomography*, Ph.D. Dissertation, Texas A&M University, College Station, TX, 2013.
- [540] J. Moser, A new technique for the construction of solutions of nonlinear differential equations, *Proc. Natl. Acad. Sci. USA*, **47** (1961), pp. 1824–1831.
- [541] S. Moskow and J. C. Schotland, Numerical studies of the inverse Born series for diffuse waves, *Inverse Problems*, **25** (2009), 095007.
- [542] J. Mueller and S. Siltanen, *Linear and Nonlinear Inverse Problems with Practical Applications*, *Comput. Sci. Engrg.* **10**, SIAM, Philadelphia, PA, 2012.
- [543] R. Muthupillai, D. J. Lomas, P. J. Rossman, J. F. Greenleaf, A. Manduca, R. L. Ehman, Magnetic resonance elastography by direct visualization of propagating acoustic strain waves, *Science*, **269** (1995), pp. 1854–1857.
- [544] A. Nachman, Global uniqueness for a two-dimensional inverse boundary value problem, *Ann. of Math.* (2), **143** (1996), pp. 71–96.
- [545] A. I. Nachman, J. F. Smith, R. C. Waag, An equation for acoustic propagation in inhomogeneous media with relaxation losses, *J. Acoust. Soc. Amer.*, **88** (1990), pp. 1584–1595.

- [546] A. Nachman, A. Tamasan, A. Timonov, Conductivity imaging with a single measurement of boundary and interior data, *Inverse Problems*, **23** (2007), pp. 2551–2563.
- [547] A. Nachman, A. Tamasan, A. Timonov, Recovering the conductivity from a single measurement of interior data, *Inverse Problems*, **25** (2009), 035014.
- [548] A. Nachman, A. Tamasan, A. Timonov, Current density impedance imaging, in [65, pp. 133–149].
- [549] H. Nam, *Ultrasound Modulated Optical Tomography*, Ph.D. thesis, Mathematics Department, Texas A&M University, College Station, TX, 2002.
- [550] H. Nam and D. Dobson, *Ultrasound modulated optical tomography*, preprint, 2004.
- [551] J. Nash, The imbedding problem for Riemannian manifolds, *Ann. of Math.* (2), **63** (1956), pp. 20–63.
- [552] F. Natterer, Computerized tomography with unknown sources, *SIAM J. Appl. Math.*, **43** (1983), pp. 1201–1212.
- [553] F. Natterer, Exploiting the range of Radon transform in tomography, in *Numerical Treatment of Inverse Problems in Differential and Integral Equations*, P. Deuflhard and E. Hairer (Editors), Birkhäuser-Verlag, Basel, 1983, pp. 290–303.
- [554] F. Natterer, Algorithms in tomography, *The State of the Art in Numerical Analysis (York, 1996)*, Inst. Math. Appl. Conf. Ser. New Ser. **63**, Oxford University Press, New York, 1997, pp. 503–523.
- [555] F. Natterer, An algorithm for 3D ultrasound tomography, in *Inverse Problems of Wave Propagation and Diffraction (Aix-les-Bains, 1996)*, Lecture Notes in Phys. **486**, Springer, Berlin, 1997, pp. 216–225.
- [556] F. Natterer, An initial value approach to the inverse Helmholtz problem at fixed frequency, in *Inverse Problems in Medical Imaging and Nondestructive Testing*, Springer, New York, pp. 159–167.
- [557] F. Natterer, Numerical methods in tomography, in *Acta Numerica*, Acta Numer. **8**, Cambridge University Press, Cambridge, UK, 1999, pp. 107–141.
- [558] F. Natterer, Mathematical models for medical imaging, in [120, pp. 17–32].
- [559] F. Natterer, *The Mathematics of Computerized Tomography*, Wiley, New York, 1986; reprinted in 2001 by SIAM.
- [560] F. Natterer, *Possibilities and Limitations of Tomography*, presentation at IMA, 2000; abstract and slides available at <http://www.ima.umn.edu/gps/abstract/natterer1.html>.
- [561] F. Natterer, Inversion of the attenuated Radon transform, *Inverse Problems*, **17** (2001), pp. 113–119.
- [562] F. Natterer, Algorithms in ultrasound tomography, in *Radon Transforms and Tomography (South Hadley, MA, 2000)*, Contemp. Math. **278**, AMS, Providence, RI, 2001, pp. 49–56.
- [563] F. Natterer, Inverting the attenuated vectorial Radon transform, *J. Inverse Ill-Posed Problems*, **13** (2005), pp. 93–101.
- [564] F. Natterer, Imaging and inverse problems of partial differential equations, *Jahresber. Deutsch. Math.-Verein.*, **109** (2007), pp. 31–48.

- [565] F. Natterer, Ultrasound tomography with fixed linear arrays of transducers, in [153, pp. 253–265].
- [566] F. Natterer, Reflectors in wave equation imaging, *Wave Motion*, **45** (2008), pp. 776–784.
- [567] F. Natterer, X-ray tomography, *Inverse Problems and Imaging*, in Lecture Notes in Math. **1943**, Springer, Berlin, 2008, pp. 17–34.
- [568] F. Natterer, Incomplete data problems in wave equation imaging, *Inverse Problems Imaging*, **4** (2010), pp. 685–691.
- [569] F. Natterer, Reflection imaging without low frequencies, *Inverse Problems*, **27** (2011), 035011.
- [570] F. Natterer, Possibilities and limitations of time domain wave equation imaging, *Tomography and Inverse Transport Theory*, Contemp. Math. **559**, AMS, Providence, RI, 2011, pp. 151–162.
- [571] F. Natterer, Photo-acoustic inversion in convex domains, *Inverse Problems Imaging*, **6** (2012), pp. 315–320.
- [572] F. Natterer, Reflection imaging of layered media without using low frequencies, *Inverse Problems*, **29** (2013), 035001.
- [573] F. Natterer, M. Cheney, B. Borden, Resolution for radar and x-ray tomography, *Inverse Problems*, **19** (2003), pp. S55–S63.
- [574] F. Natterer and A. Faridani, Basic algorithms in tomography, in *Signal Processing Part II: Control Theory and Applications*, Springer, New York, 1990, pp. 321–334.
- [575] F. Natterer and E. Ritman, *Past and Future Directions in X-Ray Computed Tomography (CT)*, Vol. 12, 2002, pp. 175–187.
- [576] F. Natterer and F. Wübbeling, A propagation-backpropagation method for ultrasound tomography, *Inverse Problems*, **11** (1995), pp. 1225–1232.
- [577] F. Natterer and F. Wübbeling, *Mathematical Methods in Image Reconstruction*, Monogr. Math. Model. Comput. **5**, SIAM, Philadelphia, PA, 2001.
- [578] F. Natterer and F. Wübbeling, Marching schemes for inverse acoustic scattering problems, *Numer. Math.*, **100** (2005), pp. 697–710.
- [579] M. Neto, F. Duarte, A. J. da Silva Neto, *An Introduction to Inverse Problems with Applications*, Springer, Heidelberg, 2013.
- [580] H.-M. Nguyen and M. S. Vogelius, Approximate cloaking for the full wave equation via change of variables, *SIAM J. Math. Anal.*, **44** (2012), pp. 1894–1924.
- [581] H.-M. Nguyen and M. S. Vogelius, Full range scattering estimates and their application to cloaking, *Arch. Ration. Mech. Anal.*, **203** (2012), pp. 769–807.
- [582] L. V. Nguyen, A family of inversion formulas in thermoacoustic tomography, *Inverse Problems Imaging*, **3** (2009), pp. 649–675.
- [583] L. V. Nguyen, On singularities and instability of reconstruction in thermoacoustic tomography, in [65, pp. 163–170].
- [584] L. V. Nguyen, *Mathematical Problems of Thermoacoustic Tomography*, Ph.D. Dissertation, Texas A&M University, College Station, TX, 2010.

- [585] S. Nilsson, *Application of Fast Backprojection Techniques for Some Inverse Problems of Integral Geometry*, Linkoeping Studies in Science and Technology, Dissertation 499, Department of Mathematics, Linkoeping University, Linkoeping, Sweden, 1997.
- [586] L. Nirenberg, An abstract form of the nonlinear Cauchy-Kowalewski theorem (Collection of articles dedicated to S. S. Chern and D. C. Spencer on their sixtieth birthdays), *J. Differential Geom.*, **6** (1972), pp. 561–576.
- [587] L. Nirenberg, Variational and topological methods in nonlinear problems, *Bull. Amer. Math. Soc. (N.S.)*, **4** (1981), pp. 267–302.
- [588] L. Nirenberg, *Lectures on Linear Partial Differential Equations*, CBMS Reg. Conf. Ser. Math. **17**, AMS, Providence, RI, 1983.
- [589] C. J. Nolan and M. Cheney, M. Synthetic aperture inversion, *Inverse Problems*, **18** (2002), pp. 221–235.
- [590] F. Noo, R. Clackdoyle, J.-M. Wagner, Inversion of the 3D exponential X-ray transform for a half equatorial band and other semi-circular geometries, *Phys. Med. Biol.*, **47** (2002), pp. 2727–2735.
- [591] F. Noo and J.-M. Wagner, Image reconstruction in 2D SPECT with 180° acquisition, *Inverse Problems*, **17** (2001), pp. 1357–1371.
- [592] S. J. Norton, Reconstruction of a two-dimensional reflecting medium over a circular domain: Exact solution, *J. Acoust. Soc. Am.*, **67** (1980), pp. 1266–1273.
- [593] S. J. Norton and M. Linzer, Ultrasonic reflectivity imaging in three dimensions: Exact inverse scattering solutions for plane, cylindrical, and spherical apertures, *IEEE Trans. Biomed. Engng.*, **28** (1981), pp. 200–202.
- [594] P. S. Novikov, Sur le problème inverse du potentiel, *Dokl. Akad. Nauk SSSR*, **18** (1938), pp. 165–168.
- [595] R. G. Novikov, Une formule d'inversion pour la transformation d'un rayonnement X, *C. R. Acad. Sci. Paris Sér. I Math.*, **332** (2001), pp. 1059–1063.
- [596] R. G. Novikov, An inversion formula for the attenuated X-ray transformation, *Ark. Mat.*, **40** (2002), pp. 145–167.
- [597] R. Novikov, On the range characterization for the two-dimensional attenuated X-ray transform, *Inverse Problems*, **18** (2002), 677–700.
- [598] L. Oksanen and G. Uhlmann, *Photoacoustic and thermoacoustic tomography with an uncertain wave speed*, arXiv:1307.1618.
- [599] O. Öktem, *Comparing Range Characterizations of the Exponential Radon Transform*, Res. Reports Math. 17, Department of Mathematics, Stockholm University, Sweden, 1996.
- [600] O. Öktem, Extension of separately analytic functions and applications to range characterization of the exponential Radon transform, in *Complex Analysis and Applications (Warsaw, 1997)*, Ann. Polon. Math. **70**, 1998, pp. 195–213.
- [601] O. Öktem, Reconstruction methods in electron tomography, in [153, pp. 289–320].
- [602] G. Ólafsson and E. T. Quinto (Editors), *The Radon Transform, Inverse Problems, and Tomography (American Mathematical Society Short Course, January 3–4, 2005, Atlanta, Georgia)*, Proc. Symp. Appl. Math. **63**, AMS, Providence, RI 2006.

- [603] G. Ólafsson and R. J. Stanton, On the life and work of S. Helgason, in [661, pp. 21–42].
- [604] J. Ophir, I. Cespedes, H. Ponnekanti, Y. Yazdi, X. Li, Elastography: A quantitative method for imaging the elasticity of biological tissues, *Ultrason. Imaging*, **13** (1991), pp. 111–134.
- [605] A. A. Oraevsky, R. O. Esenaliev, S. L. Jacques, F. K. Tittel, Laser optoacoustic tomography for medical diagnostics principles, *Proc. SPIE*, **2676** (1996), 22.
- [606] A. A. Oraevsky, S. L. Jacques, R. O. Esenaliev, F. K. Tittel, Laser-based ptoacoustic imaging in biological tissues, *Proc. SPIE*, **2134A** (1994), pp. 122–128.
- [607] A. A. Oraevsky and A. A. Karabutov, Time-resolved detection of optoacoustic profiles for measurement of optical distribution in tissues, in [766, Chapter 10].
- [608] A. A. Oraevsky and A. A. Karabutov, Optoacoustic tomography, in [789, Chapter 34].
- [609] L. V. Ovsjannikov, *Analiticheskie gruppy: Vvedenie v teoriyu beskonechnykh nepreryvnykh grupp preobrazovanii* [Analytic groups: Introduction to the theory of infinite continuous transformation groups] (in Russian), Novosibirsk. Gosudarstv. Univ., Novosibirsk, Russia, 1972.
- [610] L. Päivärinta and J. Sylvester, Transmission eigenvalues, *SIAM J. Math. Anal.*, **40** (2008), pp. 738–753.
- [611] V. P. Palamodov, Nonlinear artifacts in tomography (in Russian), *Dokl. Akad. Nauk SSSR*, **291** (1986), pp. 333–336.
- [612] V. P. Palamodov, Some singular problems in tomography, in *Mathematical Problems of Tomography*, Transl. Math. Monogr. **81**, AMS, Providence, RI, 1990, pp. 123–140.
- [613] V. P. Palamodov, Inversion formulas for the three-dimensional ray transform, in *Mathematical Methods in Tomography (Oberwolfach, 1990)*, Lecture Notes in Math. **1497**, Springer, Berlin, 1991, pp. 53–62.
- [614] V. P. Palamodov, Some mathematical aspects of 3D X-ray tomography, in [659, pp. 199–210].
- [615] V. P. Palamodov, Localization of harmonic decomposition of the Radon transform, *Inverse Problems*, **11** (1995), pp. 1025–1030.
- [616] V. P. Palamodov, An inversion method for an attenuated x-ray transform, *Inverse Problems*, **12** (1996), pp. 717–729.
- [617] V. P. Palamodov, Reconstruction from limited data of arc means, *J. Fourier Anal. Appl.*, **6** (2000), pp. 25–42.
- [618] V. P. Palamodov, Impedance tomography, inverse scattering, and phase space analysis, in *Partial Differential Equations*, Amer. Math. Soc. Transl. Ser. 2 **206**, AMS, Providence, RI, 2002, pp. 177–192.
- [619] V. P. Palamodov, Stability in diffraction tomography and a nonlinear “basic theorem,” *J. Anal. Math.*, **91** (2003), pp. 247–268.
- [620] V. P. Palamodov, *Reconstructive Integral Geometry*, Birkhäuser, Basel, 2004.
- [621] V. P. Palamodov, Characteristic problems for the spherical mean transform, in *Complex Analysis and Dynamical Systems II*, Contemp. Math. **382**, AMS, Providence, RI, 2005, pp. 321–330.
- [622] V. Palamodov, Remarks on the general Funk-Radon transform and thermoacoustic tomography, *Inverse Problems and Imaging*, **4** (2010), pp. 693–702.

- [623] V. P. Palamodov, An analytic reconstruction for the Compton scattering tomography in a plane, *Inverse Problems*, **27** (2011), 125004.
- [624] G. Paltauf, P. Burgholzer, M. Haltmeier, O. Scherzer, Thermoacoustic tomography using optical line detection, *Proc. SPIE*, **5864** (2005), pp. 7–14.
- [625] G. Paltauf, R. Nuster, P. Burgholzer, Characterization of integrating ultrasound detectors for photoacoustic tomography, *J. Appl. Phys.*, **105** (2009), 102026.
- [626] G. Paltauf, R. Nuster, M. Haltmeier, P. Burgholzer, Thermoacoustic computed tomography using a Mach-Zehnder interferometer as acoustic line detector, *Appl. Opt.*, **46** (2007), pp. 3352–3358.
- [627] G. Paltauf, R. Nuster, M. Haltmeier, P. Burgholzer, Experimental evaluation of reconstruction algorithms for limited view photoacoustic tomography with line detectors, *Inverse Problems*, **23** (2007), pp. S81–S94.
- [628] G. Paltauf, J. A. Viator, S. A. Prahl, S. L. Jacques, Iterative reconstruction algorithm for optoacoustic imaging, *J. Acoust. Soc. Am.*, **112** (2002), pp. 1536–1544.
- [629] J. E. Pasciak, *A Note on the Fourier Algorithm for Image Reconstruction*, Brookhaven National Laboratory, Upton, NY, 1981.
- [630] V. I. Passechnik, A. A. Anosov, K. M. Bograchev, Fundamentals and prospects of passive thermoacoustic tomography, *Critical Rev. Biomed. Eng.*, **28** (2000), pp. 603–640.
- [631] S. K. Patch, Thermoacoustic tomography—Consistency conditions and the partial scan problem, *Phys. Med. Biol.*, **49** (2004), pp. 1–11.
- [632] S. Patch, Photoacoustic or thermoacoustic tomography: Consistency conditions and the partial scan problem, in [793, pp. 103–116].
- [633] S. K. Patch and M. Haltmeier, Thermoacoustic tomography—Ultrasound attenuation artifacts, *IEEE Nuclear Science Symposium Conference*, **4** (2006), pp. 2604–2606.
- [634] S. K. Patch and O. Scherzer, Photo- and thermo-acoustic imaging (Guest Editors’ Introduction), *Inverse Problems*, **23** (2007), pp. S01–S10.
- [635] G. P. Paternain, M. Salo, G. Uhlmann, *Tensor tomography on surfaces*, *Invent. Math.*, **193** (2013), pp. 229–247.
- [636] G. P. Paternain, M. Salo, G. Uhlmann, *On the range of the attenuated ray transform for unitary connections*, arXiv:1302.4880.
- [637] G. P. Paternain, M. Salo, G. Uhlmann, The attenuated ray transform for connections and Higgs fields, *Geom. Funct. Anal.*, **22** (2012), pp. 1460–1489.
- [638] R. Pauen, *Non-Trapping Conditions and Local Energy Decay for Hyperbolic Problems*, Thesis, Konstanzer Schriften in Mathematik und Informatik, Nr. 132, 200.
- [639] J. Peetre, Une caractérisation abstraite des opérateurs différentiels, *Math. Scand.*, **7** (1959), pp. 211–218.
- [640] J. B. Pendry, D. Schurig, D. R. Smith, Controlling electromagnetic fields, *Science*, **312** (2006), pp. 1780–1782.
- [641] J. B. Pendry, D. Schurig, D. R. Smith, Calculation of material properties and ray tracing in transformation media, *Opt. Exp.*, **14** (2006), 9794.

- [642] Physorg.com, *The Mathematics of Cloaking*, 2006, <http://www.physorg.com/news86358402.html>.
- [643] I. Ponomarev, Correction of emission tomography data. Effects of detector displacement and non-constant sensitivity, *Inverse Problems*, **10** (1995), pp. 1–8.
- [644] I. Ponomarev (Ponomaryov), *Numerical Analysis of Problems of Tomography, Radiotherapy, and Photonic Crystal Theory*, Ph.D. Dissertation, Mathematics Department, Wichita State University, Wichita, KS, 1997.
- [645] D. A. Popov, The generalized Radon transform on the plane, the inverse transform, and the Cavalieri conditions, *Funct. Anal. Appl.*, **35** (2001), pp. 270–283.
- [646] D. A. Popov, The Paley–Wiener theorem for the generalized Radon transform on the plane, *Funct. Anal. Appl.*, **37** (2003), pp. 215–220.
- [647] D. A. Popov and D. V. Sushko, A parametrix for the problem of optical-acoustic tomography, *Dokl. Math.*, **65** (2002), pp. 19–21.
- [648] D. A. Popov and D. V. Sushko, Image restoration in optical-acoustic tomography, *Problems Information Transmission*, **40** (2004), pp. 254–278.
- [649] N. G. Preobrazhensky and V. V. Pikalov, *Reconstructive Tomography in Gas Dynamics and Plasma Physics*, Nauka, Novosibirsk, Russia, 1987.
- [650] J. Qian, P. Stefanov, G. Uhlmann, H. Zhao, An efficient Neumann series-based algorithm for thermoacoustic and photoacoustic tomography with variable sound speed, *SIAM J. Imaging Sci.*, **4** (2011), pp. 850–883.
- [651] E. T. Quinto, The dependence of the generalized Radon transform on defining measures, *Trans. Amer. Math. Soc.*, **257** (1980), pp. 331–346.
- [652] E.T. Quinto, Null spaces and ranges for classical and spherical Radon transforms, *J. Math. Anal. Appl.*, **90** (1982), pp. 408–420.
- [653] E.T. Quinto, The invertibility of rotation invariant Radon transforms, *J. Math. Anal. Appl.*, **91** (1983), pp. 510–522.
- [654] E. T. Quinto, Singular value decompositions and inversion methods for the exterior Radon transform and a spherical transform, *J. Math. Anal. Appl.*, **95** (1983), pp. 437–448.
- [655] E. T. Quinto, Tomographic reconstructions from incomplete data and numerical inversion of the exterior Radon transform, *Inverse Problems*, **4** (1988), pp. 867–876.
- [656] E. T. Quinto, Singularities of the X-ray transform and limited data tomography in \mathbb{R}^2 and \mathbb{R}^3 , *SIAM J. Math. Anal.*, **24** (1993), pp. 1215–1225.
- [657] E. T. Quinto, An introduction to X-ray tomography and Radon transforms, in [602, pp. 1–23].
- [658] E.T. Quinto, T. Bakhos, S. Chung, Local tomography in 3-D SPECT, in *Mathematical Methods in Biomedical Imaging and Intensity-Modulated Radiation Therapy (IMRT)*, CRM Ser. 7, Ed. Norm., Pisa, 2008, pp. 321–348.
- [659] E.T. Quinto, M. Cheney, P. Kuchment (Editors), *Tomography, Impedance Imaging, and Integral Geometry*, Lectures in Appl. Math. **30**, AMS, Providence, RI, 1994.

- [660] E.T. Quinto, L. Ehrenpreis, A. Faridani, F. Gonzalez, E. Grimberg (Editors), *Radon Transforms and Tomography*, Contemp. Math. **278**, AMS, Providence, RI, 2000.
- [661] E. T. Quinto, F. Gonzalez, J. G. Christensen (Editors), *Geometric Analysis and Integral Geometry*, Contemp. Math. **598**, AMS, Providence, RI, 2013.
- [662] E.T. Quinto and O. Öktem, Local tomography in electron microscopy, *SIAM J. Appl. Math.*, **68** (2008), pp. 1282–1303.
- [663] J. Radon, Über die Bestimmung von Funktionen durch ihre Integralwerte längs gewisser Mannigfaltigkeiten, *Ber. Verh. Sächs. Akad.*, **69** (1917), pp. 262–277.
- [664] J. V. Ralston, Solutions of the wave equation with localized energy, *Comm. Pure Appl. Math.*, **22** (1969), pp. 807–823.
- [665] A. Ramm, Inversion of limited-angle tomographic data, *Comput. Math. Appl.*, **22** (1992), pp. 101–111.
- [666] A. G. Ramm, Injectivity of the spherical means operator, *C. R. Math. Acad. Sci. Paris*, **335** (2002), pp. 1033–1038.
- [667] A. Ramm and A. Katsevich, *The Radon Transform and Local Tomography*, CRC Press, Boca Raton, FL, 1996.
- [668] A. Ramm and A. Zaslavsky, Reconstructing singularities of a function from its Radon transform, *Math. Comput. Modelling*, **18** (1993), pp. 109–138.
- [669] K. Ren and G. Bal, On multi-spectral quantitative photoacoustic tomography in diffusive regime, *Inverse Problems*, **28** (2012), 025010.
- [670] K. Ren, G. Bal, A. H. Hielscher, Frequency domain optical tomography based on the equation of radiative transfer, *SIAM J. Sci. Comput.*, **28** (2006), pp. 1463–1489.
- [671] K. Ren, H. Gao, H. Zhao, A hybrid reconstruction method for quantitative PAT, *SIAM J. Imaging Sci.*, **6** (2013), pp. 32–55.
- [672] K. Ren and H. Zhao, *Quantitative fluorescence photoacoustic tomography*, to appear in SIAM J. Imag. Sci., 2013.
- [673] V. Retakh (Coordinating Editor), D. McDuff, S. Tabachnikov, M. Saul, *Israel Moiseevich Gelfand, Part II*, Notices Amer. Math. Soc., **60** (2013), pp. 162–171.
- [674] V. Retakh (Coordinating Editor), I. M. Singer, D. Kazhdan, A. Vershik, B. Konstant, S. Gindikin, P. Lax, A. Zelevinsky, *Israel Moiseevich Gelfand*, Notices Amer. Math. Soc., **60** (2013), pp. 24–49.
- [675] B. Rigaud and J.-P. Morucci, Bioelectrical impedance techniques in medicine. Part III: General concepts and hardware, *Critical Reviews in Biomedical Engineering*, **24** (1996), pp. 467–597.
- [676] B. Rigaud, J.-P. Morucci, N. Chauveau, Bioelectrical impedance techniques in medicine. Part I: Bioimpedance measurement, *Critical Reviews in Biomedical Engineering*, **24** (1996), pp. 257–351.
- [677] V. G. Romanov, Reconstructing functions from integrals over a family of curves, *Sib. Mat. Zh.*, **7** (1967), pp. 1206–1208.

- [678] R. Roşu, On overdetermined systems associated with integral geometry transform in the real projective space, in [132, pp. 261–266], 1987.
- [679] F. Rouvière, Inverting Radon transforms: The group-theoretic approach, *Ensign. Math.*, **47** (2001), pp. 205–252.
- [680] F. Rouvière, *On Radon transforms and the kappa operator*, preprint, 2006; available online at <http://math.unice.fr/~frou/recherche/Radon06a.pdf>.
- [681] B. Rubin, Fractional differentiation and spherical Radon transforms, *Fract. Calc. Appl. Anal.*, **3** (2000), pp. 435–437.
- [682] B. Rubin, Inversion of exponential k -plane transforms, *J. Fourier Anal. Appl.*, **6** (2000), pp. 185–205.
- [683] B. Rubin, Inversion formulas for the spherical Radon transform and the generalized cosine transform, *Adv. Appl. Math.*, **29** (2002), pp. 471–497.
- [684] B. Rubin, Notes on Radon transforms in integral geometry, *Fract. Calc. Appl. Anal.*, **6** (2003), pp. 25–72.
- [685] B. Rubin, Reconstruction of functions from their integrals over k -planes, *Israel J. Math.*, **141** (2004), pp. 93–117.
- [686] B. Rubin, Riesz potentials and integral geometry in the space of rectangular matrices, *Adv. Math.*, **205** (2006), pp. 549–598.
- [687] B. Rubin, Inversion formulae for the spherical mean in odd dimensions and the Euler-Poisson-Darboux equation, *Inverse Problems*, **24** (2008), 025021.
- [688] B. Rubin, The Radon transform on the Heisenberg group and the transversal Radon transform, *J. Funct. Anal.*, **262** (2012), pp. 234–272.
- [689] H. Rullgård, An explicit inversion formula for the exponential Radon transform using data from 180° Arkiv för matematik, **42** (2004), pp. 353–362.
- [690] H. Rullgård, Stability of the inverse problem for the attenuated Radon transform with 180° degrees data, *Inverse Problems*, **20** (2004), pp. 781–797.
- [691] I. Sabadini and D. Struppa (Editors), *The Mathematical Legacy of Leon Ehrenpreis*, Springer, New York, 2012.
- [692] X. Saint-Raymond, *Elementary Introduction to the Theory of Pseudodifferential Operators*, CRC Press, Boca Raton, FL, 1991.
- [693] B. E. A. Saleh and M. C. Teich, *Fundamentals of Photonics*, Wiley-Interscience, New York, 1991.
- [694] M. Salo, *Calderón Problem*, lecture notes, University of Helsinki, 2008, http://www.rni.helsinki.fi/~msa/teaching/calderon_lectures.pdf.
- [695] M. Salo and G. Uhlmann, The attenuated ray transform on simple surfaces, *J. Differential Geom.*, **88** (2011), pp. 161–187.
- [696] A. A. Samarskii and P. N. Vabishchevich, *Numerical Methods for Solving Inverse Problems of Mathematical Physics*, Inverse and Ill-posed Problems Series, Walter de Gruyter, Berlin, 2007.
- [697] L. A. Santalo, *Integral Geometry and Geometric Probability*, Cambridge University Press, Cambridge, UK, 2004.

- [698] F. Santosa, Inverse problem holds key to safe, continuous imaging, *SIAM News*, **27** (1994), pp. 1 and 16–18.
- [699] F. Santosa, M. Vogelius, A backprojection algorithm for electrical impedance imaging, *SIAM J. Appl. Math.*, **50** (1990), pp. 216–241.
- [700] O. Scherzer (Editor), *Mathematical Models for Registration and Applications to Medical Imaging*, Math. in Industry 10, The European Consortium for Mathematics in Industry (Berlin), Springer-Verlag, Berlin, 2006.
- [701] O. Scherzer (Editor), *Handbook of Mathematical Methods in Imaging*, Springer-Verlag, Berlin, 2010.
- [702] O. Scherzer, M. Grasmair, H. Grossauer, M. Haltmeier, F. Lenzen, *Variational Methods in Imaging*, Appl. Math. Sci. **167**, Springer, New York, 2009.
- [703] L. Schmetterer, Reminiscences to Johann Radon, in [277, pp. 26–28].
- [704] J. C. Schotland, Inversion formulas and fast image reconstruction algorithms in optical tomography, in [153, pp. 367–387].
- [705] J. C. Schotland, Path integrals and optical tomography, in *Mathematical and Statistical Methods for Imaging*, Contemp. Math. **548**, AMS, Providence, RI, 2011, pp. 77–84.
- [706] R.T. Seeley, Spherical harmonics, *Amer. Math. Monthly*, **73** (1966), pp. 115–121.
- [707] E. Seeram, *Computed Tomography: Physical Principles, Clinical Applications, and Quality Control*, Third edition, Saunders, Philadelphia, 2008.
- [708] J. K. Seo and E. Je. Woo, Magnetic resonance electrical impedance tomography (MREIT), *SIAM Rev.*, **53** (2011), pp. 40–68.
- [709] J. K. Seo and E. J. Woo, Magnetic resonance elastography, in *Nonlinear Inverse Problems in Imaging*, John Wiley & Sons, Chichester, UK, 2013.
- [710] V. A. Sharafutdinov, *Integral Geometry of Tensor Fields*, V.S.P. Intl Science, Utrecht, The Netherlands, 1994.
- [711] L. A. Shepp, Scope of pure and applied tomography, *Computed Tomography (Cincinnati, Ohio, 1982)*, Proc. Sympos. Appl. Math. **27**, AMS, Providence, RI, 1982, pp. 1–6.
- [712] L. A. Shepp and J. B. Kruskal, Computerized tomography: The new medical x-ray technology, *Amer. Math. Monthly*, **85** (1978), pp. 420–439.
- [713] L. A. Shepp and B. F. Logan, The Fourier reconstruction of a head section, *IEEE Trans. Nuclear Sci.*, **NS-21** (1974), pp. 21–43.
- [714] L. A. Shepp and J. A. Stein, Simulated reconstruction artifacts in computerized x-ray tomography, in *Reconstruction Tomography in Diagnostic Radiology and Nuclear Medicine*, M. M. Ter-Pogossian, M. E. Phelps, G. L. Brownell (Editors), University Park Press, Baltimore, 1977, pp. 33–48.
- [715] L. A. Shepp and Y. Vardi, Maximum likelihood reconstruction for emission tomography, *IEEE Trans. Med. Imag.*, **1** (1982), pp. 113–122.
- [716] I. Shneiberg, Exponential Radon transform, *Doklady Akad. Nauk SSSR*, **320** (1991), pp. 567–571; English translation in *Soviet. Math. Dokl.*

- [717] I. Shneiberg, Exponential Radon transform, in [273, pp. 235–246].
- [718] I. Shneiberg, I. Ponomarev, V. Dmitrichenko, S. Kalashnikov, On a new reconstruction algorithm in emission tomography, in [273, pp. 247–255].
- [719] M. A. Shubin, *Pseudodifferential Operators and Spectral Theory*, Springer-Verlag, Berlin, 2001.
- [720] B. Simon, *Trace Ideals and Their Applications*, Second edition, Math. Surveys Monogr. 120, AMS, Providence, RI, 2005.
- [721] A. Singer, Z. Zhao, Y. Shkolnisky, R. Hadani, Viewing angle classification of cryo-electron microscopy images using eigenvectors, *SIAM J. Imaging Sci.*, 4 (2011), pp. 723–759.
- [722] M. Singh, An electronically collimated gamma camera for single photon emission computed tomography. Part I: Theoretical considerations and design criteria, *Med. Phys.*, 10 (1983), pp. 421–427.
- [723] B. Smith, Reconstruction methods and completeness conditions for two Compton data models, *J. Opt. Soc. Amer. A*, 22 (2005), pp. 445–459.
- [724] K. T. Smith, Reconstruction formulas in computed tomography, in *Computed Tomography*, Proc. Sympos. Appl. Math. 27, L. A. Shepp (Editor), AMS, Providence, RI, 1983, pp. 7–23.
- [725] K. T. Smith and F. Keinert, Mathematical foundations of computed tomography, *Appl. Optics*, 24 (1985), pp. 3950–3957.
- [726] K. T. Smith, D. C. Solmon, S. L. Wagner, Practical and mathematical aspects of the problem of reconstructing objects from radiographs, *Bull. Amer. Math. Soc.*, 83 (1977), pp. 1227–1270; addendum in *Bull. Amer. Math. Soc.*, 84 (1978), p. 691.
- [727] D. T. Smithey, M. Beck, M. G. Raymer, A. Faridani, Measurement of the Wigner distribution and the density matrix of a light mode using optical homodyne tomography: Application to squeezed states and the vacuum, *Phys. Rev. Lett.*, 70 (1993), pp. 1244–1247.
- [728] D. Solmon, Two inverse problems for the exponential Radon transform, in *Inverse Problems in Action*, P. S. Sabatier (Editor), Springer-Verlag, Berlin, 1990, pp. 46–53.
- [729] D. Solmon, The identification problem for the exponential Radon transform, *Math. Methods Appl. Sci.*, 18 (1995), pp. 687–695.
- [730] V. A. Solonnikov, Overdetermined elliptic boundary value problems, *Zap. Nauchn. Sem. Leningrad. Otdel. Mat. Inst. Steklov. (LOMI)*, 21 (1971), pp. 112–158 (in Russian); English translation in *J. Sov. Math.*, 1 (1973), pp. 477–512.
- [731] E. Somersalo, M. Cheney, D. Isaacson, E. Isaacson, Layer-stripping: A direct numerical method for impedance imaging, *Inverse Problems*, 7 (1991), pp. 899–926.
- [732] Special issue devoted to thermoacoustic tomography, *Inverse Problems*, 23 (2007), no. 6.
- [733] D. C. Spencer, Overdetermined systems of linear partial differential equations, *Bull. Amer. Math. Soc.*, 75 (1969), pp. 179–239.
- [734] P. Stefanov, *The identification problem for the attenuated X-ray transform*, arXiv:1105.1489.
- [735] P. Stefanov and G. Uhlmann, Linearizing nonlinear inverse problems and an application to inverse backscattering, *J. Funct. Anal.*, 256 (2009), pp. 2842–2866.
- [736] P. Stefanov and G. Uhlmann, Integral geometry of tensor fields on a class of non-simple Riemannian manifolds, *Amer. J. Math.*, 130 (2008), pp. 239–268.

- [737] P. Stefanov and G. Uhlmann, Thermoacoustic tomography with variable sound speed, *Inverse Problems*, **25** (2009), 075011.
- [738] P. Stefanov and G. Uhlmann, Thermoacoustic tomography arising in brain imaging, *Inverse Problems*, **27** (2011), 045004.
- [739] P. Stefanov and G. Uhlmann, Multi-wave methods via ultrasound, in [775, pp. 271–324].
- [740] E. M. Stein, *Fourier Analysis: An Introduction*, Princeton University Press, Princeton, NJ, 2003.
- [741] E. M. Stein and G. Weiss, *Introduction to Fourier Analysis on Euclidean Spaces*, Princeton University Press, Princeton, NJ, 1971.
- [742] D. Steinhauer, *A uniqueness theorem for thermoacoustic tomography in the case of limited boundary data*, arXiv:0902.2838, 2009.
- [743] D. Steinhauer, *A reconstruction procedure for thermoacoustic tomography in the case of limited boundary data*, arXiv:0905.2954, 2009.
- [744] P. E. Stott, A. Wootton, G. Gorini, E. Sindoni, D. Batani (Editors), *Advanced Diagnostics for Magnetic and Inertial Fusion*, Springer-Verlag, Berlin, 2002.
- [745] R. S. Strichartz, *A Guide to Distribution Theory and Fourier Transforms*, World Scientific, River Edge, NJ, 2003.
- [746] J. Sylvester, A convergent layer-stripping algorithm for the radially symmetric impedance tomography problem, *Comm. Partial Differential Equations*, **17** (1992), pp. 1955–1994.
- [747] J. Sylvester, Discreteness of transmission eigenvalues via upper triangular compact operators, *SIAM J. Math. Anal.*, **44** (2012), pp. 341–354.
- [748] J. Sylvester and G. Uhlmann, A global uniqueness theorem for an inverse boundary value problem, *Ann. Math.*, **125** (1987), pp. 153–169.
- [749] J. Sylvester and G. Uhlmann, The Dirichlet to Neumann map and applications, in *Inverse Problems in Partial Differential Equations*, SIAM, Philadelphia, 1990, pp. 101–139.
- [750] A. C. Tam, Applications of photoacoustic sensing techniques, *Rev. Modern Phys.*, **58** (1986), pp. 381–431.
- [751] A. Tarantola, *Inverse Problem Theory. Methods for Data Fitting and Model Parameter Estimation*, Elsevier Science, B.V., Amsterdam, 1987.
- [752] T. Tarvainen, B. T. Cox, J. P. Kaipio, S. R. Arridge, Reconstructing absorption and scattering distributions in quantitative photoacoustic tomography, *Inverse Problems*, **28** (2012), 084009.
- [753] M. E. Taylor, *Pseudodifferential Operators*, Princeton University Press, Princeton, NJ, 1981.
- [754] M. E. Taylor, *Noncommutative Harmonic Analysis*, AMS, Providence, RI, 1986.
- [755] M. E. Taylor, *Partial Differential Equations I & II*, Springer-Verlag, New York, 1997.
- [756] M. E. Taylor, *Tools for PDE*, AMS, Providence, RI, 2000.
- [757] S. I. Tetel'baum, About the problem of improvement of images obtained with the help of optical and analog instruments, *Bull. Kiev Polytech. Inst. (Izvestiya Kievskogo Politekhnicheskogo Instituta)*, **21** (1956), 222.

- [758] S. I. Tetel'baum, About a method of obtaining volume images with the help of x-rays, *Bull. Kiev Polytech. Inst. (Izvestiya Kievskogo Politekhnich. Instituta)* **22** (1957), pp. 154–160.
- [759] A. N. Tikhonov and V. Y. Arsenin, *Solution of Ill-Posed Problems*, V. H. Winston & Sons, Washington, DC, 1977.
- [760] G. P. Tolstov, *Fourier Series*, Dover, New York, 1962.
- [761] L. N. Trefethen and D. Bau, *Numerical Linear Algebra*, SIAM, Philadelphia, 1997.
- [762] O. J. Tretiak and P. Delaney, The exponential convolution algorithm for emission computed axial tomography, in *Computed Tomography*, Proc. Symp. Appl. Math. **27**, AMS, Providence, RI, 1982, pp. 25–33.
- [763] O. Tretiak and C. Metz, The exponential Radon transform, *SIAM J. Appl. Math.*, **39** (1980), pp. 341–354.
- [764] F. Treves, *Introduction to Pseudo Differential and Fourier Integral Operators*, University Ser. Math., Plenum, New York, 1981.
- [765] T. T. Truong, M. K. Nguyen, H. Zaidi, The mathematical foundations of 3D Compton scatter emission imaging, *Int. J. Biomed. Imaging*, **2007** (2007), 92780.
- [766] V. V. Tuchin (Editor), *Handbook of Optical Biomedical Diagnostics*, SPIE, Bellingham, WA, 2002.
- [767] A. Tumanov, Analytic continuation from a family of lines, *J. Anal. Math.*, **105** (2008), pp. 391–396.
- [768] H. K. Tuy, An inversion formula for cone-beam reconstruction, *SIAM J. Appl. Math.*, **43** (1983), pp. 546–552.
- [769] G. Uhlmann, Inverse boundary value problems and applications, *Astérisque*, **207** (1992), pp. 153–211.
- [770] G. Uhlmann, *Microlocal Analysis and Inverse Problems*, lecture slides (in two parts), 2001, <http://www.msri.org/publications/ln/msri/2001/jiw2001/uhlmann/1/index.html>; <https://secure.msri.org/communications/ln/msri/2001/jiw2001/uhlmann/2/banner/01.html>.
- [771] G. Uhlmann (Editor), *Inside Out, Inverse Problems and Applications*, MSRI Publications **47**, Cambridge University Press, Cambridge, UK, 2003.
- [772] G. Uhlmann, Commentary on Calderón's paper on an inverse boundary value problem, in [92, pp. 623–636].
- [773] G. Uhlmann, Visibility and invisibility, in Proceedings of ICIAM 07—6th International Congress on Industrial and Applied Mathematics, Eur. Math. Soc., Zürich, 2009, pp. 381–408.
- [774] G. Uhlmann, Calderon's problem and electrical impedance tomography, *Inverse Problems*, **25** (2009), 123011.
- [775] G. Uhlmann (Editor), *Inside out: Inverse Problems and Applications*, Vol. 2, MSRI Publications **60**, Cambridge University Press, Cambridge, UK, 2013.
- [776] B. Vainberg, The short-wave asymptotic behavior of the solutions of stationary problems, and the asymptotic behavior as $t \rightarrow \infty$ of the solutions of nonstationary problems, *Russian Math. Surveys*, **30** (1975), pp. 1–58.

- [777] B. Vainberg, *Asymptotics Methods in the Equations of Mathematical Physics*, Gordon and Breach, New York, 1982.
- [778] E. I. Vainberg, I. A. Kazak, M. L. Faingoiz, X-ray computerized back projection tomography with filtration by double differentiation. Procedure and information features, *Soviet J. Nondestructive Testing*, **21** (1985), pp. 106–113.
- [779] E. I. Vainberg, I. A. Kazak, V. P. Kurozaev, Reconstruction of the internal three-dimensional structure of objects based on real-time internal projections, *Soviet J. Nondestructive Testing*, **17** (1981), pp. 415–423.
- [780] B. K. Vainshtein and A. B. Goncharov, Determination of the spatial orientation of arbitrarily located identical particles of unknown structure from their projections, *Dokl. Akad. Nauk SSSR*, **287** (1986), pp. 1131–1134 (in Russian).
- [781] M. E. Valentinuzzi, J.-P. Morucci, C. J. Felice, Bioelectrical impedance techniques in medicine. Part II: Monitoring of physiological events by impedance, *Crit. Rev. Biomed. Engrg.*, **24** (1996), pp. 353–466.
- [782] Y. Vardi, L. A. Shepp, L. Kaufman, A statistical model for positron emission tomography, *J. Amer. Stat. Assoc.*, **80** (1985), pp. 8–20.
- [783] F. Guevara Vasquez, G. W. Milton, D. Onofrei, Exterior cloaking with active sources in two dimensional acoustics, *Wave Motion*, **48** (2011), pp. 515–524.
- [784] F. Guevara Vasquez, G. W. Milton, D. Onofrei, Mathematical analysis of the two dimensional active exterior cloaking in the quasistatic regime, *Anal. Math. Phys.*, **2** (2012), pp. 231–246.
- [785] C. L. Vaughan, *Imagining the Elephant: A Biography of Allan MacLeod Cormack*, World Scientific, River Edge, NJ, 2008.
- [786] Video recordings of lectures given at MSRI can be found online at <http://www.msri.org/web/msri/online-videos/>.
- [787] N. Ja. Vilenkin, *Special Functions and the Theory of Group Representations*, Transl. Math. Monogr. **22**, AMS, Providence, RI, 1968.
- [788] N. Ya. Vilenkin and A. U. Klimyk, *Representation of Lie Groups and Special Functions*, Vol. 1–3, Kluwer Academic Publishers, Dordrecht, The Netherlands, 1992.
- [789] T. Vo-Dinh (Editor), *Biomedical Photonics Handbook*, CRC, Boca Raton, FL, 2003.
- [790] C. R. Vogel, *Computational Methods for Inverse Problems*, Frontiers in Appl. Math. **23**, SIAM, Philadelphia, 2002.
- [791] V. Volchkov, *Integral Geometry and Convolution Equations*, Kluwer Academic Publishers, Dordrecht, The Netherlands, 2003.
- [792] J.-M. Wagner, F. Noo, R. Clackdoyle, Exact inversion of the exponential X-ray transform for rotating slant-hole (RSHT) SPECT, *Phys. Med. Biol.*, **47** (2002), pp. 2713–2726.
- [793] L. Wang (Editor), *Photoacoustic Imaging and Spectroscopy*, CRC Press, Boca Raton, FL, 2009.
- [794] L. Wang and M. A. Anastasio, Photoacoustic and thermoacoustic tomography: Image formation principles, in [701, Chapter 28].

- [795] K. Wang, C. Huang, Y. J. Kao, C. Y. Chou, A. A. Oraevsky, M. A. Anastasio, Accelerating image reconstruction in three-dimensional optoacoustic tomography on graphics processing units, *Med. Phys.*, **40** (2013), 023301.
- [796] X. Wang, Y. Pang, G. Ku, X. Xie, G. Stoica, L. Wang, Noninvasive laser-induced photoacoustic tomography for structural and functional *in vivo* imaging of the brain, *Nature Biotech.*, **21** (2003), pp. 803–806.
- [797] K. Wang, R. Su, A. A. Oraevsky, M. A. Anastasio, Investigation of iterative image reconstruction in three-dimensional optoacoustic tomography, *Phys. Med. Biol.*, **57** (2012), pp. 5399–5423.
- [798] L. V. Wang and H. Wu, *Biomedical Optics. Principles and Imaging*, Wiley-Interscience, New York, 2007.
- [799] Y. Wang, A. Yagola, C. Yang (Editors), *Computational Methods for Applied Inverse Problems*, De Gruyter, Berlin, 2012.
- [800] S. Webb, *From the Watching of Shadows—The Origins of Radiological Tomography*, Adam Hilger, Bristol, New York, 1990.
- [801] R. O. Wells, Jr., Integral geometry and twistor theory, in [132, pp. 317–336].
- [802] T. Widlak and O. Scherzer, Hybrid tomography for conductivity imaging, *Inverse Problems*, **28** (2012), 084008.
- [803] E. J. Woo and J. K. Seo, Magnetic resonance electrical impedance tomography (MREIT) for high-resolution conductivity imaging, *Physiol. Meas.*, **29** (2008), pp. R1–R26.
- [804] L. Xing and L. Lee, Image guided intensity modulated radiation therapy, in [153, pp. 479–504].
- [805] M. Xu and L.-H. V. Wang, Time-domain reconstruction for thermoacoustic tomography in a spherical geometry, *IEEE Trans. Med. Imaging*, **21** (2002), pp. 814–822.
- [806] M. Xu and L.-H. V. Wang, Universal back-projection algorithm for photoacoustic computed tomography, *Phys. Rev. E*, **71** (2005), 016706.
- [807] M. Xu and L.-H. V. Wang, Photoacoustic imaging in biomedicine, *Rev. Scientific Instruments*, **77** (2006), 041101.
- [808] Y. Xu, D. Feng, L.-H. V. Wang, Exact frequency-domain reconstruction for thermoacoustic tomography: I. Planar geometry, *IEEE Trans. Med. Imaging*, **21** (2002), pp. 823–828.
- [809] Y. Xu, L.-H. V. Wang, Time reversal in photoacoustic tomography or thermoacoustic tomography, in [793, pp. 117–120].
- [810] Y. Xu, L. Wang, G. Ambartsoumian, P. Kuchment, Reconstructions in limited view thermoacoustic tomography, *Med. Phys.*, **31** (2004), pp. 724–733.
- [811] Y. Xu, L. Wang, G. Ambartsoumian, P. Kuchment, Limited view thermoacoustic tomography, in [793, pp. 61–73].
- [812] Y. Xu, M. Xu, L.-H. V. Wang, Exact frequency-domain reconstruction for thermoacoustic tomography: II. Cylindrical geometry, *IEEE Trans. Med. Imag.*, **21** (2002), pp. 829–833.
- [813] X. Xun, B. Mallick, R. Carroll, P. Kuchment, Bayesian approach to detection of small low emission sources, *Inverse Problems*, **27** (2011), 115009.

- [814] O. Yilmaz, *Seismic Data Analysis* (two volumes), Investigations Geophys. 10, Society Exploration Geophysicists, Tulsa, OK, 2001.
- [815] Z. Yuan, Q. Zhang, H. Jiang, Simultaneous reconstruction of acoustic and optical properties of heterogeneous media by quantitative photoacoustic tomography, *Optics Express*, 14 (2006), 6749.
- [816] M. G. Zaïdenberg, S. G. Krein, P. A. Kučment, A. A. Pankov, Banach bundles and linear operators, *Russian Math. Surveys*, 30 (1975), pp. 115–175.
- [817] L. Zalcman, Offbeat integral geometry, *Amer. Math. Monthly*, 87 (1980), pp. 161–175.
- [818] G. Zangerl, O. Scherzer, M. Haltmeier, Circular integrating detectors in photo and thermoacoustic tomography, *Inverse Problems in Science and Engineering*, 17 (2009), pp. 133–142.
- [819] G.T. Zeng, R. Clack, R. Gullberg, Implementation of Tuy's cone-beam inversion formula, *Phys. Med. Biol.*, 39 (1994), pp. 493–508.
- [820] J. Zhang and M. A. Anastasio, Reconstruction of speed-of-sound and electromagnetic absorption distributions in photoacoustic tomography, *Proc. SPIE*, 6086 (2006), 608619.
- [821] H. Zhang and L. Wang, Acousto-electric tomography, *Proc. SPIE*, 5320 (2004), pp. 145–149.
- [822] H. Zhao, Time reversal based direct imaging methods, in [153, pp. 505–521].
- [823] H. Zhao (Editor), *Mathematics in Image Processing*, AMS, Providence, RI, 2013.

Index

- acousto-electric effect, 142
- acousto-electric tomography, (AET), 12, 141, 142
- acquisition surface, 98
- active interrogation, 139
- algebraic reconstruction technique (ART), 44, 84
- analysis
 - commutative harmonic, 167
 - harmonic, 165
- analytic set, 188
- artifact, 13, 40, 65
- attenuated Radon transform, 54
- audible, 70
- backprojection, 34
- Beer's law, 23
- Bell, A. G., 98
- Calderón problem, 94
- central slice formula, 32
- co-spectrum, 189
- collimation, 22
- collimator, 7, 22
- commutative harmonic analysis, 167
- Compton camera, 22, 62
- computed tomography (CT), 3, 22
 - fully 3D, 16
- conditions
 - evenness, 45
 - moment, 45
 - range, 45
- cone-beam projection, 23
- conical neighborhood, 69
- contrast, 12
- coordinates
 - normal, 27
 - polar, 47
- cost, 13
- coupled physics technique, 16, 93, 95
- Coxeter cross, 108
- current density imaging, (CDI, CDII), 12
- data
 - incomplete, 13
- detector
 - circular, 103, 105
 - integrated, 103
 - linear, 103, 104
 - planar, 103
 - point, 98
- determinant
 - regularized, 51
- Dirichlet-to-Neumann map, 88
- divergent beam transform, 25
- effect
 - photoacoustic, 98
- elastography, 11, 91
 - magnetic resonance, 12
- electrical impedance imaging, 9
- electrical impedance tomography (EIT), 9, 11
- elliptic equation, 13
- ellipticity
 - Douglis–Nirenberg, 155
- emission tomography, 5
- equation
 - elliptic, 13
 - hyperbolic, 13
 - radiative transfer, 25, 53
 - transport, 13
 - wave, 13
- \tilde{f} - multidimensional Fourier transform, 29
- factorization formula, 32
- fan-beam projection, 23
- filtered backprojection (FBP), 38, 122
- formula, 38
- in thermoacoustic tomography (TAT), 122
- filtration, 38
- focusing
 - synthetic, 141
- formula
 - central slice, 32
 - filtered backprojection (FBP), 38
 - Fourier-slice, 32
 - Poisson–Kirchhoff, 100
 - projection-slice, 32
 - ρ -filtered backprojection, 38
- forward operator
 - \mathcal{M} , 101
 - \mathcal{W} , 99
- Fourier integral operator (FIO), 15, 85
- Fourier transform, 29, 172
- Fourier-slice formula, 32
- Fredholm, 152
- Fredholm alternative, 115
- Fredholm operator, 184
- fully 3D computed tomography (CT), 80
- fully 3D imaging, 77
- fully 3D X-ray computed tomography, 16
- function
 - essentially band-limited, 42
 - ridge, 33
- \hat{g} - 1D Fourier transform, 29
- geodesic Radon transform, 89
- geometric tomography, 19

- goal in thermo-/photoacoustic tomography (TAT/PAT), 99
- Goursat problem, 79
- harmonic analysis, 165
- Helmholtz representation, 127
- high frequency tomography, 72
- Hilbert transform, 37
- Hilbert–Schmidt operators, 186
- Hölder stability, 42
- hole theorem, 48
- hybrid, 16
- hybrid method, 12, 95
- hybrid technique, 93
- hyperbolic equation, 13
- ideals
- operator, 51
- image processing, 3
- image reconstruction, 3
- image registration, 94
- image understanding, 3
- imaging
- current density, 12
 - direct, 22
 - electrical impedance, 9
 - magnetic resonance, 8
 - projection, 21
- imbedding, 50
- inaudible, 70
- incomplete data
- due to trapping, 118
 - in thermoacoustic tomography (TAT), 110
- incomplete data artifacts, 102
- index of A , 184
- instability
- exponential, 43
- integral geometry, 19, 26, 101, 117
- intensity modulated radiation therapy treatment planning, 62
- interior problem, 67
- inverse
- left, 40
- inverse conductivity problem, 94
- inverse crime, 40
- inverse problem, 3
- inverse spectral problem, 4
- inversion
- algorithm, 102
 - stability of, 42
- inversion formula, 102
- closed-form, 121
 - local, 49
 - non-local, 49
- inversion method, 12
- invertible regularizer, 184
- invisibility, 88
- invisible, 70
- John's equation, 16, 79
- John's parametrization, 16
- John's transform, 27, 28
- k -plane transform, 27
- x -operator, 80
- Λ_σ , 88
- left inversion, 40
- left regularizer, 152, 185
- left semi-Fredholm operator, 152, 185
- Lipschitz stability, 42
- local, 49
- local tomography, 72
- locality, 153
- \mathcal{M} , 101
- Mackey, G., 165
- magnetic resonance elastography (MRE), 12, 91, 94
- magnetic resonance electrical impedance tomography (MREIT), 12
- magnetic resonance imaging (MRI), 8, 11
- matrix
- Hermitian, 162
- medical imaging, 3
- Mellin transform, 32, 180
- method
- hybrid, 93
- microlocal analysis, 15, 65, 86
- Minkowski–Funk transform, 7
- mollifier, 161
- multiphysics technique, 93
- multiwave technique, 93
- Noether operator, 184
- noise
- statistical, 23
- noncommutative harmonic analysis, 167
- nontrapping condition, 182
- nonuniqueness, 41
- nonuniqueness set, 105
- normal coordinates, 27
- normal operator, 36
- nuclear magnetic resonance (NMR), 8, 87
- nuclear magnetic resonance (NMR) imaging, 87
- numerical phantom, 39
- Nyquist condition, 177, 178
- observation surface, 98
- observation time
- finite, 109, 117
 - infinite, 109, 116
- Oka's principle, 188
- “old” integral geometry, 19
- ω^\perp , 29
- operator
- Fourier integral, 85
 - Fredholm, 184
 - Noether, 184
 - spherical mean, 101
- operator ideal, 51, 186
- optical coherence tomography (OCT), 147
- optical tomography (OT), 11, 90
- oversampling, 178
- parallel beam projection, 23
- parametrix, 85, 125
- passive version of TAT, 139
- Petrovsky ellipticity, 154
- phantom
- numerical, 39
 - physical, 40
- $\Phi(E, F) \subset L(E, F)$, 184
- photo-, optoacoustic tomography (PAT/OAT), 12
- photoacoustic effect, 7, 93
- photoacoustic tomography (PAT), 97, 98
- physical phantom, 40
- point detectors, 98
- positron emission tomography (PET), 11
- principal analytic, 188
- principal value (p.v.), 38
- problem
- inverse, 3
 - inverse spectral, 4
- projection
- cone-beam, 23
 - fan-beam, 23
 - parallel beam, 23

- projection imaging, 21
 projection-slice formula, 32
 pseudodifferential operator (Ψ DO), 15, 152
 pseudolocality, 153
 $p.v.$ (principal value), 38
 quantitative PAT (QPAT), 139, 151
 radar, 11
 synthetic aperture, 149
 radiative transfer equation (RTE), 25, 53
 Radon, 7
 transform, 7, 25
 continuity, 33
 dilation invariance, 31
 Fourier inversion
 formula, 39
 inversion, 36
 range, 45
 rotation invariance, 31
 shift invariance, 30
 Radon–John transform, 27
 range conditions, 13
 in thermoacoustic tomography (TAT), 112
 range descriptions, 102
 range theorem, 46
 reflection tomography, 5
 region of interest (ROI), 49
 region of interest (ROI) imaging, 67
 regularized determinant, 187
 regularizer, 184
 resolution, 12
 ρ -filtered backprojection, 38
 ridge function, 33
 Riesz potential, 38
 right regularizer, 185
 right semi-Fredholm, 185
 S^1 , 161
 \mathcal{S} -Schwartz space, 29
 s-number, 186
 safety, 13
 sampling, 177
 sampling theorem, 178
 scan
 ultrasound, 8
 scattering amplitude, 53
 Schatten–von Neumann classes, 186
 Schwartz space, 29, 162
 semi-Fredholm operators, 185
 Shatten–Neumann class, 50
 Σ_N , 108
 signal-to-noise ratio (SNR), 68
 signed distance, 27
 single photon emission
 tomography (SPECT), 11
 singular value, 36, 43, 186
 singularity
 audible
 in thermoacoustic tomography (TAT), 111
 visible, 118
 in thermoacoustic tomography (TAT), 111
 sinogram, 28
 smoothness
 microlocal, 180
 Sobolev space, 176
 sonar, 11
 sonoelastography, 12, 91, 94
 sound speed reconstruction, 102
 spectral geometry, 4
 spectrum of the operator
 function, 189
 spherical mean operator, 101
 stability, 12, 42
 Hölder, 42
 Lipschitz, 42
 stability of reconstruction, 102
 in thermoacoustic tomography (TAT), 109
 statistical noise, 23
 Stein manifold, 188
 stiffness, 91
 sufficiency of the data, 101
 support theorem, 48
 surface
 acquisition, 97, 98
 observation, 97, 98
 synthetic aperture radar (SAR), 149
 synthetic focusing, 141
 TAT image (tomogram), 97, 98
 Tchebychev polynomial, 45
 theorem
 “hole”, 48
 range, 46
 support, 48
 thermoacoustic tomography (TAT), 12, 97
 filtered backprojection, 122
 tomographic, 3
 tomography, 3
 acousto-electric (AET), 12, 141, 142
 computed (CT), 3, 22
 discrete, 11
 Doppler, 11
 electrical impedance (EIT), 11
 electron, 11
 emission, 5, 53
 high frequency, 72
 Internet, 11
 local, 72
 luminescence, 11
 magnetic resonance electric impedance (MREIT), 12
 old, 21
 optical (OT), 11, 90
 optical coherence (OCT), 147
 photoacoustic (OAT), 12
 photoacoustic (PAT), 12, 97
 quantitative (QPAT), 151
 polarization, 11
 positron emission (PET), 11
 reflection, 5
 single photon emission
 (SPECT), 11
 thermoacoustic (TAT), 12, 97
 traditional, 21
 transmission, 5
 ultrasound (UT), 11
 ultrasound modulated optical (UMOT), 12, 141, 147
 totally real, 56
 trace class operators, 186
 traditional “old” tomography, 8
 transform
 Abel-type, 45
 divergent beam, 25
 Fourier, 29
 Hilbert, 37
 John’s, 28
 k -plane, 27
 Mellin, 32
 Radon, 7, 25, 29

- generalized, 62
geodesic, 89
weighted, 62
X-ray, 25, 29
transmission tomography, 5
transport equation, 13
trapping, 110, 118, 182
ultrahyperbolic, 79
ultrasound imaging (tomography) (UT), 11, 91
ultrasound modulated optical tomography (UMOT), 141, 147
ultrasound scan (US), 8, 141
ultrasound tomography, 11
UMOT, UOT, 12
undersampling, 178
uniqueness, 12
uniqueness set, 105
unit normal vector, 27
visibility zone, 111
visible, 70
 \mathcal{W} , 99
wave equation, 13
wavefront set, 15, 180
Whittaker–Kotel’nikov–Shannon theorem, 178
X-ray, 7
computed tomography (CT), 11, 22
picture, 21
transform, 25